Streamflow Data Assimilation for Soil Moisture Prediction

by

Christoph Rüdiger

Diplom-Ingenieur

Submitted in total fulfilment of the requirements of the degree of
Doctor of Philosophy

29 October 2006

Department of Civil and Environmental Engineering,
The University of Melbourne, Australia.

– Produced on archival quality paper –

Abstract

Soil moisture is an important variable in hydrologic land surface and climatic modelling because of its control on water and energy balance processes in and between the soil and the atmosphere. However, obtaining reliable information on soil moisture is difficult. While point ground observations are useful to determine the temporal variability of soil moisture, they are limited spatially. This is due to the accessibility of sites and number of measurements needed for spatial representation; a consequence of high spatial variability and short correlation length. On the other hand, soil moisture observations from satellite platforms allow for the coverage of large areas with a relatively high repeat cycle. Nevertheless, some limitations to the data apply. For example, it has long been known that these data are limited to a thin near-surface layer of soil for areas of low-to-moderate vegetation, due to the attenuation effects of dense vegetation on the soil moisture signal. An alternative to observing soil moisture is making estimates through hydrologic land surface modelling. However, the accuracy of a model prediction depends on its input variables and physical processes representation, which generally rely on good observations for calibration purposes. Hence, techniques need to be developed to improve the current state of soil moisture information.

The primary objective of this thesis is to develop computationally efficient methods to determine reliable soil moisture for the initialisation of global climate and weather prediction models. The focus is on areas where soil moisture remote sensing is limited in its availability, such as in the heavily forested regions of the Amazon, where improvement in the soil moisture states has been shown to have a significant impact on the quality of precipitation forecasting.

While the three techniques described above (remote sensing, point measurements and modelling) have their individual limitations,

there have been recent advances in using the diverse approaches to complement each other through the process of data assimilation, utilising their respective strengths. This thesis proposes to extend this process by inferring soil moisture states through the joint assimilation of observed streamflow and remotely sensed surface soil moisture observations into a hydrologic land surface model. A variational data assimilation approach is used, rather than a sequential assimilation approach, such as the Kalman filter to account for the time lag between rainfall in the catchment and the observed upstream runoff impact on streamflow at the catchment outlet. The approach presented in this thesis makes use of the correlation between streamflow and upstream soil moisture observations to yield an improvement in soil moisture predictions. Because of the implication of vegetation on soil moisture remote sensing, the focus of this thesis is on the use of streamflow observations to retrieve soil moisture, allowing for improved soil moisture predictions in areas of dense vegetation. However, remotely sensed surface soil moisture observations are also used when and where available.

The soil moisture estimation method developed here is applied in a number of synthetic and field case studies in the Goulburn River catchment in south-east Australia, a sub-humid to semi-arid region. In the synthetic studies, different aspects of streamflow data assimilation are investigated in single and multi-catchment scenarios. First, time scale issues of the assimilation scheme are identified, followed by identification of the impact of forcing data errors. Further, the potential for assimilating remotely sensed surface soil moisture observations in addition to streamflow observations is studied. Finally, the developed method is demonstrated with a field study using observed streamflow, forcing data and AMSR-E soil moisture products.

This is to certify that

i) this thesis comprises only my original work towards the PhD, except where indicated,

ii) due acknowledgment has been made in the text to all other material used,

iii) this thesis is less than 100,000 words in length, exclusive of tables, maps, bibliographies and appendices.

Christoph Rüdiger

empty page

This thesis is dedicated to the three most important people in my life:

My mother, Odile,

and my brother, Stephan,

for being ever so supportive, no matter which way I choose to go.

And my late grandfather, Pépère.

With deep love and respect.

Where do we come from?

Who are we?

Where do we go?

- Paul Gauguin, 1848 – 1903

"We go about our daily lives understanding almost nothing of the world. We give little thought to the machinery that generates the sunlight that makes life possible, to the gravity that glues us to the Earth that would otherwise send us spinning off into space, or to the atoms of which we are made and on whose stability we fundamentally depend. Except for children (who don't know enough not to ask the important questions), few of us spend much time wondering why nature is the way it is; where the cosmos came from, or whether it was always here; if time will one day flow backward and effects precede causes; or whether there are ultimate limits to what humans can know. There are even children, and I have met some of them, who want to know what a black hole looks like; what is the smallest piece of matter; why we remember the past and not the future; how it is, if there was chaos early, that there is, apparently, order today; and why there is a universe.

"In our society it is still customary for parents and teachers to answer most of these questions with a shrug, or with an appeal to vaguely recalled religious precepts. Some are uncomfortable with issues like these, because they so vividly expose the limitations of human understanding.

"But much of philosophy and science has been driven by such inquiries. An increasing number of adults are willing to ask questions of this sort, and sometimes they get some astonishing answers. Equidistant from the atoms and the stars, we are expanding our exploratory horizons to embrace the very small and the very large. […]"

Carl Sagan,
in "Introduction" to
A Brief History of Time
by Stephen Hawking

Acknowledgement

First, I wish to thank my mother, Odile. I would never have achieved this work without her constant support and understanding, especially for accepting me to move a second time to the other side of the world to pursue my dreams. Second, thanks have to be extended to my brother, Stephan, as always, because as the older brother he always had to fight for the rights which I was able to take for granted.

A special thanks has to go to the people at the Hydrological Sciences Branch at NASA Goddard Space Flight Center, where I had the opportunity to spend three outstanding months. In particular, I have to thank the former head of the Hydrological Sciences Branch, Paul Houser, for his invitation, sponsorship, and helpful discussions. Further, Randy Koster and Sarith Mahanama for their insight into and help with the Catchment Land Surface Model, Rolf Reichle for discussing the topic of data assimilation, and in general everybody who happily gave up some of their time to help me. Finally, Debra Scott for taking care of Cress and I during our stay at Goddard.

Further, I have to thank Garry Willgoose for providing me the opportunity to spend seven weeks at the School of Geography at the University of Leeds, a place to stay during my visit, and the countless number of interesting talks we had during that period.

Then, there are my office mates throughout these years: Steve, Matthew and Adam – long live the "Dungeon" – and Cress, who all had to endure my moods. I had a wonderful time with all of you.

Last but not least I have to thank all three of my supervisors, Jeffrey Walker, Jetse Kalma and Garry Willgoose, for their guidance and patience during the past years. Especially my thanks go to Jeffrey Walker for tolerating my view of life and being always available and open for discussions.

empty page

Table of Contents

List of Figures

List of Tables

List of Symbols

Symbol	Unit	Definition
a	-	Upstream runoff-contributing area per pixel contour length
A	km²	Catchment area
A	m²	Cross sectional area of flow
A_{sat}	-	Fraction of saturated catchment area
A_{tr}	-	Fraction of unsaturated catchment area
A_{wilt}	-	Fraction of catchment area at wilting point
A_u	km²	Upstream runoff-contributing area
b	-	Shape parameter of soil moisture profile
$\mathbf{B}$	-	Background error covariance matrix
$c_{r,i,f}$	-	Routing coefficient of flow type f in cell i
C^T	ms/°C µs/°C	Temperature correction coefficient for P_{obs}
d	m	Local depth to the water table
$\bar{d}$	m	Catchment-average water table depth
d	m	Streamflow depth
D	mm	Local soil moisture deficit
$e_{r,p}$	-	Rough bare surface emissivity at polarisation p
e_s	hPa	Saturation vapour pressure
$e_{s,p}$	-	Smooth bare surface emissivity at polarisation p
es	mm	Soil water extraction through bare soil evaporation
et	mm	Soil water extraction through evapotranspiration
ev	mm	Soil water extraction through vegetation transpiration
ET	mm	Evapotranspiration
ET_a	mm	Actual evapotranspiration
ET_p	mm	Potential evapotranspiration
f_n	-	Value of areal fraction n (A_{sat}, A_{tr}, A_{wilt})
FL_i	L	Flow length through grid cell i
$FT_{j,f}$	T	Flow time of flow type f to outlet j
G	mm	Baseflow over time step t
h	-	Effective roughness factor
$\mathbf{H}$	-	Observation operator matrix
HF_n	W/m²	Heat flux of areal fraction n (A_{sat}, A_{tr}, A_{wilt})
HF_t	W/m²	Total heat flux

i	mm	Throughfall infiltration
i	mm	Soil temperature observation depth
$\mathbf{I}$	-	Identity matrix
J	-	Cost function
K	-	Box-Cox transformation parameter
$\mathbf{K}$	-	(Kalman) gain function matrix
$K_s(surface)$	m/s	Saturated hydraulic conductivity of the surface soil layer
L_t	m^2/m^2	Leaf area index
M_D	mm	Catchment soil moisture deficit
$M_{D,\max}$	mm	Maximum catchment soil moisture deficit
$\mathbf{M}_k$	-	Model operator matrix at time step k
M_{rz}	mm	Root zone excess
M_{se}	mm	Surface excess
$M_{se\text{-}max}$	mm	Maximum surface excess
n	-	Manning's roughness coefficient
N	-	Normalised period of sensor measurement
$N_{cp,i}$	-	Number of cells contributing to streamflow for a given time step
$N_{cp,all}$	-	Number of all cells contributing to streamflow in a catchment
o	-	Offset for temperature correction
p	deg	Horizontal or vertical polarisation
P	hPa	Atmospheric pressure
P	kg/m^2	Precipitation
P	m	Wetted perimeter of flow
P^{25}	ms µs	Period measurement standardised to 25°C
$P_{0.0}$	ms µs	Average period measurement for oven dry soil at 25°C
$P_{0.4}$	ms µs	Optimised soil specific period at a moisture content of 0.4v/v and a temperature of 25˚C
P_{obs}	ms µs	Observed period measurement
P_t	kg/m^2	Precipitation throughfall
q_t	-	Observed response
$\mathbf{q}_t$	-	Observed response vector
$\mathbf{Q}$	-	Added error matrix
Q	m^3/s	Streamflow
$Q_{conv,i,k}$	m^3/s	Unit converted streamflow at time step i, caused by

		precipitation event *k*
$Q_{CLSM,i,k}$	$kg/(m^2d)$	CLSM modelled instantaneous runoff at time step *i*, caused by precipitation event *k*
$Q_{out,i,k}$	m^3/s	Streamflow at time step *i*, caused by precipitation event *k* at the catchment outlet
Q_s	kg/kg	Specific humidity of air
Q_s	kg	Surface runoff
Q_t	-	Transformed observation
$Q_{tot,i,k}$	m^3/s	Total streamflow from all cells at time step *i*, caused by precipitation event *k* at the catchment outlet
$Q_{tot,i,lower}$	m^3/s	Total streamflow at the outlet of a lower catchment at time step *i*
$Q_{tot,i+lag,upper}$	m^3/s	Total streamflow coming from an upper catchment at time step *i+lag* at the outlet of a lower catchment,
$Q^{comb}_{tot,i,lower}$	m^3/s	Total streamflow at the outlet of a lower catchment at time step *i*, resulting from $Q_{tot,i,lower}$+ $Q_{tot,i+lag,upper}$
r^i_T	-	Average daily soil temperature ratio at depth *i*
R	mm	Streamflow at the catchment outlet
$\mathbf{R}$	-	Observation error matrix
R_h	m^2/m	Hydraulic radius
R_i	-	Normalised number of pixels contributing to streamflow for a given time step *i*
$R_{s,h}$	-	Surface reflectivity coefficient at horizontal polarisation
$R_{s,p}$	-	Surface reflectivity coefficient at nadir and polarisation *p*
$R_{s,v}$	-	Surface reflectivity coefficient at vertical polarisation
RRF	-	Rainfall Reduction Factor
s	1/°C	Slope for temperature correction
S	m/m	Streambed slope in flow direction
S_i	m/m	Slope of grid cell *i*
SI	-	Stress index
SM	mm	Soil moisture storage in the catchment
SWI	-	Soil wetness index
t	s	Model time step
T	K	Air temperature
T	°C	Observed soil temperature
$T_{b,p}$	K	Brightness temperature at polarisation *p*
T_c	K	Canopy temperature
T^i_d	°C	Average daily soil temperature at depth *i*

T_s	K	Effective surface temperature
$u_i(t)$	-	Routing response function
$V_{i,f}$	L/T	Flow velocity of flow type f in cell i
$w(z)$	v/v	Soil water content at depth z from the surface
w_p	km	Unit contour length
W_r	kg/m^2	Interception reservoir
$\bar{x}$	-	Catchment-average CTI value
$\mathbf{X}$	-	Model state vector
$\mathbf{X}_0$	-	Initial model state vector
$\mathbf{X}_k^a$	-	Analysed model state vector at update time step k
$\mathbf{X}_k^b$	-	Background model state vector at update time step k
$\mathbf{x}_t$	-	Model input vector
z	m	Water table depth from the surface
$\mathbf{Z}$	-	Observation vector
$\hat{\mathbf{Z}}$	-	Predicted observation vector
α	v/v	Slope of the linear function of the sensor calibration
β	-	Shape parameter of function N
β	-	Local pixel slope
$\boldsymbol{\beta}$	-	Model parameter and state vector
$\boldsymbol{\gamma}$	-	Augmented parameter vector
$\boldsymbol{\gamma}_0$	-	Optimum augmented parameter vector
Γ	-	Surface reflectivity
Γ	-	Vegetation transmissivity
Γ_0	-	Derivative matrix $\partial\varepsilon/\partial\gamma$
ε	F/m	Complex dielectric constant
$\boldsymbol{\varepsilon}_t$	-	Random error vector
η_t	-	Transformed error
θ	deg	Incidence angle from nadir
θ	v/v	Volumetric soil moisture content
θ_i	-	Moving average (MA) parameter
θ_{obs}	v/v	Observed soil moisture content
θ_{sat}	v/v	Saturation soil moisture content
θ_{wilt}	v/v	Soil moisture content at wilting point
λ	-	Box-Cox transformation parameter

λ_M	-	Marquardt search parameter
ν	1/m	Change with depth of the hydraulic saturated conductivity
σ_0	-	Standard deviation of the error distribution for the optimum parameter and states
$\boldsymbol{\Sigma}$	-	Covariance error matrix
τ	-	Optical depth
τ_1	1/s	Time scale parameter 1
τ_2	1/s	Time scale parameter 2
τ_{ip}	-	Optical depth caused by precipitation interception at polarisation P
τ_l	-	Optical depth caused by litter
τ_p	-	Total optical depth polarisation P
τ_{sp}	-	Optical depth caused by standing vegetation at polarisation P
φ_i	-	Autoregressive (AR) parameter
Φ	v/v	Soil porosity
ψ_s	m	Matric potential
ω	-	Scattering albedo
Ω	-	Error covariance matrix

Glossary

Key Acronyms

AMSR-E	Advanced Microwave Scanning Radiometer for the Earth Observing System
ASA	Australian Soils Atlas
AWS	Automated Weather Station
BoM	Bureau of Meteorology (Australia)
CASMM	Catchment-average Soil Moisture Monitoring
CLSM	Catchment Land Surface Model
CTI	Compound Topographic Index
DEM	Digital Elevation Model
DIPNR	Department of Infrastructure, Planning, and Natural Resources (Australia)
ERS	European Remote Sensing programme
GCM	General Circulation Model
GDAS	Global Data Acquisition System
GSWP-2	2nd Global Soil Wetness Project
LAI	Leaf Area Index
LSM	Land Surface Model
MPDI	Microwave Polarisation Difference Index
RFI	Radio-frequency Interference
SASMAS	Scaling and Assimilation of Soil Moisture and Streamflow project
SMMR	Scanning Multichannel Microwave Radiometer
SMOS	Soil Moisture and Ocean Salinity
TDR	Time Domain Reflectometry

Definition of Key Terms

assimilation window	Observation window of a pre-defined period, including the series of observations to be assimilated into the model.
catchment deficit	Soil water lacking the soil moisture profile to reach saturation.
cell-to-cell routing	Routing of water particles from cell to cell, with interaction between surface and soil water in each cell.
control run	Baseline simulation as for comparison with the open-loop simulations and simulations after assimilation.
degraded forcing scenario	Model predictions from simulations with errors included in the forcing data.
equilibrium soil moisture profile	A soil moisture profile in equilibrium is the condition, when pressure head gradient and gravity are in balance and is only changed by changes in the soil moisture content.
excess (surface and root zone)	Soil water in exceeding or lacking the water profile at equilibrium
initial states	Initial values of model prognostic variables.
nested catchment	"Nested catchments" describes subcatchments located in a larger catchment. Streamflow observations at a subcatchment outlet are the sum of all upstream catchments, while all other hydrologic and flux processes are modelled for each subcatchment individually.
observation depth	Soil depth from which soil moisture information is retrieved through remote sensing.
optical depth	Optical thickness of the vegetation cover over soil
real study	Experiment based on the use of observations/forcing data measured in the field.
runoff	Expression for the combined horizontal subsurface and surface water fluxes.
source-to-sinfk routing	Direct routing of water particles from their source directly to the outlet of the catchment, without further interaction with the surrounding terrain.
streamflow	Horizontal water flux through the river system.
synthetic study	Experiment based on the use of data/observations created through model runs, to replace field observations.
time of concentration	Period of maximum travel time of precipitated water as runoff to the catchment outlet.
true observations	Synthetic observations created with an open-loop simulation, which are used in the synthetic studies to replace field observations.

Chapter One

1 Introduction

This thesis presents a new approach to improving soil moisture state estimation in a hydrologic land surface model, through the assimilation of streamflow and – where available – surface soil moisture observations using a variational-type data assimilation scheme. The rationale for this thesis is to develop a methodology for soil moisture initialisation in global climate and weather prediction models for regions where remote sensing cannot provide information on soil moisture.

A series of numerical twin experiments have been undertaken to demonstrate the approach. First, the general feasibility of the approach was tested in a single-catchment synthetic study, and the impact of errors in the forcing data and model assessed. Second, the applicability of the approach for regional modelling was tested in a nested multi-catchment synthetic study. The thesis concludes with a demonstration of the approach for an experimental catchment, using observed streamflow and remotely sensed surface soil moisture from the Advanced Microwave Scanning Radiometer for the Earth Observing System (AMSR-E) for assimilation. Observed streamflow and root zone soil moisture are used for verification of the assimilation scheme.

1.1 Importance of Soil Moisture

Water plays an important role in a multitude of environmental fields: humans and most other life forms need water to survive; it is an important factor in agriculture (eg. Suojala-Ahlfors and Salo, 2005); it influences soil erosion (eg. Fitzjohn et al., 1998); and most significantly the amount of water in the soil controls several hydrological and climatological processes (eg. Entekhabi et al., 1996; Dirmeyer et al., 1999). In hydrology, the amount of soil moisture controls the partitioning of precipitation between infiltration water (which in turn is transferred into subsurface storage and baseflow) and surface runoff (Descroix et al., 2002; Castillo et al., 2003), and therefore river discharge and flooding. In a climatological context, soil moisture content controls the land surface and atmospheric energy exchange. Furthermore, soil moisture regulates the bare soil evaporation, influences plant transpiration (eg. Wetzel and Chang, 1987; Ács, 2003) and photosynthesis (Rodriguez-Iturbe et al., 2001), and plant transpiration and stomatal resistance of plants are affected by soil moisture stress (eg. Calvet et al., 2004).

Soil moisture is particularly important for the initialisation of climate models. It has been shown in several studies that improvements in the initial soil moisture content can significantly improve the predictability of precipitation and air temperatures (Delworth and Manabe, 1989; Koster et al., 2000a; Koster and Suarez, 2003). Koster et al. (2000a) and Koster and Suarez (2003) have shown that there is an improvement in precipitation predictability for their model when soil moisture prediction is constrained (over and above that from sea surface temperature; Fig. 1.1). The largest effect of soil moisture on the land surface-atmosphere interactions has been observed for dry and intermediate soil moisture content (Koster et al., 2004), since for wet conditions evapotranspiration is controlled by radiation rather than changes in soil moisture. Moreover, soil moisture "memory" influences the atmospheric conditions over long periods (Beljaars et al., 1996; Shinoda and Yamaguchi, 2003), due to its long decay timescales. Therefore, soil moisture is important for the prediction of seasonal changes in precipitation, temperature (Mahanama and Koster, 2003) and evaporative fraction (Dirmeyer et al., 2000). Consequently, reliable soil moisture estimates must be

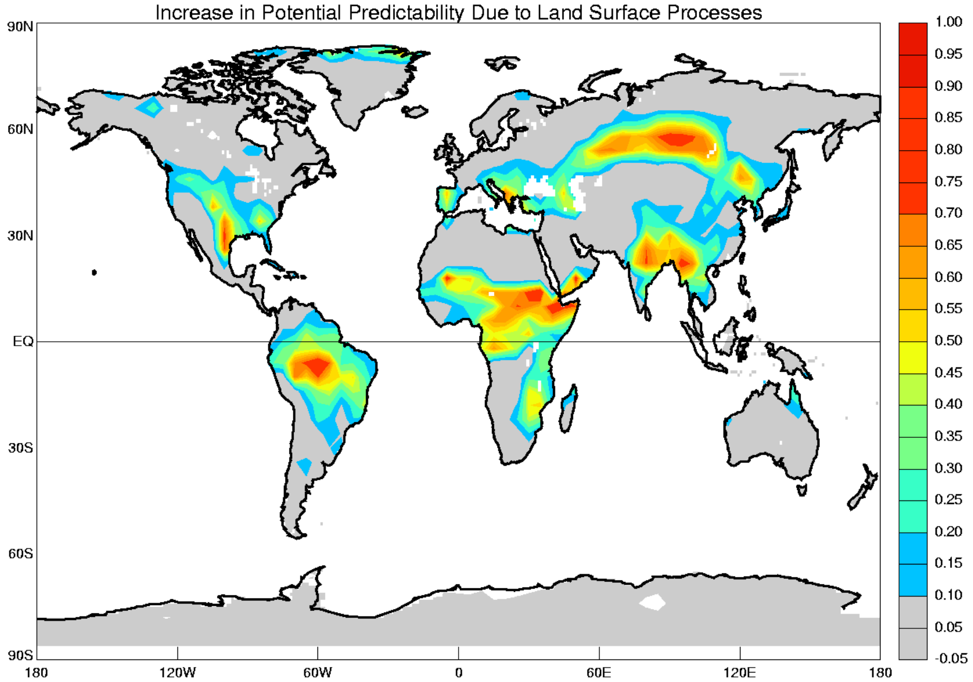

Figure 1.1. Potential improvement in northern hemisphere summertime predictability of precipitation when improved soil moisture information is available in addition to sea surface temperature (from Koster et al., 2000a).

obtained to improve land surface model initialisation and hence the predictability of weather and climate.

1.2 *Statement of Problem*

Despite its importance, there is no operational system for global soil moisture prediction. The reason for this is that the users who can benefit from such a system require frequent information on root zone soil moisture content across large areas (Schmugge et al., 1980); it is difficult to satisfy these requirements and the technological advances required are only now reaching maturity.

Three different techniques are available to obtain soil moisture values for hydrologic and climate modelling purposes: i) point ground measurements, ii) remote sensing, and iii) modelling (Fig. 1.2). However, these techniques only provide limited information or are inherently inaccurate.

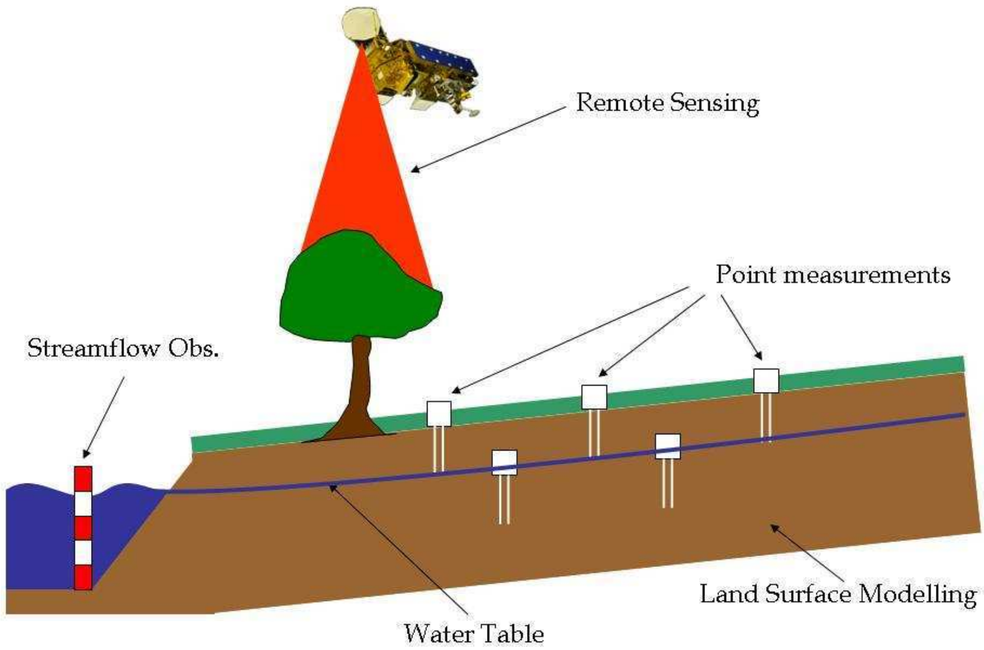

Figure 1.2. Schematic of the soil moisture estimation problem. Point measurements can only cover a limited area, remote sensing signals are masked by dense vegetation, land surface models provide an areal estimate of the root zone soil moisture, and streamflow observations give information of the aggregated upstream moisture conditions.

While point ground measurements are a good tool to determine the temporal variability of surface, root zone and profile soil moisture, a very large number of these measurements are needed to obtain even a catchment wide accurate estimate of average soil moisture, unless a catchment average soil moisture monitoring (CASMM) site is determined (Grayson and Western, 1998). The need for a large number of monitoring sites is caused by the heterogeneity of soil properties, topography, land cover and vegetation use over short distances. The non-linearity of these processes makes simple upscaling from a single point ground observation difficult (eg. Brunsell and Gillies, 2003; Arrigo and Salvucci, 2005). Therefore, the point ground measurements are typically limited to local or regional scales, because of logistical and financial limitations. The integration of regional soil moisture observations throughout the world into the Global Soil Moisture Data Bank (Robock et al., 2000) is a first effort to

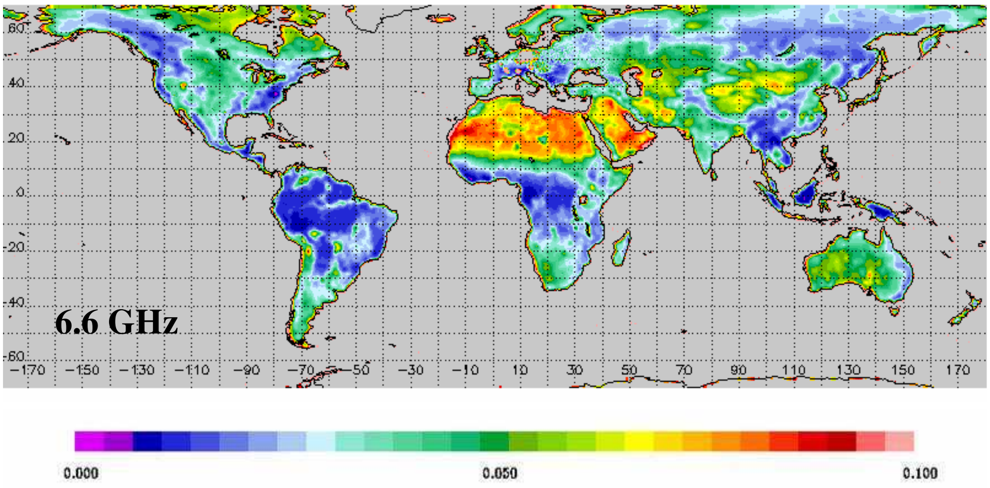

Figure 1.3. The microwave polarisation difference index (MPDI) derived from the Scanning Multichannel Microwave Radiometer (SMMR) 6.6GHz data. A low MPDI (blue) represents dense vegetation and a high MPDI (red) a low level of vegetation (E. Njoku, personal communication). An MPDI of greater than ~0.02 is required for soil moisture estimation from C-band remote sensing.

satisfy the needs for regular publicly available soil moisture observations.

In contrast to point measurements, remote sensing provides a good spatial average of surface soil moisture over a whole region with a single overpass. However, remote sensing of soil moisture is only available for regions with low-to-moderate vegetation, as dense vegetation masks the soil moisture signal (Jackson, 1982). This is the case for a large portion of the Earth's surface when using the C-band observations currently available (Fig. 1.3). Furthermore, remote sensing platforms only detect the near-surface soil moisture content, with the observation depth of the soil moisture being on the order of a few centimetres (Jackson et al., 1981). Instruments that operate in the microwave spectrum have an observation depth of between 1/10 to 1/4 of the wavelength (eg. C-band has a wavelength of ~5cm with an observation depth of between 0.5 and 1cm) (eg. Wilheit, 1978; Njoku and Entekhabi, 1996; Schmugge et al., 2002). However, knowledge of the root zone soil moisture is needed to correctly model evapotranspiration, as plant transpiration is governed by the soil water available in the root zone (eg. Calvet, 2000). Moreover, satellite overpasses have a repeat time of about 2 to 3 days for passive microwave sensors (Njoku et al., 2003) and up to one month for active microwave sensors (Crosson et al., 2002; Zribi et al., 2005). The difference between these two types of microwave remote sensing is that passive microwave remote sensors have coarser spatial resolution (10's km) than active microwave remote sensors (10's m) and therefore cover a larger area of the Earth's surface with each overpass.

The alternative to observations is modelling, and this is the approach most commonly used to date for soil moisture estimation, particularly for weather and climate forecasting. However, the output from hydrologic land surface models cannot be better than the forcing data or the model itself, which suffer from observational errors and biases (eg. Maurer et al., 2001), and assumptions made about physical processes within the soil and between the land surface and the atmosphere (Jackson et al., 1981). Additionally, poor models are not capable of producing good predictions, even with good forcing data. Moreover, Houser et al. (2001) showed that even when the same parameter and atmospheric forcing data are used in different models, the soil moisture predictions from the models vary widely. Fig. 1.4 shows the difference in root zone soil moisture prediction for two commonly used hydrologic land surface models in climate modelling, with differences in root zone soil moisture prediction as great as 10%v/v, being more than one-quarter of the dynamic range.

Despite the shortcomings of these approaches, it has been proposed (Entekhabi et al., 1994) and shown (eg. Houser et al., 1998; Lakshmi and Susskind, 2001; Walker and Houser, 2001) that the individual strengths of the three approaches can be combined to

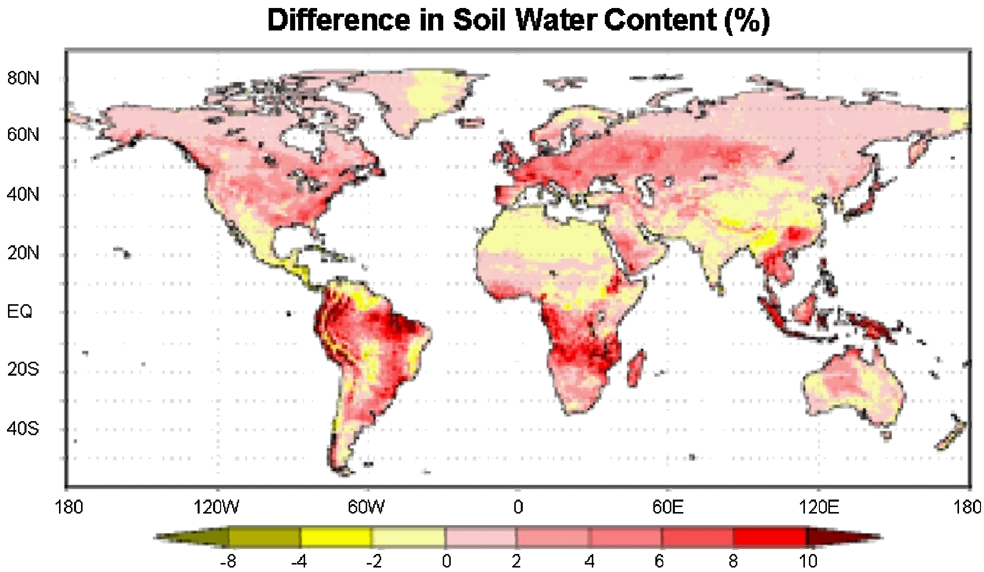

Figure 1.4. Difference in root zone soil moisture prediction for the Global Data Acquisition System (GDAS) and Mosaic land surface models (from Houser et al., 2001).

provide good soil moisture prediction through the use of various data assimilation techniques. The data assimilation techniques that have been used can be distinguished into two different approaches: i) sequential data assimilation such as the Kalman Filter (Kalman, 1960) and its derivatives (eg. Reichle et al., 2002ab; Walker et al., 2002; Aubert et al., 2003) in which model states are updated for each time a new observation becomes available and ii) variational data assimilation schemes (eg. Le Dimet and Talagrand, 1986; Duan et al., 1992; Rabier et al., 1992; Reichle et al., 2001ab; Vrugt et al., 2003), which minimise an objective function using the observations within a certain time window (or assimilation window). These techniques have been used to assimilate remotely sensed regional soil moisture observations (eg. Houser et al., 1998) to improve the spatial distribution of soil moisture, and point observations for the retrieval of the soil moisture profile (eg. Walker et al., 2002).

While both assimilation techniques have been shown to lead to improved model predictions, real soil moisture observations are still required for assimilation purposes. However, satellite missions such as AMSR-E can provide this information only for areas of low-to-moderate vegetation (eg. Jackson, 1982; Njoku and Chan, 2006) and point measurements can only be used on local scales due to personnel and instrument limitations and may not be representative of the catchment average soil moisture (Grayson and Western, 1998), which would introduce a bias into the model. Coincidentally, a large portion of the regions identified by Koster and Suarez (2003) to have the greatest soil moisture impact on precipitation predictability (Fig. 1.2), are also the regions with greatest model soil moisture uncertainty (Fig. 1.3), and regions of dense vegetation cover where remotely sensed soil moisture information is not readily available (Fig. 1.4). In other words, if precipitation predictability improvements are to be achieved in these regions, alternative approaches for improving soil moisture estimates must be sought.

To overcome the shortcoming of surface soil moisture availability for data assimilation in densely vegetated areas, it is proposed that streamflow data be assimilated into the hydrologic land surface model, as these data are a direct measure of the upstream water balance and can be measured to a satisfactory accuracy (Sivapalan, 2003). This proposed approach may be seen as an addition to the assimilation of surface soil moisture observations and is aimed at increasing the accuracy of the latter approach, by constraining the retrieval algorithm with additional information.

A number of soil moisture assimilation studies exist. While successful, the majority of these studies focused on the assimilation of on-site collected soil moisture observations (eg. Heathman et al., 2003) or remotely sensed surface soil moisture observations (eg. Enthekabi et al, 1994; Walker and Houser, 2001, Crosson et al., 2002; Montaldo and Albertson, 2003) to improve root zone soil moisture predictions. Other studies have focussed on the improvement of streamflow predictions, either by assimilating streamflow observations to improve the streamflow forecast itself (eg. Georgakakos and Smith, 1990; Schreider et al., 2001; Aubert et al., 2003; Seo et al, 2003; Madsen and Skotner, 2005) or through the assimilation of remotely sensed soil moisture (eg. Pauwels et al., 2002; François et al., 2003). Moreover, Crow et al. (2003) assimilated streamflow and surface soil moisture in order to calibrate model parameters, rather than improving soil moisture prediction. However, these studies were either synthetic, did not consider the vegetation limitations on remote sensing, were not directed at improving the soil moisture, or suffered from other limitations in the conception of the assimilation scheme or study set up.

Only a very limited number of studies has considered the retrieval of soil moisture states from streamflow data assimilation (Aubert et al., 2003; Seo et al., 2003; Pauwels and de Lannoy, 2006). In their study Pauwels and de Lannoy (2006) used a Kalman filter variant with a fixed lag in the streamflow, which includes the soil moisture states of several time steps (equal or larger than the time of concentration within the catchment). However, this approach is not practical when the time of concentration in the catchment is large, as a large number of soil moisture states has to be simultaneously updated (Seo et al., 2003). Furthermore, this study was only undertaken for a single, small catchment under relatively wet conditions. Additionally, the use of the fixed-lag Kalman Filter would be limited, if the study was undertaken for large, nested catchment networks, as one streamflow observation then relates to different soil moisture states in different catchments, which would have different times of concentration. Finally, it is a purely synthetic study, that has no real surface soil moisture observations to support the validity of the assimilation scheme.

This thesis investigates the potential to improve climate model soil moisture initialisation through a variational-type assimilation of streamflow and remotely sensed soil moisture data when available, with a focus on the use of streamflow data. As this is a demonstration study with a focus on soil moisture improvement, rather than on the impact on precipitation prediction, an uncoupled hydrologic land surface model (as used by a fully coupled climate prediction model) is used, forced with observed atmospheric data. The following section describes more fully the objectives and scope of this thesis.

1.3 *Objectives and Scope*

The principal objective of this thesis is the development and demonstration of a methodology to improve model soil moisture state estimation through the assimilation of streamflow data into a hydrologic land surface model. In order to prove the feasibility of the approach the research tasks included:

a) Collection of field data required for model data assimilation, forcing and validation.

b) Development and integration of a streamflow model with a hydrologic land surface model currently used in a coupled climate prediction model.

c) Implementing the data assimilation scheme with the hydrologic land surface model, to allow soil moisture states to be updated with observed streamflow and/or near-surface soil moisture.

d) Determining the implications of errors in forcing data and model parameters for the assimilation scheme, due to introduced uncertainties in the observations and model output.

e) Finding the appropriate assimilation window length.

f) A comparison of (i) streamflow assimilation, (ii) near-surface soil moisture assimilation, and (iii) joint assimilation of both observations.

g) Understanding the implications involved with application to more complex, nested stream networks.

h) Demonstration of the developed approach on an experimental catchment.

As mentioned previously, the objective of this thesis is to retrieve soil moisture information for regions where near-surface soil moisture measurements are not available. Nevertheless, it is assumed that some areas within the experimental catchment are sufficiently cleared of vegetation, so that remotely sensed surface soil moisture information can be assimilated.

1.4 Outline of Approach

The approach taken in this research consisted of three progressive steps. First, a synthetic study was undertaken for a single catchment as a proof-of-concept that soil moisture within this catchment could be retrieved from the assimilation of streamflow observations observed at the outlet of the catchment. Second, a synthetic study was undertaken for a nested catchment network as a proof-of-concept that upstream soil moisture states could be retrieved from the assimilation of streamflow observations, where streamflow from some of the upstream catchments was not monitored. Third, a field study was conducted to demonstrate how the approach works under real-world conditions. As such, the results from the earlier steps provided insights into how the system would respond in the subsequent steps.

The synthetic studies were also used to answer some fundamental science questions. These science questions included (i) the differences in the performance when assimilating streamflow and surface soil moisture separately, (ii) the likely behaviour in the presence of model, forcing, or observation error, and (iii) the optimal length of an assimilation window. These month- to year-long twin studies, consisted of a truth run initialised from a model spin-up, several degraded simulations initialised with poor soil moisture estimates and parameters, and an assimilation run during which observations from the truth run were assimilated into the degraded run.

The field study was conducted in the Goulburn River experimental catchment specifically set up for this research. While the synthetic studies allowed the identification of individual strengths and weaknesses of the assimilation scheme by artificially driving the model with poor data, these results may not translate into the real field environment, which made a field study necessary. First, observed streamflow and surface soil moisture were individually and jointly assimilated into the model with observed forcing data, and without any prior calibration of the model. This serves to show how the assimilation scheme would likely perform in a typical application of the methodology. Next the model soil moisture parameters were adjusted to correspond better to the observed dynamic range (ie. the observed lowest and highest soil moisture content), the model was modified to simulate the change in the hydrologic response to cracking soil, and observed point rainfall was modified based on the water balance determined from the field observations. This serves to show how the assimilation scheme performs under a more ideal situation.

1.5 Structure of Thesis

This thesis consists of 8 chapters which can be divided into six major parts:

Part 1 – a review section (Chapters 1-2);

Part 2 – the data and catchment under investigation (Chapter 3)

Part 3 – the description of the models and the assimilation scheme used (Chapter 4)

Part 4 – synthetic studies on the feasibility of the proposed technique (Chapters 5-6);

Part 5 – application of the technique to real data (Chapter 7); and

Part 6 – conclusions and recommendation for future work (Chapter 8).

A literature review is given in Chapter 2, where the importance of soil moisture in land surface-atmosphere models, remote sensing of environmental variables, hydrologic land surface modelling, data assimilation approaches, and past achievements are reviewed and discussed for their relevance to this research.

The synthetic and field studies were conducted for the Goulburn River experimental catchment in south-east Australia. This field data was collected as part of the Scaling and Assimilation of Soil Moisture and Streamflow (SASMAS) project – of which this thesis is a part – and is presented in Chapter 3 together with the ancillary data required for this thesis. The available remotely sensed data is also outlined, together with an explanation of limitations and potential sources of errors.

A review of the hydrologic land surface model, development of a routing model, and explanation of the variational-type assimilation scheme used for soil moisture retrieval in this thesis are presented in Chapter 4.

Chapter 5 uses the models introduced in Chapter 4 in a synthetic case study for a single subcatchment of the Goulburn River experimental catchment. In the first part of Chapter 5, the synthetic forcing data sets are presented. This synthetic study demonstrates the applicability of the proposed assimilation scheme and leads to an understanding of the technique, before it is used in a multi-catchment synthetic study in Chapter 6.

A model validation and the field study demonstration of the assimilation methodology are performed in Chapter 7. The forcing, observation and evaluation data used in this study are those from Chapter 3.

A discussion of results, conclusions and recommendations for future research on improved estimation of soil moisture states is given in Chapter 8.

Chapter Two

2 Literature Review

This chapter presents an overview of the significance of soil moisture information for climate modelling, followed by a discussion of the methods to obtain soil moisture information, specifically through microwave remote sensing and hydrologic modelling. The respective strengths and limitations of these methods are discussed in the light of their possible combination through the process of data assimilation. Finally, advances in hydrologic data assimilation are reviewed and a new approach to obtain soil moisture information within a catchment through streamflow data assimilation is proposed.

2.1 Importance of Soil Moisture for Climate Modelling

Climate modelling has been used to predict future climate change, in response to such occurrences as anthropogenic influences. The effects studied range from high-altitude atmospheric processes (Jin et al., 2005) to land surface-atmosphere interactions (Douville, 2003; Hay and Clark, 2003; Koster et al., 2004), the influence of increased CO_2 (Enting and Pearman, 1987), and the impact on local climate due to global climate change (Chiew et al., 1995) and oceanic processes such as the El Niño Southern Oscillation (ENSO; Chiew and McMahon, 2002). However, soil moisture plays an equally significant role in climate modelling, as it regulates the energy and water fluxes between the land surface and the atmosphere.

Shuttleworth (1991) has shown that coupling a model of land surface-atmosphere interactions with a hydrological land surface model can improve the quality of climate model results. Consequently, climate models have been run together with hydrologic land surface models (LSMs) to more accurately describe land surface processes. These land surface processes eventually allow the quantification of possible changes in the environment, such as increasing drought conditions. Such changes may be natural, due to changes in soil moisture conditions and vegetation cover or due to land cover changes following human activities, and are represented in the energy and water balances (Pitman, 2003).

Several synthetic studies have also shown that an improvement to the initial surface soil moisture states had significant positive impact on the predictability of precipitation and air temperatures (Delworth and Manabe, 1989; Koster et al., 2000a; Koster and Suarez, 2003). This is because soil moisture has a significant influence on different temporally and spatially distributed environmental processes (Delworth and Manabe, 1988 and 1989), as it controls the infiltration capacity of the soils (Richards, 1931; Philip, 1957) and consequently the partitioning of precipitation into surface and subsurface runoff (eg. Descroix et al., 2002; Castillo et al., 2003). Furthermore, the availability of soil moisture is a major control on the level of evapotranspiration from plants (eg. Wetzel and Chang, 1987; Ács, 2003) and their stomatal resistance (eg. Calvet et al., 2004). In particular, the lack of soil moisture causes the plants to be water stressed and stops evapotranspiration under extreme conditions.

Because the soil moisture status controls the latent and sensible heat fluxes between the land surface and the atmosphere, it contributes to the heat and water balances between the atmosphere and the land surface. Consequently, soil moisture directly influences the air temperature and air humidity, thus affecting cloud formation (Betts et al., 1996). Furthermore, soil moisture has been shown to "memorise" anomalies within the land surface water budget (Beljaars et al., 1996; Shinoda and Yamaguchi, 2003), meaning that soil moisture is a slowly changing variable that "stores" information on the preceding soil moisture conditions. This has a significant impact on long-term climate modelling, due to the long decay timescales of soil moisture (eg. soil moisture decline after precipitation events may take several weeks to restore the initial conditions). This memory results in an influence on the prediction of seasonal changes in different environmental variables such as precipitation and temperature (Georgakakos et al., 1995; Koster and Suarez, 2001; Mahanama and Koster, 2003).

The above discussion demonstrates that soil moisture plays an important role in modelling atmospheric water and energy budgets (Wetzel et al., 1996). It is therefore essential to understand and quantify the processes related to soil moisture and to predict and observe soil moisture states within a region, or better still the whole land surface of the Earth, and ultimately implement this knowledge into general circulation models (GCM) to improve the predictions from these models (Koster et al., 2004).

The influence of soil moisture on the water and energy balance is largest when the heat fluxes are constrained by water availability in the soil (eg. in temperate, sub-humid, and arid regions), rather than by incoming radiation (as in humid regions such as the tropics). Consequently, experimental catchments have to be set up in areas that provide these environmental conditions.

Even though LSMs are widely used to predict soil moisture conditions, their predictions have to be used with caution. Assumptions about the physical processes and their variability, poor parameter estimates, and observational errors in the forcing data lead to the introduction of errors in the prediction of soil moisture through LSMs (Jackson et al., 1981). Consequently, LSMs have to be improved using available information. Such information may come in the form of in-situ or remotely sensed soil moisture observations (Jackson et al., 1981). In the following sections, techniques to acquire soil moisture information are discussed.

2.2 *Techniques of Soil Moisture Data Acquisition*

Three major techniques are commonly used to provide soil moisture estimates: i) in-situ point observations, ii) remotely sensed observations, and iii) hydrologic land surface modelling. However, despite extensive research in the observation of soil moisture and the use of all the three mentioned observation techniques in operational modelling systems, some critical issues remain unsolved. In the following sections, the different techniques are introduced and their respective advantages and limitations discussed.

2.2.1 In-situ Point Observations

Traditional techniques of in-situ soil moisture measurements include point measurements, with sensors such as the Trase® Time Domain Reflectometry (TDR) probes or Campbell Scientific Water Content Reflectometers, or simply gravimetric measurements of soil moisture (see Walker et al. (2004a) for a detailed review of different techniques). While the first two methods are non-destructive methods and can be repeated for the same soil, the gravimetric measurements require collection of soil samples and subsequent analysis in the laboratory and therefore cannot be repeated in the field with the same soil sample. The aforementioned soil moisture probes are generally permanently installed in the ground and measure the dielectric constant of the soil, which changes with the amount of water stored in the soil (Wang and Schmugge, 1980), with only little destruction to the soil sample during the insertion process.

There are several limitations to the use of in-situ soil moisture observations. While they provide accurate and detailed information on the vertical profile of soil moisture at a single point in space, there is only a limited area that can be monitored with this approach. Soil moisture sensors are expensive and due to the short spatial correlation length of soil moisture, point measurements need to be closely spaced if they are to provide information on the spatial variability of soil moisture. This makes large-scale, high-density instrumentation of field sites economically and logistically infeasible. Furthermore, the measurement of soil moisture with handheld instruments is only feasible over small areas, shallow depths, and short periods.

An extensive amount of work has been undertaken in regard to soil moisture distribution within a catchment and its importance to hydrological processes (Grayson and Western, 1998; Yoo, 2001). Grayson and Western (1998) have undertaken research into the variability of near-surface soil moisture and its correlation to remotely sensed data, and assessed the possibility of identifying representative monitoring sites within a catchment. They showed that even on a small scale, the soil moisture variability is significant between the points of observation. This has significance for field studies, when lumped model outputs are compared with observed point measurements, as such sites would be used to represent the catchment-wide soil moisture average. Furthermore, the identification of such sites would reduce the number of required soil moisture monitoring stations within a catchment, and therefore the financial costs involved in instrumentation of a catchment. While Grayson and Western (1998) concluded that catchment average soil moisture monitoring (CASMM) sites must exist within a catchment, it remains difficult to a priori determine their exact location.

A way to estimate sampling errors when using point measurements and satellite based instruments together has been developed by Yoo (2001), finding that in-situ measurements are ineffective on larger scales, where spacing between the soil moisture sensors becomes too large to adequately capture the spatial variability of soil moisture and consequently the observational error. In his work, Yoo (2001) found that the threshold for the experimental catchment used in his study was at about 100-200m spacing between the stations. Thus, it was suggested to use ground-based techniques only for small-scale observations, of less than basin-scale.

2.2.2 Remote Sensing in Hydrology

Remote sensing is defined in this thesis as the measurement of a certain quantity of emitted or reflected electromagnetic energy from a location other than the point of observation, specifically measured by instruments operated on air- and space-borne platforms. Thus, this definition includes all observable wavelengths from X-ray to radio bands.

An exemption to this definition is the Gravity Recovery and Climate Experiment (GRACE) satellite. In the case of GRACE, its two satellites fly in a tandem formation and make use of their capability to detect changes in the gravitational field of the Earth (Rodell and Famiglietti, 2001). With this new type of remote sensing the long-term changes in the total regional water storage can now be quantified. Nevertheless, the temporal resolution of GRACE data is in the order of 4 weeks and therefore cannot detect short term dynamics, which are occurring during and after rainfall events. Moreover, the spatial resolution is ~1000km, which is not sufficient for hydrologic land surface modelling as an input to climate modelling. Since short term dynamics are important for hydrologic and climate modelling, observations from GRACE are therefore not considered in this thesis. Furthermore, GRACE provides the integrated soil moisture throughout the soil. It is not possible to distinguish between surface and root zone soil moisture, or groundwater. However, adequate information about these quantities are required to properly model heat and water fluxes between the land surface and the atmosphere.

Some environmental variables measured in the different wavelengths include vegetation cover and type in the visible and infrared bands (eg. Askne et al., 2003; Cohen et al., 2003; Wen and Su, 2004); cloud cover in the visible band (eg. Berendes et al., 2003); thermal surface information with infrared and near-infrared bands (eg. French et al., 2005); surface soil moisture content with microwave bands (eg. Njoku and Enthekabi, 1996; Zribi et al., 2003; Walker et al., 2004b); and rainfall intensity with radar (eg. Sorooshian et al., 2002). While infrared has been shown to be useful for the observation of hydric stress or for disaggregation purposes of low resolution microwave observations (Merlin et al., 2005), it only provides information on the soil skin, whereas microwave observations are obtained for the soil surface layer of up to several centimetres (Jackson et al., 1981). Because of this better observation depth, microwave observations are considered in this thesis.

The last 25 years have seen an intensifying research into the use of remotely sensed data for soil moisture measurement and its application in hydrologic modelling (see Schmugge et al., 2002 for a detailed review). Work has also been undertaken to retrieve soil moisture information from visible and thermal observations (Su et al., 2002), however this review will focus on the application of microwave remote sensing to observe surface soil moisture. While the work by Su et al. (2002) determines the soil moisture deficit through the observation of evapotranspiration and the subsequently derived drought index, microwave remote sensing is a more direct observation of soil moisture. The microwave signal is directly related to the dielectric constant in the soil (Jackson et al., 1981), rather than the modelled response of vegetation to changes in the soil moisture store, which limits the assumptions made to derive the soil moisture product.

The large contrast between land and water surface emissions in the microwave band makes microwave bands the ideal frequency range for soil moisture remote sensing (Schmugge et al., 2002). Moreover, earlier research has shown a high sensitivity of microwave measurements to changes in the soil moisture conditions (eg. Schmugge et al., 1974; Jackson et al., 1981), when compared to observations in other bands, such as visible or thermal. Another advantage of observing emissions in the microwave band over other bands is that atmospheric conditions (eg. caused by clouds or aerosols) do not show a significant influence on the observed signal (Uitdewilligen et al., 2003) and are therefore negligible.

Microwave remote sensing is distinguished into two different types: i) passive (eg. Njoku and Entekhabi, 1996; Owe et al., 2001) and ii) active (eg. Du et al., 2000; Magagi and Kerr, 1997; Walker et al., 2004b). In passive microwave remote sensing, electromagnetic waves naturally emitted from the Earth's surface are measured, while in active microwave remote sensing emissions are sent out by the instrument and the returned signal from the Earth's surface is measured and related to the soil moisture content. Both active and passive microwave remote sensing have shown a good correlation with soil moisture (Engman and Chauhan, 1995). The resolution of active microwave remote sensing is generally several magnitudes higher than the resolution of passive microwave remote sensing (tens of metres against tens of kilometres). However, active microwave remote sensing of soil moisture is also very sensitive to local soil roughness changes (Moran et al., 1998; Walker et al., 2004b) and more importantly, the satellite overpass repeat rate of active instruments is significantly lower than for active instruments (eg. 35 days for the instrument on ERS-2, against 2 or 3 days for passive instruments). Due to these limitations of active microwave remote sensing and the availability of data from the Advanced Microwave Scanning Radiometer for the Earth Observing System (AMSR-E; Njoku et al., 2003) – which are obtained in the passive mode – the following discussion focuses on passive microwave remote sensing.

Surface soil moisture remote sensing is an indirect technique, obtained by observing the horizontally and vertically polarised brightness temperatures (Owe et al., 2001). Generally, this has been in C-band (~4 to 7GHz), due to a lack of instruments operating in L-band (~1 to 4GHz). While most instruments provide data from several bands, such as the Scanning Multichannel Microwave Radiometer (SMMR; Gloersen and Barath, 1977) and AMSR-E, the C-band measurements are used due to the lower impact of atmospheric water content on the signal, its better observation depth, and the reduced effect of surface roughness compared with other frequencies (Wigneron et al., 1995). Factors such as terrain slope and vegetation cover interfere with satellite measurements (Jackson et al., 1982), which is less significant in passive than in active microwave remote sensing, as the scattering effect from the land surface has a lesser influence in the coarser resolution of the passive observations.

The soil microwave emission observed is defined as the brightness temperature (T_b) in Kelvin. Over a smooth and bare surface, this is expressed through (Ulaby et al., 1986)

$$T_{b,p} = e_{s,p} T_s , \qquad (2.1)$$

where $e_{s,p}$ is the smooth surface emissivity of the surface layer at polarisation p (horizontal or vertical); and T_s is the effective temperature of the surface layer [K]. The emissivity $e_{s,p}$ may be further written as

$$e_{s,p} = 1 - R_{s,p}, \tag{2.2}$$

where $R_{s,p}$ is the bare surface reflectivity at polarisation p. While all soil layers contribute to the soil microwave emission, the contribution of the deeper soil layers decreases as a function of the soil depth. The depth of this contributing layer is referred to as the skin depth or observation depth, which is generally defined as 1/10 to 1/4 of the observation wavelength of the respective channel (Jackson et al., 1981; Owe et al., 2001). $R_{s,p}$ is expressed through the Fresnel equations for smooth surfaces

$$R_{s,h} = \left| \frac{\cos\theta - \sqrt{\varepsilon - \sin^2\theta}}{\cos\theta + \sqrt{\varepsilon - \sin^2\theta}} \right|^2 \tag{2.3}$$

and

$$R_{s,v} = \left| \frac{\varepsilon\cos\theta - \sqrt{\varepsilon - \sin^2\theta}}{\varepsilon\cos\theta + \sqrt{\varepsilon - \sin^2\theta}} \right|^2, \tag{2.4}$$

where subscripts h and v represent the horizontal and vertical polarisation, respectively; θ is the incidence angle from nadir (deg); and ε is the complex dielectric constant, which is the sum of its real and imaginary components.

Surface roughness and vegetation affect the signal and reduce the sensitivity of the emission to soil moisture conditions (Jackson et al., 1982). The emissivity of a rough bare surface ($e_{r,p}$) is defined as (Choudhury et al., 1979)

$$e_{r,p} = 1 - R_{s,p}\exp(-h\cos^2\theta), \tag{2.5}$$

or when substituting eq. (2.2) into eq. (2.5)

$$e_{r,p} = 1 - \left(1 - e_{s,p}\right)\exp(-h\cos^2\theta), \tag{2.6}$$

where h is an empirical measure of the surface roughness, depending on the surface conditions. Choudhury et al. (1979) and Wang et al. (1983) found typical values for the surface roughness ranging from 0.1 (grasslands and wheat) to 0.5 (recently tilled fields).

The vegetation effects on the emission are quantified using the τ-ω approach, which takes into account the optical penetration depth (τ) of the signal through, and the scattering (ω) of emitted waves within the vegetation. The vegetation transmissivity Γ is described with (Mo et al., 1982)

$$\Gamma = \exp\left(\frac{-\tau}{\cos\theta}\right). \qquad (2.7)$$

This expression allows the influence of vegetation to be taken into account, and Mo et al. (1982) expressed the brightness temperature from a vegetated rough surface as

$$T_b = T_s e_r \Gamma + (1-\omega) T_c (1-\Gamma) + (1-e_r)(1-\omega) T_c (1-\Gamma)\Gamma, \qquad (2.8)$$

where T_c is the canopy temperature [K]. Eq. (2.7) and (2.8) show that with increasing vegetation cover the emission from the soil surface is increasingly masked and additionally the emitted microwave signal from the vegetation is increased.

Recent work (Saleh et al., 2006) has shown that the total optical depth is not only a function of the optical depth caused by standing vegetation, but is also increased by litter and rainfall interception. Consequently, Wigneron et al. (2007) adjusted their radiative transfer model to allow for a more detailed definition of τ as

$$\tau_p = \tau_{sp} + \tau_l + \tau_{ip}, \qquad (2.9)$$

where the subscript p represents the vertical or horizontal polarisation; s is the index for standing vegetation; l stands for litter; and i for interception water. While τ_{sp} was previously a linear function of the vegetation water content (VWC), Wigneron et al.

(2007) adjusted this, so that τ_{sp} is now a function of the leaf area index (LAI), while τ_l and τ_{ip} are functions of the litter water content (LWC) and the interception reservoir, respectively. Nevertheless, water interception and litter water content are not readily observable and have to be estimated using empirically derived equations. This example shows that the retrieval process of soil moisture from remote sensing introduces a high level of uncertainty.

Past and current missions of microwave remote sensing for soil moisture retrieval include i) short-term airborne experiments and ii) satellite-based missions. Airborne experiments include the Electronically Steered Thin Arrary Radiometer (ESTAR) measurements during the Southern Great Plains experiment (SGP97; Jackson et al., 1999; Guha et al., 2003), the AirSar missions (Western et al., 2004), the Soil Moisture Experiments in 2002 (SMEX02; Njoku et al., 2004), and the recent National Airborne Field Experiment (NAFE'05; Walker et al., 2005). Satellite-based instruments include the European Remote Sensing (ERS) satellites (Wagner et al., 1999), NASA's SMMR (Gloersen and Barath, 1977) and AMSR-E (Njoku et al., 2003), and ESA's future Soil Moisture and Ocean Salinity mission (SMOS; Kerr et al., 2001). While SMMR and AMSR-E data is available for bands at and above 6.6GHz, SMOS will be the first space-borne L-band mission, scheduled for launch in early 2008 (Y. Kerr, personal communication).

It is important to note that airborne and satellite instruments have significantly different resolutions, with airborne instruments typically having a higher resolution. The resolution of microwave bands, as observed from space, is often in the order of several kilometres and can therefore cover a large area in a short time (Njoku et al., 2003), whereas instruments with higher resolutions take longer for global coverage.

Geophysical properties, land form and vegetation have an impact on the satellite data. The presence of large forested areas within a satellite footprint – which normally represents the averaged brightness temperature of the observed area from which soil moisture information is retrieved – leads to inaccurate interpretation of the satellite observations (Jackson et al., 1982; Owe et al., 2001), as the vegetation cover masks the soil moisture signal. Moreover, the impact of radio-frequency interference (RFI) on the microwave signal has been gradually increasing over the last 20 years. This impact was first observed in SMMR data over northern Spain in the early 1980s (R. de Jeu, personal communication). This effect is also observable in the current AMSR-E products, as television relay and auxiliary broadcasting, and radar use other than for navigation (eg. rainfall radars) are close to the channels used by AMSR-E (Li et al., 2004; Njoku et al., 2005). It was shown that RFI results in a bias of up to 7K in the observed brightness temperature of the 6.9GHz band. As a consequence, the current AMSR-E retrieval algorithm for soil moisture is based on the 10.7GHz observations (Njoku et al., 2003). This results in a soil moisture product which is based on observations with only a few millimetres of observations depth and significant effects due to vegetation cover.

Remote sensing instruments operating with active microwave sensors, while providing higher resolutions, suffer from surface roughness, presence of surface vegetation and topographic conditions, due to the increased sensitivity to these surface conditions (Ulaby et al., 1978). Therefore, the future SMOS mission operating in the protected band at 1.4GHz is expected to provide soil moisture products, with a significantly lower impact from vegetation, roughness and RFI. The reasons for these reduced influences are that L-band is less affected by vegetation, due to the longer wavelength as compared to C-band, surface roughness effects should be reduced, and L-band is internationally protected for space and earth exploration missions. In particular, the latter results in a spectral distance to wireless communication emissions, which should allow for lower background noise in the signal.

2.2.3 Hydrologic Land Surface Models

An alternate means to the measurement of soil moisture is hydrologic land surface modelling, which relies upon atmospheric forcing data, such as precipitation, temperature and incoming radiation, to drive the model. A hydrologic land surface model (LSM) simulates the physical conditions of the modelled area and produces a model output by using more or less complex water balance models (Pitman, 2003). Fig. 2.1 presents a schematic of an LSM.

Hydrologic land surface models exist in varying complexities, from simple spatially averaged (or lumped) rainfall-runoff models with one soil layer to complex distributed models with multiple soil layers. Generally, hydrologic land surface models are forced with atmospheric observations (precipitation, air temperature, vapour pressure, and incoming radiation), which are used to drive the physical processes in the soil and vegetation, and provide predictions of energy and water fluxes. In LSMs, precipitation water is partitioned into infiltration and runoff components, governed by two different physical processes: i) saturation excess runoff and ii) infiltration excess runoff. Over saturated areas, the precipitated water is directly transferred into surface runoff, because the saturated state of the soil prevents more water from infiltrating into the soil (Dunne and Black, 1970). Conversely, precipitated water over unsaturated soils is infiltrated into the soil at the rate of the infiltration capacity of the soil, which may change with the soil moisture conditions (Richards, 1931). Any water in excess of the

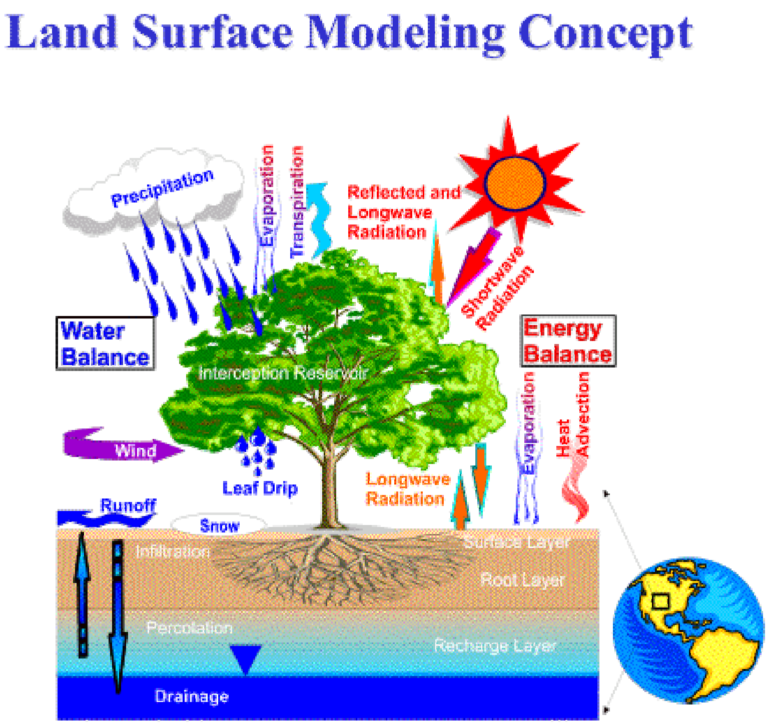

Figure 2.1. Schematic of a land surface model (from NASA's Land Information Systems (LIS) homepage; www.lis.gsfc.nasa.gov).

infiltration rate is either transferred into surface runoff (Horton, 1933, 1940) or remains ponding on the surface until it is infiltrated or evaporated. The infiltrated water percolates through the soil, increasing the soil moisture content and affecting bare soil evaporation and vegetation transpiration, and consequently the energy and water budget between the soil and the atmosphere.

The information on the energy and water budget from the LSMs is then used to provide atmospheric General Circulation Models (GCMs) with information about the boundary layer between the soil surface and the atmosphere. This feedback has been shown in several studies to impact on the performance of GCMs (Koster et al., 2000a, 2003, 2004; Douville, 2003), and in particular on the predictability of air temperature and precipitation. However, the LSMs used are not perfect and are merely representations of natural processes, containing errors in their results due to errors in the forcing data (Berg et al., 2003; Mahanama and Koster, 2005) and model parameters (Boulet et al., 1999), and simplifications in the model physics. This was further highlighted by Ajami et al. (2004) and Hogue et al. (2006). In their respective studies, they have shown that varying the parameter sets of sub-catchments in a semi-distributed model does not result in a significant improvement of the model predictions, while a more detailed distribution of the model forcing data in their studies led to an improvement. Consequently, Hogue et al. (2006) concluded that no "perfect" model exists.

2.3 Data Assimilation

To reduce the level of uncertainty in model predictions, observed data may be used to update the model states through the process of data assimilation. This process brings the predictions closer to the observations using knowledge about observational and model errors. The field of data assimilation is divided into two major approaches: i) sequential data assimilation and ii) variational data assimilation. The terminology of data assimilation is similar for both approaches. The change of an initial model state is called an "update", which is generally achieved through an "analysis" of the model (or "background") state by reducing the difference between predictions and observations, based on different statistical methods. From the model state, the model predicts or "forecasts" the model trajectory through time.

Sequential data assimilation updates the state of a variable at one point in time using an error estimate derived from the previous data to better resemble an observed value (Fig. 2.2a). Variational data assimilation uses available data to find an optimal value for the initial states of a model, so that predicted values best fit the observed values within a defined period known as an assimilation window (Fig. 2.2b).

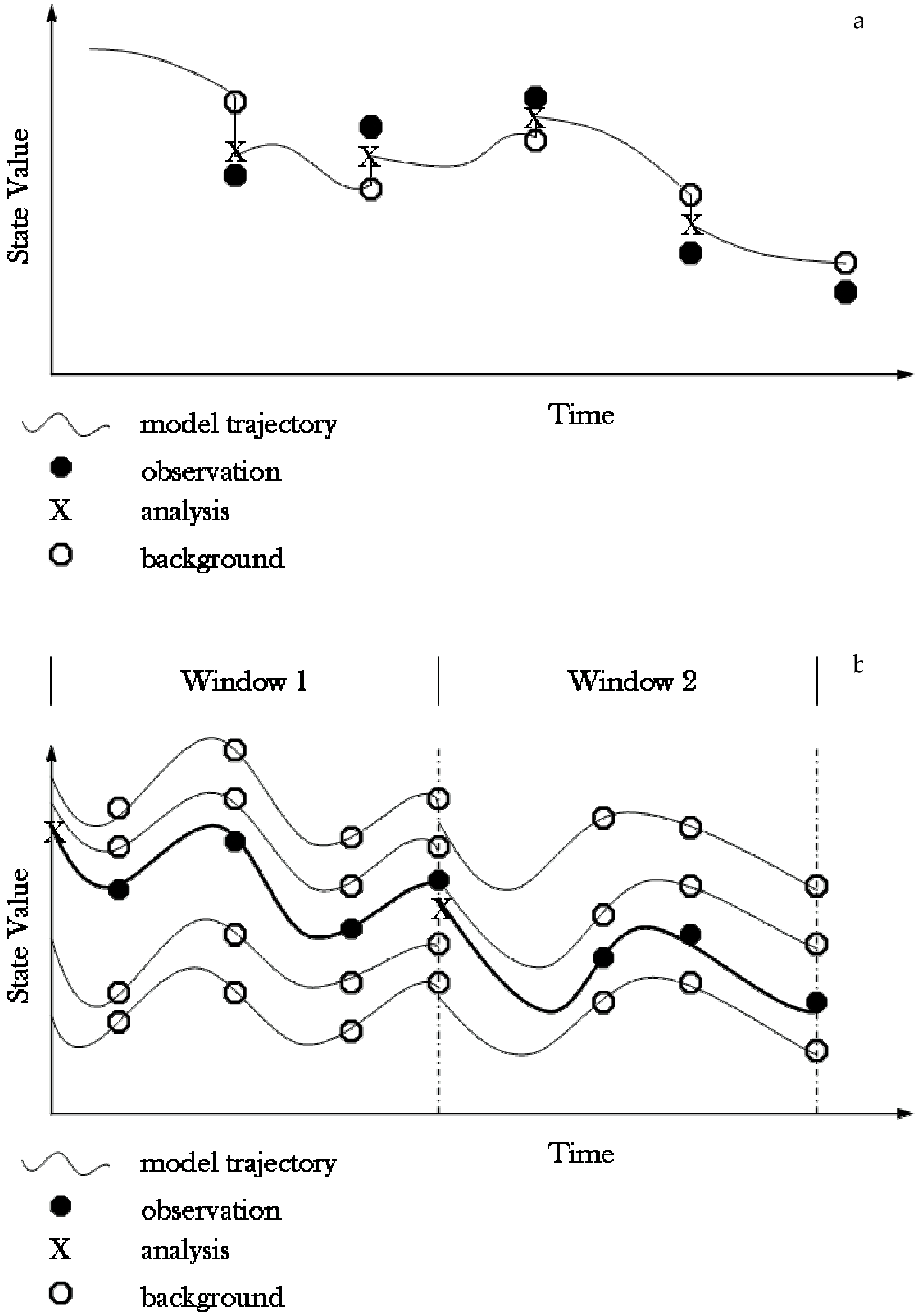

Figure 2.2. Schematic of a) sequential, and b) variational data assimilation (after Walker and Houser, 2005).

2.3.1 Sequential Data Assimilation

In sequential data assimilation, the model states **X** are analysed and updated each time new observations **Z** become available. The Kalman Filter (Kalman, 1960) is the most widely known sequential data assimilation technique, using both forecast and update steps.

This means that the model predicts a certain observation value $\hat{\mathbf{Z}}$ (say streamflow discharge) up to a point in time when an observed value $\mathbf{Z}$ (e.g. from a gauging station) is known. This knowledge is then used to analyse the background state by

$$\mathbf{X}_k^a = \mathbf{X}_k^b + \mathbf{K}\left(\mathbf{Z}_k - \hat{\mathbf{Z}}_k\right), \qquad (2.10)$$

where the superscripts a and b refer to the analysed and background state values respectively; k is the time step of the update; $\left(\mathbf{Z}_k - \hat{\mathbf{Z}}_k\right)$ is the innovation vector; and $\mathbf{K}$ is the gain function given by

$$\mathbf{K} = \mathbf{B}\mathbf{H}^T\left(\mathbf{H}\mathbf{B}\mathbf{H}^T + \mathbf{R}\right)^{-1}, \qquad (2.11)$$

where $\mathbf{B}$ and $\mathbf{R}$ are the background and observation error covariance matrices respectively; and $\mathbf{H}$ is the observation operator matrix. The gain describes the relative uncertainty in prediction and observation variances and ranges from 0 to 1, given the special case where $\mathbf{X}$ and $\mathbf{Z}$ are in the same space. A gain value of 0 then represents no confidence in the observation while a value of 1 represents no confidence in the predictions.

In addition to the model state, the Kalman filter is also used to update the model error covariance matrix by

$$\mathbf{B}^a = \left(\mathbf{I} - \mathbf{K}\mathbf{H}\right)\mathbf{B}^b\left(\mathbf{I} - \mathbf{K}\mathbf{H}\right)^T + \mathbf{K}\mathbf{R}\mathbf{K}^T, \qquad (2.12)$$

where $\mathbf{I}$ is the identity matrix. The updated values are then propagated by the model until the next update step by adding an error term $\mathbf{Q}$ to the model error covariance forecast

$$\mathbf{B}_{k+1}^b = \mathbf{M}_k\mathbf{B}_k^a\mathbf{M}_k^T + \mathbf{Q}_k, \qquad (2.13)$$

where $\mathbf{M}_k$ is the model operator matrix.

The key assumptions of the Kalman Filter are that the error terms are uncorrelated and have a Gaussian distribution. Moreover, the original Kalman Filter requires models to be linearised, which significantly limits its application in hydrologic and climate modelling, due to the inherent non-linearity of natural processes. Consequently, the Kalman Filter underwent further development (Extended Kalman Filter (eg. Gelb, 1974); Ensemble Kalman Filter (Evensen, 1994); see Reichle et al. (2002a) for a comparison study of Extended and Ensemble Kalman Filter). While the model operator remains linearised in the Extended Kalman Filter, the Ensemble Kalman Filter uses the information of an ensemble of model simulations to determine the background error covariance matrix. The Ensemble Kalman Filter therefore has two advantages over the Extended Kalman Filter: i) it does not require the linearization of the model, and ii) it provides a better understanding of the model background error, through the spread of the ensemble of the model predictions.

In terms of computational costs, the Kalman Filter becomes expensive for large problems. In particular, the inversion of the large covariance matrices in order to determine the gain function poses a significant problem (Walker et al., 2001). Numerous studies exist which deal with variations of the Kalman Filter. The difference of these studies is generally the calculation of **K**, or rather **Q** within **K**, which can be difficult to achieve. In particular, the background error term **Q** included in the calculation of **K** often poses a problem. Consequently, **K** is often only approximated (Walker and Houser, 2005), for example by assuming constant background errors.

2.3.2 Variational Data Assimilation

In contrast to the sequential data assimilation techniques, variational data assimilation techniques use assimilation windows (generally of fixed length), which contain a number of observations, and update the model states at the beginning of the assimilation window so that the predictions show a best fit with the observations across that time period. New assimilation windows begin after the last time step of the previous window. The best fit between observations and model predictions is achieved by minimising the cost or objective function J

$$J = \frac{1}{2}\left(\mathbf{X}_0 - \mathbf{X}_0^b\right)^T \mathbf{B}_0^{b-1}\left(\mathbf{X}_0 - \mathbf{X}_0^b\right) + \frac{1}{2}\sum_{k=0}^{n-1}\left(\mathbf{Z}_k - \hat{\mathbf{Z}}_k\right)^T \mathbf{R}_k^{-1}\left(\mathbf{Z}_k - \hat{\mathbf{Z}}_k\right), \tag{2.14}$$

where the initial state vector after and before he analysis is expressed with $\mathbf{X}_0$ and $\mathbf{X}_0^b$, respectively; $\mathbf{B}_0^b$ is the background error covariance matrix; $\mathbf{Z}_k$ and $\hat{\mathbf{Z}}_k$ are the observation and the model predicted observation at time step k of n time steps, respectively; and $\mathbf{R}_k$ is the observation error covariance matrix.

The cost function J can be minimised using different approaches, through the use of adjoints (Talagrand and Courtier, 1987) or the simplification of the observation operator matrix (Balsamo et al., 2004; Zhan et al., 2006). The derivation of an adjoint (which is essentially an operator that allows to propagate information back in time through the model space) to determine the sensitivity of a model to changes in its initial states has the distinct advantage that it requires only one forward and one backward run. An adjoint allows the determination of the influence of changes of the state equations on the objective function. The initial conditions of the catchment will be used as variables within the adjoint equation to determine the propagation of certain information backwards in time through the model. A forward equation is then used to determine the state estimate (Reichle et al., 2001a).

The development of the adjoint is a difficult process (Reichle et al., 2002a) and has to be derived anew after every change to the model. To counter the requirement to derive adjoints of the model, Balsamo et al. (2004) developed a simplified 2-dimensional variational data assimilation technique, which allows to determine the sensitivity of the model for each observation within the assimilation window. Balsamo et al. (2004) assumed that the observation operator matrix **H** in eq. (2.11) can be linearised by

$$\mathbf{H}^T = \begin{pmatrix} \dfrac{\delta \hat{\mathbf{Z}}_1}{\delta \mathbf{X}_0} \\ \vdots \\ \dfrac{\delta \hat{\mathbf{Z}}_{n-1}}{\delta \mathbf{X}_0} \end{pmatrix}. \tag{2.15}$$

Through this approach the changes to the model prediction at any given time, based on a change in the initial state, are calculated. This allows the sensitivity of the model to be determined by brute-force, requiring n+1 model runs, where n is the number of model states. Moreover, the main assumption of this approach is that the changes of the model prediction behave linearly in relation to the perturbation of the initial model states. While the assumption of a linear behaviour of the model is more limiting than for the derivation of the sensitivity through an adjoint, it has the advantage of simplicity.

Other schemes that fall under the definition of variational data assimilation as given in this thesis are, iterative brute-force optimisation approaches, as they simply reduce the least square cost function

$$J = \left(\mathbf{Z}_k - \hat{\mathbf{Z}}_k\right)^2 \tag{2.16}$$

by determining the initial value that propagates the model trajectory to best fit the observations, without taking into account background or observation errors (Calvet and Noilhan, 2000). Such methods find the best fit of model and observations by changing the initial states iteratively. Moreover, the observation and prediction vectors of the expression $\left(\mathbf{Z}_k - \hat{\mathbf{Z}}_k\right)$ may be replaced within this simple brute force cost function with skill or cost functions, such as the Nash criteria (Nash and Sutcliffe, 1970), which is widely used in streamflow modelling to assess the quality of streamflow predictions. However, this would not allow the further evolution of this simple cost function to the traditional variational assimilation scheme with the inclusion of observational and model errors. For such formulations, the Nash criteria can only be used as a qualitative description of the results of assimilation run, but it cannot be used within the objective function.

2.4 Data Assimilation in Hydrology

A large number of studies have been published, especially in the recent years, which are concerned with the assimilation of data to improve soil moisture. The literature research showed that data assimilation is a widely known and extensively used tool in streamflow assimilation for streamflow forecasting and soil moisture assimilation for soil moisture updating, however the possibility to utilise the water balance of a hydrologic model to initialise initial soil moisture states through streamflow data assimilation has mostly been neglected.

While generally successful, the majority of the studies in data assimilation in hydrology have focussed on the assimilation of ground-based (Heathman et al., 2003) and remotely sensed (Walker and Houser, 2001, Crosson et al., 2002; Reichle et al., 2002ab; Walker et al., 2002; Montaldo and Albertson, 2003) surface soil moisture observations to improve root zone soil moisture predictions or streamflow predictions (Jackson et al., 1981; Pauwels et al., 2001). Other studies dealt with the assimilation of streamflow data for improving streamflow predictions (Georgakakos and Bras, 1982; Georgakakos and Smith, 1990; Awwad et al., 1994; Madsen and

Skotner, 2005). Streamflow data assimilation has only recently been considered as a tool for soil moisture initialisation (Aubert et al., 2003; Pauwels and de Lannoy, 2006). Finally, Mahfouf et al. (1991) and Balsamo et al. (2004) assimilated screen level variables (air temperature and relative humidity at 2m) into their SVAT models to retrieve root zone soil moisture. However, this assimilation technique requires a functional land surface-atmosphere interchange of the water and heat fluxes, which can introduce further errors into the retrieval process.

The applicability of remotely sensed soil moisture data for streamflow prediction was shown early by Jackson et al. (1981). Their research comprised the use of a hydrologic land surface model using different data sources (precipitation and/or remotely sensed soil moisture) for their observations. The data assimilation technique was to simply replace simulated soil moisture values with measured values as soon as they became available. Jackson et al. (1981) were able to show the importance of soil moisture updating for hydrologic land surface modelling and concluded that "periodic measurements of areal soil moisture […] could be used to correct soil moisture simulation errors caused by other factors and to improve runoff estimates" (Jackson et al., 1981, p. 317). Even though it was acknowledged in the same paper that streamflow data was often the only observation data available, it was not suggested to use this available streamflow data for soil moisture correction within the model. While Jackson et al. (1981) assimilated the data as it was, Pauwels et al. (2001) stated that the importance of spatial distribution of soil moisture to improve streamflow was not examined in earlier papers.

Reichle et al. (2002a) assimilated synthetic L-band (1.4 GHz) radiobrightness data into a hydrologic land surface model using the

Ensemble Kalman filter (EnKF) and tested its performance compared to a simulation of near-surface soil moisture without applying any data assimilation. It was found that the EnKF performed well and reduced the error in soil moisture by up to 80%, depending on the number of ensembles used. While the application of soil moisture data assimilation was merely for a one-dimensional model, Walker et al. (2002) modified the Kalman filter for its use in a three-dimensional application. In their study, they simplified the covariance forecasting approach and used the assimilated near surface soil moisture data to update the vertical soil moisture profile.

As mentioned in section 2.2.2, soil moisture observations from space are limited to areas with low-to-moderate vegetation, due to the masking effect of the soil moisture signal through the vegetation cover. Consequently, the studies presented so far are only applicable for such areas. Thus, the assimilation of remotely sensed surface soil moisture cannot be applied to large forested regions such as the Amazon or south-east Asia. However, it was shown particularly for these regions that an improvement of soil moisture would significantly increase the potential predictability of precipitation (Koster et al., 2004). As Jackson et al. (1981) stated, streamflow is often the only observed quantity available for a catchment, the potential of using this observations to initialise soil moisture has to be considered.

In Georgakakos and Bras (1982) the authors developed a linearised flood routing scheme in order to accommodate the mostly linear forecasting techniques. The focus of their research was on the updating of streamflow data within hydrologic land surface models using the simulated soil moisture data to determine the influx into the reservoirs – thus assuming the model as being correct – and observed streamflow data. The potential of streamflow data to be used as a means to update the soil moisture states within the model was neglected. Georgakakos and Smith (1990) used the Extended Kalman Filter to improve real-time streamflow forecasting from a rainfall-runoff model. However, rather than updating the soil moisture in the model, they improved the model parameters responsible for flow-routing in the hydrologic and routing segments of the model and their results were only compared against streamflow observations from two catchments, neglecting any discussion on the soil moisture conditions. Awwad et al. (1994) used a Kalman filter for streamflow updating while simultaneously updating the catchment parameters and background noise of their rainfall-runoff model with other filters. In their study, only precipitation and streamflow were observed, soil moisture was only simulated. As in Georgakakos and Bras (1982), the soil moisture product was then only used within the model to influence runoff production from the catchments. Even though the potential of parallel updating techniques were available, they were not used together.

Other studies, which included the possibility to retrieve soil moisture states from streamflow data assimilation, are those of Crow et al. (2003) and Seo et al. (2003). In their study, Crow et al. (2003) assimilated streamflow and surface soil moisture in order to calibrate model parameters, rather than finding the correct initial soil moisture states. Finally, Seo et al. (2003) derived an adjoint to retrieve the soil moisture initial states for three independent catchments in the United States to forecast streamflow. They found that a variational data assimilation approach is a good tool for such an inverse problem and presents an advantage over sequential data assimilation techniques. However, Seo et al. (2003) did not have any field observations to validate their retrieved initial soil moisture states and only assessed the model performance in terms of the accuracy of the streamflow predictions.

The weakness of the presented studies is that they solely focussed on the model performance for streamflow forecasting. In all studies, soil moisture states were accepted as modelled by the LSMs without any further validation of their accuracy. Moreover, most studies only updated parameters or states, which were part of the runoff routing processes. There are only two papers, which have recognised the limitation of these studies to simple streamflow forecasting. In these papers, soil moisture as well as streamflow data have been jointly assimilated to update their respective states in order to improve the hydrologic land surface model output of streamflow prediction.

In the first paper, Aubert et al. (2003) used the information obtained from their field measurements to update a) the soil moisture states within the hydrological model with soil moisture data and b) modelled streamflow output with streamflow data, treating both variables as two parallel but independent states. However, this paper has several shortcomings. First, the updating of the soil moisture states was done for the time step of the observations. As streamflow is the product of a combination of precipitation and soil moisture preceding the time of observation of streamflow, an updating of soil moisture at the same time as the streamflow observation can only have an effect on future streamflow conditions. Consequently, the forecasting of the streamflow events was improved. Second, the paper focussed only on the improvement of the streamflow events and failed to show an improvement in the soil moisture predictions of the model. Finally, the study was undertaken for a period over which the model was calibrated, which already showed good results for streamflow, with only two weeks of open-loop simulations.

Aubert et al. (2003) used the extended Kalman Filter, which only updates the state variables at the previous time step. This conflicts with streamflow being influenced by the soil moisture conditions over a longer period (Seo et al., 2003). This problem was recognised by Pauwels and de Lannoy (2006). In their study, they used the retrospective Ensemble Kalman Filter (REnKF), which augments the state vector $\mathbf{X}_k$ to include not only the model states at time k, but also the soil moisture states of several time steps before time k, so that all model states at time k-1 to k-(n_c+n_y-1) are included. In this case, n_c is the time of concentration and n_y is the time of observation. The model is then required to be rerun for the time window n_c+n_y-1, with the new initial conditions. However, this is not practical when the time of concentration in the catchment is large, and a large number of soil moisture states have to be simultaneously updated (Seo et al., 2003). The reason is that cross-covariance matrices would have to be determined for each model state in each catchment over the whole time of concentration. Thus, this approach would become infeasible. Consequently, Pauwels and de Lannoy (2006) applied their assimilation scheme only to a single, small catchment with a relatively small time of concentration in a synthetic twin experiment with real meteorological forcing and streamflow observations. However, soil moisture observations were not available to verify the model performance.

2.5 *Proposed Approach*

Despite the demonstrated importance of soil moisture for hydrological modelling, land surface–atmosphere interactions, weather forecasting and so on, there is no working soil moisture prediction system in place, in particular for areas of dense vegetation. Thus, research into the correct initialisation of soil moisture is of a high priority.

Although much work has been undertaken to improve soil moisture and streamflow predictions, the majority of the studies are limited to surface soil moisture assimilation. Moreover, this approach cannot be applied globally, due to the technical constraints in the observation technique (dense vegetation cover masking the soil moisture signal). While other studies have recognised that streamflow observations are often available and can be used to constrain model predictions, the focus of these studies has been on the improvement of the streamflow predictions themselves, rather than the soil moisture states. Only two studies have recognised that streamflow observations may be used to update soil moisture states. However, both have applied Kalman Filter-type assimilation techniques, which are infeasible for large catchment networks.

To address the shortcomings identified in global soil moisture estimation, a data assimilation scheme is proposed that assimilates streamflow observations to update soil moisture states. Streamflow observations are used as they are an integrator of precipitation response to upstream soil moisture status and are independent of the vegetation cover in the catchment. Because of the time-delay response of catchment runoff to precipitation, a variational assimilation approach is pursued, with an assimilation window that is equal or larger than the time of concentration of the catchment.

The proposed approach consists of several steps. First, a hydrologic land surface model is spun-up in an initialisation phase, Then, streamflow observations are obtained which are required for the assimilation into the LSM. Third, streamflow observations are assimilated into the model to update the initial soil moisture states of the model. These three steps are the general overview of an operational system. For the development and evaluation of the proposed assimilation scheme, different synthetic studies are undertaken to study the assimilation scheme under different forcing and parameter scenarios, and eventually in a real study, where the soil moisture predictions are compared with in-situ soil moisture observations from the catchment. These four steps are presented in the following sections in more detail.

2.5.1 Model Initialisation Phase

To initialise a hydrologic land surface model, a number of different techniques area available. The most widely used techniques are the spin-up of the LSM, and the use of the field capacity (after extensive rain periods) (Ragab, 1995) or residual water content (after extensive dry periods) (Walker, 1999). While the spin-up is based on the hydraulic equilibrium of the model after several years of spin-up (Jackson, 1980), the initialisation of the model with soil moisture at field capacity or residual water content requires some knowledge of the antecedent weather conditions. For the hydrologic land surface model of this thesis, it was decided to spin up the model over ten years. Because of the limited amount of years with observations, the model had to be spun up repeatedly over a certain period, in order to obtain stable conditions throughout the catchment (eg. the soil moisture content and the heat and water fluxes have to be in equilibrium; ie. the fluxes physically correspond to the forcing data and the environmental conditions, without causing inconsistencies between surface conditions, such as soil temperatures and moisture, and the energy and water fluxes to the atmosphere).

2.5.2 Observational Data

Observational data is required for the assimilation and verification of the model and the assimilation scheme. The observation data obtained included streamflow observations for the assimilation and root zone soil moisture observations for the verification, at different locations throughout the catchment.

2.5.3 Prediction and Assimilation Phase

The last initialisation data from the spin-up period are used to initialise the prediction run of the model. This prediction run provides estimates of the streamflow from the catchment. Furthermore, the model predicts soil moisture changes, and heat and water fluxes in the catchment. The model is forced with the same atmospheric forcing data as used during the spin-up period. Since forcing data contains errors, even well parameterised models will contain errors in their predictions.

To improve such erroneous model predictions, a variational data assimilation scheme is applied to improve the model initial states. The assimilated streamflow observations are compared against the predictions, in order to determine the error of the predictions in relation to the observations. The model initial states are then updated to reduce this error. The model is then run forward with the new initial states, to obtain improved predictions. This process is repeated until the best combination of initial states is found.

2.5.4 System Development and Testing

The soil moisture prediction system presented in this thesis was developed through four major studies, in order to determine:

i) the general applicability of streamflow data assimilation for soil moisture predictions,

ii) an optimal assimilation window length,

iii) the identification of the impact of errors in forcing data and parameters on the retrieval process, and possible solutions to the problems,

iv) the applicability of the proposed approach to nested catchments with only a limited number of point of observations,

v) the possibility of a joint assimilation of streamflow and remotely sensed surface soil moisture assimilation.

During the different studies of this thesis, the size of the catchment structure is gradually expanded. First, runs with a simple model set up (one catchment, no routing) are undertaken with synthetic data. The use of synthetic data provides a tool to verify the accuracy of the model and its performance, as the results should be "perfect", meaning that the predicted results should be the same as the results given by the simulation with synthetic data. Then, the assimilation scheme is tested in further synthetic studies for one- and multi-catchment scenarios to study the approach under different scales. These studies include experiments with errors introduced to the forcing data and model parameters, in order to gain an understanding of the effects of such errors on the retrieval accuracy. Finally, the proposed soil moisture prediction system is tested in a field data study, using real observations.

Additional data is assimilated in this thesis in the form of remotely sensed surface soil moisture observations. These observations originate from open-loop simulations for the synthetic studies and real satellite C-band observations for the field study.

2.6 Chapter Summary

The importance of soil moisture for climate and hydrologic land surface modelling has been discussed. However, the acquisition of soil moisture observations within a catchment is problematic, due to economic and technical limitations. Different methods to determine soil moisture were presented, including in-situ measurements, remote sensing and hydrologic modelling, and their advantages and limitations discussed.

Recent work on data assimilation in hydrology for the improvement of streamflow and soil moisture predictions through data assimilation has also been presented. This review showed that only a small number of papers have been published on the topic of streamflow data assimilation for the retrieval of initial soil moisture states. Moreover, these papers were shown to have limitations in their approaches, as they were either based on synthetic studies or used assimilation schemes which are not feasible techniques for multi-catchment studies.

Based on the review in this chapter, a new approach was suggested, which will allow the joint assimilation of streamflow and surface soil moisture observations simultaneously for a multiple number of catchments.

Chapter Three

3 Field Data

This chapter describes the study catchment and the collected data required for the use in the proposed streamflow assimilation scheme (see Chapter 2). The descriptions presents the experimental catchment and data collected for the development and verification of a runoff routing model (Chapter 4), and modelling and assimilation purposes of two synthetic studies (Chapters 5 and 6) and a field study (Chapter 7). In addition to data on soil moisture and streamflow, the hydrologic land surface model used in this thesis (see Chapter 4 for a detailed description of the model) requires precipitation, air pressure and temperature, saturated vapour pressure, long wave and short wave downwelling radiation, and wind speed data.

The data presented in this chapter was collected in support of the Scaling and Assimilation of Soil Moisture and Streamflow project (SASMAS; see www.sasmas.unimelb.edu.au) of which this thesis is a part. Data was collected throughout the Goulburn River experimental catchment at 6 stream gauges, 2 automated weather stations, and 26 soil moisture monitoring sites; a new universal calibration method for the soil moisture sensors was also developed. Additionally, three stream gauges operated by the Department of Infrastructure, Planning and Natural Resources (DIPNR) and a further three weather stations, operated by the Bureau of Meteorology (BoM), are located within or in the vicinity of the catchment. Ancillary data such as elevation, and soil and vegetation properties are also described.

The soil moisture observations serve as a verification of the hydrologic land surface model itself, as well as a verification of the streamflow assimilation field demonstration in Chapter 7. Due to the persistent severe drought in the region only few detailed flow measurements could be taken at the SASMAS sites. Consequently, a full calibration of the project-operated stream gauges was not possible, meaning that these data could not be used in a quantitative way.

The siting and installation of the monitoring sites was a collaborative effort from the three post-graduate students involved in the SASMAS project. Due to the location of the sites, the students based in Newcastle were responsible for the downloading of loggers and infrastructure maintenance, while the author of this thesis focused on calibration issues, quality control and archiving of the data.

3.1 Catchment Description

The catchment used for the modelling studies in this thesis is the 6,540km^2 Goulburn River experimental catchment, which itself is a tributary to the Hunter River in New South Wales, Australia (Fig. 3.1). The catchment extends from 31°46′S to 32°51′S and 149°40′E to 150°36′E, with elevations ranging from 106m in the floodplains to 1257m in the northern and southern mountain ranges (Fig. 3.2a). The typical terrain slope as derived from the national 250m digital elevation model (DEM; AUSLIG (now Geoscience Australia), 2001) has a median of 8%, with a maximum of 71%.

This catchment was chosen for (i) its relatively large area of predominantly low to moderate vegetation cover in the north of the catchment (Fig. 3.2b) for satellite soil moisture remote sensing studies; (ii) its dense vegetation in the southern region for which no remotely sensed surface soil moisture information is available; (iii) the lack of maritime effects in order to avoid mixed pixel responses

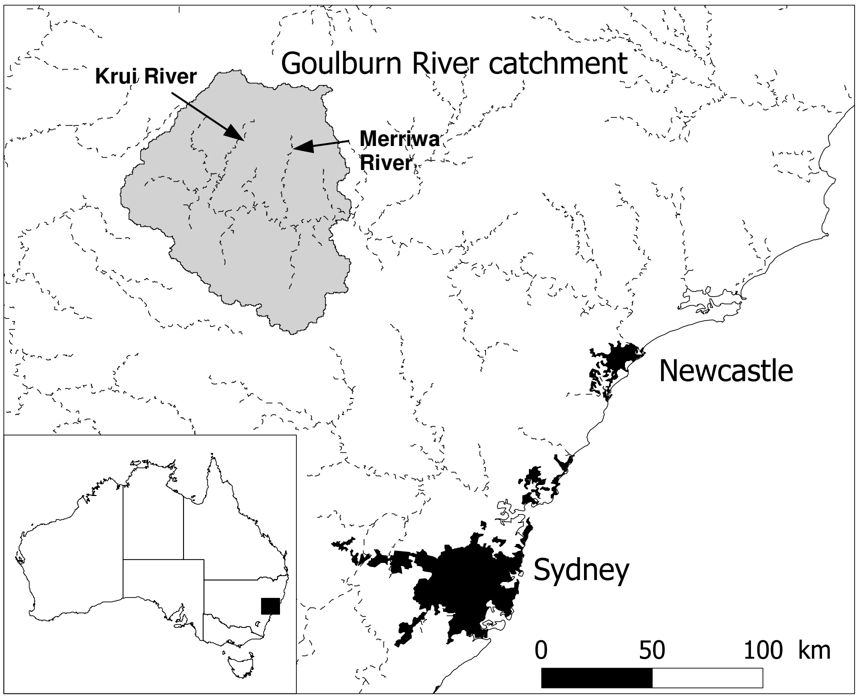

Figure 3.1. Location of the Goulburn River experimental catchment (shaded in grey) in south-east Australia.

from ocean and land data within satellite measurements; (iv) the distinct soil type distributions with basalt derived soils in the north and sandstone derived soils in the south; (v) the topographic variation including flood plains, undulating hills and mountainous terrain; (vi) the absence of regulation in the river system; (vii) no soil moisture interactions with groundwater due to the deep aquifer; (viii) it is believed that irrigation in the region has no influence on the streamflow; and (ix) its relative proximity to Newcastle.

The Goulburn River runs generally from west to east, with tributaries from the north and south, meaning the catchment is dominated by easterly and westerly aspects. The main catchment has two more intensively monitored subcatchments, the Krui River (562km^2) and Merriwa River (651km^2) in the northern half of the catchment (Fig. 3.3). Additionally, a densely monitored 175ha micro-catchment is located on a property called "Stanley", situated in the lower reach of the Krui River catchment (Fig. 3.3). A detailed

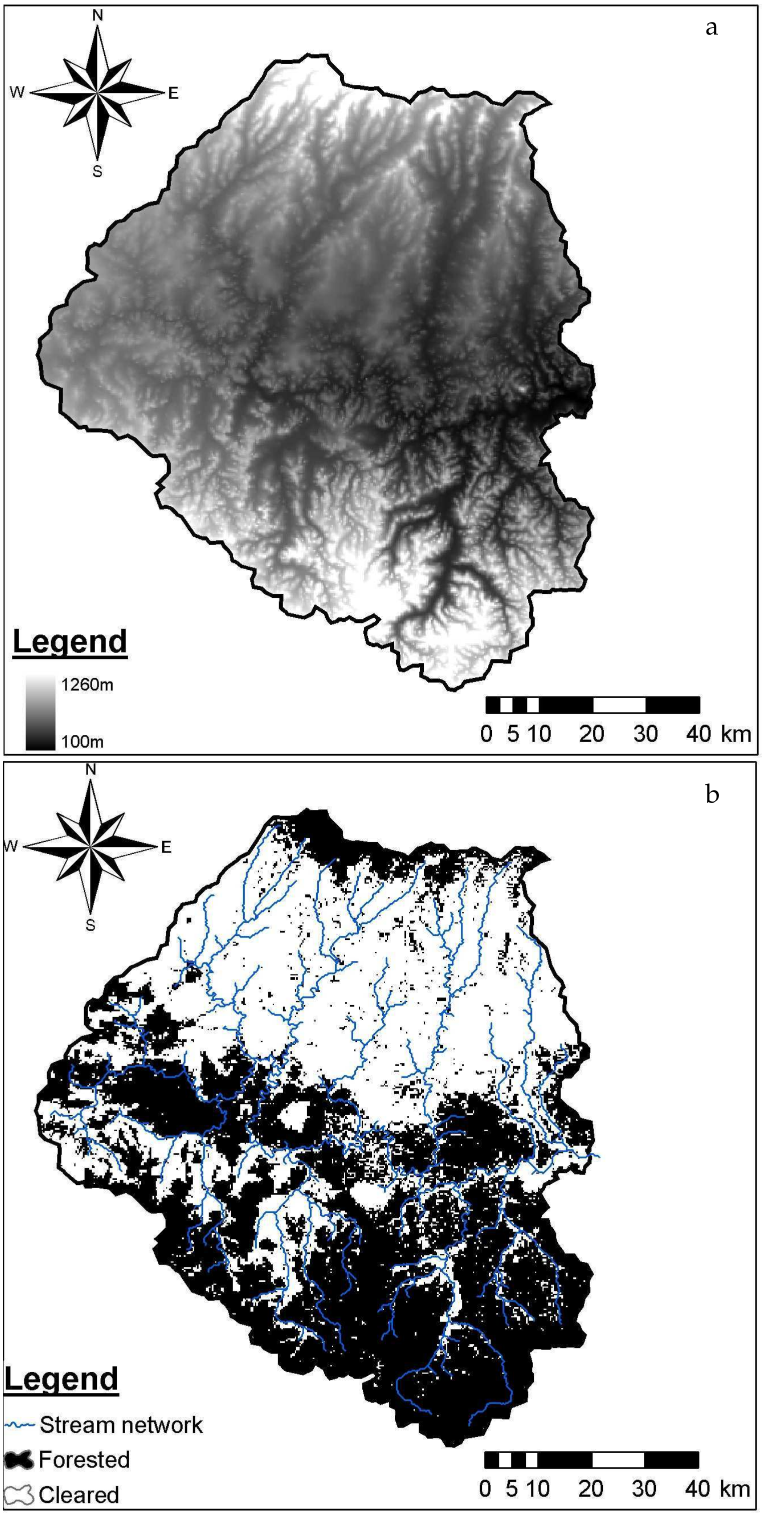

Figure 3.2. a) Elevation data and b) vegetation map, showing cleared and forested (black) areas for the Goulburn River catchment.

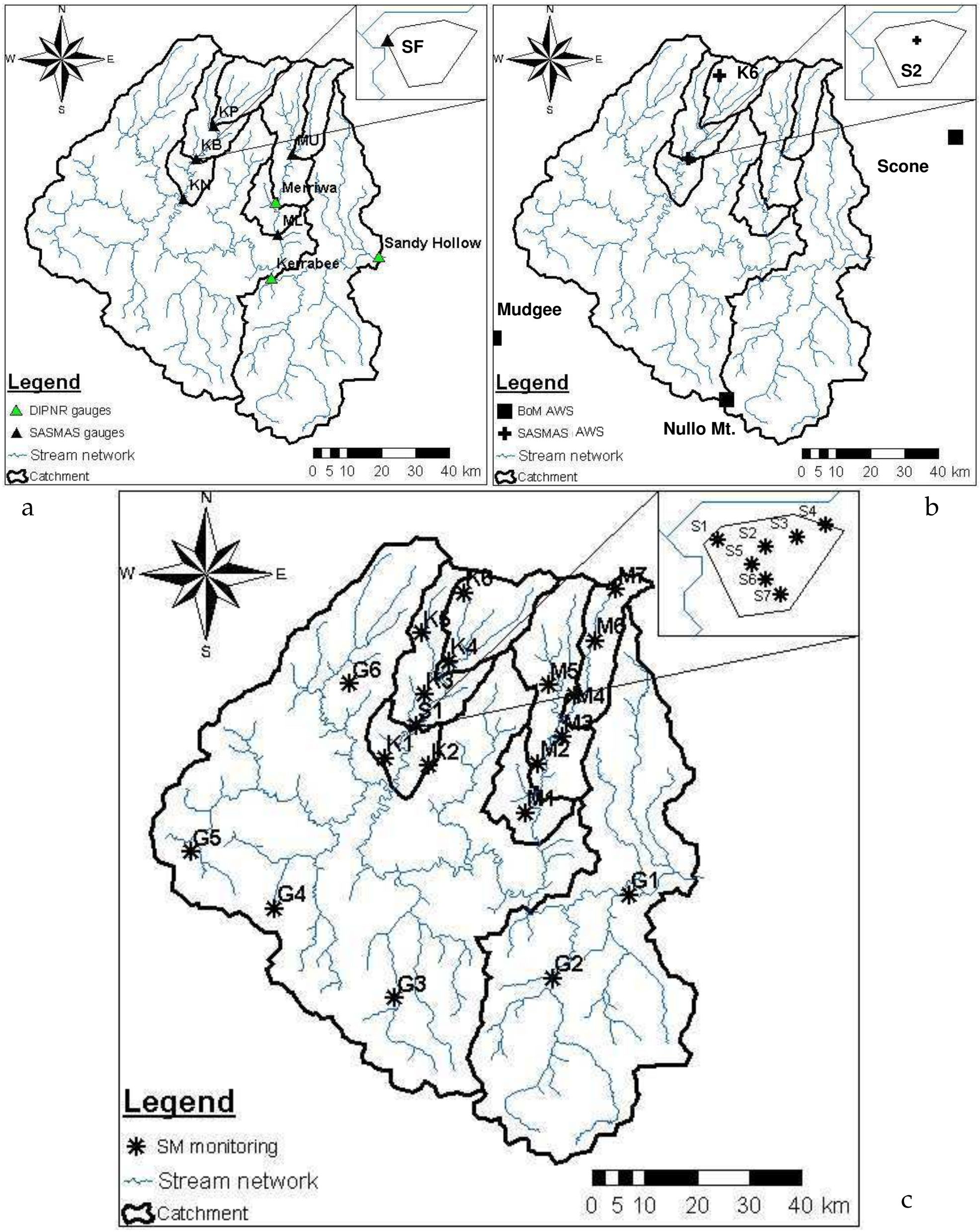

Figure 3.3. Location of monitoring sites and subcatchment delineations. The inset shows the set-up of the microcatchment on "Stanley". a) Stream gauges, b) climate stations, and c) soil moisture monitoring sites. The numbering of the monitoring sites follows the location of the sites (G = Goulburn, K = Krui, M = Merriwa, S = Stanley; soil moisture monitoring sites received a number as index while stream gauges in the Merriwa catchment received a character designating lower or upper and in the Krui site specific characters (P = Pembroke, B = Krui Bridge, and N = Neverfail.

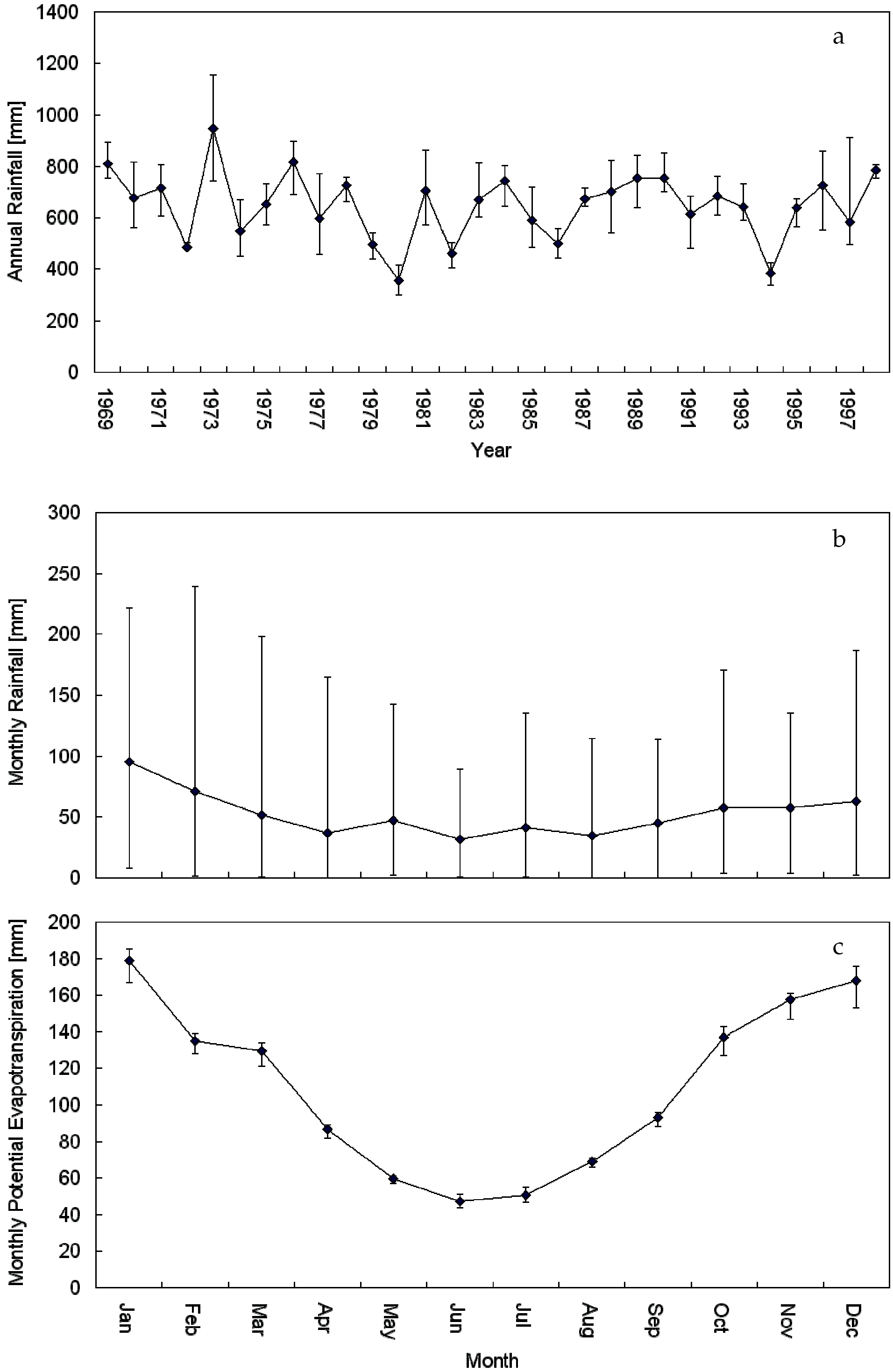

Figure 3.4. a) Annual and b) monthly rainfall patterns from 9 collecting rain gauges within the Goulburn River catchment for the years 1969 – 1998 (BoM, personal communication), and c) 30 year monthly averages of evapotranspiration (BoM, 1988). The solid line represents the average values while the whiskers show the spatial variability in a) and c), and both spatial and temporal variability in b).

overview of the stations is presented in Appendix A1.

The general climate within the region – based on the classification of long term averages – is described as subhumid or temperate (Stern et al., 2000), with significant variation in the annual rainfall (Bridgman, 1984). Similarly, the monthly maxima and minima show some variation between the rain gauges throughout the catchment (Fig. 3.4). However, the climate during the period of monitoring (2002-2005) could be described as semi-arid to arid. While the average annual rainfall in the Goulburn River catchment is approximately 650mm, it varies from 575mm to 1180mm depending on altitude (Fig. 3.5a). Major rainfall events generally occur during the southern hemisphere summer with an average monthly precipitation of 68mm, while the minimum monthly average precipitation occurs in June with 32mm. The average annual areal potential evaporation ranges from 1240mm to 1360mm (Fig. 3.5b). The minimum monthly areal potential evaporation is reached in July with an average of 47mm and the maximum is observed in January, reaching 185mm. Monthly mean maximum temperatures reach approximately 30°C in summer and 14°C in winter, with mean minimum values of 16°C and 2°C, respectively (BoM, 1988). Except for elevated areas, frost is unlikely to occur during daytime in winter, but nighttime minimum temperatures in winter are frequently less than 0°C.

The catchment soil types are derived from two distinct geological conditions. The northern part of the catchment consists mainly of Tertiary basalt, while the southern part consists mainly of Triassic sedimentary rock formations (Atkinson, 1966; Story et al., 1963). Hence, the soil types in the north are predominantly clayey and silty soils, while the soils in the south are mainly sandy, being derived from the underlying sandstone formations. The soil types in the

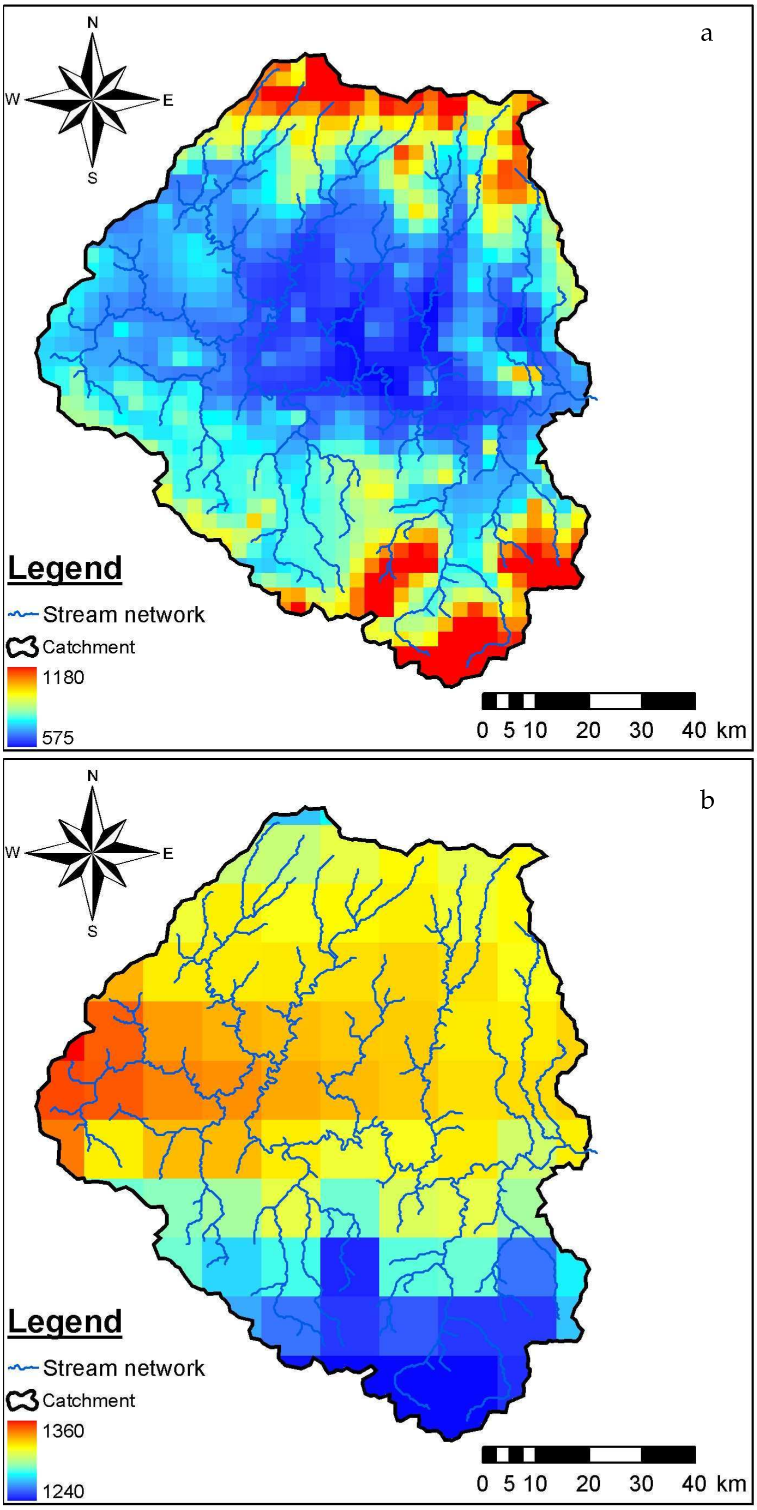

Figure 3.5. a) Annual average rainfall and b) annual average areal potential evapotranspiration. Both data sets were compiled with 30 years of data (1961-1990) interpolated from various stations in the region (BoM, 1988).

Table 3.1. Specific soil types within the top 30cm at the soil moisture monitoring sites.

Station	*Clay %*	*Silt %*	*Sand %*	*Soil Type*	*Salinity [dS/m]*
G1	8	15	77	Sandy loam	0.044
G2	21	56	23	Silt loam	0.225
G3	64	25	11	Clay	0.304
G4	11	13	76	Sandy loam	0.012
G5	9	17	74	Sandy loam	0.046
G6	33	35	32	Clay loam	0.201
K1	23	51	26	Silt loam	0.516
K2	6.5	8.5	85	Loamy sand	0.008
K3	71	23	6	Clay	0.472
K4	54	36	10	Clay	0.308
K5	62	26	12	Clay	0.368
K6	35	44	21	Clay loam	4.454
M1	6.5	21.5	72	Sandy loam	0.021
M2	0	6	94	Sand	0.141
M3	36	43	21	Clay loam	0.290
M4	25	49.5	25.5	Loam	0.129
M5	69	21	10	Clay	0.545
M6	51	17.5	31.5	Clay	0.135
M7	35	40	25	Clay loam	0.398
S1	54	40	6	Clay	0.170
S2	39	35	26	Clay loam	0.126
S5	46	42	12	Silt clay	n/a
S6	41	28	31	Clay	n/a
S7	16	52	32	Silt loam	n/a

eastern floodplains are a mixture of both types, due to the mixing of the river sediments (a detailed overview over the geological conditions in the Goulburn River are given by Martinez (2004)). An overview of the surface 30cm soil type at the various soil moisture monitoring sites (based on laboratory analyses) is presented in Table 3.1.

3.2 *Catchment Monitoring*

3.2.1 Locations of Instrumentation

The Goulburn River experimental catchment has been instrumented since September 2002. The catchment monitoring includes surface and root zone soil moisture, soil temperature, meteorological and streamflow measurements.

Five streamgauges were installed in the two focus catchments (Krui and Merriwa River catchments), adding to the 3 existing streamgauges operated by the New South Wales Department of Infrastructure, Planning and Natural Resources (DIPNR), allowing the main catchment to be subdivided into smaller modelling units. This includes 3 subcatchments in the Krui, 3 subcatchments in the Merriwa, and a further 2 divisions of the Goulburn River (Fig. 3.3a). A partial Parshall flume (Bos, 1976) was also installed in the "Stanley" microcatchment to monitor local runoff from a small catchment.

The automatic weather stations were sited close to existing infrastructure and to assess anticipated spatial variability, resulting in one station at the centre of the Goulburn River experimental catchment and a second station in high terrain in the north of the catchment, supplementing BoM sites to the east, south and west (Fig. 3.3b). This resulted in having automatic weather stations located in both the upper and lower reaches of the Krui focus catchment, and in the centre of the "Stanley" microcatchment.

A total of 26 soil moisture and temperature monitoring sites were chosen on the basis of i) being representative monitoring sites, ii) having a spatial distribution across the experimental catchment, and iii) their accessibility (Fig. 3.3c). The representative monitoring site objective was addressed by choosing mid-slope locations with typical vegetation, soil, and aspect, so that they represented catchment average soil moisture monitoring sites (CASMM; Grayson and Western, 1998). Although beyond the scope of this thesis, the spatial distribution was chosen to give a concentration of measurements in the open cropping and grazing land to the north for application to remote sensing measurements, while achieving a good distribution for model verification within the chosen focus catchments and the broader Goulburn River catchment.

3.2.2 Streamflow Data

Streamflow has been measured at 8 locations throughout the catchment, with 3 of these stream gauging stations (Sandy Hollow, Kerrabee and Merriwa; see Fig. 3.3a) being operated by the New South Wales Department of Infrastructure, Planning and Natural Resources (DIPNR).

Streamflow at the project operated sites has been observed with Solinst Model 3001 Leveloggers, which measure and record the local water pressure every 20 minutes. The instruments are not vented and hence raw data are corrected for atmospheric pressure measured at the "Stanley" microcatchment (see Appendix A2 for the detailed preliminary calibration of the sensors and the respective cross-sections). Three of the project's 5 stream gauging sites are located along the Krui River and 2 are located along the Merriwa River, complementing the single DIPNR gauge near the town of Merriwa. The water level observations for 2003 and 2004 at the DIPNR-operated streamflow monitoring site south of Merriwa are shown in Fig. 3.6. Fig. 3.6 shows that the Merriwa River (and equally the Krui River) is an ephemeral stream, with long periods of no or very low flow. The majority of the streamflow occurs during large events, as a consequence of intensive precipitation.

For the calibration efforts of the SASMAS stream gauges, the monitoring sites were surveyed to determine the shape and

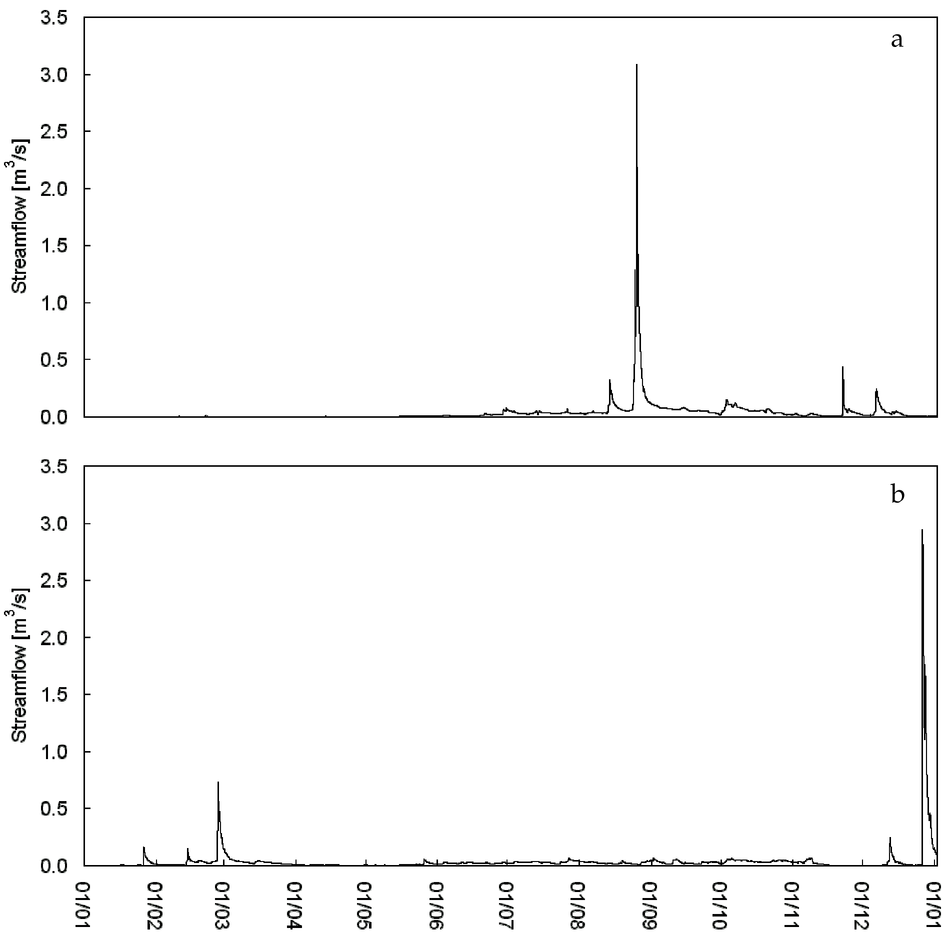

Figure 3.6. Streamflow at the DIPNR site near Merriwa for a) 2003 and b) 2004.

longitudinal slope of the respective cross sections (see Fig. 3.7 for an example). For the calibration, Manning's equation was used

$$Q = \frac{S^{\frac{1}{2}} R_h^{\frac{2}{3}} A}{n}, \tag{3.1}$$

where Q is the streamflow [m^3/s]; S is the slope in flow direction [m/m]; R_h is the hydraulic radius [m^2/m]; A is the cross sectional area of the flow [m^2]; and n is Manning's roughness coefficient. To allow adequate calculation of the streamflow in relation to the flow depth for the preliminary rating curves, n was estimated following Cowan's (1956) method that takes into consideration adjustment factors for the conditions of the bed (eg. obstructions and roughness), the vegetation, any surface irregularities and the variations in the cross section of the flow. Additionally, local channel conditions of

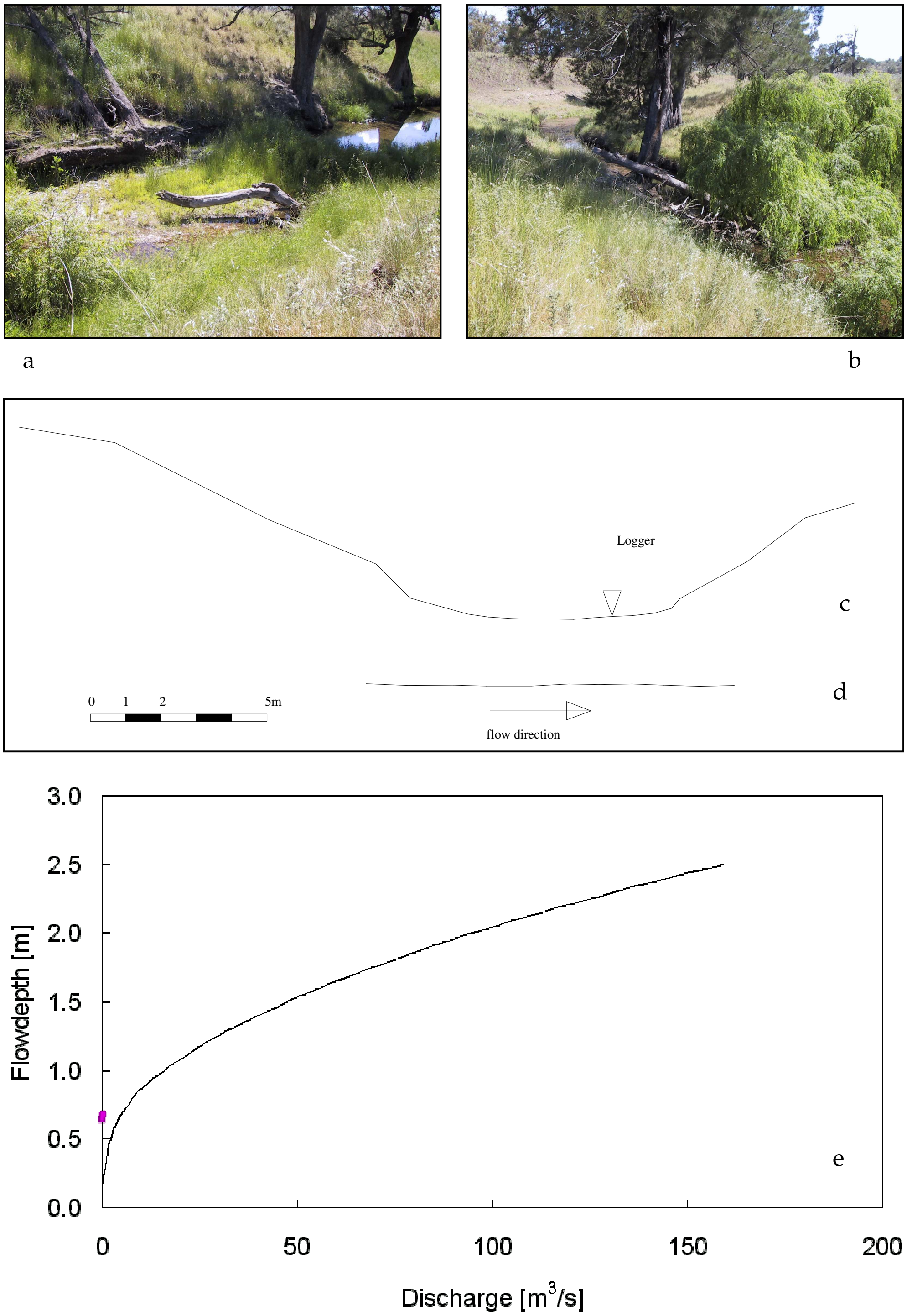

Figure 3.7. View of stream gauge MU (upper reaches of the Merriwa River). a) View north, b) view west c) cross section in flow direction at the location of the logger (identical horizontal and vertical scale), d) slope along the flow direction, and e) preliminary rating curve (solid line) and two calibration measurements (squares).

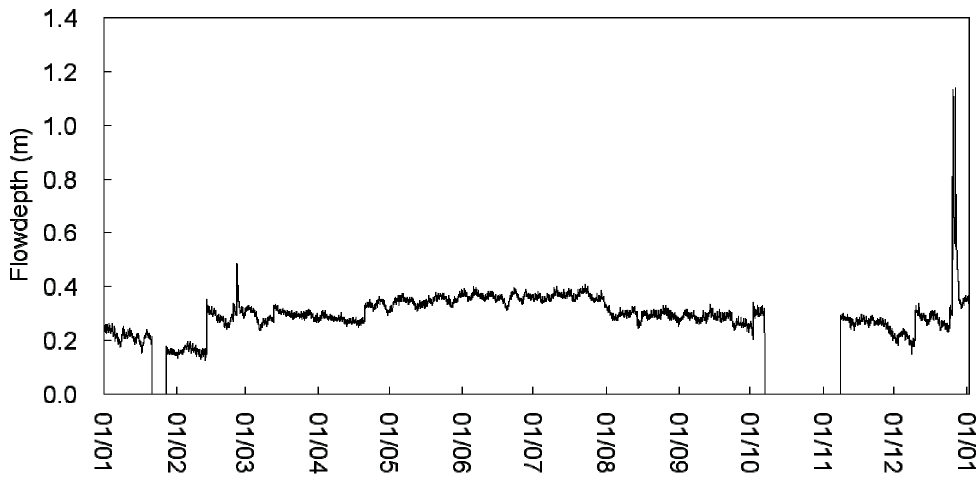

Figure 3.8. Example of the observed flowdepth at stream gauge MU for the year 2004, showing a pattern similar to the observed streamflow at Merriwa.

the gauging sites were compared with published *n* values for similar sites (Barnes, 1967; U.S. Geological Survey).

Several sets of flow velocity measurements were taken across the streams at different flow depths. However, due to the persistent drought in the area, both Krui and Merriwa Rivers presented few opportunities for the collection of rating curve calibration and validation data (see for example the lack of data points on the preliminary rating curve in Fig. 3.7e) and therefore were not used for the development of the preliminary rating curves. Nevertheless, the observed flow depth is available for qualitative comparisons of observations and model output while the rating curves undergo further development for future studies, but is not used for assimilation in Chapter 7. Fig. 3.8 shows the observed flow depth at the stream gauge MU. The first flow velocity measurements showed that a flow depth of less than 0.5m does not produce observable streamflow. Consequently, the flow depth shown for 2004 only resulted in streamflow towards the end of the year. The other streamflow event at the beginning of 2004 (see Fig. 3.6) is not shown here, as no reliable atmospheric pressure data was available during these periods to correct the instrument. All cross sections and flow velocity measurements are presented in detail in Appendix A2.

Runoff from the "Stanley" microcatchment has been monitored with a 1ft 6in (46cm) partial Parshall flume located at the outlet of the catchment. A stilling well at the side of the flume houses an Solinst Levelogger (replacing an Innovonics MD4W water level logger in March 2005), which measures and records the water level at 20 minute intervals. The calibration relationship for this flume is presented by Bos (1976) and has been confirmed in laboratory experiments (Walker, 1999). Since the installation of the flume, there has been no runoff recorded from this site. However, the inlet from the flume to the stilling well is located 3mm above the flowbed of the flume. It is therefore possible that small flow events with a flow depth of less than 3mm have taken place without having been recorded. Nevertheless, as neither deposited material nor sedimentation or erosion downstream is observed at this site, it is assumed that no such runoff event has taken place.

3.2.3 Meteorologic Data

The Goulburn River experimental catchment operates two automatic weather stations, located in the lower and upper reaches of the Krui catchment respectively (Fig. 3.3b). A schematic for the automatic weather station setup at "Stanley" (S2) and "Spring Hill" (K6) is given in Fig. 3.9. The northern weather station at K6 is at an elevation of 739m and includes an air temperature and relative humidity sensor at 2m, wind speed sensor at 3m, tipping bucket rain gauge, and 3 soil temperature sensors (150, 450 and 750mm). The southern weather station at S2 is located at an elevation of 376m and includes a pyranometer, wind speed and direction sensors at 3m, air temperature, relative humidity and barometric pressure sensors at 2m, a 4-way radiometer at 1m (installed in April 2004, replacing a net radiometer, which was installed at the beginning of the project),

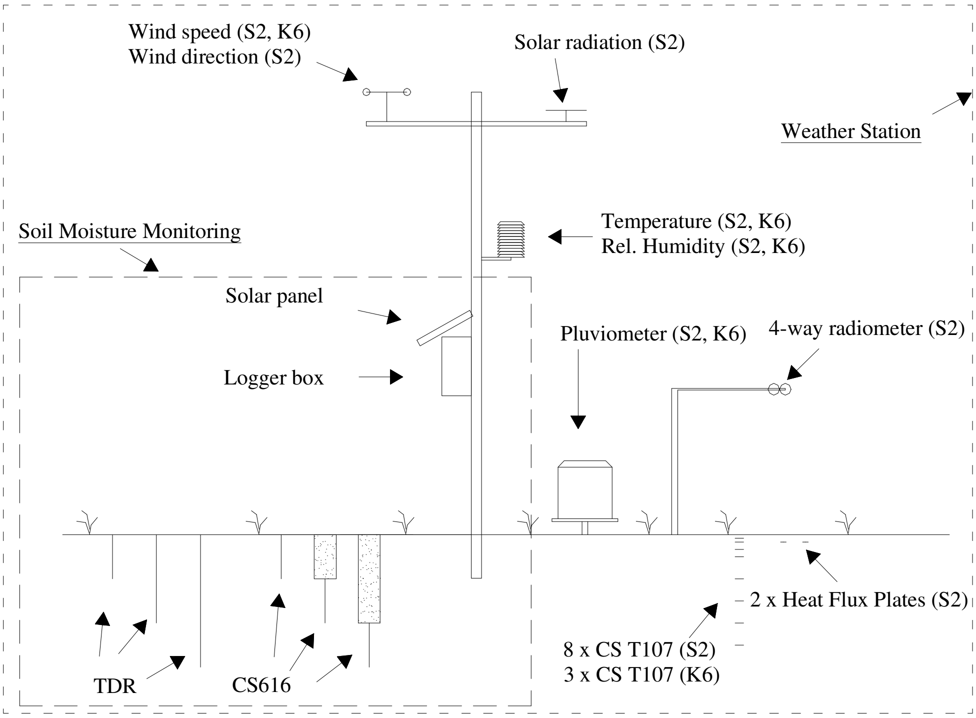

Figure 3.9. Schematic of the weather (large box) and soil moisture monitoring stations (small box).

tipping bucket rain gauge, 2 heat flux plates at 50mm depth, and 8 soil temperature sensors (25, 50, 100, 150, 300, 450, 600, 750mm). The meteorologic measurements are taken every minute and the averaged logged every 20 minutes. Rainfall data is logged for each tip of the 0.2mm tipping bucket. These two automatic weather stations also measure and record soil moisture data at three depths, as described in section 3.2.4.

Sample data for the year 2004 from the weather stations at S2 and K6 are shown in Fig. 3.10 and 3.11. The gaps in the data result from failures of the logger. The main differences in the meteorological data between the weather stations at S2 and K6 originate from the different elevations of the stations. The temperature at S2 is generally higher than at the higher elevation site at K6. Furthermore, rainfall intensity and quantity vary between the two sites with more rainfall occurring throughout the year at K6.

Three other BoM automated weather stations (AWS) are located in

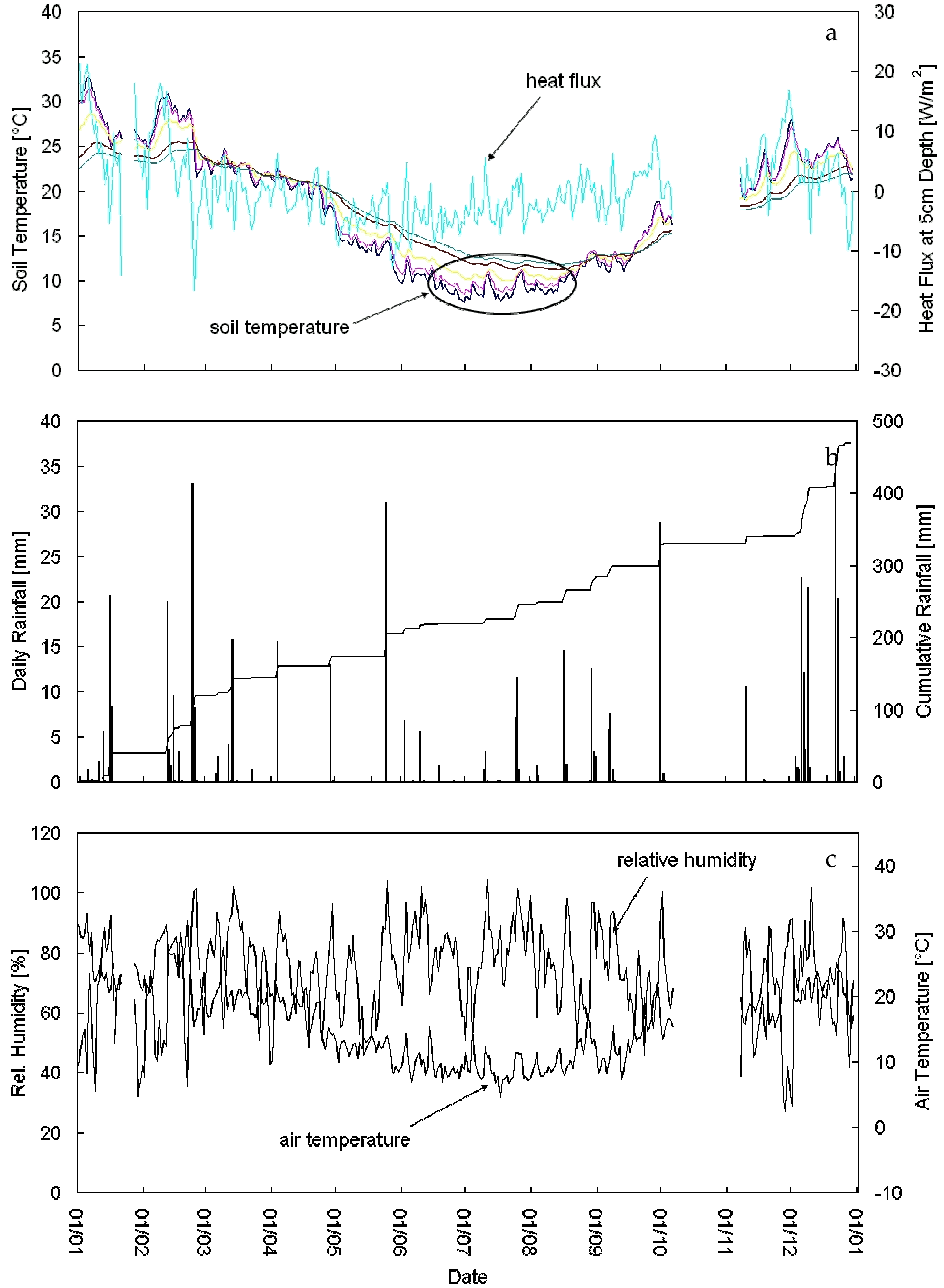

Figure 3.10. Sample data (daily averages of 2004) from the weather station at S2. a) sensible heat flux (turquoise) at 25mm and soil temperatures at depths of 100, 150, 300, 450, 600, 750mm, b) daily and cumulative rainfall, and c) relative humidity and air temperature.

the region: Scone (east), Mudgee (west) and Nullo Mountain (south). These stations provide air temperature and rainfall data. Numerous collecting rain gauges, operated by the BoM, are located in and around the catchment and provide daily 9am rainfall observations (Fig. 3.12).

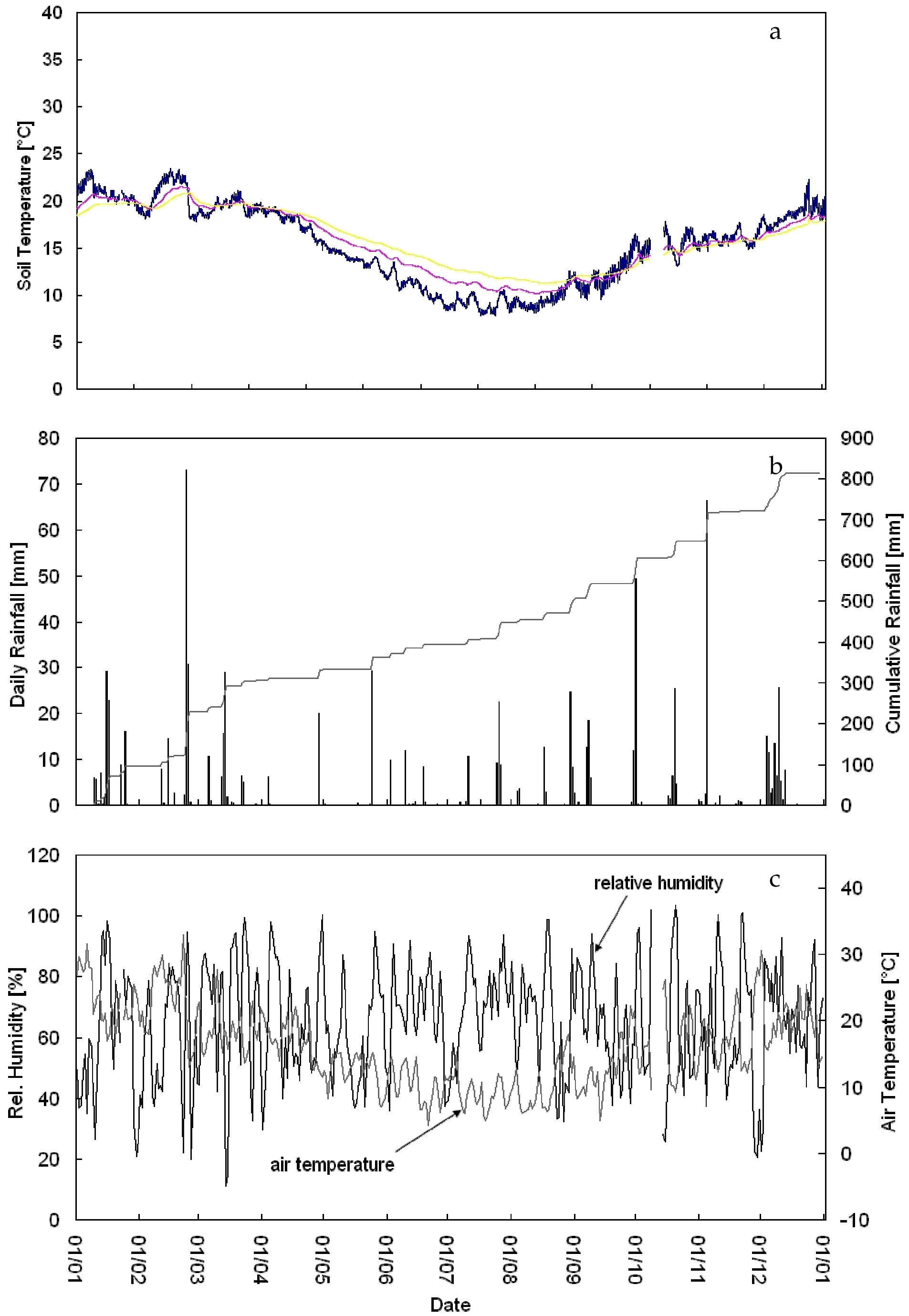

Figure 3.11. Sample data (daily averages of 2004) from the weather station at K6. a) soil temperatures at depths of 150, 450, and 750mm, b) daily and cumulative rainfall, and c) relative humidity and air temperature.

The hydrologic land surface model used in this thesis requires incoming longwave and shortwave radiation as forcing data. However, the 4-way radiometer installed at the weather station at S2 was not in operation for the period that the experiments in this thesis

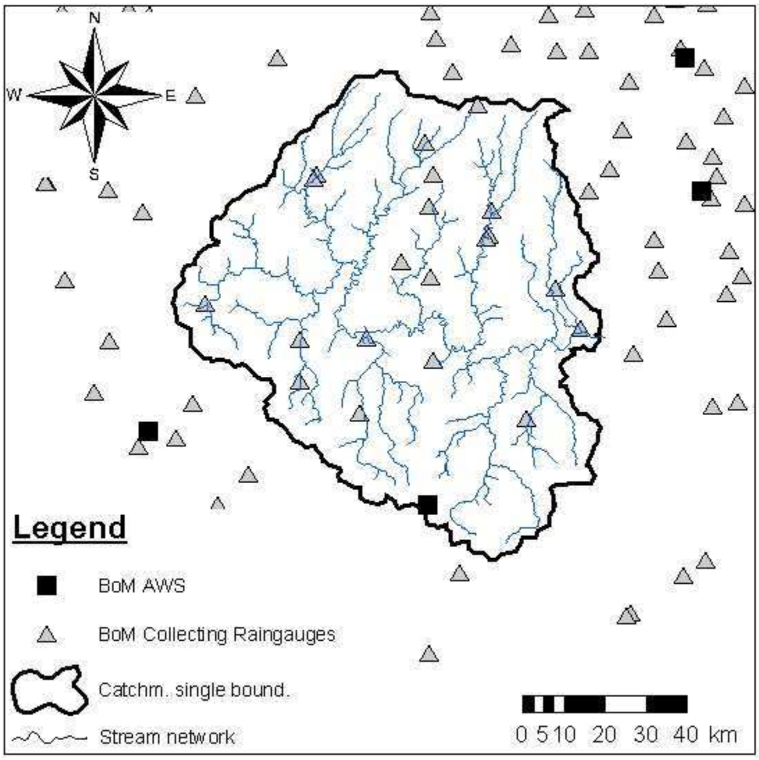

Figure 3.12. Location of collecting rain gauges and AWS operated by the BoM.

focus on (April 2003 to March 2004). Since only a net-radiometer was in operation in the catchment during the period in question, other sources of radiation data were required. Radiation data from the National Centers for Environmental Prediction Global Data Acquisition System (NCEP GDAS) radiation data sets (Derber et al, 1991) were used as this was considered to be more accurate than calculating the longwave and shortwave radiation from the net observed radiation and an estimated albedo.

3.2.4 Soil Moisture Data

Soil moisture profile monitoring was installed at 26 sites throughout the Goulburn River experimental catchment, with each site having up to three vertically inserted Campbell Scientific CS616 water content reflectometers (Campbell Scientific Inc., 2002) over depths of 0-300, 300-600 and 600-900mm, respectively (see Fig. 3.9). The siting of the soil moisture monitoring sites followed closely the general description of CASMM sites in Grayson and Western (1998), ie. a site generally located mid-slope, with representative soil and vegetation for the local area. However, this siting was undertaken using local points of reference to determine the representativeness of the sites (soil, vegetation, and slope). A comparison of the local and subcatchment CTI was later undertaken, showing most sites were within one half of a standard deviation to the subcatchment-wide average. However, some sites were found to have large CTI, which signifies flat terrain (unless it is located within a river, then the most significant factor in the CTI is the contributing upstream area), even though these sites were known to be on relatively steep terrain (eg. M7). The reason for this is small errors in the collocation of site coordinates and the maps, resulting in pixel shifts, which is particularly significant in areas where flat terrain is directly adjacent to steep hillslopes.

The exact number of soil moisture sensors installed at a site was determined by the depth to the bedrock, being less than 900mm in some cases and therefore limiting the number of sensors at sites with shallower soils. A Campbell Scientific T107 temperature sensor was installed over a depth of 120 to 180mm (the average 150mm depth being the midpoint of the soil moisture reflectometers installed at 0-300mm) at all soil moisture monitoring sites. The soil temperature data is required for temperature correction of the soil moisture sensor readings. The CS616 sensors ensured a continuous observation of the temporal and spatial soil moisture variability throughout the soil profile, with sensors read every minute and averages stored once every 20 minutes. The temperatures for deeper soil depths were estimated from the relationships with deeper soil temperature measurements at S2 and K6 (see section 3.2.4.2).

Two focus catchments were created by establishing 7 soil moisture monitoring sites in each of the major subcatchments (6 individual sites in the Krui River catchment in addition to the "Stanley" microcatchment (with 7 sites) and 7 individual sites in the Merriwa River catchment), with a further 6 sites installed in the remaining Goulburn River catchment (Fig. 3.3c). The intensively monitored "Stanley" microcatchment was designed to explore the spatial variation of soil moisture across local scales, which is not part of this thesis. Moreover, the higher density of soil moisture monitoring sites in the Krui River and Merriwa River catchments allows for work in the spatial organisation of soil moisture throughout the northern part of the catchment, supports work undertaken in the validation of hydrologic land surface models and the validation and scaling of satellite measurements (Hemakumara et al., in review).

The sensor response to soil moisture varies with salinity, density, soil type and temperature, requiring a detailed sensor calibration for each site using both laboratory and field measurements (see section 3.2.4.3). Moreover, during the installation of the soil moisture sensors, care had to be taken not to damage the rods of the sensor during the insertion into the soil, as damage would distort the sensor response. The insertion of the sensor cannot be avoided as the soil around the sensor has to be undisturbed in order to be representative of the surroundings.

3.2.4.1 Sensor Installation

The deeper soil moisture sensors (at depths of 300-600mm and 600-900mm, respectively) and the soil temperature sensors were installed by excavating the overlying soil layers. The soil was removed with a manually operated auger, in order to limit the mixing of soil. Moreover, the excavated soil was collected in the order of its removal and stored in the same order, before refilling. Recompaction of the soil was undertaken to the same approximate density of the original soil column. The soil was not wetted during the installation process so as to minimise disturbance and hence time to retrieve representative soil moisture data.

Installation of the probe itself was achieved by physically pushing the two 3.2mm diameter 300mm long probes into the soil. Such an installation can prove to be difficult, especially if pebbles/rocks are present in the soil and/or the soil is dry. Probe installation was undertaken in September to maximise the likelihood of favourable soil moisture content conditions, however the clay soil was still quite stiff in many instances.

As the sensors are delicate and easily bent, care had to be taken so that the rods of the water content reflectometers did not bend during the insertion process, thus distorting the signal of the sensor. To minimise sensor damage, pilot probes were first inserted for sites where the probes could not easily be inserted directly, thus presetting the insertion path in the soil. The pilot probes have steel rods of 300mm length and a diameter slightly less than the diameter of the reflectometer rods to ensure a close fit of the leader holes with the sensor rods and minimise the potential for air gaps, as air gaps lead to incorrect soil moisture observations (eg. Baker and Lascano, 1989).

3.2.4.2 Extrapolation of Deep Soil Temperatures

As CS616 sensors are particularly sensitive to soil temperature fluctuations, Campbell Scientific T107 temperature sensors were installed vertically with their midpoint at 150mm below the soil surface, to provide a continuous record of soil temperature at the midpoint of the 0-300mm CS616 sensors at each monitoring site for temperature corrections. In order to apply the correction to deeper soil moisture sensors, a method for extrapolating the deeper soil temperature observations from S2 and/or K6 to the other Goulburn soil moisture stations had to be developed. As no soil temperature

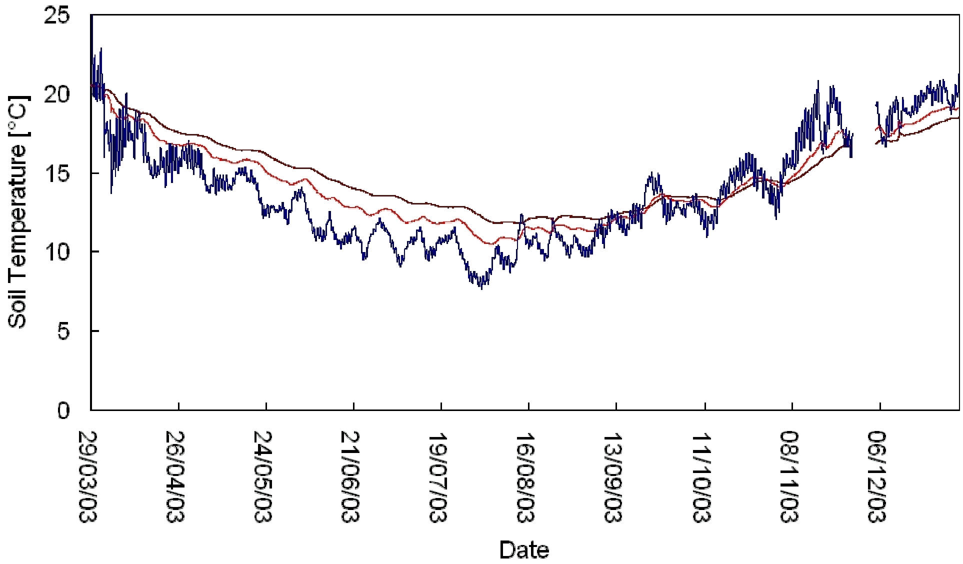

Figure 3.13. Soil temperatures at "Spring Hill" (K6) at 150mm (blue), 450mm (red) and 750mm (brown).

data was available for a depth of 450mm at S2 (due to an early failure of the sensors at 25, 50 and 450mm), the soil temperature data from 600mm were used (ie. the average of the midpoints of the soil moisture sensors at 300-600mm and 600-900mm). Thus, it was assumed for all monitoring sites that the temperatures at 450 and 750mm were the same as at 600mm or that the introduced error was negligible and that they could thus be estimated from the temperature at 600mm. The weather station at K6 has sensors installed at 450 and 750mm and therefore, the average temperature of these sensors was compared against the temperature at a depth of 600mm at S2. As the deeper soil temperatures (at 450 and 750mm) only differ by a maximum of 2°C (Fig. 3.13), the assumption that the temperature at 600mm can be used was not expected to be limiting as a difference of 2°C has only little impact on the measured period of the sensor.

The spatial extrapolation methodology developed here is based on the ratio of the soil temperature sensor at a given depth to the observations at 150mm by

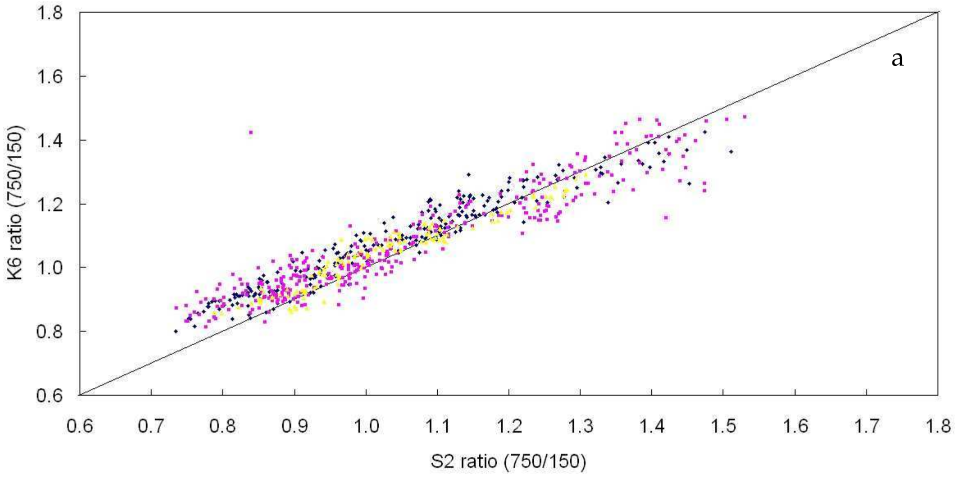

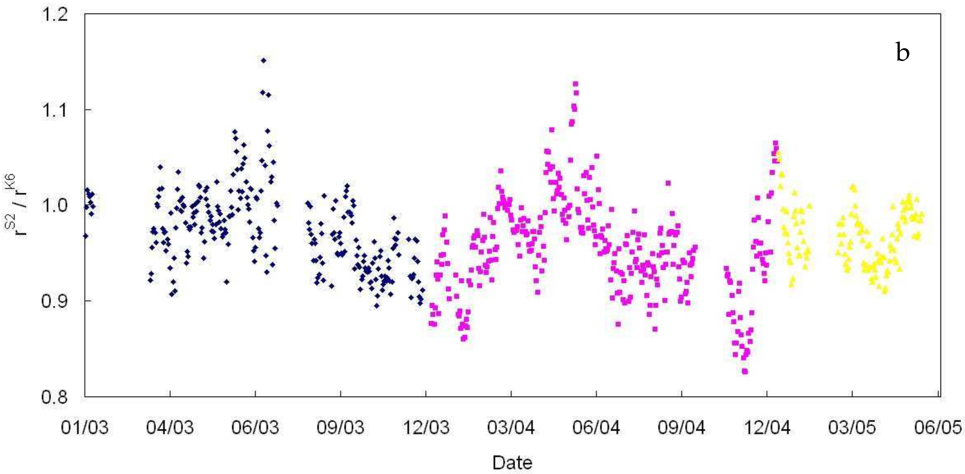

Figure 3.14. Correlation of daily soil temperature ratios between "Stanley" (S2) and "Spring Hill" (K6) weather stations. a) two years of observations from mid-2003 to mid-2005 and b) temporal behaviour of the ratio of r_T^i at both stations (Blue: 2003, Pink: 2004, Yellow: 2005).

$$r_T^i = \frac{\overline{T}_d^i}{\overline{T}_d^{150}}, \tag{3.2}$$

where r_T^i is the temperature ratio at depth i; $\overline{T}_d^i$ is the daily average of the soil temperature. The ratios for both S2 and K6 data were shown to be consistent (Fig. 3.14a), even though located in two extreme locations of the catchment (low and flat against high and rugged terrain). Therefore, it was assumed that this ratio approach could be reliably used at other locations within the Goulburn River catchment.

The ratio of the daily averages was chosen to avoid the noise originating from the near-surface temperature fluctuations resulting from local variations on a sub-daily scale. In order to calculate the deeper temperatures at the individual sites, the respective 150mm temperature measurement at the monitoring site was multiplied with the ratio of S2 (for the majority of the sites) or K6 (for M7 as it is located at a higher elevation, similar to K6). Even though the ratios of the two stations are approximately the same, the approach of using the two different ratios is aimed at getting consistency in the data (data from higher elevation for sites are temperature corrected with the ratio at the higher station, similarly lower sites are temperature corrected with the ratio at S2). This approach yields a daily average temperature at 600mm for the other monitoring sites, from which the 450mm or 750mm were estimated (as mentioned above, it was assumed that the temperatures at both depths were equal to the temperature at 600mm). Use of a daily average temperature estimate is valid as the soil temperatures at 450mm and 750mm do not undergo the same diurnal fluctuations as the temperatures at 150mm (Fig. 3.13).

However, a seasonal pattern is visible when plotting the temporal evolution of the ratio of the r_T^i values (ie. $r_T^{750}(S2)/r_T^{750}(K6)$) at those two sites for a depth of 750mm (Fig. 3.14b), with low values in summer and high values in winter. The explanation for this seasonal pattern is that in summer time the temperature difference between the shallow and deeper layer is smaller in the lower regions (S2) than in higher regions (K6), whereas it is the opposite in winter time. In summer, the deeper soil layers at S2 reach higher temperatures than at K6 and therefore result in smaller values for r_T^i, while in winter the deeper soil layers do not cool down as significantly, consequently resulting in higher r_T^i values than at K6.

To assess the potential temperature error in the above approach, the temperature at a depth of 600mm was calculated for K6 using the temperature ratio at S2 and the temperature at 150mm at K6 and then compared against the observed temperatures at 750mm. The RMSE in the calculated temperature was determined with 1.12°C and the maximum error was 2.97°C. Furthermore, in order to quantify the resulting error in the estimated soil moisture, the error is determined for a worst-case scenario. The largest temperature effect on the CS616 is observed in section 3.2.4.5 for a wet loam. Assuming an error in the temperature of 3°C (30 and 33°C) and an observed period of 40µs (wet conditions) results in an error of approximately 0.022v/v in the volumetric moisture content. This error is almost identical with the accuracy of the instrument, published by the manufacturer (Campbell Scientific Inc., 2002).

The extrapolation of the temperatures assumes that the ratio of r_T^i at S2 and K6 is constant at 1. However, while this is true as an average over one year, the ration of r_T^i varies between 0.9 and 1.1 depending on the season (Fig. 3.14b). This seasonal pattern was not filtered out for the calculations. As the anomalies introduce a maximum error in r_T^i of approximately 10%, it would result in an error of about 0.002v/v and can therefore be assumed to be negligible, as all other soil types are less affected by changes in the temperature. Moreover, due the drought during the data collection, the soils are not likely to be saturated.

3.2.4.3 Sensor Calibration

The soil moisture sensors used throughout the Goulburn River experimental catchment are Campbell Scientific CS616 Water Content reflectometers. This sensor indirectly measures the dielectric constant of the soil, which ranges from 3 for dry soil to 80 for water. The CS616 operates with an operational frequency of oscillation of about 70MHz in free air (up to a maximum of 175MHz in the soil), making it more susceptible to changes in particle size distribution and temperature than time domain reflectometry (TDR), which operate at higher frequencies (Seyfried and Murdock, 2001). Consequently, soil dependent calibration equations had to be developed, as the general equation provided by the manufacturer does not take into account differences in soil type (Campbell Scientific Inc., 2002).

Several studies have been undertaken to investigate the signal changes of TDR sensors (eg. Gong et al., 2003) and the CS615 (eg. Quinones et al., 2003; Western and Seyfried, 2005) under varying soil and temperature conditions. Western and Seyfried (2005) developed standardised calibration equations for the CS615, the predecessor of the CS616, which operates over a lower frequency range. As both sensors work under the same principles, the equations developed in that study for the CS615 were adopted as the starting point for the CS616 calibration.

The equations developed by Western and Seyfried (2005) are

$$\theta = 0.4N^{\beta} \tag{3.3}$$

and

$$N = \frac{P^{25} - P_{0.0}}{P_{0.4} - P_{0.0}}, \tag{3.4}$$

where θ is the soil moisture content [v/v]; β is the shape parameter of the function; N is the normalised period of the sensor measurement; P^{25} is the temperature corrected (to 25°C) period measurement of the sensor [ms] at the current moisture content, effectively eliminating the temperature effects on the sensor; $P_{0.0}$ is the average period for oven dried soil at a temperature of 25°C [ms]; $P_{0.4}$ is the optimised soil specific period at a moisture content of 0.4v/v and a temperature of 25°C [ms]. The temperature correction for P^{25} is given by Western and Seyfried (2005) as

$$P^{25} = P_{obs} - C^{T}(T - 25), \tag{3.5}$$

where P_{obs} is the observed period measurement [ms]; C^T is a temperature correction coefficient [ms/°C]; and T is the observed soil temperature [°C]. Western and Seyfried (2005) found that the temperature correction coefficient C^T was constant for a given soil moisture content over a varying temperature range, when plotting T against P_{obs}, which allowed to calculate the period measurement at 25°C (P^{25}) with a linear regression. Moreover, it was found that C^T varied for the same soil type with soil moisture content, when plotting C^T against P^{25}. Consequently, Western and Seyfried (2005) defined C^T as

$$C^T = sP^{25} + o\,, \tag{3.6}$$

where s is the slope and o is the offset of the temperature correction function. Therefore substituting (3.6) into (3.5) gives

$$P^{25} = \frac{P_{obs} - o(T-25)}{1 + s(T-25)}\,, \tag{3.7}$$

and the calibrated soil moisture may be calculated from eqns. (3.3), (3.4) and (3.7).

As the CS615 sensor operates in a different frequency range from the CS616, it was found in laboratory experiments for this thesis that the CS615 calibration parameters ($P_{0.0}$, $P_{0.4}$, s, o, β) of Western and Seyfried (2005) could not be used. Moreover, it was found that the temperature correction was also soil type dependent, and that the calibration function of eq. (3.3) was better described by a curvilinear, rather than a simple exponential relationship (see section 3.2.4.4).

3.2.4.4 Laboratory Calibration Approach

For the purpose of developing specific calibration parameters for the CS616, a laboratory experiment was set up as shown in the schematic in Fig. 3.15. In this experiment oven dried soil samples from the monitoring sites were placed in containers of 150mm

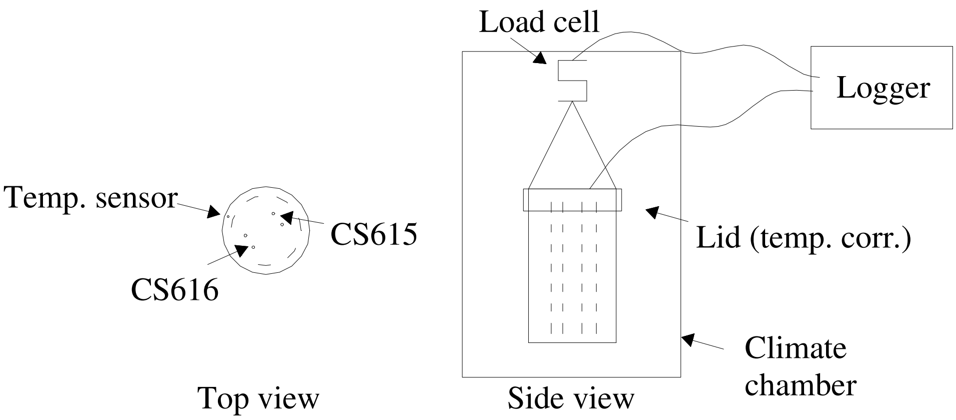

Figure. 3.15. Schematic of the laboratory set up for the calibration of the water content reflectometers.

diameter and 400mm length, instrumented with a CS616, CS615 (for cross-correlation studies (not presented here)), and a temperature sensor (a thermocouple at 150mm depth, placed in the centre of the soil column). The containers were suspended from load cells, which were constantly measuring the change in weight of the soil, through which the volumetric soil moisture content was calculated. The temperature was changed when the thermocouple had reached a constant temperature for at least two hours, assuming a homogeneous soil temperature profile.

In the studies of Quinones et al. (2003) and Western and Seyfried (2005), the soil moisture content of the sample was increased by removing the soil from the containers, adding extra water and then replacing the sample into the container. In contrast, the soil moisture content was increased in this experiment by adding water to the top of the container and allowing time for the water to fully infiltrate into the soil column. It was assumed that the water was properly infiltrated when the period measurement of the sensor did not show any more changes. This approach was chosen over that of the earlier studies, as it would not be guaranteed that the soil moisture at the field sites would be homogeneously distributed throughout the soil column as precipitation water infiltrates from the top, and a homogenous soil moisture profile in the laboratory experiment would therefore introduce a bias in the calibration results. Moreover, repeated recompaction of the sample would likely result in more variability in the results due to changes in soil structure and density.

In an initial experiment, a dry-down approach was tested. For this approach the soil column was saturated by infiltrating water through the bottom of the container until water was ponding on the surface of the soil. The container was then suspended from the load cells as described previously. However, the ambient temperature had to be set to 60°C to speed up the dry-down process, which took considerable time (in the order of 4 weeks). This approach showed some limitations. First, the dry-down of the soil was not fully achieved and the residual moisture required a further oven drying of the soil to obtain the $P_{0.0}$ values. Second, the dry-down of the soil took about 4 weeks, a long period compared to the 5 to 8 days of the final experimental setup. Finally, the high operational temperature is not a realistic field temperature and resulted in a quick drying of the surface and bottom of the soil column with a delayed effect in its centre. This led to unrealistic gradients in the moisture distribution throughout the soil column. As a consequence of these undesirable effects, the previously described approach was chosen.

3.2.4.5 Revised Temperature Correction

In contrast to the study by Western and Seyfried (2005), it was found that when P^{25} was plotted against C^T, the relationship changed with soil type as well as soil moisture (Fig. 3.16a). Consequently, soil specific s and o values (see eq. 3.6) had to be developed (Table 3.2). Fig. 3.16a shows that the slope is steeper for soils with progressively finer particles, such as clay and loam. Accordingly, soils with a large quantity of sand particles are less affected by temperature changes.

Two different functions were derived from the data: i) a best fit to

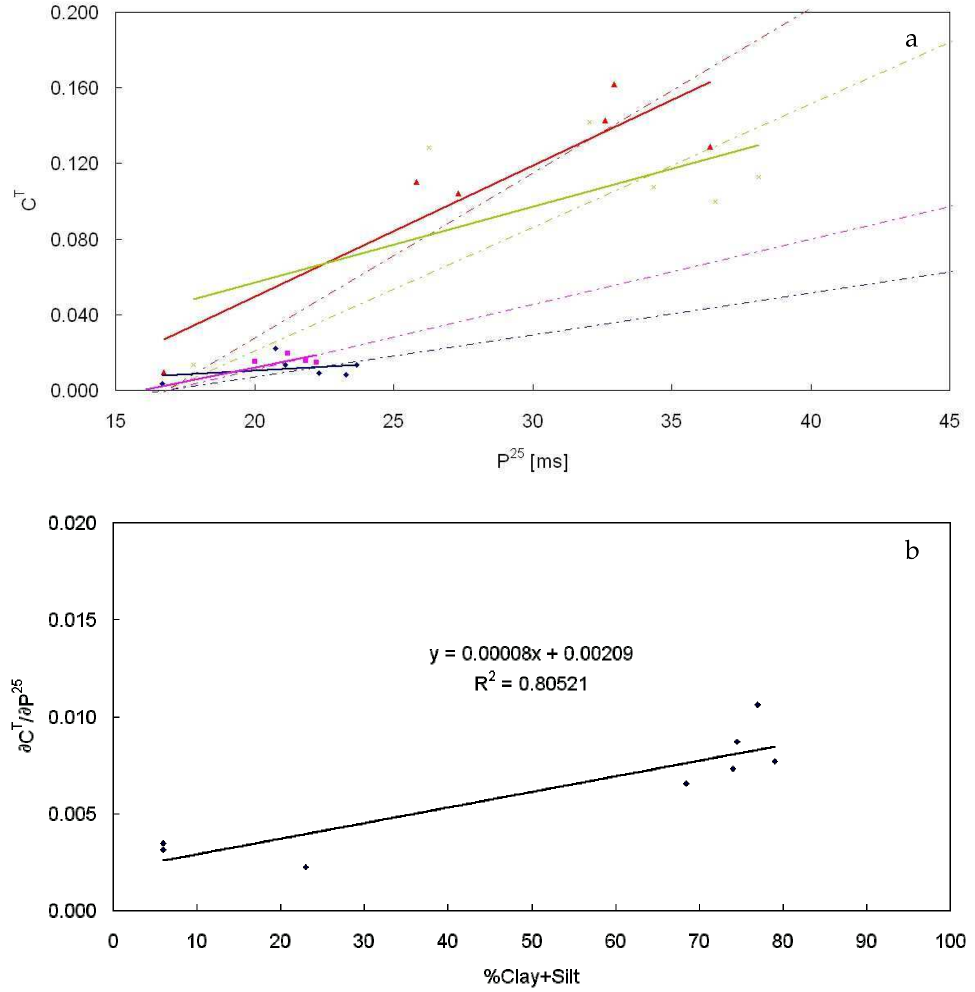

Figure 3.16. Correlation between a) soil specific C^T and P^{25} values and b) slope (s) of the C^T function with forced offset (o) as a function of clay plus silt fraction of the soil samples. Red: Loam (M4), Green: Clay (M6), Pink: Sand (M2), Blue: Sandy Loam (G1). Individual measurements on (a) are represented by the symbols, best fit trend lines are the solid lines, and fitted lines with an intersection at 16.8µs are dashed-dotted. The blue symbols on (b) represent the different soil types from all experiments, with a best fit trend line fitted to the data.

the observed data and ii) a best fit to the observed data for a function forced to intercept the x-axis at 16.8µs (Fig. 3.16a and Table 3.2). The period value of 16.8µs was the average $P_{0.0}$ value for all oven dried soil samples (irrespective of the particle size), with a standard deviation of 0.46µs. Moreover, the value was temperature independent for dry soils. Fig. 3.17 shows an application of these two temperature correction functions to the temperature effects

Table 3.2. Soil specific temperature correction parameters.

Soil Type	*Slope (fitted and with forced intercept)*	*Offset (fitted and with forced intercept)*
Sand	0.00345 / 0.00257	-0.05796 / -0.04318
Sandy Loam	0.00222 / 0.00393	-0.03730 / -0.06602
Loam	0.00872 / 0.00805	-0.14650 / -0.13542
Clay	0.00654 / 0.00757	-0.10987 / -0.12718
Silt Loam	0.01062 / 0.00825	-0.17842 / -0.13860
Clay Loam	0.00768 / 0.00841	-0.12902 / -0.14129

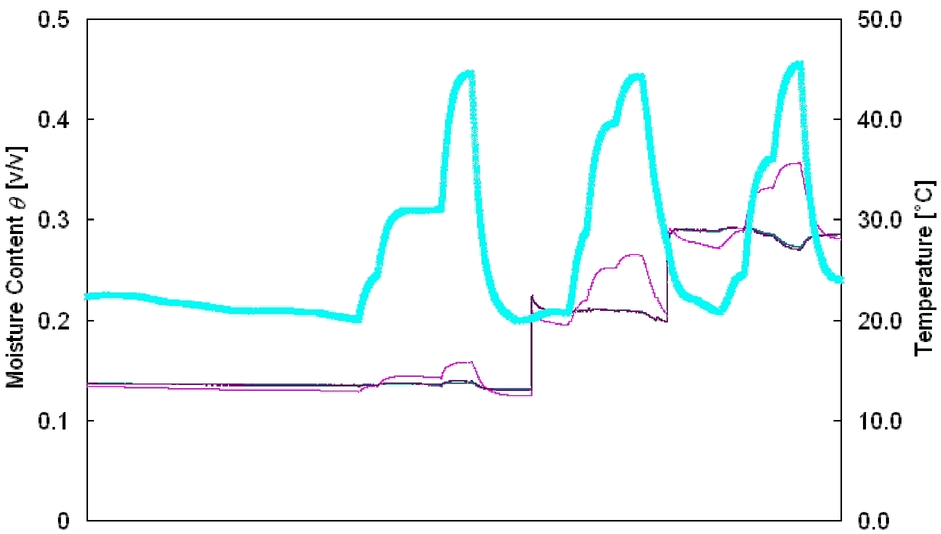

Figure 3.17. Influence of temperature (turquoise) on the observed (pink) soil moisture content. Temperature corrected soil moisture observations are shown in green (best fit) and blue (best fit with forced intersect).

observed for a loam (M4), with a significant temperature impact on the observed soil moisture content clearly seen. Moreover, the difference between the "best fit function" and "forced" correction functions is shown to be negligible. It was also found that the slope s of the temperature correction function could be related to the soil particle size distribution (Fig. 3.16b). As the soil types in the catchment are either sandy or clayey, no intermediate soil types were available and tested. To verify the results and particular the linear fit of Fig. 3.16b, a larger range of soil types has to be included in order to obtain a general relationship.

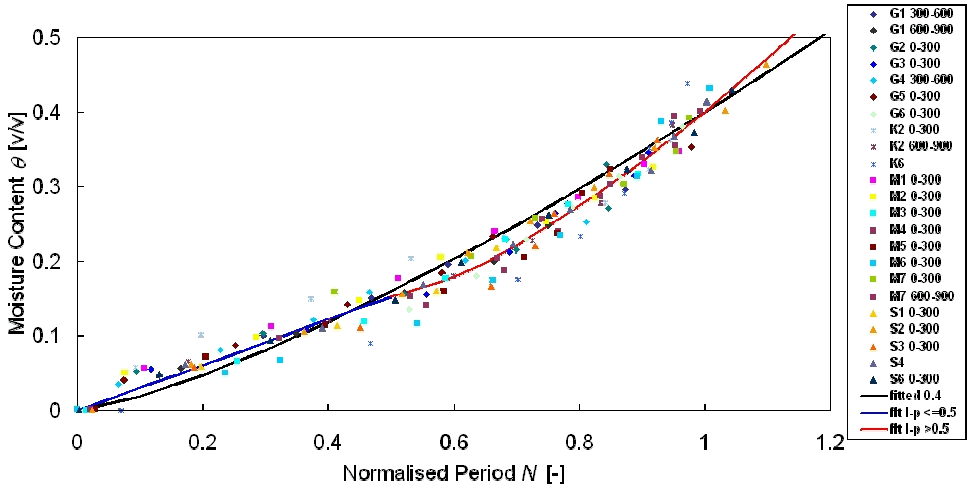

Figure 3.18. Relationship between normalised period and soil moisture content for the different soil moisture monitoring sites. The best fit function after Western and Seyfried (2005) is shown in black. The linear part of the new function is shown in blue and the non-linear part is shown in red.

Using the fitted particle size relationship for slope together with the offset term from the forced intercept, the temperature corrected period measurement for a loamy soil showed some overcorrection for the higher soil moisture content (Fig. 3.17). However, the error in the resulting soil moisture was found to be not more than the sensor's expected accuracy (±0.02v/v). All other soil types have smaller temperature correction errors and therefore this overcorrection was deemed acceptable.

3.2.4.6 *Revised Calibration Function*

As in Western and Seyfried (2005), the soil specific optimised $P_{0.4}$ values were obtained by jointly optimising equations (3.3) and (3.4) using a quasi-Newton optimisation that minimises the least square error of all soil samples, resulting in a curve of the observations normalised to 0.4 and collapsed onto a narrow band (Fig. 3.18). A minimum of 5 soil moisture observations were available for each soil type. The least square error was calculated from the difference between the gravimetric measurements in the laboratory and the calculated soil moisture content from eq. (3.3) and (3.4). The fitted curve was found to have a root mean square error (RMSE) of 0.023v/v, which is marginally better than the RMSE of 0.025v/v obtained by Western and Seyfried (2005) for the CS615. However, a visual analysis of the shape of the distribution of the values in Fig. 3.18 suggested that a linear relationship for $N \leq 0.5$ and a non-linear relationship for $N > 0.5$ would be more appropriate. In the majority of the soils tested, a value of $N = 0.5$ is near the transition point from free soil water to bound soil water, ie. near the wilting point (Wang and Schmugge, 1980). The wilting point was therefore used as the transition between a linear and a non-linear function.

Following this assumption, eq. (3.4) was modified to

$$\theta = \alpha N \qquad \text{for } N \leq 0.5 \qquad (3.8a)$$

and

$$\theta = 0.5\alpha + \left(\frac{0.4 - 0.5\alpha}{0.5^{\beta}}\right)(N - 0.5)^{\beta} \qquad \text{for } N > 0.5, \qquad (3.8b)$$

where α is the slope of the linear function. Calculating the $P_{0.4}$ and β values for eq. (3.8) resulted in an improved RMSE of 0.017v/v for the soil moisture calibration (Fig. 3.18). The different optimised $P_{0.4}$ values are given in Table 3.3 for seven soil types (averaged from all available $P_{0.4}$ values for the individual soils) and in Table 3.4 for all individual soil samples. In Fig. 3.19 the estimated soil moisture content is plotted against the observed soil moisture content, showing a good relationship between the two data sets.

In contrast to the findings of Western and Seyfried (2005) for the CS615, a strong correlation between optimised $P_{0.4}$ and soil type and/or density was found for the CS616 ($r^2 = 0.84$ for percentage clay+silt, $r^2 = 0.85$ for percentage sand, $r^2 = 0.89$ for density; Fig. 3.20). The application of the averaged values to soils, that were not part of the optimisation process (ie. the deeper soil samples were excluded for this process) resulted in a range of RMSEs for the individual samples of 0.013 to 0.046v/v, being the same range as the soil sample

Table 3.3. Soil type specific average optimised $P_{0.4}$ values.

Soil type	*$P_{0.4}$ [μs]*	*Std. Dev. [μs]*	*# of samples*
Sand	27.2915	---	1
Sandy Loam	28.0147	1.1863	4
Loam	40.3563	---	1
Clay	39.2833	1.3371	5
Silt Loam	33.0705	---	1
Loamy Sand	30.1702	---	1
Clay Loam	39.9405	2.6418	5

Table 3.4. Optimised $P_{0.4}$ values for all individual soil samples. The depth values correspond to the soil depth from which the samples were taken. The first $P_{0.4}$ value is the value obtained by optimising the simple non-linear function according to Western and Seyfried (2005) and the second $P_{0.4}$ value was obtained by optimising the new function. The soil types are: C – Clay, CL – Clay Loam, L – Loam, LS – Loamy Sand, S – Sand, SaL – Sandy Loam, SiL – Silt Loam, SC – Silty Clay.

Site	*Soil Type*	*Depth*	*$P_{0.4}$ (W&S)*	*$P_{0.4}$*
G1	SaL	300-600	31.9979	30.9944
G1	SaL	600-900	29.3738	28.8232
G2	SiL	0-300	33.9663	33.0761
G3	C	0-300	41.3296	40.1388
G4	SaL	300-600	27.2022	26.6669
G5	SaL	0-300	27.9118	27.5468
G6	CL	0-300	40.9520	39.6823
K2	LS	0-300	30.7458	30.4098
K2	LS	600-900	30.4849	29.9306
K3	C	0-300	39.1293	40.3067
K5	C	0-300	40.0411	37.0723
K6	CL	0-300	45.3478	44.7094
M1	SaL	0-300	28.2488	27.9364
M2	S	0-300	27.7113	27.2915
M3	CL	0-300	38.3421	37.1620
M4	L	0-300	41.6288	40.3563
M5	C	0-300	42.5362	40.8890
M6	C	0-300	40.7082	39.7318
M7	CL	0-300	42.5453	41.8521
M7	CL	600-900	39.4491	38.6910
S1	C	0-300	40.3480	38.6011
S2	CL	0-300	38.1013	37.8775
S3	not avail.	0-300	39.7388	38.4282
S4	not avail.	0-300	36.8656	36.3024
S6	SiC	0-300	37.4548	37.0558

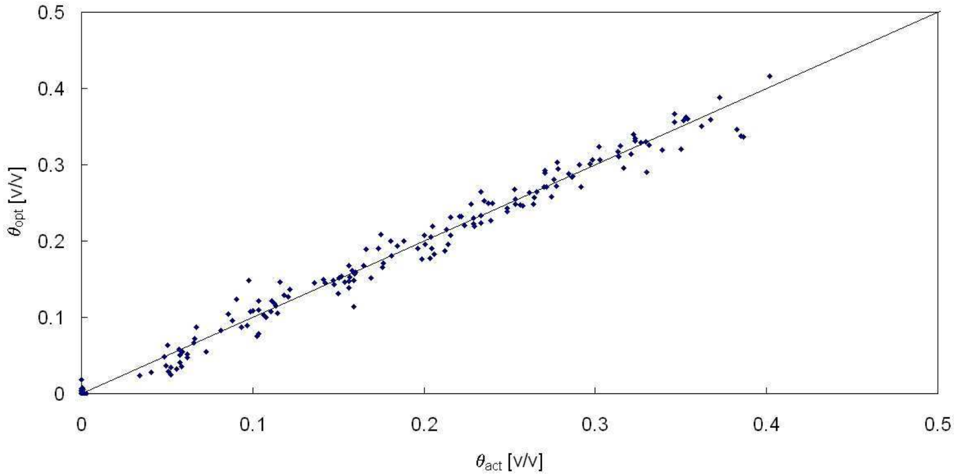

Figure 3.19. Correlation between estimated and observed soil moisture content.

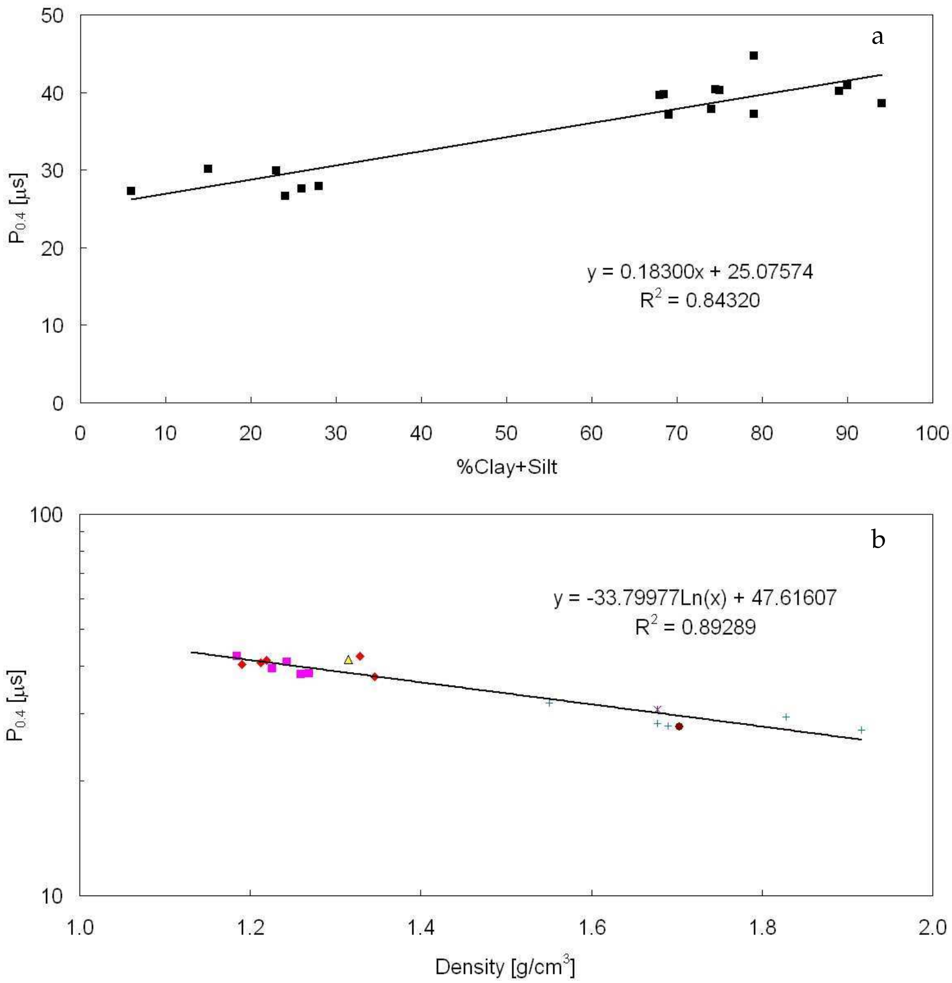

Figure 3.20. Correlation between a) clay and silt content and b) density with optimised $P_{0.4}$ values. In b) red diamonds represent clay, pink squares clay loam, yellow triangles loam, purple star loamy sand, brown circle sand, and green crosses sandy loam.

specific $P_{0.4}$ values. It was therefore concluded that the average soil type specific $P_{0.4}$ values in Table 3.3 may be used in eq. (3.4) to calculate the normalised period N. However, some of those averaged soil type specific values were obtained with only a few soil samples and therefore are in need of further verification (Table 3.3).

3.2.4.7 Salinity Correction

A further effect on the sensor response comes from changes in salinity. However, no salinity impact was observed for the soil samples, apart from one sample (K6), which was the only soil sample outside of the manufacturer recommended electric conductivity of 2dS/m (Table 3.1) threshold (Campbell Scientific Inc., 2002). While the results for the soil sample from K6 showed a significant impact of salinity on its signal, the other samples did not show any noticeable effects caused by salinity.

A recent study discussing the effects of salinity on CS615 sensor responses found bulk soil salinity to be an important factor, but no calibration relationship could be established from their data (Kim and Benson, 2002). Moreover, as only one site exceeded the manufacturer's threshold, a further calibration for salinity effects was not undertaken, as it would have been beyond the scope of this thesis.

3.3 AMSR-E Soil Moisture

The current instrument providing remotely sensed microwave observations is the Advanced Microwave Scanning Radiometer for Earth Observing Systems (AMSR-E) launched on 4 May 2002 on the Aqua satellite operated by the National Aeronautics and Space Administration (NASA). The microwave channels on AMSR-E are operating in the 6.925, 10.65, 18.7, 23.8, 36.5, 89.0GHz frequencies.

The most sensitive channel to surface soil moisture on board Aqua is the C-band channel (6.925GHz). The spatial resolution at 6.925GHz is 74km x 43km, but it has been binned to a 0.25°x0.25° geographic grid due to oversampling. The Aqua satellite is in a sun-synchronous orbit with approximately 14 orbits each day. However, due to significant radiofrequency interference in C-band, in particular over the United States, current soil moisture retrieval algorithms only use the channels above C-band (Njoku et al., 2003[1]). This higher frequency data is less sensitive to soil moisture changes and only represents the top few millimetres of the soil, rather than the 1 to 2cm layer observed at C-band.

Comparison of the obtained AMSR-E soil moisture product with the 0-300mm soil moisture observations at the monitoring sites located within the Goulburn River catchment shows that AMSR-E data lacks the expected dynamics, particularly during wet periods (Fig. 3.21), despite significant precipitation events after DoY 224. While the compared depths are significantly different to each other (300mm observed with the water content reflectometers against 1mm observed with AMSR-E) and are consequently difficult to compare, it would be assumed that the shallower depth of the satellite observations would provide a more significant response to precipitation than the deeper layers. Nevertheless, the impact of small or short precipitation events may not be observed by the satellite due to the overpass repeat rate of up to three days, during which the surface layer may undergo a wetting up and drying down.

[1] Near the completion of the write-up of this thesis a new AMSR-E soil moisture product was being made available to the author (de Jeu and Holmes, personal communication). This new soil moisture product was derived from the brightness temperatures at 6.925, 10.65 and 37GHz with a different algorithm than that used to create the product obtained for their use in the studies of this thesis (Njoku et al., 2003). Preliminary analyses of this new product showed a better correlation between in-situ measurements and satellite observations, than for the data developed with the algorithm by Njoku et al. (2003).

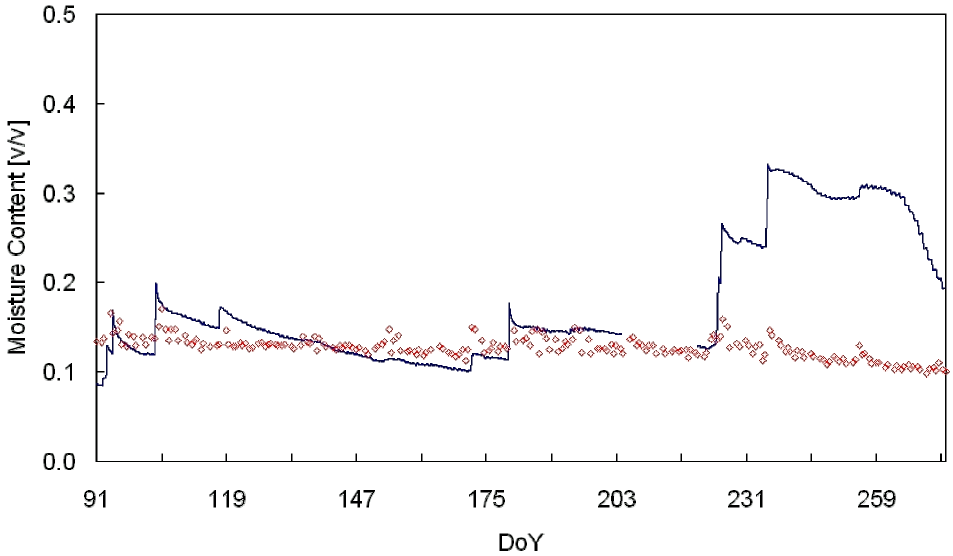

Figure 3.21. Comparison of AMSR-E surface soil moisture (red diamonds) and 0-300mm in-situ field observations for a 6 months period in 2003, including a dry and a wet period.

Furthermore, the AMSR-E footprint covers a relatively large area (see above) and point measurements were shown to have a high spatial variability throughout the Goulburn River experimental catchment. Therefore, a point measurement may represent local effects rather than the areal averages of a satellite footprint and may have a different response pattern.

However, the general trend of the observations in the first part of the year shows a good agreement between ground and space-based observations for the first part of the observation period. This general trend allows the AMSR-E data to be used in the assimilation of surface soil moisture into CLSM.

3.4 *Ancillary Data*

3.4.1 Vegetation Data

Vegetation information was obtained from Second Global Soil Wetness Project (GSWP-2) 0.25°x0.25° vegetation maps (Dirmeyer et al., 2002). The vegetation parameters required by the hydrologic land surface model are greenness and LAI. Catchment-wide in-situ observations of these parameters over a large temporal and regional scale are infeasible, as it would require detailed samples, analyses and manpower to achieve. Furthermore, high resolution information, if it were available, would have to be upscaled to (sub-) catchment scales, potentially introducing a further degree of error into the modelling.

3.4.2 Soil Parameters

All soil parameters required for CLSM, with the exception of soil depth, were obtained from the global Food and Agriculture Organisation (FAO) digital soil map at 5′×5′ resolution. These maps provide an overview of dominant soil types. The required soil parameter values have been determined from the study of Cosby et al. (1984). Consequently, these values contain inaccuracies due to factors such as the resolution of the maps from which they were derived and the pedotransfer functions used, as these are generally developed for global applications. While this does not affect the performance of the model in terms of synthetic studies, it may affect real studies and introduce a further bias due to the inherent uncertainty on the soil parameters.

A further source of soil parameter data is the Australian Soils Atlas (ASA; Northcote, 1960, 1979), from which average soil depths for the individual catchments were derived. While the ASA provides high resolution soil information it does not provide some of the parameters needed within CLSM. Therefore, to preserve consistency, the generic soil parameter values based on FAO data were kept for the simulations.

3.4.3 Elevation Data

The elevation data used to derive the compound topographic index (CTI; Gessler et al., 1995)) was extracted from the 9′′

(approximately 250m) DEM (Fig. 3.2) for all of Australia, which can be downloaded for free from the Geoscience of Australia website. Released in 2001, the current version of the DEM has had several alterations in order to improve data accuracy following a collaborative effort between the Australian Surveying and Land Information Group (AUSLIG, 2001) and the Centre for Resource and Environmental Studies (CRES) at the Australian National University.

3.5 Subcatchment Disaggregation

The disaggregation of the Goulburn River catchment into smaller modelling units or subcatchments initially followed the location of the stream gauges and the distribution of the dominant soil types throughout the catchment. Stream gauge locations coincide with subcatchment delineation as much as possible, however the stream gauges near the confluence of Krui and Goulburn, and Merriwa and Goulburn are located some distance upstream of the confluences to avoid an impact of the flow depth in the Goulburn River on the Krui and Merriwa Rivers.

For the purpose of the synthetic studies presented in this thesis, the Goulburn River catchment was split into 8 subcatchments, while 16 subcatchments were used for the field application (Fig. 3.22). The more detailed disaggregation of the main catchment for the field study became necessary, during the verification process of the model results for the field study (see section 7.4), because of problems with the correct modelling of the streamflow within the Goulburn River catchment. The single catchment synthetic study in Chapter 5 focuses on the upper Krui River subcatchment (Catchment 2). While the first part of Chapter 6 (multi-catchment synthetic study) comprises all three subcatchments of the Krui River (Catchments 2, 3 and 4), the second part comprises all 8 subcatchments of the

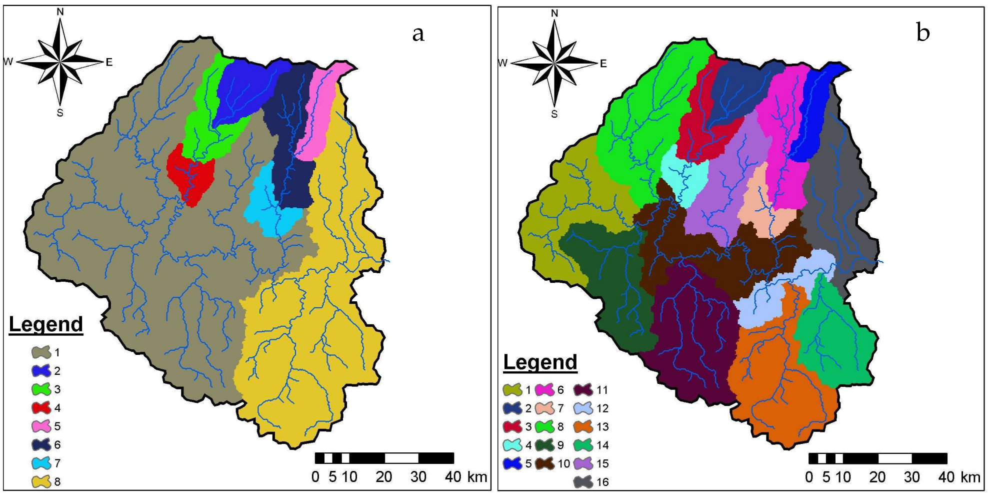

Figure. 3.22. Subcatchment disaggregation into a) 8 (synthetic data study) and b) 16 (real data study) subcatchments.

Goulburn River experimental catchment upstream from the stream gauge at Sandy Hollow.

For the real data study the catchment was further disaggregated into a total of 16 subcatchments. While the subcatchments in the Krui River and Merriwa River catchments remained as in the synthetic study, Catchments 1 and 8 were further disaggregated to allow a better representation of the soil conditions in the Goulburn River catchment. This further disaggregation split up the large subcatchments into all their respective subcatchments.

3.6 Intra-Station Variability of Soil Moisture

Sample data for 2004 from site M6 is shown in Fig. 3.23, with Fig. 3.23a showing the raw and temperature corrected period measurements and Fig. 3.23b showing the calculated soil moisture content. The data shows significant soil moisture changes for the CS616 installed in the first 300mm, with only minor changes for the sensor installed at 300-600mm. This figure also shows the effect of the drought throughout 2004 on the deeper soil moisture conditions, when hardly any recharge to the deeper soil layers occurred.

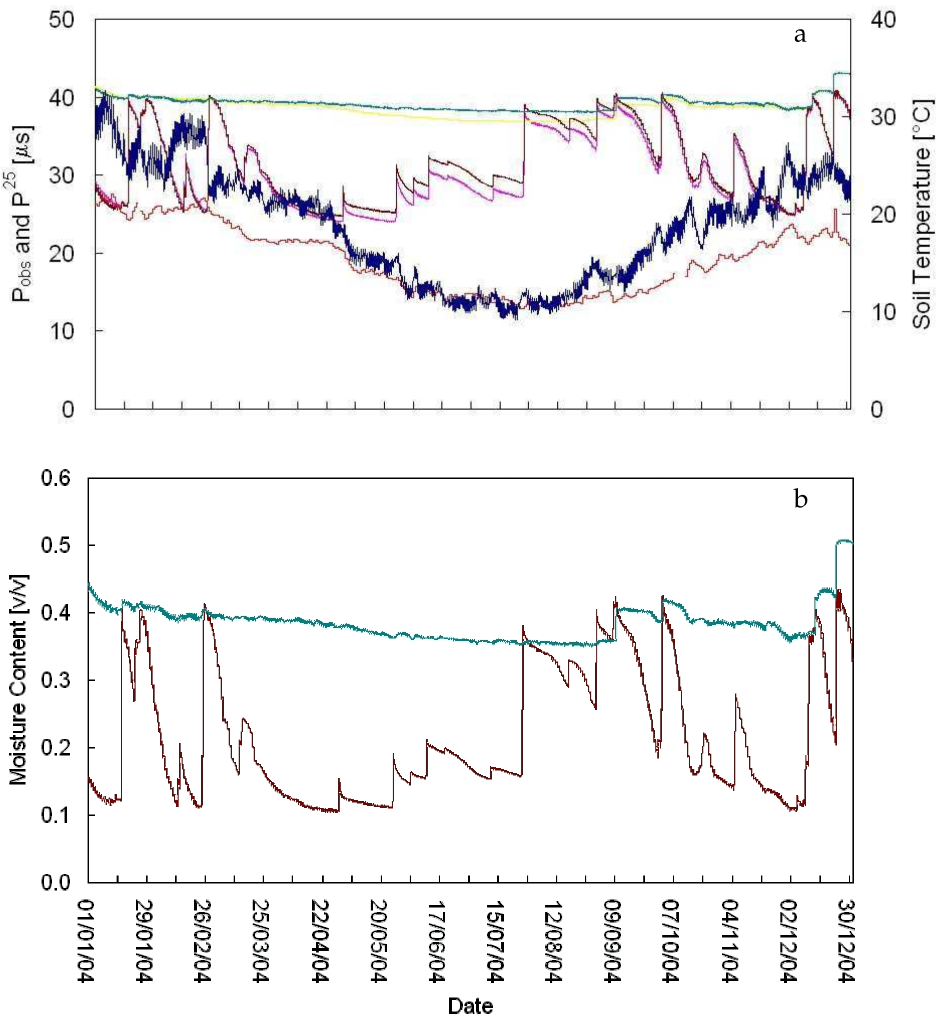

Figure 3.23. a) P_{obs} (for 0-300mm (pink) and 300-600mm (yellow)) and P_{25} (for 0-300mm (brown) and 300-600mm (green)) for the sensors at M6 at depths of 0-300 and 300-600, and the observed (blue) and estimated (red) soil temperature at 150mm and 450mm. b) Respective soil moisture content at 0-300mm (pink) and 300-600mm (green).

Fig. 3.24 shows the soil moisture variability for different soil moisture monitoring stations in the Goulburn River catchment. This variability is expected, considering the differences in soil type (see section 3.1). The RMSE of the observed root zone soil moisture at individual sites as compared to the average calculated from all sites from the Goulburn River catchment is shown in Fig 3.25. The density of monitoring sites within the whole Goulburn River catchment is approximately one site per 325km^2 and ranges from one site per 53km^2 to one site per 113km^2 in the smaller focus subcatchments. The variability presented here is calculated from all

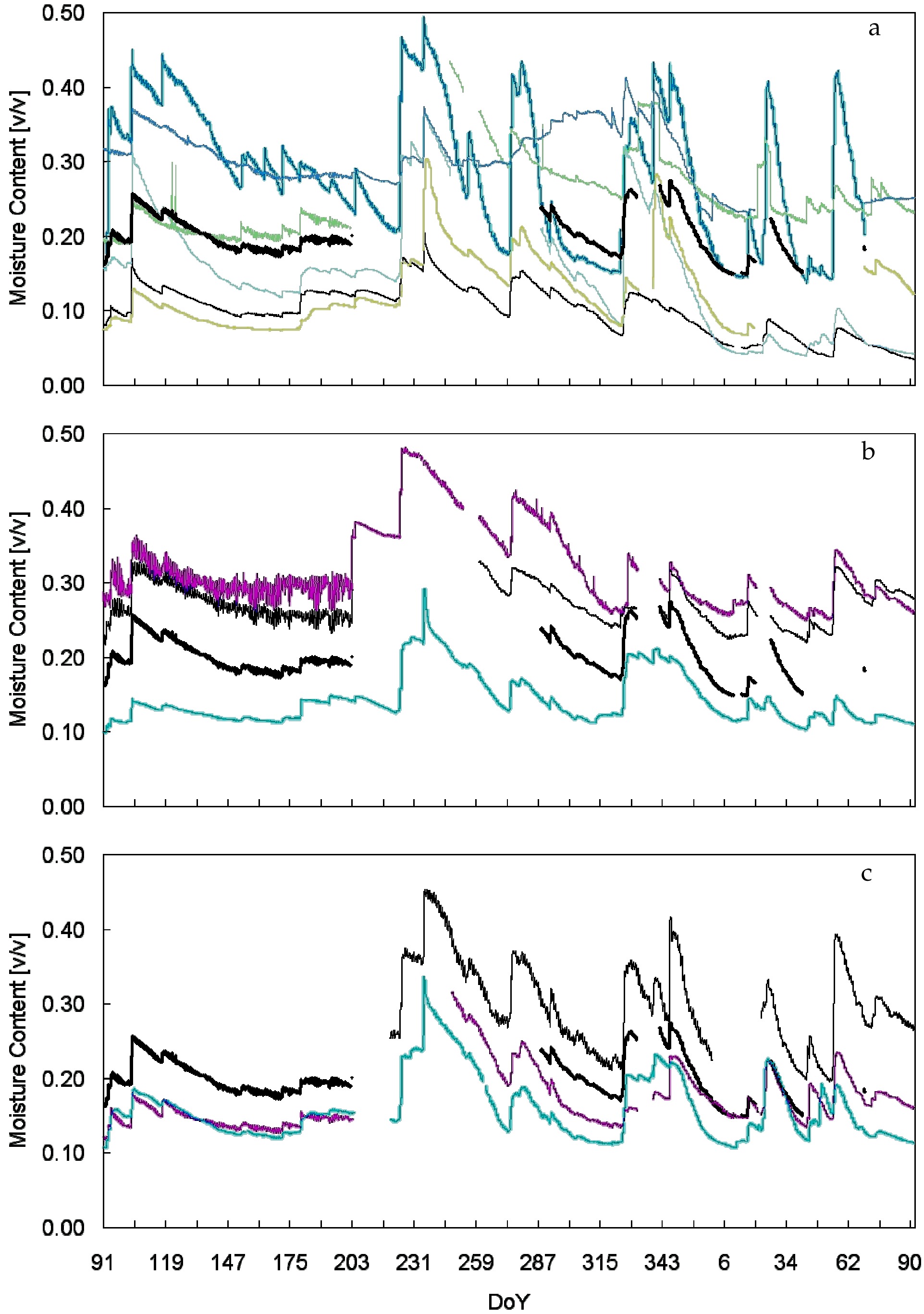

Figure 3.24. Average root zone soil moisture content for the Goulburn catchment (thick black line) and 17 soil moisture monitoring sites in a) the larger Goulburn River catchment, b) the Krui River catchment, and c) the Merriwa River catchment, for the 12-month period of 1 April 2003 to 31 March 2004.

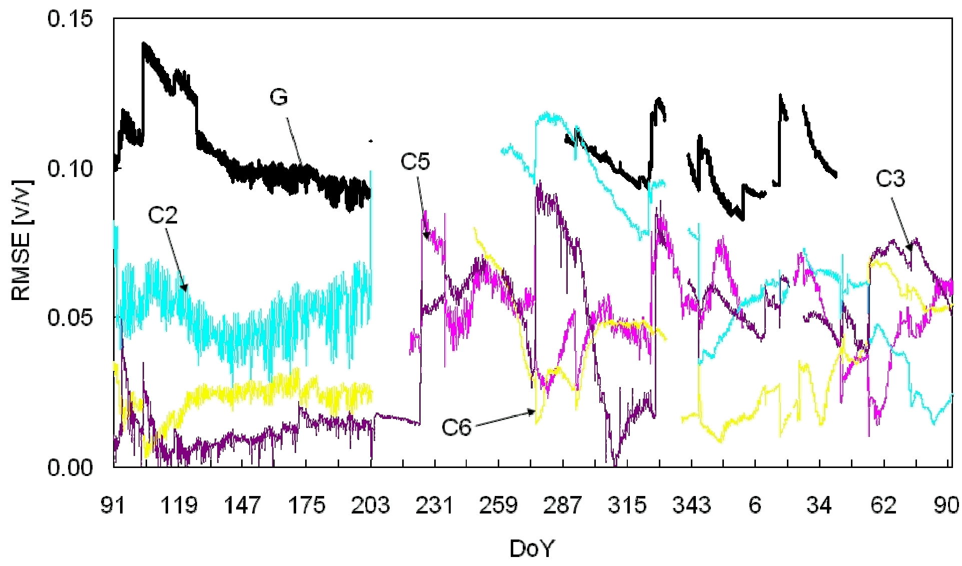

Figure 3.25. RMSE of the stations within the Goulburn (G; 1 soil moisture monitoring site per 325km^2), Catchment 2 (1 site per 108km^2), Catchment 3 (1 site per 113km^2), Catchment 5 (1 site per 56km^2) and Catchment 6 (1 site per 113km^2), for the 12-month period of 1 April 2003 to 31 March 2004.

the sites within a (sub-)catchment in relation from their calculated average root zone soil moisture within the respective (sub-) catchment. It is clearly shown that the higher density of sites within the subcatchments results in a smaller error, than in the main catchment with a lesser density of monitoring sites.

This statement is supported in Fig. 3.26a, where the error with increasing density of monitoring sites and for smaller, more homogeneous catchments is reduced. This is largely due to the two main soil types (clayey and sandy) within the Goulburn River catchment, which lead to a significant intra-station variability in the soil moisture observations at the stations throughout the catchment. Moreover, the spatial variability of the smaller catchments appears to vary around a value of about 0.05v/v.

To further the understanding of the overall error in the soil moisture, rather than its temporal evolution, the soil moisture content at the different monitoring sites were analysed in terms of their intra-station variability and the error when only a limited

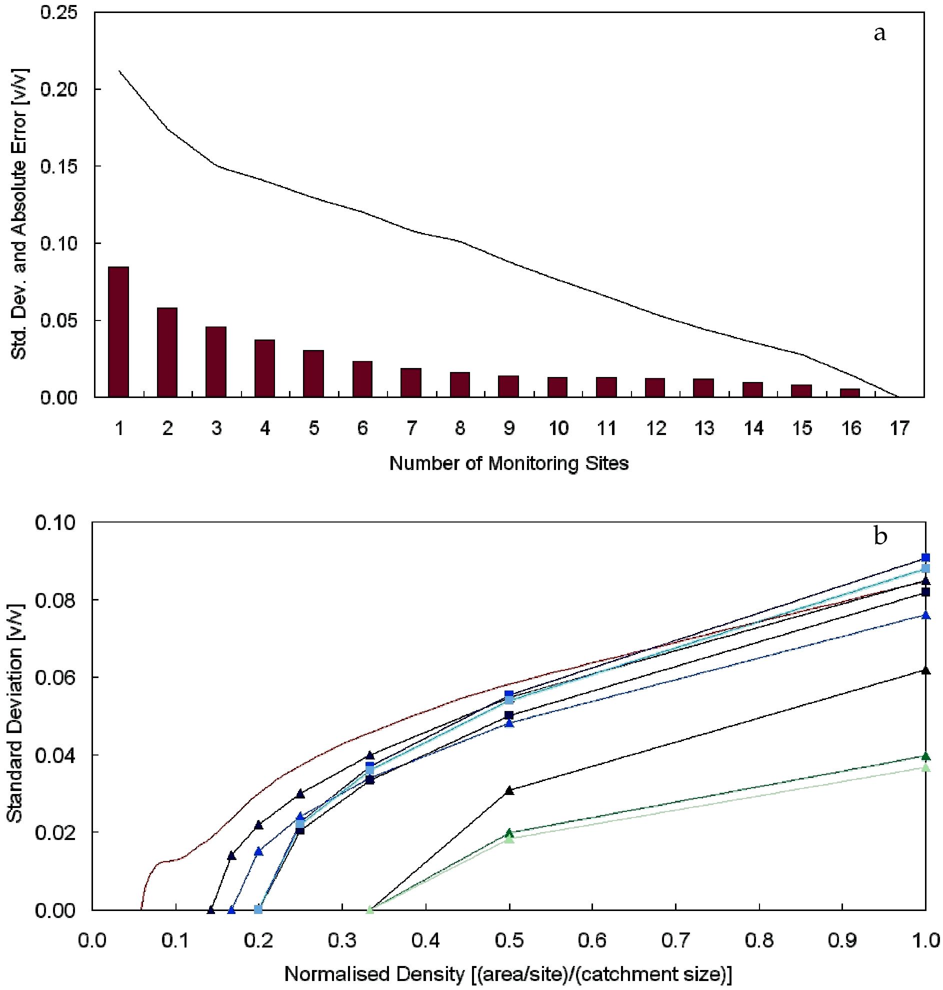

Figure 3.26. a) Maximum error (line) and standard deviation (columns) for soil moisture in the Goulburn River catchment, using observations from an increasing number of monitoring sites. b) Standard deviation of the soil moisture in the Goulburn (red line), the whole Krui (squares) and Merriwa (triangles) River catchments (blue lines), and the Merriwa River subcatchments (green lines). Lighter colours show increasing profile depth.

number of catchments are available to calculate the soil moisture average. In this analysis the deviation from the catchment-wide soil moisture average (which was calculated by using data from all 17 available monitoring sites) was determined, when using data from 1 up to 17 monitoring sites to calculate an estimated average. The number of available sites is limited, as the seven sites on the "Stanley" focus catchment are not regarded as seven individual sites, but rather as one single site. The total number of all possible combinations is shown in Table 3.5.

Table 3.5. Total number of possible combinations of soil moisture monitoring sites, given 17 available sites.

Number of Sites in Calculation	*Number of Combinations*
1 or 16	17
2 or 15	136
3 or 14	680
4 or 13	2380
5 or 12	6188
6 or 11	12376
7 or 10	19448
8 or 9	24310
17	1

The analysis was undertaken on three different levels. First all subcatchments containing two or more monitoring sites were studied, then the Krui and Merriwa Rivers subcatchments, and finally the whole Goulburn River catchment.

The results show that initially the addition of sites does significantly improve the standard deviation of the estimated soil moisture average (Fig. 3.26a). However, the higher the density of monitoring sites, the less significant the impact from additional monitoring sites on the standard deviation. For the Goulburn River catchment that level is achieved, when a combination of 8 monitoring sites or more are used. The standard deviation at this level is 0.016v/v, with a maximum error of 0.101v/v. The low standard deviation allows the conclusion that for a heterogeneous catchment such as the Goulburn River, a density of about 1 site per 800km^2 (8 sites per 6,540km^2, or one site every 28km) may be sufficient to estimate the catchment-wide soil moisture average.

Fig. 3.26b shows the normalised density (area per site divided by catchment area) plotted against the standard deviation to allow a direct comparison between the catchments. The change in the standard deviation is close to 0 between 8 and 13 monitoring sites and then increases again with 14 or more monitoring sites (Fig.

3.26a). This may be an effect of the two main soils types within the catchment, as the more homogeneous catchments of the Krui and Merriwa Rivers do not show the same behaviour.

An interesting aspect of Fig. 3.26b is that the initial change per added monitoring site appears to be similar for all catchment scales with a small offset between the different catchment dimensions, with the standard deviation becoming smaller for smaller catchments. However, this effect may be localised and other catchments and their respective subcatchments may show different behaviour. Therefore, further data from other catchments are required to support these results. Table 3.6 summarises the standard deviation, and the maximum error for all subcatchments and their respective soil moisture profiles for 0-300, 300-600 and 600-900mm, if all available sites within the specified catchments are included in the calculation of the catchment wide root zone soil moisture average. The maximum error and the standard deviation are significant throughout the catchments. This is due to the high spatial variability of soil texture, even in small catchments.

These results, in particular those for the smaller subcatchments, have an important significance for the discussion of the field study in Chapter 7. It is shown here that a high variability between the soil moisture observations at different monitoring stations exists even within small catchments and that the observations at two monitoring sites in a catchment vary significantly. As the chosen hydrologic land surface model calculates the lumped soil moisture in a catchment a direct comparison between the model results and the point observations will be limited, due to the catchment specific level of uncertainty in the representativeness of the observations.

Table 3.6. Summary of the absolute maximum error and standard deviation of the soil moisture observations for all subcatchments in the Krui River and Merriwa River catchments (for upper, middle and lower reaches and for the entity of the catchments), and the Goulburn River catchment.

Catchment		*# of Sites*	*Depth of Profile [mm]*	*Max. Error [v/v]*	*Stand. Dev. [v/v]*
Krui	Upper K4, K6	2	0-300	0.141	0.058
		2	0-600	0.123	0.061
		2	0-900	0.119	0.067
	Middle K3, K5	2	0-300	0.100	0.035
		2	0-600	0.085	0.041
		2	0-900	0.107	0.048
	Lower K2	1	0-300	Only one site	
		1	0-600	Only one site	
		1	0-900	Only one site	
	All	5	0-300	0.187	0.082
		5	0-600	0.205	0.091
		5	0-900	0.204	0.088
Merriwa	Upper M4, M6, M7	3	0-300	0.137	0.040
		2	0-600	0.091	0.042
		1	0-900	Only one site	
	Middle M2, M3, M5	3	0-300	0.188	0.062
		3	0-600	0.106	0.037
		1	0-900	Only one site	
	Lower M1	1	0-300	Only one site	
		1	0-600	Only one site	
	All	7	0-300	0.227	0.085
		6	0-600	0.201	0.076
		2	0-900	0.108	0.040
Goulburn	All	17	0-300	0.211	0.085
		15	0-600	0.250	0.088
		9	0-900	0.192	0.098

3.7 *Chapter Summary*

This chapter has described streamflow, meteorological and soil moisture observations collected within the Goulburn River experimental catchment for the modelling, assimilation and verification purposes of this thesis. Ancillary data has also been presented, including DEM, LAI, greeness, and long wave and short wave downwelling radiation. Furthermore, the calibration of streamflow gauges and soil moisture sensors has been presented. The lack of sufficient streamflow events throughout the duration of this thesis has prevented the development of reliable rating curves, with more observations required for verification purposes. Consequently, the additional streamflow data collected as part of this data set could not be used for quantitative purposes at this time.

The collected data consists of long-term meteorologic, soil moisture, and streamflow observations over a relatively large scale, making it an important data set. As monitoring will continue until the end of 2007, this data set will have significance for other projects dealing with soil moisture and climate modelling. For that reason, the data are being made accessible on the internet at www.sasmas.unimelb.edu.au.

Chapter Four

4 Models

The land surface assimilation scheme proposed in Chapter 1 and 2 for climate model initialisation requires the selection of i) suitable land surface and routing models, and ii) an appropriate assimilation approach. This chapter provides a brief discussion of available models and approaches before describing the land surface model, the routing model and the assimilation approach selected for the research described in this thesis.

4.1 Soil Moisture and Streamflow Model Requirements

For the modelling of streamflow, soil moisture, sensible heat flux and evapotranspiration, a model is required which provides these variables as diagnostic variables, so that observations can be compared to model output. Furthermore, the assimilation of streamflow and surface soil moisture requires that soil moisture content, or another variable representing the soil moisture state in the model, is available as a prognostic variable.

4.2 Review of Land Surface Modelling

4.2.1 General Discussion

The list of hydrologic models available is endless, ranging from simple rainfall-runoff models to complex LSMs, dealing with a multitude of input parameters. Rainfall-runoff models, such as SimHYD (Chiew et al., 2002) or the Hydrologic Research Center Distributed Hydrologic Model (HRCDHM; Carpenter et al., 2001) are not appropriate for the research of this thesis, as they do not model surface-to-atmosphere energy and water fluxes – which are required in modelling climate feedback –, but rather require evapotranspiration as model forcing data. Furthermore, a large number of rainfall-runoff models only deal with one soil layer (eg. SimHYD; IHACRES, Jakeman et al., 1990, Jakeman and Hornberger, 1993). As one aspect of the present thesis is the assimilation of information in addition to streamflow observations, such as remotely sensed surface soil moisture, a multi-layer model is essential. Therefore, the focus of this discussion is on LSMs that comply with the requirements of this thesis (modelling of energy and water fluxes and runoff, and providing model results from different soil layers).

Within the last three decades LSMs have undergone a significant evolution. Pitman (2003) groups LSMs into three generations, based on the definitions of Sellers et al. (1997). First-generation models such as the bucket model by Manabe (1969) were simplified water and energy balance models that were not capable of accurately modelling the diurnal or seasonal cycles of the energy and water balances. Furthermore, soil depth and water capacity were assumed to be constant and a soil moisture threshold was defined below which evapotranspiration was limited. Second-generation models are defined as those capable of simulating temperature and soil moisture in multiple layers and including a heat and moisture transfer from the vegetation to the atmosphere. However, Pitman (2003) points out that the major limitation of second generation LSMs is their empirical representation of canopy conductance, which led to the inclusion of plant physiology into third-generation LSMs.

The various models are further divided into distributed and lumped models. Distributed models perform a full energy and water balance for each modelled cell (a cell represents the modelling unit at the model resolution) individually (eg. the Interactions between the Soil Biosphere and Atmosphere model (ISBA; Noilhan and Planton, 1989)). These cells are disaggregated in some LSMs into tiles and surface covers (eg. ISBA; Variable Infiltration Capacity model (VIC; Wood et al., 1992; Liang et al., 1994), Mosaic LSM (Koster and Suarez, 1992, 1996)). On the other hand, lumped or semi-distributed models such as the Catchment Land Surface model (CLSM; Koster et al., 2000b) account for the spatial variability within their cells implicitly rather than explicitly. This is achieved using probability density functions, which are functions of the average soil moisture content within the modelled catchment, or information from the dominant soil or vegetation type.

Out of the large number of different LSMs (and consequently different model philosophies), it is necessary to identify a model that is suitable for the purpose of this thesis (see section 4.1), since the aim of this project is not to produce a new hydrologic model, but rather to improve the performance of existing models. Most hydrologic models support only one type of surface runoff generation (either infiltration (Horton, 1933 and 1940; see Beven (2004) for a detailed review) or saturation excess (Dunne and Black, 1970) runoff). Those models have performed well when their respective runoff generation scheme dominated the runoff generation processes within the catchment, but faced inaccurate results when the hydrologic conditions changed (Nijssen et al., 1997; Lohmann et al., 1998). Consequently, it is imperative to identify models that consider both processes. Additionally, it is preferred to use a LSM, which has been used in climatologic studies.

4.2.2 Model Selection

The above discussion has reduced the number of possible LSMs for the use in this thesis considerably. Two models comply well with the requirements of this thesis: i) VIC and ii) CLSM. In this section, both LSMs are first briefly compared. While VIC has been proven to work well at both small (e.g. Wooldridge et al., 2001) and global (e.g. Lettenmaier, 2001) scales, CLSM has mainly been applied in continental or global studies (eg. Koster et al., 2004). Considering the scale of the Goulburn River catchment (~6500km^2), this would suggest the use of VIC as the most appropriate model. However, the more complex structure of VIC leads to a contrary decision which will be discussed in the remainder of this section.

Since the objective of this thesis is the assimilation of streamflow to retrieve soil moisture within a catchment, the semi-distributed approach of VIC with different vegetation types within a modelling unit, significantly increases the number of retrieved soil moisture states, and therefore leads to a significant under-determination of the retrieval process. This is the case, because tiling of the vegetation types requires either the retrieval of the individual soil moisture states in each of the vegetation tiles at the same time, or a disaggregation algorithm to transfer a single catchment-wide average soil moisture state into the different soil moisture states in the vegetation tiles. The advantage of CLSM in this case is the use of three prognostic variables to account for the soil moisture distribution throughout the catchment. Consequently, the assimilation scheme has to determine only these three variable states (from which the soil moisture states are calculated) to allow for a retrieval of the soil moisture within the catchment.

The alternative use of a single average value for the soil moisture states is not adequate for VIC, as it would adversely affect the evapotranspiration rates from the different tiles, because their soil moisture states would not be individually modelled. On the other hand, the retrieval of a larger number of soil moisture states from one single streamflow observation creates an underdetermined system to be solved by the assimilation scheme, which will cause difficulties in the accuracy of the soil moisture retrieval.

The main advantage of VIC over CLSM in regard of their respective use in GCMs is the explicit treatment of different vegetation types through tiling of the modelling units rather than having the area covered by the dominant vegetation. However, as explained above this causes significant problems for the approach presented in this thesis. Moreover, the aim of this thesis is the general proof of concept of streamflow data assimilation. For this purpose a "simpler" LSM is sufficient.

The number of parameters required as direct input parameters by VIC far exceeds those of CLSM. While additional parameters may be seen as an advantage, because of improved representation of the physical processes, it is usually a disadvantage due to the limited amount of information on vegetation processes and plant species both globally and in the Goulburn River experimental catchment. A detailed calibration of VIC would require a thorough study of the vegetation conditions in the catchment, which is beyond the scope of this thesis.

Finally, and most importantly, CLSM has been used in combination with climate model research (Koster and Suarez, 2003; Koster et al., 2004) and in data assimilation studies (Sun et al., 2004; Walker and Houser, 2004; Ni-Meister et al., 2006). Therefore, CLSM was chosen as the LSM used in this thesis.

4.3 Catchment Land Surface Model (CLSM)

The Catchment Land Surface Model (CLSM; Koster et al., 2000; Ducharne et al., 2000) is a catchment-based land surface model (LSM), which unlike traditional land surface models uses catchments as modelling units, rather than grid cells. As diagnostic model predictions, CLSM produces catchment-wide averages of soil moisture content and energy fluxes and surface runoff. The effects of subscale variability on infiltration, surface runoff and energy fluxes are treated explicitly in three different zones (saturated, unsaturated, water-stressed), using topographic information from a DEM. This topographic information is derived from the compound topographic index (CTI), which represents the topographic features of the upstream terrain within a catchment through a function of runoff-contributing upstream area and slope

$$CTI = \ln\left(\frac{a}{\tan\beta}\right), \tag{4.1a}$$

with

$$a = \frac{A_u}{w_p}, \tag{4.1b}$$

where a is the area contributing to the runoff at this point (A_u) per unit contour length (w_p) upstream of the point of interest; and β is the local slope.

The hydrology of CLSM is based on the TOPMODEL approach (Beven and Kirkby, 1979), with which the average water table depth is calculated within the catchment. Combining the knowledge of the catchment-average water table depth ($\bar{d}$) and the statistical information of the CTI within the catchment, the water table depth at any point within the catchment is estimated with

$$d = \bar{d} - \frac{1}{\nu}\left[\ln\left(\frac{a}{\tan\beta}\right) - \bar{x}\right], \tag{4.2}$$

where d is the local water table depth [m]; ν is a parameter describing the change with depth of the hydraulic saturated conductivity [1/m]; and $\bar{x}$ is the mean value of the CTI within the catchment. The units of the variables presented in this section are in accordance with their definition in CLSM (Koster and Suarez, 1996; Koster et al., 2000) and are not further simplified.

Because the TOPMODEL approach assumes equilibrium soil moisture profile conditions (a soil moisture profile in equilibrium is the condition, when the pressure head gradient and gravity are in balance and is only changed by changes in the soil moisture content due to infiltration or evaporation and transpiration), modifications were required to allow for nonequilibrium conditions, caused by water fluxes within the soil. For that purpose, Koster et al. (2000) introduced three prognostic variables, that allowed to describe the water profile and the nonequilibrium conditions. The introduced prognostic variables implicitly describe the equilibrium water content of the soil layer, and the short term changes in the soil moisture storage within the catchment. Those three prognostic variables are: i) the catchment deficit, which represents the amount of water that would have to be added to the current soil moisture condition per unit area to achieve saturation of the soil (a catchment deficit of 0 represents a fully saturated soil); ii) the root zone excess, which represents any short term change in the storage of water in excess of or lacking the amount of water calculated from the water balance equilibrium in the root zone; and iii) the surface excess, which represents, similarly to the root zone excess, any short term changes to the water balance in the top soil layer (Fig. 4.1).

The catchment deficit is determined by using the information on the water table depth and the actual soil moisture content profile above the water table. The soil moisture profile above the water table is determined by the equilibrium equation of Clapp and Hornberger (1978)

$$w(z) = \left(\frac{\psi_s - z}{\psi_s} \right)^{-\frac{1}{b}}, \tag{4.3}$$

where $w(z)$ is the water content [v/v] at depth z [m] above the water table; ψ_s is the matric potential [m]; and b is a soil parameter defining the shape of the soil moisture profile above the water table [-]. The

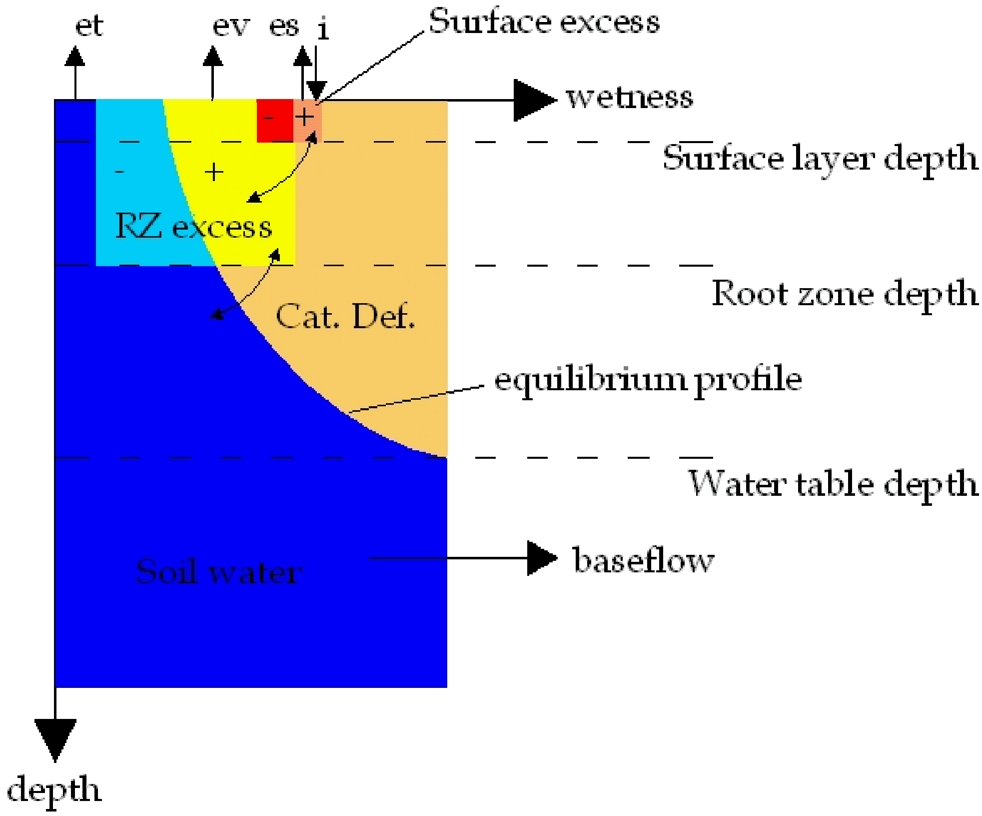

Figure 4.1. Schematic of CLSM, showing the water fluxes from the different soil layers, with evapotranspiration from the moisture profile (et), transpiration from the root zone (ev), infiltration into the surface layer (i) and bare soil evaporation from the surface layer (es). Furthermore, the equilibrium water profile is plotted. Positive and negative surface and root zone excesses are highlighted in the upper part of the soil (after Walker and Houser, 2001).

integration of 1-$w(z)$ above the water table yields the local moisture deficit at any point. Given the variability of the soil moisture (and consequently the local moisture deficit D) throughout the catchment (Fig. 4.2), an integration of the local moisture deficit over the catchment yields the catchment deficit with

$$M_D = \frac{1}{A}\int_A D dA, \qquad (4.4)$$

where M_D is the catchment deficit; A is the total catchment area; and D is the local moisture deficit.

While the calculation of the catchment deficit assumes a water profile in equilibrium, root zone and surface excess values allow for

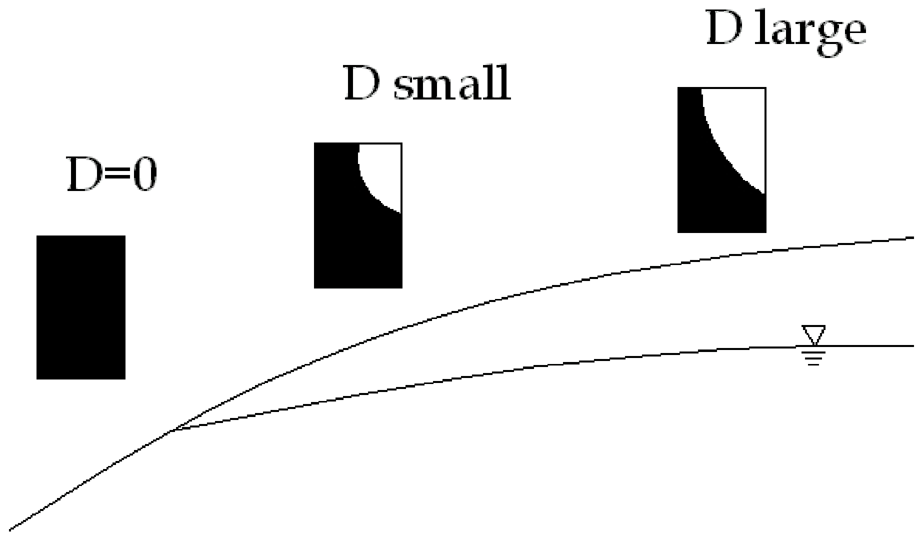

Figure 4.2. Distribution of the local moisture deficit throughout a catchment (after Koster et al., 2000).

the definition of the nonequilibrium soil moisture conditions, ie. mean short-term soil moisture content deviations from the average conditions in surface and in root zone layer. Both values represent the soil moisture response to infiltration and evapotranspiration of precipitation water. While the root zone excess quantifies the departure of the soil moisture conditions in the root zone from the equilibrium, any surface excess quantifies the soil moisture conditions of the surface layer relative to the root zone excess. In case of infiltration the root zone and surface excess values are both positive and in case of evapotranspiration both values are negative, and an excess of 0 means that the respective layers do not show any deviation from the equilibrium soil moisture profile.

The moisture transfer between the surface layer and the root zone, and between the root zone and the catchment deficit takes place if the root zone and surface excesses are out of equilibrium (ie. not 0). In the case of a positive excess value, water is transferred to the lower layer. Vice versa, if the excess values are negative, water is transferred into the respective water store where there is a deficit. When water is transferred into the moisture profile (decreasing catchment deficit), the depth to the water table decreases (i.e. the water table rises). Similarly, when water is transferred from the profile into the root zone the depth to the water table increases. This again shows the differences between the catchment deficit and the excess values. The catchment deficit is the theoretical average representing the whole soil moisture profile, while the excesses are only deviations from this profile in the respective layer, which impact on the profile only due to water transfer between the layers, occurring after the disturbance in the equilibrium. The equations for moisture transfer from the surface soil to the root zone layer and from the root zone to the soil profile are given as (Koster et al., 2000)

$$\Delta M_{rz} = -\Delta M_{se} = M_{se} \frac{\Delta t}{\tau_2} \tag{4.5a}$$

$$\Delta M_D = \Delta M_{rz} = -M_{rz} \frac{\Delta t}{\tau_1} \tag{4.5b}$$

where M_{rz} is the root zone excess [mm]; M_{se} is the surface excess [mm]; M_D is the catchment deficit [mm]; Δt is the time step [s]; and τ_1 and τ_2 are empirical time scale parameters [1/s], defining the moisture transfer rate between the soil layers. Note that a decrease in the surface layer excess leads to an increase in the root zone excess, so ΔM_{rz} and ΔM_{se} have different signs. Note also that an increase in the root zone excess leads to a decrease in the catchment deficit, therefore ΔM_{rz} and ΔM_D are both positive. The moisture transfer rates τ_1 and τ_2 between M_D, M_{rz} and M_{se} are determined, prior to the model runs, in offline calculations for a wide range of combinations of catchment deficit and excesses. The offline calculation of the time scale parameters avoids the necessity to solve Richards' equation at every time step, decreasing computational requirements. Given the water transfer equations 4.5a and 4.5b, the water balance equations for the three prognostic variables are thus

$$M_{se}^{t+1} = M_{se}^{t} - \Delta M_{se}^{t} + i - es \,, \tag{4.6a}$$

$$M_{rz}^{t+1} = M_{rz}^{t} + \Delta M_{se}^{t} - \Delta M_{rz}^{t} - ev \text{, and} \tag{4.6b}$$

$$M_{D}^{t+1} = M_{D}^{t} - \Delta M_{rz}^{t} + G + et \text{,} \tag{4.6c}$$

where the superscripts t and $t+1$ denote the beginning and the end of the respective time step; i is the infiltration [mm]; es is the bare soil evaporation [mm]; ev is the vegetation transpiration [mm]; G is the baseflow [mm]; and et is the evapotranspiration [mm].

The knowledge of the prognostic variables and their probabilistic distribution throughout the catchment allows the calculation of the saturated, unsaturated (soil moisture between saturation and wilting) and water-stressed (soil moisture reaching the wilting point) areal fractions of the catchment. Saturated and unsaturated areal fractions are only determined when the water table is located above the bedrock. Ducharne et al. (2000) present a detailed study on the development of the τ_1 and τ_2 and the derivation of the probability density functions (pdf) required to determine these areal fractions.

Precipitated water is first routed through an interception reservoir with a capacity of

$$W_r = 0.1 L_t \text{,} \tag{4.7}$$

where W_r is the interception reservoir [kg/m^2]; and L_t is the leaf area index of the vegetation type in the catchment [m^2/m^2]. Consequently, the throughfall P_t is defined as

$$P_t = P - W_r \text{,} \tag{4.8}$$

where P is the total precipitated water [kg/m^2]. Where infiltration takes place, the infiltration rate (i) is set equal to P_t. The relationship between W_r and L_t was chosen arbitrarily, but is consistent with the requirements of the Project for Intercomparison of Landsurface Parameterization Schemes (PILPS; Henderson-Sellers et al., 1993).

In CLSM, surface runoff from the catchment is taking place instantaneously during the time step of the precipitation, with the three areal fractions of the catchment contributing with different processes to the runoff production. While all throughfall is transferred into surface runoff over saturated areas (eq. 4.9a), unsaturated areas only contribute with a fraction of their area to the surface runoff (eq. 4.9b), and water-stressed areas do not contribute to surface runoff at all. Furthermore, in the case of a negative surface excess (dryness) none of the unsaturated area contributes to surface runoff. This leads to the following equations for the surface runoff production:

$$Q_s = P_t A_{sat} \qquad \text{for } M_{se} \leq 0 \qquad (4.9a)$$

and

$$Q_s = P_t \left(A_{sat} + A_{tr} \frac{M_{se}}{M_{se-\max}} \right) \qquad \text{for } M_{se} > 0, \qquad (4.9b)$$

where Q_s is the surface runoff [kg/m^2]; A_{sat} is the fraction of the saturated area [m^2]; A_{tr} is the fraction of the unsaturated area [m^2]; and $M_{se\text{-max}}$ is the maximum value of the surface excess [mm]. While saturation excess runoff is explicitly modelled, the linear change of the contributing area in eq. 4.9b implicitly represents infiltration excess runoff production (Koster et al, 2000). Baseflow from the catchment is only produced, when the water table is located above the bedrock with

$$G = \frac{K_s(surface)}{\nu} e^{-\bar{x}-\nu\bar{d}} \qquad (4.10)$$

where G is baseflow [m/s]; $K_s(surface)$ is the saturated hydraulic conductivity of the surface soil layer [m/s]; ν is a parameter describing the change with depth of the hydraulic saturated conductivity [1/m]; $\bar{x}$ is the mean value of the CTI within the catchment [-]; and $\bar{d}$ the average water table depth [m]. No

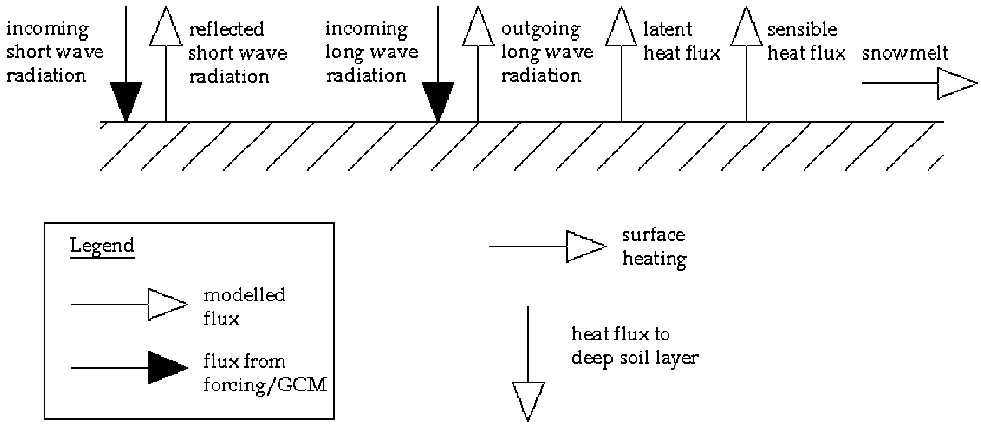

Figure 4.3. Schematic of the energy balance calculations within CLSM, with required forcing data input and internally calculated energy fluxes (after Koster and Suarez, 1996).

baseflow is produced, when the water table is located below the bedrock.

The energy balance within CLSM is calculated at each time step by a one-dimensional soil-vegetation-atmosphere-transfer model (Fig. 4.3), individually for each of the three areas (saturated, unsaturated, and water-stressed) (Koster and Suarez, 1992, 1996). The magnitude of the resistance changes with changing soil moisture conditions, as the resistance to these processes is soil moisture dependent (the resistance is set to small non-zero values for saturated areas, and to moderate values in the unsaturated areas). Both, evaporation and transpiration are completely shut off when the soil becomes water-stressed.

The three areal fractions maintain their individual surface temperatures at the surface (soil surface and canopy). However, the soil heat flux calculations in the deeper soil layers are performed for the catchment as a whole, as it is assumed that deeper soil temperatures do not have any spatial variability (Fig. 4.4; snow is shown on this schematic for a complete representation, though it was not required in the study of this thesis). The heat flux transfer between the soil layers is calculated through linear diffusion,

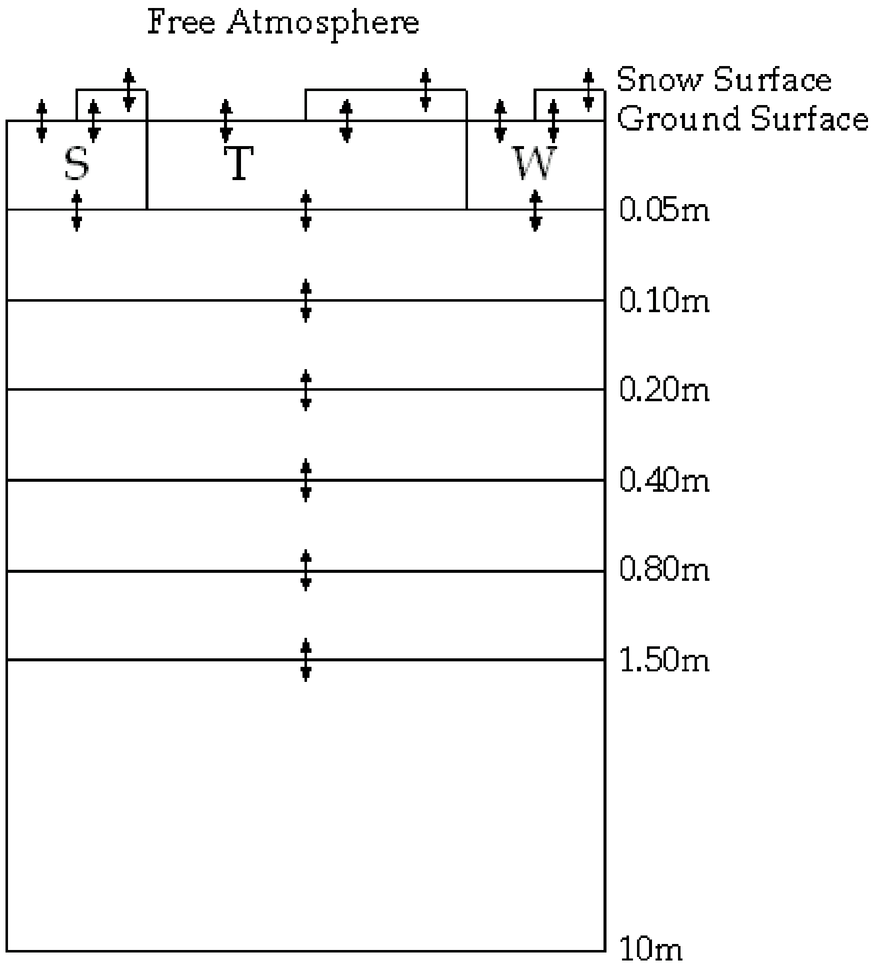

Figure 4.4. Schematic of the thermal heat flux calculations within CLSM (after Koster et al., 2000). The areal fractions are represented by S (saturated), T (transient – unsaturated), and W – water-stressed.

according to the heat gradient between the two adjacent layers. The three different heat fluxes from the surface soil layer to the second single layer are averaged according to the areal fraction of the overlying soil moisture condition (saturated, unsaturated, water-stressed), so that

$$HF_t = \sum_{n=1}^{3} f_n HF_n \,, \qquad (4.11)$$

where HF_t is the total heat flux and HF_n is the heat flux from the respective areal fraction n [W/m^2]; and f_n is the value of the areal fraction n.

The forcing parameters in CLSM are long wave and short wave downward radiation, wind speed, precipitation, air temperature, air saturation, and vapour pressure. In this thesis, apart from the radiation forcing which is in 6-hourly time steps, all forcing input data are provided in 20-minute time steps. A detailed description of the forcing data is given in Chapter 3. In addition to the forcing data, vegetation and soil parameters have to be prescribed to the model. For the vegetation, these are provided by monthly average of greenness and leaf area index (LAI) of the modelled catchments, obtained from external data banks. The required soil parameters are the soil depth, porosity, wilting point, saturated hydraulic conductivy of the soil surface, and matric potential. Generally, these parameters are obtained from global vegetation and soil maps. The soil parameters are used to calculate the maximum catchment deficit, the maximum value of the surface and root zone excesses, and the time scale parameters τ_1 and τ_2.

For further details, exceeding the scope of this model description, the reader is referred to Koster and Suarez (1992, 1996), who give a detailed description of the energy transfer component of the model; to Koster et al. (2000), who give a full model description of CLSM; and to Ducharne et al. (2000) who present the derivation of the model parameters described in this section.

4.4 *Routing Model*

4.4.1 General Discussion

Most LSMs (including CLSM) do not generally include water runoff routing, but rather produce an instantaneous, lumped runoff value from each grid cell or catchment. However, runoff from a catchment at the catchment outlet does not coincide with the precipitation over the catchment. Runoff is rather a variable distributed over time, as a function of antecedent soil moisture, surface conditions and precipitation intensity and may occur several hours or days after the precipitation event took place. Consequently, it is necessary to incorporate a routing model into the hydrologic model, in order to rout the runoff through the catchment structure (through surface, subsurface and streamflow routing). Moreover, Georgakakos and Bras (1982) showed that especially under relatively dry conditions, with only few major flood events (such as in the Goulburn River experimental catchment), the routing model is important for the performance of the whole model. Therefore, a detailed analysis of existing models is required for the study reported in this thesis.

Routing models are divided into two major categories: i) linear (unit hydrograph, fixed parameters in time) (Jakeman et al., 1990; Lohmann et al., 1996; Olivera et al., 2000), and ii) non-linear routing models (routing of water through each individual grid cell, surface runoff-soil moisture interactions, variable parameters through time and space) (Moore and Grayson, 1991; Atkinson et al., 2003; Ducharne et al., 2003).

A requirement for non-linear models is the explicit knowledge of the soil moisture content in each individual pixel (in a distributed LSM). However, complex non-linear models a) require more computational resources, b) influence soil water contents along the river due to their interaction with the surroundings, and c) require the knowledge of soil moisture at any time within each individual grid cell. In particular the latter is in contrast to the discussion in the previous sections, where it was decided that a distributed model will not be used in this thesis. Consequently, the following review concentrates on the use of linear routing models.

Stewart et al. (1999) showed that several processes influence the way a flood wave propagates in a river system and introduced a complex finite element model in order to model flood behaviour. Detailed information on the streambed conditions are required to allow for the application of this model, yet such information is not available in the present case. On the other hand, Arnell (1999) used a linear routing model, where the runoff from one cell was defined as being uncorrelated to the next cell. The runoff in each cell was modelled independently of any neighbouring cells and the parameter calibration was independent of streambed information. Arnell (1999) defined catchments, rather than pixels of a LSM as cells, which is the same philosophy as in CLSM. However, while Arnell's (1999) model showed good results for humid areas (England and Ireland), it encountered some problems for dry (SW France) and nordic (Norway; frozen soils) regions. This may have been an effect of calibrating fixed routing parameters to monthly streamflow events, without taking into account the high variability of the surface and stream conditions in regions with ephemeral streams.

Other linear models have been described in the literature by Jakeman et al. (1990), Lohmann et al. (1996), Nijssen et al. (1997), and Olivera et al. (2000). The simplest routing model is represented by the unit hydrograph approach (Jakeman et al., 1990), for which a static distribution over a given time window is applied to the instantaneous runoff, in order to redistribute its runoff over time. Because of its simplicity and low computational cost, and the generally large level of uncertainty of flow conditions within a catchment (eg. depth-discharge relationship), the unit hydrograph approach is used in some operational systems (eg. Météo France; E. Martin, personal communication).

Linear models are further distinguished between cell-to-cell and source-to-sink models (Olivera et al., 2000). In cell-to-cell models the runoff is calculated for each individual cell, according to the antecedent soil moisture capacity (eg. Lohmann et al., 1996; Nijssen et al., 1997) and the surface-subsurface water exchanges, using time-invariant parameter sets, before the runoff is routed into the neighbouring cell. On the other hand, source-to-sink models determine the travel time from the point of origin to the catchment sink (ie. the catchment outlet), without taking into consideration antecedent soil moisture conditions or interactions with downstream cells. The total of the contributions of each source at the outlet of the catchment is then taken as a representation of the unit hydrograph (eg. Naden, 1993; Olivera et al., 2000).

Cell-to-cell models are excluded from further discussion in this section because they require an explicit knowledge of the soil moisture conditions at smaller then the catchment scale, which is not required in source-to-sink models. In source-to-sink models, it is only necessary to determine the flow length and flow velocity, and the resulting travel time of the surface, subsurface and stream runoff. With the assumption that the flow routing parameters are constant at least over time, if not in space, a fixed unit hydrograph is determined using the surface characteristics of the catchment, which are known through DEMs and vegetation maps (both are available for the Goulburn River catchment) for each subcatchment outlet.

The source-to-sink approach presents the best solution for the routing purposes identified in this thesis. While it is a method, which is simple to establish, it implicitly takes into account catchment characteristics, such as slope, catchment area and surface conditions. A discussion of the routing model developed for the work in this thesis is presented in the following section.

4.4.2 Model Development

As CLSM produces instantaneous runoff for each output time step (in general hourly) and each individual subcatchment, it is necessary to apply a routing model to the modelled runoff, in order to introduce a delay function for the flow conditions. This routing model is required to internally rout the subsurface and surface runoff within an individual catchment to the stream network, and then to rout the streamflow through this network to the regional catchment outlet. In the previous section, a number of inherently different routing models were discussed, concluding that the source-to-sink approach by Olivera et al. (2000) represented the best method to be applied for the work of this thesis.

In the present section, an adaptation of the source-to-sink model of Olivera et al. (2000) is presented. The major difference between the approach presented here and the original work by Olivera et al. (2000) is the empirical development or calibration of some parameters in the source-to-sink model, and the application of the model to subcatchments rather than continents. These changes are required for the multi-catchment synthetic and field studies in Chapters 6 and 7, for which information about the hydrograph at the subcatchment outlets is necessary. Furthermore, this new version of the source-to-sink model is a two-level source-to-sink approach, in which each subcatchment is first treated individually with its own sink and then each subcatchment sink is in turn treated as a source with just one single sink at the outlet of the Goulburn River catchment.

Like in Olivera et al. (2000), flow direction and flow paths were derived for the new approach from a DEM (in the present case from the 250m DEM presented in Chapter 3). The theoretical response function $u_j(t)$ in Olivera et al. (2000) was replaced here with a semi-empirical unit hydrograph for each subcatchment. First it was assumed, that the velocities of surface sheet flow, subsurface flow and streamflow can be described with Manning's equation

$$V_{i,f} = \frac{1}{n} R_h^{2/3} S_i^{1/2} \tag{4.12}$$

where $V_{i,f}$ is the flow velocity [m/s], with f denoting the three types of flow (subsurface flow, surface sheet flow, streamflow) and i the cell index; n is Manning's roughness coefficient; R_h is the hydraulic radius of the flow [m^2/m], and S_i is the slope of the grid cell i [m/m], with the assumption that the subsurface water table is parallel to the surface slope. However, in order to remove the lack of knowledge of R_h and n, the function

$$\frac{R_h^{2/3}}{n} = \frac{5}{3} c_{r,i,f} \tag{4.13}$$

was introduced to simplify Manning's equation; where $c_{r,i,f}$ is a routing coefficient; and the factor $\frac{5}{3}$ is included to allow for the kinematic wave propagation in the flow velocity calculations. For this function, it was assumed that the ratio between the hydraulic radius and Manning's roughness coefficient remained constant for all flow intensities. Substituting eq. (4.13) in eq. (4.12) gives the new equation for the flow velocity

$$V_{i,f} = \frac{5}{3} c_{r,i,f} S_i^{1/2}. \tag{4.14}$$

The product of flow length and flow velocity is the travel time through each cell to the sink of the cell

$$FT_{j,f} = \sum_{i=j}^{n} FL_i \times V_{i,f}^{-1}, \tag{4.15}$$

where $FT_{j,f}$ is the flow time to the outlet; j is the index of the upstream pixel; n is the number of pixels in the downstream flow path from j; FL_i is the flow length of pixel i. Fig. 4.5 shows the calculated flow times for the whole Goulburn River experimental catchment.

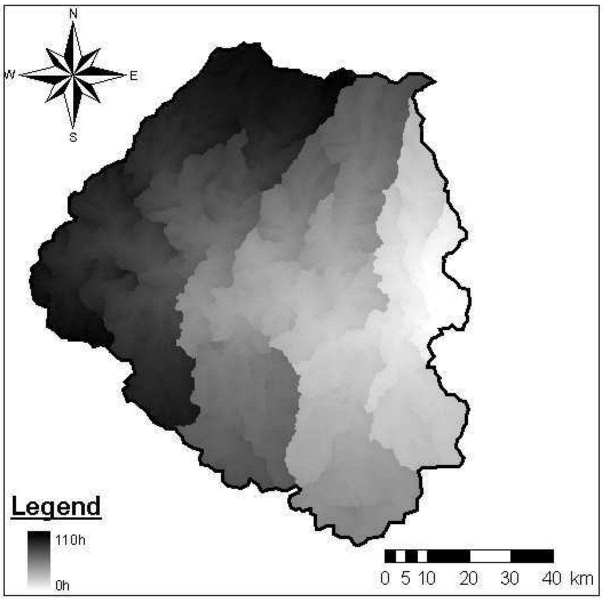

Figure 4.5. Flow time for all cells to the outlet of the Goulburn River experimental catchment, as derived with the method described in the text.

Summarising the contribution from all pixels at the subcatchment outlet produces a distribution of runoff intensity. The pixels contributing to the streamflow at a given time step are then normalised to the total number of pixels in the subcatchment with

$$R_{t1,t2} = \frac{\sum_{i=t1}^{t2} N_{cp,i}}{N_{cp,all}}, \tag{4.16}$$

where $R_{t1,t2}$ is the normalised number of pixels (or contributing areal fraction) for a given time step $i=[t1,t2]$; $N_{cp,i}$ and $N_{cp,all}$ are the numbers for contributing pixels for a given time step and all contributing pixels within a catchment, respectively. This normalised distribution of pixels contributing to the streamflow at the sink at any one time was then used to derive a unit hydrograph (Fig. 4.6). To obtain the streamflow quantity at the subcatchment outlet, the developed unit hydrograph is multiplied with the modelled instantaneous streamflow

$$Q_{out,i,k} = Q_{conv,i,k} \times R_i, \tag{4.17}$$

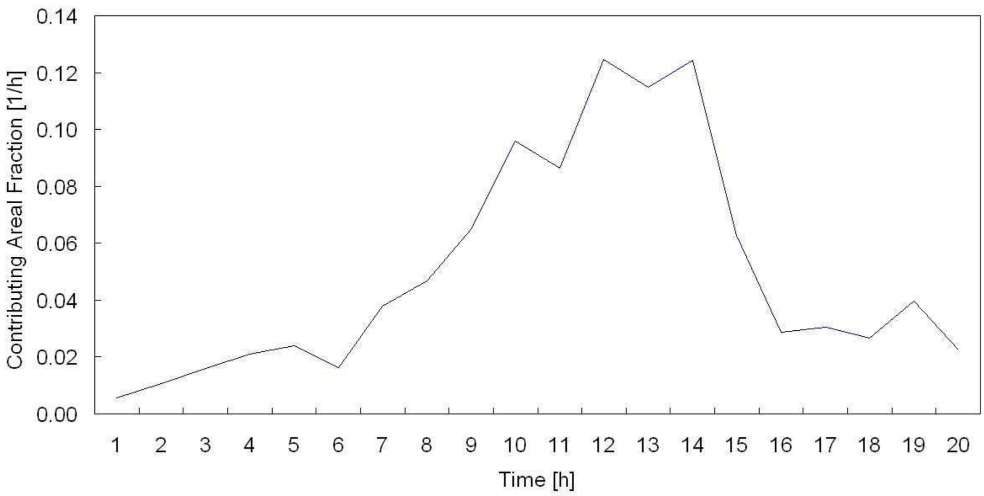

Figure 4.6. Unit hydrograph for surface flows for a subcatchment of the Goulburn River experimental catchment.

where Q is the streamflow [m³/s]; the subscripts denote "at the outlet" (*out*) and modelled streamflow (*conv*) [m³/s]; the time step of the observation (*i*); and an identifier for the rain event (*k*).

As individual rain events may produce streamflow events that are within the catchment response times (max($FT_{j,f}$)) of the previous event, simple redistribution of the runoff is not sufficient, as the events are overlapping. The accumulation of the individual runoff events was achieved by adding the runoff matrices at the outlet

$$Q_{tot,i} = \sum_{k=1}^{n} \begin{bmatrix} Q_{out,i,k} \\ \ldots \\ Q_{out,w,k} \end{bmatrix}_k , \qquad (4.18)$$

where w is the sum of the duration of the precipitation events and max($FT_{j,f}$).

Because precipitation and streamflow events were observed within the Goulburn River catchment, the routing coefficient $c_{r,i,f}$ was calibrated against these observations. This was undertaken by adjusting $c_{r,i,f}$ so that the unit hydrograph showed a best fit with the observed hydrograph at the sink. A detailed example of the calibration process is presented in Appendix A3.2.

To this point, the described approach generally follows the one-level source-to-sink model described by Olivera et al. (2000). However, as mentioned previously, in order to rout the water at the subcatchment sink to the outlet of the main catchment, the model had to be extended to allow for a second level of routing. This second level treats the streamflow at the sink of each subcatchment as a source, with its sink at the outlet of the main catchment. The approach is, apart from the different definition of sources and sink, identical with the model described above. Nevertheless, further calibration of $c_{r,i,f}$ for the stream network is not necessary, as it has been calibrated on the first level.

4.5 Data Assimilation Scheme

4.5.1 General Discussion

There are several requirements for the streamflow assimilation scheme implemented by the soil moisture prediction system developed in this thesis, as identified in the literature review of Chapter 2. Most importantly, the assimilation scheme must be able to relate the soil moisture states to the streamflow observation, accounting for the time delay between runoff generation at the hillslope and its subsequent observation impact downstream some time later. There are fundamentally only two different assimilation approaches (sequential and variational data assimilation), and earlier discussion in the literature review concluded that the variational data assimilation approach was more appropriate for this application. The reason for this was that a sequential assimilation scheme could not easily relate the observations at an instant in time back to the soil moisture state conditions during the rainfall event, which produced the runoff, especially for large nested catchments.

In its pure form, the variational assimilation scheme uses an adjoint (Talagrand and Courtier, 1987; Courtier et al., 1998) to find the Jacobian of a cost function *J* (see eq. 2.14). The alternative is a "brute force" approach, which numerically finds the Jacobian of the cost function through methods such as forward difference. This Jacobian is then used to find the optimal initial condition values to best match the observations through the cost function, which typically requires quantification of the model and observation errors (generally assumed fixed within the assimilation window). The optimisation is then achieved using a multi-objective optimisation scheme. This data assimilation approach can be likened to calibration, but rather than calibrating for an optimal parameter set, the optimal initial state values (ie. soil moisture) are sought for a given assimilation window.

4.5.2 Description of NLFIT

Numerous optimisation routines exist, however for the work presented in this thesis, it was decided to use the Bayesian nonlinear regression suite NLFIT (Non-Linear FIT; Kuczera, 1983ab, 1994), which uses the shuffled complex evolution method (Duan et al., 1992, 1994). NLFIT was chosen, as it is capable to deal with the long timeseries of observations and model predictions, and does not require the derivation of an adjoint. Furthermore, response and error cross-correlations are calculated within NLFIT and do not have to be specified by the user. Moreover, as NLFIT is a brute-force optimisation scheme, background and model errors are not taken into consideration and do not require prior definition.

In this application, NLFIT is used to minimise a cost function of the observed and predicted streamflow (and later surface soil moisture) over an assimilation window. The optimisation is realised by changing the initial soil moisture state variables until the best fit between predicted and observed streamflow timeseries within a preset assimilation window is achieved. These changes are carried out according to the method chosen (Gauss-Marquardt or Shuffled Complex Evolution; see below), and search the parameter space for the global maximum, based on their individual statistical assumption.

Determination of background and observation errors is not a straightforward task and requires detailed analyses of the model processes, and the instrumentation and observation errors. Given the limited time period from which observations were available for this study and the extreme conditions in the ephemeral rivers of the Goulburn River catchment during the recent drought, an optimisation approach, which does not require such estimates of the background and observation errors internally had to be chosen. Furthermore, it was decided to apply a brute force approach, because the derivation of an adjoint has been shown to be difficult, in particular for large non-linear models.

In its most general form the regression model of NLFIT is defined as

$$\mathbf{q}_t = \mathrm{f}(\mathbf{x}_t, \boldsymbol{\beta}) + \boldsymbol{\varepsilon}_t, \quad \text{with } t = 1,.....,n, \tag{4.19}$$

where $\mathbf{q}_t$ is the observed response vector (eg. streamflow, soil moisture); $\mathbf{x}_t$ is the input vector (eg. forcing data); $\boldsymbol{\beta}$ is the vector of the model parameters or states; and $\boldsymbol{\varepsilon}_t$ is a random error vector. In this regression model, the model parameters or states in $\boldsymbol{\beta}$ are optimised, in order to produce the vector $\mathbf{q}_t$ which best fits with the available observations. The error model of NLFIT assumes in its basic case that $\boldsymbol{\varepsilon}_t$ is a random error with an expected value of zero and a constant variance σ^2, which signifies that the errors are normally distributed. Moreover, $\boldsymbol{\varepsilon}_t$ includes both background and observation errors. These assumptions mean that the predictive model is capable to predict the average of the observations correctly.

For a single observation type, with no assumed errors, the cost function of eq. (2.14) is then reduced to the simple least square function

$$J = \min_{\beta} \sum_{t=1}^{n} \varepsilon_t^2 = \min_{\beta} \sum_{t=1}^{n} \left(q_t - \mathrm{f}\left(x_t, \beta\right)\right)^2 , \qquad (4.20)$$

where J is the cost function; n is the number of time steps within the assimilation window; q_t is the observation; x_t is the predicted value and β is the model parameter or initial state.

If the assumption of normality in the error distribution is violated, for example if the relative error grows with the magnitude of the observed variable, the error model is rewritten in the more general form (Box and Jenkins, 1976)

$$\eta_t = \varphi_1 \eta_{t-1} + \ldots + \varphi_p \eta_{t-p} + \varepsilon_t + \theta_1 \varepsilon_{t-1} + \ldots + \theta_q \varepsilon_{t-q} , \qquad (4.21)$$

where η_t is the transformed error; φ_i are p numbers of autoregressive parameters (AR); and θ_i are q numbers of moving average (MA) parameters. While in theory any number of AR and MA parameters may be chosen, it is recommended to limit them to one or two parameters each (G. Kuczera, personal communication). In a more simple form, η_t is

$$\eta_t = Q_t - \mathrm{E}(Q_t), \qquad (4.22)$$

where the observation Q_t is transformed through (Box and Cox, 1964)

$$Q_t = \frac{(q_t + K)^{\lambda} - 1}{\lambda} \qquad \text{for } \lambda \neq 0 \qquad (4.23a)$$

and

$$Q_t = \log(q_t + K) \qquad \text{for } \lambda = 0 , \qquad (4.23b)$$

with K and λ being transformation parameters and where the transformed predicted response is defined as

$$\mathrm{E}(Q_t) = \frac{(\mathrm{f}(x_t,\beta)+K)^\lambda - 1}{\lambda} \qquad \text{for } \lambda \neq 0 \qquad (4.24a)$$

and as

$$\mathrm{E}(Q_t) = \log(\mathrm{f}(x_t,\beta)+K) \qquad \text{for } \lambda = 0. \qquad (4.24b)$$

Because of this transformation, the predicted response is now the median response of time step t.

In NLFIT, two different search algorithms for the global optimum may be chosen, which are distinctly different in their methodology. These two algorithms are i) the Gauss-Marquardt algorithm (Press et al., 1986) and ii) the Shuffled Complex Evolution (SCE-UA) algorithm (Duan et al., 1992 and 1994). While the majority of the work in this thesis was undertaken with the SCE-UA algorithm, the Gauss-Marquardt algorithm was tested in a single catchment study were undertaken with the. Consequently, both algorithms are described here.

4.5.2.1 Gauss-Marquardt Algorithm

The first type of search algorithm NLFIT uses is the Gauss-Marquardt algorithm (Press et al., 1986), which is a combination of the steepest (or gradient) descent and the Gauss-Newton algorithms, to determine the search direction within the parameter space. The steepest descent method follows the steepest gradient in the parameter space from the point of initialisation, in order to determine the optimum state value. The Gauss-Newton algorithm is an iterative method for an ellipsoid parameter space, in which the user has to provide the algorithm with an initial guess of the parameter vector **β**, which is then updated iteratively by

$$\beta^{k+1} = \beta^k - \left(J_f(\beta^k)^T J_f(\beta^k)\right)^{-1} J_f(\beta^k)^T \mathrm{f}(\beta^k), \qquad (4.25)$$

where $J_f(.)$ is the Jacobian of the function f(.) for the parameter vector β at guess k. The transition of the algorithms between the steepest descent and the Gauss-Newton method is achieved by multiplying the diagonal elements of the Hessian matrix with the scalar parameter λ_M. A value of zero signifies that the search method is purely based on the Gauss-Newton algorithm, with the method approaching the steepest gradient algorithm as λ_M is increased.

In order to determine the shape of the posterior distribution function of the parameter vector γ, the cost function $J(\gamma)$ is expanded through a second-order Taylor expansion about the optimum value γ_0, which yields

$$J(\gamma) = J(\gamma_0) + \frac{\partial J(\gamma)}{\partial(\gamma)}(\gamma - \gamma_0) + \frac{1}{2}(\gamma - \gamma_0)^T \frac{\partial^2 J(\gamma)}{\partial \gamma^2}(\gamma - \gamma_0), \tag{4.26}$$

or for the optimal solution, where $\frac{\partial J(\gamma)}{\partial \gamma} = 0$,

$$J(\gamma) = J(\gamma_0) + \frac{1}{2}(\gamma - \gamma_0)^T \frac{\partial^2 J(\gamma)}{\partial \gamma^2}(\gamma - \gamma_0). \tag{4.27}$$

The covariance matrix for this function, given some prior information at point p in the parameter space on the observations and the parameter β, is defined as

$$\Sigma = -\left(\frac{\partial^2 J(\gamma)}{\partial \gamma^2}\right)^{-1} = \left(\Sigma_p^{-1} + \frac{1}{\sigma_0^2}\Gamma_0^T \Gamma_0\right)^{-1}, \tag{4.28}$$

where

$$\Gamma_0 = \frac{\partial \varepsilon}{\partial \gamma}, \tag{4.29}$$

which depends on the model response to changes in the parameter β (ie. $\frac{\partial f(x_t, \beta)}{\partial \beta}$). If no prior information on observations and parameter estimates is available, Σ_p^{-1} is equal to 0, and the covariance matrix of eq. (4.28) is reduced to

$$\Sigma = \left(\frac{1}{\sigma_0^2} \Gamma_0^T \Gamma_0 \right)^{-1}. \tag{4.30}$$

The cost function in eq. (4.20) is presented for the simple case of one type of observation. For joint fitting of different data sets, such as streamflow and surface soil moisture as presented in Chapters 5 to 7, the cost function becomes

$$J(\boldsymbol{\gamma}) = \sum_{t=1}^{n} \boldsymbol{\varepsilon}_t^T \boldsymbol{\Omega}^{-1} \boldsymbol{\varepsilon}_t + (\boldsymbol{\gamma} - \boldsymbol{\gamma}_p)^T \boldsymbol{\Sigma}_p^{-1} (\boldsymbol{\gamma} - \boldsymbol{\gamma}_p), \tag{4.31}$$

where $\boldsymbol{\Omega}$ is the error covariance matrix of the errors of the different jointly fitted data sets; $\boldsymbol{\gamma}$ are the response vectors; and $\boldsymbol{\Sigma}_p$ is the covariance matrix of the different response vectors at point p. Eq. (4.31) is essentially equal to the general cost function of eq. (2.14).

4.5.2.2 Shuffled Complex Evolution (SCE-UA) Algorithm

The objective functions used for the optimisation process in the SCE-UA algorithm are identical to those presented in eq. (4.20) for a single type of observation and eq. (4.31) for joint fitting of different data sets. However, the search function is fundamentally different to the Gauss-Marquardt algorithm. The SCE-UA algorithm is the result of merging different aspects of three other optimisation algorithms: i) the simplex procedure (Nelder and Mead, 1965), ii) the competitive evolution (Holland, 1975), and iii) the controlled random search (Price, 1987). In brief, this merged algorithm samples a number of points from the state space and ranks them according to the value of the cost function, rather than searching along a steepest descent direction as in the Gauss-Marquardt algorithm. This process is repeated until the objective function fulfils a predefined criterion.

An exhaustive description of the SCE-UA algorithm and an example for its optimal use are presented in Duan et al. (1992 and 1994) and the reader is referred to these publications for more details. Nevertheless, it is required to outline the general functionality of the

SCE-UA. In the first step, a random sample of data points is chosen from the feasible data space. The feasible data space is predefined by the user (eg. through the physically possible range of soil moisture states), while the number of samples (s) is automatically determined as the product of the chosen number of complexes (p) and the number of required data points within a complex (m), which has to be larger than the dimension of the problem (n; eg. number of soil moisture states). For an objective function that is to be minimised, the samples are then ranked according to their value, with the smallest value ranked first. These ranked samples are then partitioned into the predefined number of complexes (so that every j^{th} data point is located in complex j). In each of these complexes, the data point with the largest value is replaced with another data point, using the Competitive Complex Evolution (CCE) algorithm (which is outlined in more detail further below). The results of the different complexes are then regrouped into a full sample population and the lowest value checked against the convergence limit. In case the convergence limit is not reached, the new sample population is again ranked and partitioned into complexes. This procedure is repeated either a predefined number of times or until the objective function has converged with the convergence limit.

The CCE algorithm, which is a subroutine of the SCE algorithm, is used to replace the lowest ranking data point with a more likely data point. It functions in principle similar to the general SCE algorithm, in that it samples a number of data points from the respective complex (obtained from the main SCE-UA routine) to form a subcomplex and then ranks the data points in this subcomplex. From this subcomplex, the data point with the highest value of the objective function is then removed and the centroid of the remaining data points calculated. Based on this centroid, a new data point is calculated and substituted into the vacant space of the removed data

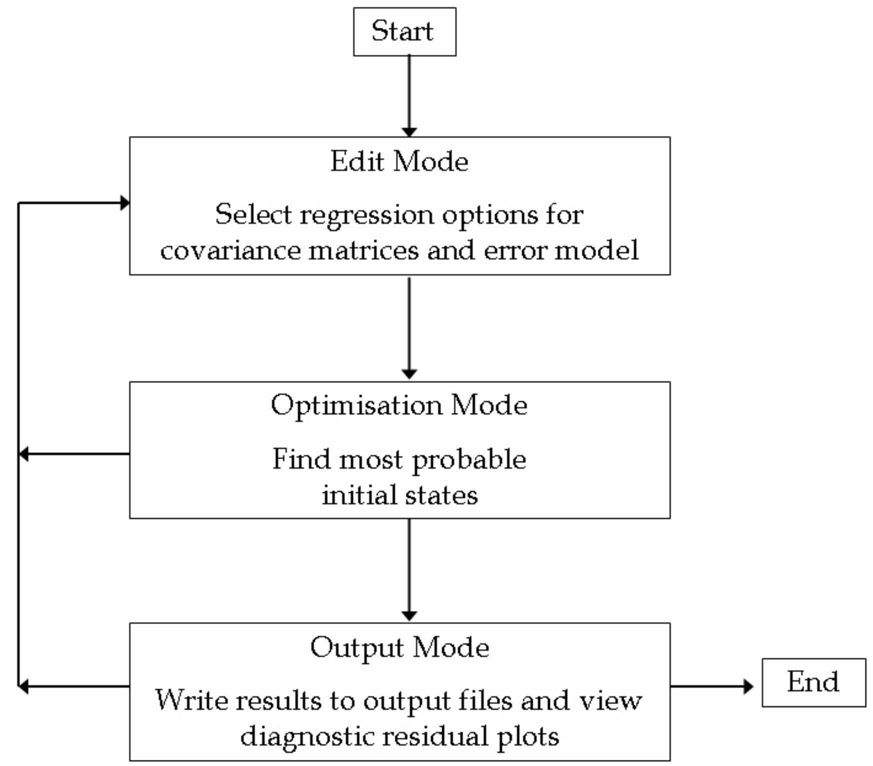

Figure 4.7. Schematic of NLFIT.

point, which eventually results in an improved subsample. This process may be repeated several times for each complex. All complexes are then regrouped into the full sampled population and the process is restarted by creating a new set of complexes.

The advantage of the SCE-UA method is that the re-shuffling of the complexes after each evaluation step allows the exchange of information between each of the complexes, rather than allowing the different complexes to determine their own minimum (Duan et al., 1992). Moreover, it results in a focus on one single data point within the state space within each complex.

4.5.3 Application of NLFIT

While the previous section has presented the mathematical background of NLFIT, a basic application of NLFIT is illustrated here. Fig. 4.7 shows the schematic of NLFIT, with Edit, Optimisation, and Output Modes. In the Edit Mode, the regression algorithm is selected, and the initial guess of the states and error model parameters are entered. In the Optimisation Mode, the model is run and the most probable set of initial model states is found. In its current form, NLFIT communicates with the model through a user defined subroutine of its own code, so that the model is only linked to NLFIT through the passing of input and output values (predictions and states). Finally, in the Output Mode the results are analysed using the diagnostic tools built into NLFIT. NLFIT can be relaunched after either the Optimsation Mode or the Output Mode, if no optimisation has been achieved.

This section serves to provide an overview of the assumptions made during the optimisation process. An exhaustive description of NLFIT and its application is given by Kuczera (1983ab, 1994) and Duan (1992). The reader is referred to these publications for more details.

4.5.3.1 Edit Mode

In the Edit Mode, the first two steps are to inform the model of the sources of the computed derivatives and any prior information (ie. mean, standard deviation, and covariance matrix) on the model states. For the work in this thesis, NLFIT was always used to compute the derivatives based on the internal finite difference method, and it was assumed that no prior information on the model states existed.

Any data record may contain observations which should not be included in the optimisation process for various reasons (eg. the data being obvious outliers). NLFIT allows observations to be censored on the basis of significance or quality. For example, in an ephemeral stream, no-flow conditions do not contain sufficient information about the soil moisture states in the upstream catchment. The sole information these observations provide is that either precipitation or antecedent soil moisture conditions (or both together) did not suffice to produce streamflow. While the no-flow conditions may represent a significant portion of all observations within one assimilation window, they may not contain sufficient information about the upstream flow conditions to justify their inclusion in the analysis.

In the following step of the Edit Mode, NLFIT requires the user to define the states, which are to be optimised. As the retrieved states in this thesis were the three prognostic moisture variables of CLSM (catchment deficit, root zone and surface excess), the maximum and minimum values of these states were determined in a preliminary study. This was achieved by setting these initial states to unrealistically high or low values, which were then automatically reset by the model to its actual maximum and minimum values. In the case of the catchment deficit, the lower boundary is 0mm (saturation) and the maximum catchment deficit ($M_{D,\max}$), which is a function of porosity, soil depth, and soil moisture profile in the catchment. The maximum excess values generally depend on the catchment deficit. Therefore, their extreme, albeit exaggerated, values can be determined, when the catchment deficit is set to 0 or $M_{D,\max}$. In case of a saturated soil, the root zone and surface excesses were set to unrealistically dry conditions and in case of $M_{D,\max}$, were set to unrealistically wet conditions. Following the results of this preliminary study, the initial guesses of the state values were set to the average of the maximum and minimum (in case of the excesses, the average value is 0, as it represents the equilibrium soil moisture condition, described in section 4.3). During the same step within the Edit Mode, the initial perturbation for the search function was to be defined, and was set to 10% of the initial guess (catchment deficit) or 10% of the maximum value (root zone and surface excess).

The choice of the error model is an iterative step. Kuczera (1994) recommended that a normal distribution of the errors should initially be assumed and that the optimisation scheme should therefore be run first with the simple least square error model of eq. (4.20). This assumption would be corrected after a first optimisation run, when information on the error distribution is available, through the knowledge of residual variance and the calculated cross-correlation (the latter only if more than one state was optimised). In case the errors are not normally distributed, the user is then in the position, to introduce the Box-Cox parameters λ and K, and any autoregressive or moving average parameters (ARMA). This is undertaken in an iterative process, where the optimisation is rerun with new parameters, until the residual errors are transformed into a normal distribution.

4.5.3.2 Optimisation Mode

In the first step of the Optimisation Mode, λ_M and the search step fraction are set. While the first guess of λ_M should aim to be around 0.1 to 0.2 (G. Kuczera, personal communication), it should reach 0 when near the optimum value (Kuczera, 1994). The search step fraction is used to disaggregate the initial search vector into smaller segments. At the end of each of these segments, the slope of the function along the search vector is evaluated and if found to increase, the direction of the search vector is changed. The value of the search vector during the work for this thesis was generally set to values between 0.1 and 0.33. Depending on the level of convergence of the cost function with its optimum, the fraction should be gradually increased.

When run in the shuffled complex evolution mode (Duan et al., 1992), NLFIT allows to define upper and lower boundaries of the state values. While these are again the minimum and maximum values of the three prognostic soil moisture states, a more realistic approach was chosen for the catchment deficit. While the root zone and surface excess values were allowed to vary between their respective maximum and minimum values (as they would during major precipitation events or long-lasting droughts), an informed decision was made for the range of the catchment deficit. As it was known that the region was under a severe drought during the 12-month study period, and that even the artificially wet conditions of the true observations in the synthetic studies did suffer from these dry conditions, it was assumed that the catchment deficit could only vary between 50-100% of its maximum value. This assumption constrains the optimisation process somewhat, as it reduces the possible range of values for the initial states.

After the optimisation run is complete, NLFIT provides information on the different states. Most importantly, it identifies states which did not have any impact on the changes of the predicted response, which is followed by a recommendation to exclude such states from the retrieval process.

4.5.3.3 Output Mode

In the Output Mode NLFIT produces various graphs, which help to analyse the optimisation process and to validate or discard the assumptions made initially in the Edit and Optimisation Modes. In particular, the graphs show the time series of predictions and observations, the residual error against the predicted response, and the normal probability plot are important tools.

While the time series graph helps to determine whether there are any inconsistencies in the dynamics of the model or any temporal drifts, the two other graphs (residual error against the predicted response and normal probability) help to assess whether the assumptions about the error model were indeed correct. The residual error against predicted response graph indicates, whether the residual error is changing with the magnitude of the observations. If this is the case, the errors are not normally distributed. Similarly, the normal probability graph should plot as a straight line if the errors were normally distributed. Any deviation from this signifies that this assumption is not valid, and that it must be corrected by changing the error model for the optimisation process, or altering the Box-Cox and ARMA parameters. The optimisation process is finalised, when the cost function cannot be reduced any further or the response function has become insensitive to changes in the initial states.

4.6 Chapter Summary

This chapter has presented the hydrologic land surface model, routing model, and assimilation scheme used throughout this thesis, selected following conclusions drawn from the literature assessment of Chapter 2. The chosen land surface model is the Catchment Land Surface Model (CLSM), because of its use in GCMs studies and data assimilation studies. As there was no routing model in the CLSM, a simple linear routing model with three runoff parameters for stream, surface and subsurface runoff has been developed, using a simplification of Manning's equation. The data assimilation scheme uses the variational approach, but with a brute force approach for the calculation of the model state Jacobian. State optimisation is achieved using the NLFIT implementation of the shuffled complex evolution method.

Chapter Five

5 Single-Catchment Synthetic Study

This chapter presents a single-catchment synthetic study as a proof of concept for the land surface assimilation scheme proposed in Chapter 2 for climate model initialisation. This synthetic study uses the forcing and catchment parameter data from Chapter 3, with the uncoupled land surface model, routing model, and assimilation scheme presented in Chapter 4. This is the first step towards the multi-catchment synthetic and field data studies presented in Chapters 6 and 7, respectively. This chapter identifies the impact of: i) assimilation window length, ii) atmospheric forcing errors; iii) model parameter errors, and iv) inclusion of satellite-type surface soil moisture values when and where available, on land surface initialisation.

The true forcing data and observations are presented in detail, before the experiments of this study are described. Each of the different experiments of this study (assimilation window length, forcing and parameterisation errors, and joint assimilation) is presented in two parts. First, the reader is introduced to the control experiments of the particular experiment, and then the assimilated model runs are discussed.

The synthetic studies in the present and following chapter were developed as twin experiments, consisting of four parts:

i) the development of a reference simulation (the true environment),

ii) the development of (synthetic) observations,

iii) the assimilation of the synthetic observations into a control simulation, and

iv) an analysis of the simulations after the assimilation runs.

5.1 *True Forcing*

The same true forcing scenarios were used for the synthetic studies presented in Chapters 5 and 6. Therefore, the true forcing data is presented only in this section. The true forcing data set is the basis of the different forcing scenarios, which are presented at the beginning of each section. Reference is made to this forcing data set throughout both the current chapter and Chapter 6.

5.1.1 Data Compilation

The atmospheric forcing data required by CLSM are 2m wind speed, precipitation, air temperature, specific humidity, air pressure, and long wave and short wave downwelling radiation. To impose a maximum amount of reality in the synthetic studies, real forcing data were used from weather stations within or nearby the Goulburn River catchment. These data were acquired from SASMAS weather stations operated as part of the Goulburn River experimental catchment, several automated weather stations (AWS) operated by the BoM, and the Global Data Acquisition System (GDAS). Apart from the two 6-hourly GDAS radiation data sets, all of the required forcing data were available in 20 minute intervals. The AWS and GDAS data were only used to infill unobserved or missing data from the SASMAS data sets (see Chapter 3). While the data was compiled from different sources, they were applied directly to Catchment 2 of the Goulburn River experimental catchment (Fig. 5.1), without any consideration for inconsistencies. This is an adequate assumption in synthetic studies, as the observations are derived from this compiled data set.

The compiled data set for the period chosen for the purpose of the

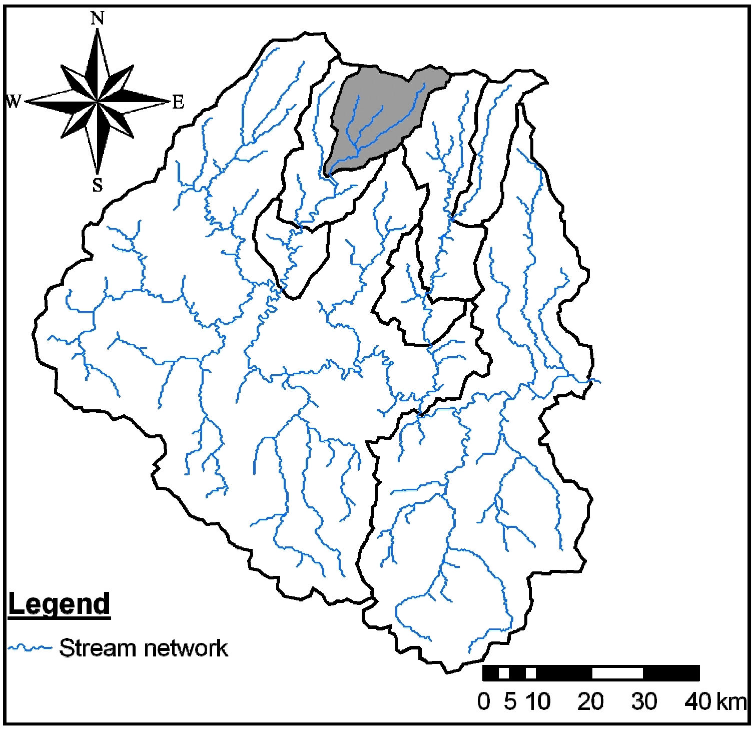

Figure 5.1. Location of Catchment 2 within the Goulburn River experimental catchment.

synthetic studies in this thesis extended from April 2003 (day 91 in 2003) through a full 12-month period until the end of March 2004 (day 91 in 2004). The choice of a full year of record ensured that at least one wet and one dry season was included within the study period. Moreover, this particular 12-month period included two major streamflow events (one in winter and one in summer), whereas no major runoff event occurred in the winter of 2004. This ensured the production of significant runoff events and changes in soil moisture during the study period.

The use of multiple data sets circumvented large gaps in the forcing data, with any gaps filled using overlapping data sets from different locations (Fig. 5.2). While most forcing variables were available from more than one station, only one source of atmospheric pressure was available (S2). Therefore, missing atmospheric pressure data were replaced with other periods, which had similar climatic conditions (temperature, precipitation) observed at other

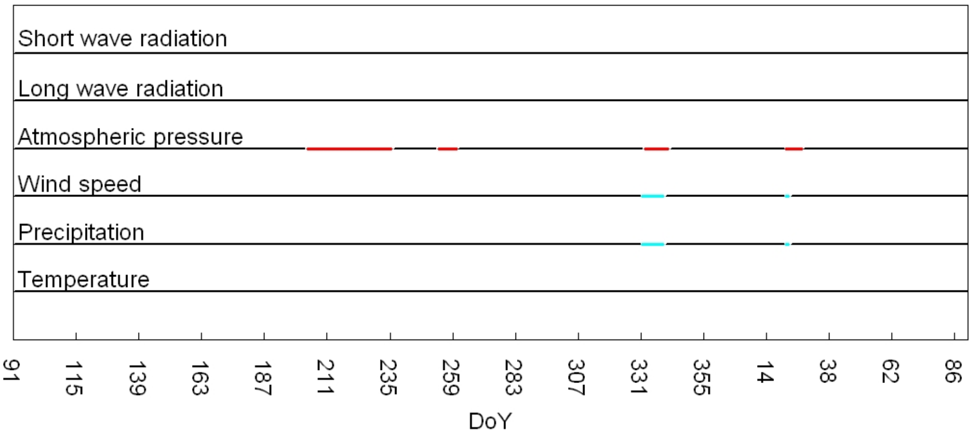

Figure 5.2. Schematic of the gap-filling in the forcing data throughout the 12-month period. Black lines are from one single station, red lines are observations inserted from other periods, and blue lines are from other stations.

weather stations. This avoided inconsistencies within the temporal evolution of the forcing data (eg. between air temperature and relative humidity). Data gaps in the remaining forcing fields were filled with data observed at the same time at the other weather stations. Any inconsistencies in the data due to the spatial distance between the different station locations were assumed to have a negligible impact on the physical processes in the model. Spatial variability of the forcing data within the single catchment, due to elevation or local climatic conditions, was not taken into consideration. Though it was shown that high resolution rainfall data has a positive impact on streamflow modelling in a lumped model (St-Hilaire et al., 2003), the present approach of forcing data compilation was chosen to simplify the synthetic studies by eliminating spatial effects from the forcing data in order to focus on the potential of the data assimilation scheme.

Precipitation and wind data were taken from the higher elevation climate station of the SASMAS project (K6) to artificially overcome the severe drought conditions in the region (higher precipitation rate); atmospheric pressure at 2m from the weather station at S2; and air temperature data were obtained from the BoM AWS at Scone, as it constituted the most consistent data set with the least gaps. The gaps in the temperature data at Scone were generally in the order of 1 to 10 hours and were linearly interpolated between the last preceding and first succeeding observed temperatures. The specific humidity was estimated using the temperature and pressure data from the respective weather stations with

$$Q_s = \frac{0.622 e_s}{P - 0.378 e_s}, \tag{5.1a}$$

and

$$e_s = 6.11 \exp^{\frac{17.26(T-273.16)}{T-35.86}}, \tag{5.1b}$$

where Q_s is the specific humidity of the air [kg/kg]; e_s is the saturation vapour pressure [hPa]; P is the atmospheric pressure [hPa]; and T is the air temperature at 2m [K].

5.1.2 Evaluation and True Observation Data

The conditions of the true simulation were derived from a repeated 10-year spin-up with the same one year of true forcing data (with the assumption of no data or model errors) over the 12-month period to obtain stable, non-changing water and energy balance conditions. The initial guess of the model states were assumed to be average values (initial soil temperatures were set to observed air temperatures, interception reservoir to 0mm, catchment deficit to 100mm, root zone and surface excess to 0mm, ground heat fluxes were set to 0 W/m^2). The spin-up was achieved by using the last restart data set of the previous year of simulation to initialise the new year of simulation. After 10 years of spin-up, the model was run a further year with the spun-up restart parameters, in order to produce the true data set. The true observations are denoted "True" on the figures in Chapters 5 and 6 (see Table 5.1 for a detailed overview of the naming conventions for the different scenarios).

Table 5.1. Description of forcing data sets for synthetic studies. The model states for the wet initial conditions are M_D=50mm, M_{rz}=0mm, M_{se}=0mm.

Forcing Scenario	*Description*
True	Using the *true synthetic* data set
1	As for *true* data but with wet initial conditions
2	As for *1* but with precipitation +20% and radiation -30%
3	As for *1* but with precipitation -20% and radiation +30%
4	As for *1* but with precipitation +20%, white noise radiation and average initial conditions
5	As for *4* with degraded soil parameters

The hydrologic land surface model was not calibrated to any real observations for the synthetic studies of this thesis and the model parameters for greenness, LAI, and soil were obtained from the respective data sets, as described in Chapter 3. Nevertheless, for the purpose of these synthetic experiments the model output was considered to be perfect, meaning that the model correctly represented environmental conditions. While the streamflow and near-surface soil moisture output were used as observational data for the assimilation experiments in Chapters 5 and 6, root zone soil moisture, sensible heat flux and evapotranspiration output were used as evaluation data.

The time step of the model output was set to one hour. The output generated by CLSM with the most significance for the studies presented here consists of streamflow and soil moisture (surface and root zone) to determine the performance of the assimilation scheme, and sensible heat flux and evapotranspiration to control the improvement the assimilation scheme has on the land surface-atmosphere interactions.

Fig. 5.3 presents the soil moisture propagation of the true data set

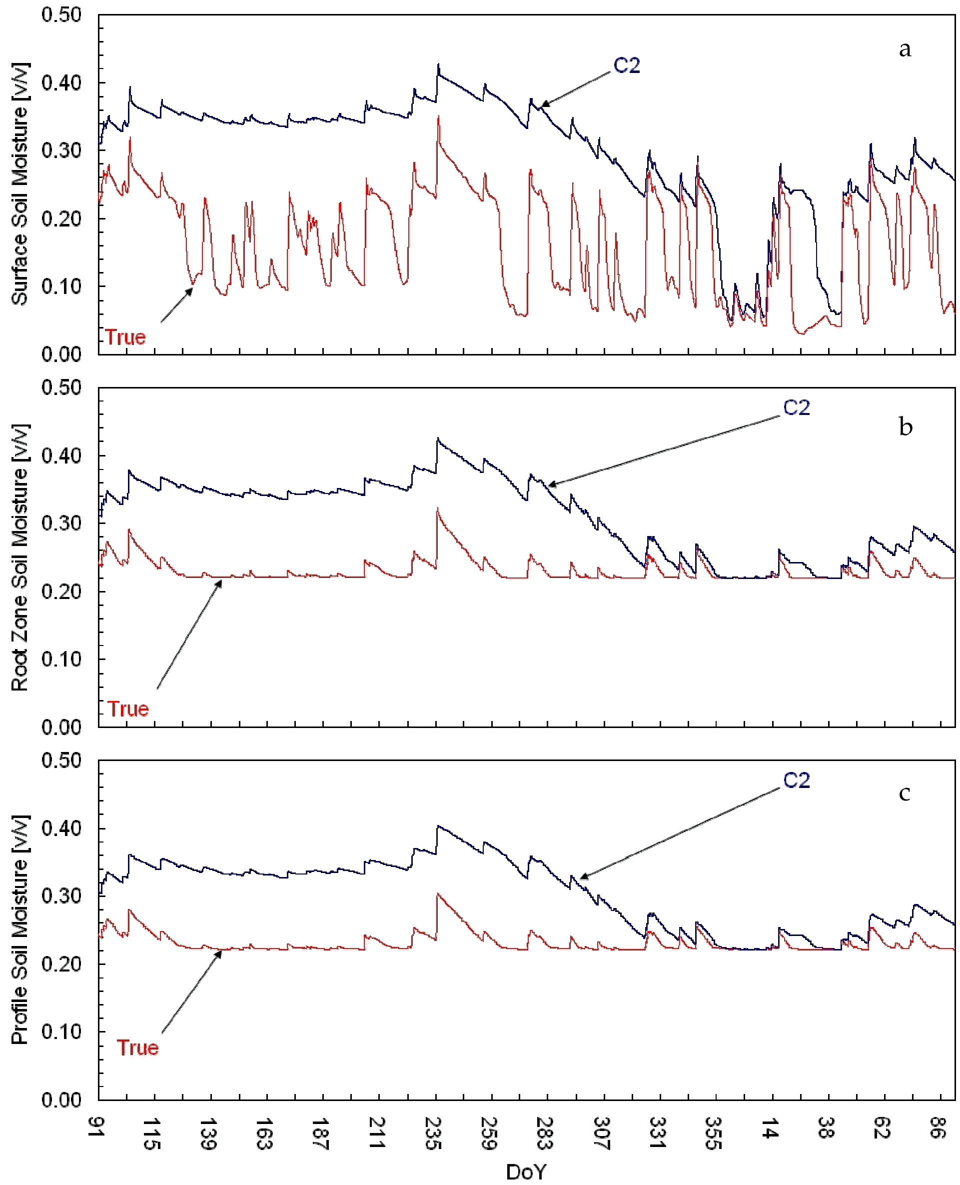

Figure 5.3. Soil moisture from true observations and C2 control runs for Catchment 2. a) Surface soil moisture, b) root zone soil moisture and c) profile soil moisture.

for the 12-month period. Due to the drought conditions in the region, the true root zone and profile soil moisture content were close to the wilting point throughout the year and showed only significant responses to strong precipitation events. On the other hand, surface soil moisture underwent a high variability over the same period. It had a quick response to all precipitation events, as these events throughout the year wetted up the surface layer, but moisture was either quickly evaporated or transferred into lower soil

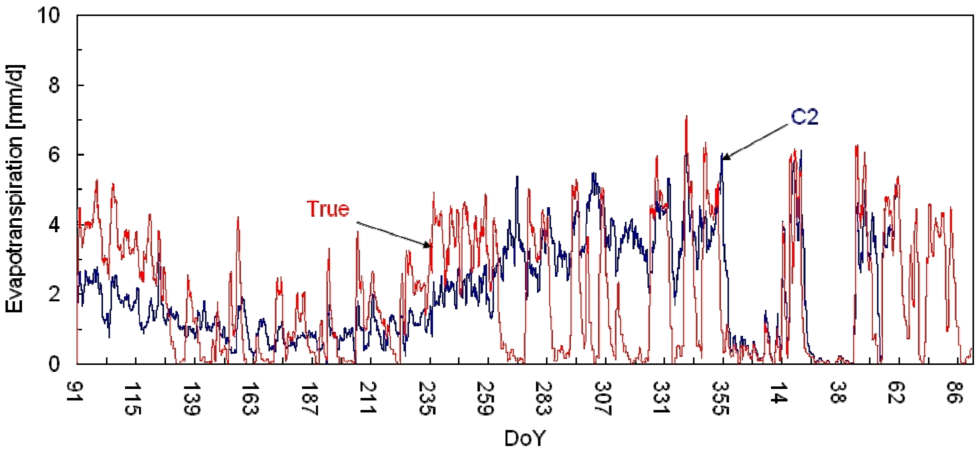

Figure 5.4. Daily averaged evapotranspiration from true and C2 control runs for Catchment 2.

layers. Furthermore, the surface soil moisture decreased below the wilting point, when root zone and profile soil moisture content reached this threshold. This caused the surface soil moisture to be decoupled from the deeper layers. A decoupling takes place in the model, when the soil moisture stores reach the wiling point. At this point in the simulation, profile and root zone soil moisture can not dry down further, while the surface layer is not restricted by the wilting point and can dry down further. Because no further exchange from the deeper soil moisture stores to the surface layer takes place, the surface layer soil moisture becomes independent of the deeper soil moisture conditions, until the deeper stores can again contribute to the water exchange between the layers.

Fig. 5.4 shows the daily averaged evapotranspiration rate for Catchment 2 for the 12-month period. When the root zone and profile soil moisture content reached wilting point, only limited evapotranspiration was available. The most significant evapotranspiration events took place when sufficient soil moisture was available, ie. evapotranspiration was limited by radiation rather than soil moisture in the true data set.

The true streamflow for the 12-month period is presented in Fig. 5.5. Three major streamflow events were simulated for 2003,

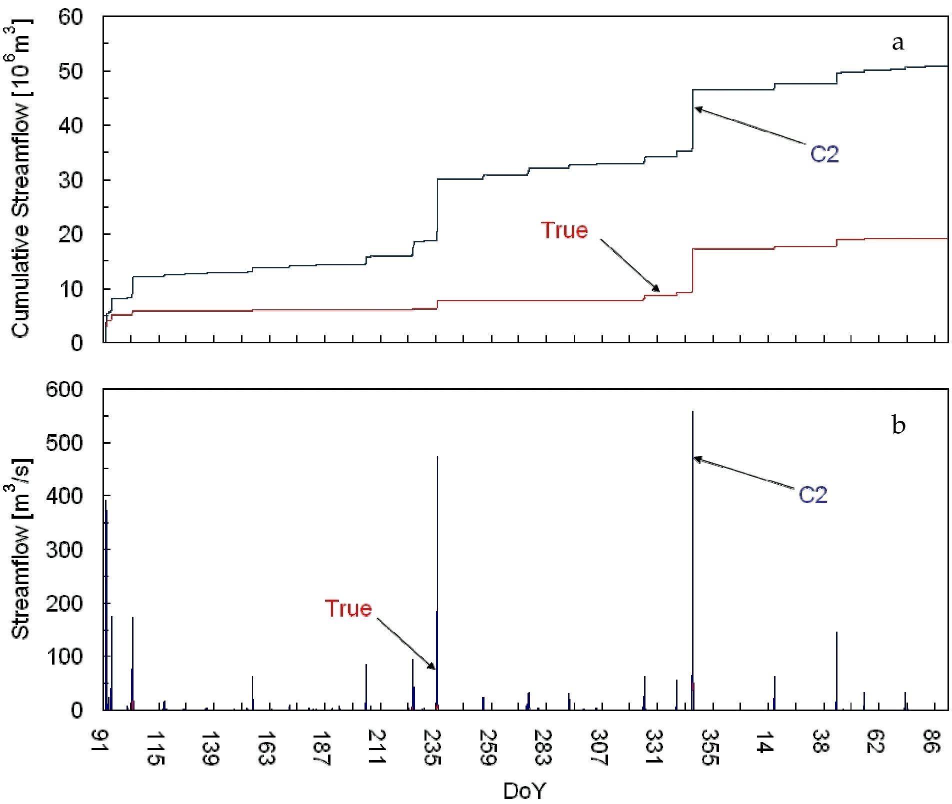

Figure 5.5. a) Cumulative and b) hourly streamflow from true and C2 control runs for Catchment 2.

coinciding with major precipitation events. These three events produced over 80% of the cumulative streamflow from Catchment 2. Several months showed only small or no streamflow, particularly in the first half of the 12-month period. Any streamflow events within the observed period were solely due to strong precipitation events, exceeding the infiltration capacity of the soil. Light or medium precipitation events did not cause any significant streamflow, as the runoff-contributing area was small and infiltration capacity was rarely exceeded.

5.2 *Setting of Assimilation Parameters*

An initial test using the Gauss-Marquardt and SCE methods showed that the SCE method has two significant advantages over the Gauss-Marquardt method. While the computational time was slightly reduced, more importantly, it allowed setting upper and lower boundaries for the retrieved variables. This resulted in a more accurate retrieval, as the number of mathematically (but not physically) possible local minima was reduced. Because of these results, the study undertaken in this thesis is based on the retrieval of the initial states using the SCE method. For more complex problems than the one presented in this thesis, with only a relatively small number of retrieved variables, it is recommended to first use the SCE method followed by the Gauss-Marquardt method (G. Kuczera, personal communication).

As briefly mentioned in Chapter 4, the river system of the Goulburn River experimental catchment consists of ephemeral streams, which results in a high number of streamflow observations with no measured flow. This situation has implications for the error distribution of model and observations, as it introduces a bias in the data towards no-flow conditions. The inclusion of the observations would mean that these observations would be included in the calculation of the objective function and the variance. Therefore, values that do not change in response to initial conditions have to be filtered from the input list. The most important reason for this is that any non-changing data points may adversely affect the calculation of the variance, as they introduce a bias in their calculation, because they are not sensitive to changes in the initial states. Furthermore, the only information available from no-flow conditions is that the soil moisture is below the threshold for the production of the surface runoff and consequently streamflow. However, this may include a range of soil moisture conditions, which is not a sufficiently constraining information. In ephemeral streams, no-flow conditions dominate in the summer and therefore, the objective function would be tending to accommodate the best fit mainly to these observations. If, for example, 744 observations were available for one month and 250 out of these would have a value of 0, only 494 observations would be considered within the assimilation window.

As a further constraint to the assimilation process, the range of possible initial states was limited to values ranging from 50-100% of $M_{D,\max}$, while the excesses were unconstrained. These limits were introduced in order to limit the search range and to reduce the possibility of finding local optima of the cost function in the state space. Moreover, the initial guess to determine the first search direction was generally set to ±10% of the initial guess of the soil moisture state.

Finally, the setting of the Box-Cox transformation and ARMA error model parameters is an iterative process and depends particularly on the normality of the observations and predictions. Consequently, those parameters vary from case to case and potentially need to be revised after a first assimilation run, in order to improve the performance of the assimilation scheme. For that purpose, it is required to study the residual plots and adjust the parameters accordingly, in order to obtain a near-normal distribution. This was done throughout the experiments. The parameters Box-Cox transformation and ARMA error model parameters, and the residual plots are not presented within this thesis, as they were different for each assimilation run (as explained above).

5.3 Assimilation Window Length

The focus of this experiment is on the optimal assimilation window length required for streamflow assimilation. This is investigated by comparing the performance of a year-long assimilation window against twelve sequential month-long assimilation windows for the same period.

5.3.1 Control Run

The forcing data used for the control and assimilation simulations contained a wet bias in the radiation (-30%) and precipitation data sets (+20%), in addition to an initialisation of the simulation with averaged soil moisture states. Initially, the experiment was intended to be degraded by only a wet initialisation of the soil moisture states. However, a change of the forcing scenarios from forcing scenario 1 to scenario 2 was necessary because the extreme drought conditions during the 12-month period forced the modelled soil moisture content to be identical with the true observations after two months when using true forcing data, even with a wet initialisation (near saturation). As this model-resetting negates the need for data assimilation, the control run needed to contain larger and more realistic errors. The results of this control run are presented alongside the true run in Figs. 5.3 to 5.5.

The soil moisture conditions were significantly different to those of the true observations (Fig. 5.3). Soil moisture did not reach the wilting point until day 355, consequently the surface soil moisture was never decoupled from the root zone and profile soil moisture until this time, as it happened early in the 12-month period for the true run (see section 5.1.2). As a consequence, the surface soil moisture did not undergo the same high variability as the true observations. This changed in the summer period, when increased air temperatures and longer radiation periods dried the catchment down to the wilting point, regardless of the wet bias in the forcing data.

During the summer period only one significant rainfall event took place. These dry conditions caused the degraded model predictions and the true soil moisture observations to be almost identical, due to the lack of incoming water. The reason for this effect was that the catchment deficit reached its maximum value, meaning that the soil moisture had reached its prescribed lower boundary, from which the model could not depart. However, at the end of the summer a divergence of true and control run was again observed, as the influence of air temperature and radiation was reduced and the wet bias again dominated the model performance.

The evapotranspiration from the control run shown in Fig. 5.4 demonstrates the cycle expected from an evapotranspiration rate not limited by soil moisture availability. The lower evapotranspiration rate of C2, as compared to the true observations near the start and middle of the simulation period (days 91-115 and 235-259), was a consequence of the reduced downwelling long wave and short wave radiation. After day 259, evapotranspiration was only observed when sufficiently strong precipitation events occurred, as evapotranspiration was water limited during the summer period. On the other hand, C2 evapotranspiration continued unrestricted due to the availability of soil moisture and higher summer radiation and temperatures. Because of true and C2 soil moisture being almost identical after day 355, the true and C2 evapotranspiration rates showed a similar behaviour, with slightly lower evapotranspiration rates for C2, due to the wet bias in the forcing data.

Total and hourly streamflow (Fig. 5.5) were significantly higher for the C2 control run, due to the wet bias in the forcing data. Furthermore, the antecedent soil moisture conditions in the catchment caused an additional increase in the surface runoff (Chapman, 1963), as they reduced the infiltration capacity of the soil. Nevertheless, the majority of the total streamflow in the 12-month period was caused by the same three streamflow events, as for the true scenario.

Table 5.2. Definition of assimilation runs. The numbering of the model output after assimilation follows the notation for the control runs (Table 5.1). While control runs are labelled with the character C, the assimilation runs are labelled with characters to identify the type of data assimilated (R streamflow assimilation only; SM surface soil moisture assimilation only; and RS joint assimilation of streamflow and surface soil moisture).

		Assimilation of....		
		Streamflow	*Soil Moisture*	*Both Obs.*
Forcing Data	*True*	R1	SM1	RS1
	Wet Bias	R2	SM2	RS2
	- year-long	Ra2	---	---
	- month-long	Rm2	---	---
	Dry Bias	R3	SM3	RS3
	Random	R4	SM4	RS4
	- degrad. soil	R5	---	---

5.3.2 Year-long Assimilation Window

In this experiment, a full year of streamflow data was assimilated into the hydrologic model, by using a single year-long assimilation window. This study shows the effects long assimilation windows have on the model predictions, in particular when forcing data are inaccurate. Furthermore, the predictions from this study are later used for comparison against the hydrologic model predictions after data assimilation with shorter assimilation windows, to determine the optimal length of assimilation windows.

The assimilation of one year of streamflow observations with a year-long assimilation window (Ra2; see Table 5.2 for a summary of the assimilation scenario name definitions) resulted in an improved retrieval of the initial soil moisture state of all soil moisture layers (Fig. 5.6, Table 5.3) and the subsequent simulation. However, the wet bias in the forcing data resulted in a divergence from the true observations quickly after the simulation start. This divergence resulted in the predictions after the assimilation to be close to the control run C2 after day 235, with a full convergence after day 320.

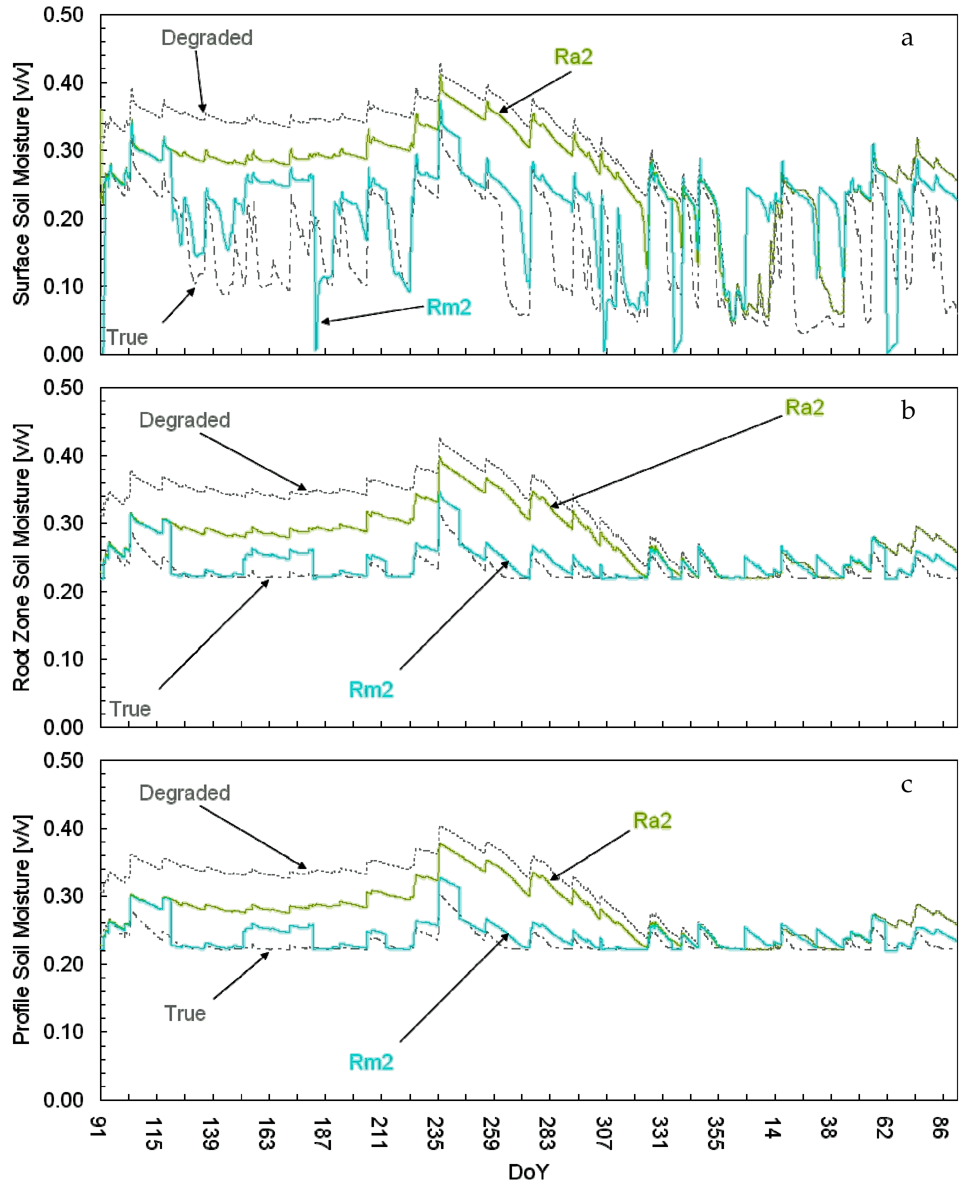

Figure 5.6. Year-long and twelve sequential month-long assimilation window results for streamflow assimilation only. a) Surface , b) root zone, and c) profile soil moisture. The experiment labels are: "True" for the "true" model output; "Degraded" for control run C2; Ra2 for results after assimilation with a one year assimilation window; Rm2 for the results after sequential assimilation of the one-month assimilation windows.

Because of the exceptionally dry season, both control run and assimilated run were close to the true observations after day 320. As a consequence of the inaccurate simulation of soil moisture, both streamflow and evapotranspiration were not adequately predicted (Figs. 5.7 and 5.8) throughout the year.

Table 5.3. RMSE for the volumetric water content, evapotranspiration, and the streamflow for the year-long experiment. The data in brackets is calculated without the summer period, whereas the first number is calculated with the full year of data, and best results are shown in bold.

	Surface *[v/v]*	*Root Zone* *[v/v]*	*Profile* *[v/v]*	*ET* *[mm/d]*	*Streamflow* *[m^3/s]*
Control	0.156 (0.179)	0.095 (0.122)	0.086 (0.112)	1.629 (1.616)	28.66 (36.29)
Annual	0.126 (0.137)	0.061 (0.077)	0.056 (0.070)	1.577 (1.580)	21.41 (26.01)
Monthly	**0.095 (0.077)**	**0.026 (0.031)**	**0.025 (0.031)**	**0.827 (0.694)**	**15.66 (18.57)**

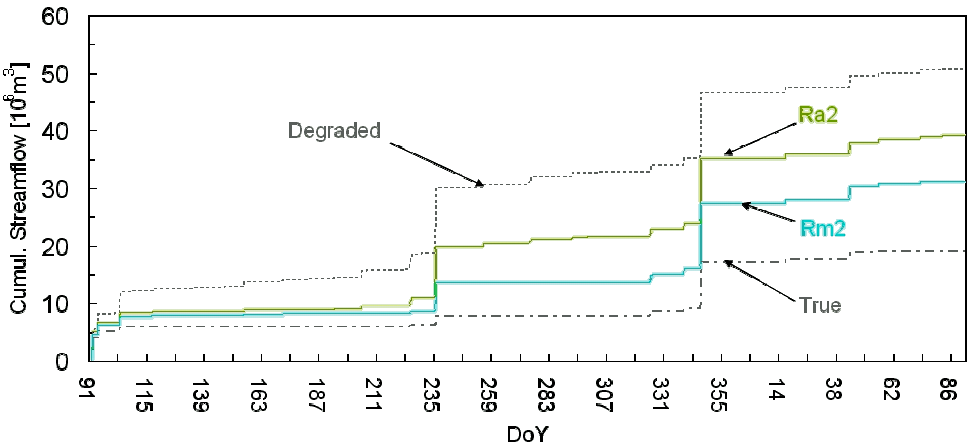

Figure 5.7. Streamflow prediction after streamflow assimilation with year-long and twelve sequential month-long assimilation windows.

Several important aspects are observed in this experiment. First, while the assimilation of streamflow data with a year-long assimilation window improved the initial soil moisture states within the model, the assimilated model prediction diverged from the true observations towards the degraded model predictions in winter (Fig. 5.6). This was due to the wet bias in the forcing data, and the response to the precipitation event around day 235, which led to a wetting of the catchment. Moreover, while the assimilated model output was dried down to the wilting point during summer, where it closely resembled the true observations, the assimilated model predictions showed an identical behaviour to the degraded model

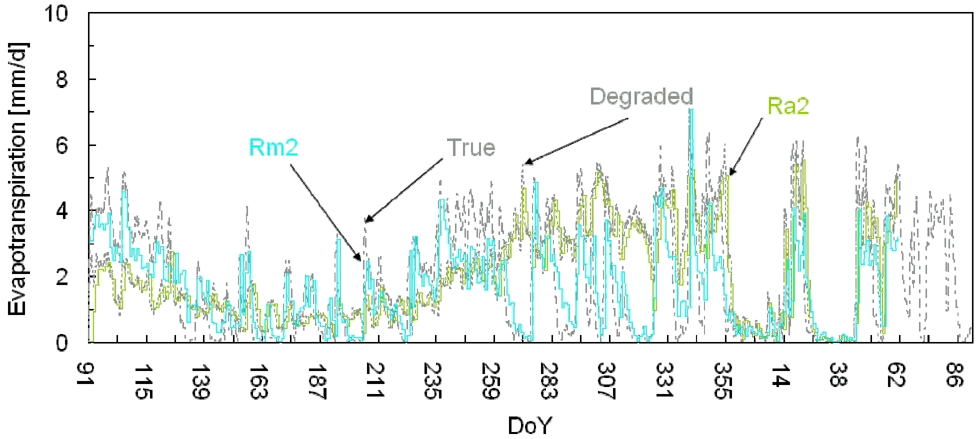

Figure 5.8. Evapotranspiration results after streamflow assimilation with year-long and twelve sequential month-long assimilation windows.

predictions which again diverge from the true observations towards the end of summer. This may be seen as a loss of memory of the soil moisture about its improvement of the initial states. However, the year-long assimilation window had the knowledge of the model reaching this extreme, as this information is implicitly included in the streamflow observations. Nevertheless, the assimilation scheme considered the above results as the best possible fit. The assimilation scheme was unable to make further improvements as the initial soil moisture states could not be reduced below the wilting point, as an initialisation of the model below the wilting point was not allowed and automatically reset by the model.

From these results, it was concluded that year-long assimilation windows are not adequate. This was not an unexpected result, as the presence of forcing and model biases resulted in a divergence of the model from the true observations, due to the accumulation of the forcing errors within the model. Therefore, it was suggested to apply the same streamflow assimilation scheme to a sequence of shorter assimilation windows for the same 12-month period.

5.3.3 Sequential Month-long Assimilation Windows

In order to compare the performance of assimilation windows with different lengths, this section presents the results from twelve sequential month-long assimilation windows over the same 12-month period as in the previous section. In this case, the initial estimates of soil moisture for the subsequent month-long assimilation windows are the predicted soil moisture at the end of the previous month.

The assimilation of streamflow observations with twelve individual month-long assimilation windows (Rm2) showed significant improvement in soil moisture prediction throughout the 12-month period, as compared to the year-long assimilation window (Fig. 5.6). At the same time, streamflow and evapotranspiration were also improved. However, some inaccuracies in the simulation of streamflow and evapotranspiration are evident. They are manifested in the continuing streamflow overestimation (Fig. 5.7) and in particular the underestimation of the evapotranspiration rate (Fig. 5.8). Both were due to the bias in the forcing data. While the streamflow was overestimated due to increased water input into the model, the reduced evapotranspiration rate was due to the reduced downwelling long wave and short wave radiation. A further reduction of the streamflow was not possible, as it would have required an initialisation of the model below the wilting point, however, this was not allowed by the model. The shut down of evapotranspiration was better modelled than with the year-long assimilation window, because soil moisture reached the wilting point on several occasions and therefore restricted evapotranspiration, which led to a high variability in the surface soil moisture.

A significant improvement in soil moisture is observed from the start of the simulation through until the end of December (day 355).

At this point, there was no obvious improvement over the year-long assimilation window experiment or control run. This was caused by the dry summer conditions, driving the model soil moisture to the wilting point, which resulted in assimilated and true observations to be almost identical. However, from about the beginning of March (day 62), the month-long assimilation window predictions again outperformed the predictions for soil moisture from the year-long assimilation window, as the predictions from the year-long assimilation window diverged from the true observations.

The temporal drift apparent in the timing of the dry-down of surface soil moisture (for the month-long assimilation windows) originated from the different times when the root zone reached its wilting point, at which it could not provide any more water through capillary effects to the surface layer. Because the forcing data contained a wet bias in the precipitation, the time when this threshold was reached was later in the assimilation run than in the true simulation, consequently leading to a temporal drift in the decoupling of the surface soil moisture. While the root zone and profile soil moisture did not reach their wilting point, water was still transferred to the surface layer. However, the surface layer dried out when no more water was provided from the lower moisture stores.

Fig. 5.6 shows a further important result. The soil moisture in the period of day of year 152-181 was significantly overestimated as compared to the truth, after the assimilation of one month of data. This was due to the extremely low-flow conditions during that period, where the assimilation scheme was not able to find a best fit to the low streamflow. The reason for this is that the hardly present streamflow provided only limited knowledge about the soil moisture condition in the catchment. As a consequence, the assimilation scheme found a local minimum in the almost flat state space and identified this as the global minimum as the objective function around this point increased. This was verified by relaunching NLFIT from this point with changed search parameters, which resulted in the retrieval of the same values. Nevertheless, the error of this false initialisation was corrected with the next assimilation window, during which a streamflow event containing sufficient information was observed. From these results, it is concluded that the assimilation scheme is immediately self-correcting, when the required information becomes available

In general, the overall performance of the monthly assimilation scheme significantly improved the model predictions. This shows that the assimilation windows have to be kept as short as the model or the environmental conditions allow. The limiting environmental conditions in the present case are the time of concentration for the catchment or the inclusion of at least one streamflow event, to allow the transfer of information from all parts of the catchment within one assimilation window. If the latter is not the case, the assimilation scheme fails to identify the global optimum.

The reason for the significant improvement between the year-long and the month-long windows is that the bias in the forcing data introduced a persistent error by constantly increasing the stored water. This error in the water storage has to be corrected for. Using shorter assimilation windows avoids the accumulation of large errors in the predictions, which otherwise had to be compensated for by large errors in the initial soil moisture states.

In the subsequent sections and later in Chapters 6 and 7, only month-long sequential assimilation windows are used. As shown above, month-long assimilation windows provide a better performance than year-long assimilation windows in the presence of significant model drift from the true observations, due to errors in model physics and/or forcing. While it is desirable to have shorter windows than one month, the conditions in the Goulburn River experimental catchment do not allow for this due to the extensive no- and low-flow conditions. Moreover, the focus of this thesis is a general proof of concept of streamflow assimilation. Detailed improvements to the assimilation scheme are beyond the scope of this thesis and will be left for future research (see section 8.3).

Furthermore, it is shown on Fig. 5.6 that profile and root zone soil moisture were similar throughout the year. Therefore, profile soil moisture will neither be discussed nor its results shown on the figures throughout the remainder of this thesis, because it was assumed to be equal to the root zone predictions.

5.4 *Impact of Forcing Data Errors*

In this experiment, true streamflow observations were assimilated into the model forced with different forcing data scenarios to demonstrate the feasibility of streamflow assimilation when the forcing data is subjected to observational errors, and to identify limitations of the assimilation scheme under such conditions. This experiment was undertaken for a one-month simulation period, only (August 2003), as it was shown in the previous section that month-long assimilation windows are preferable to longer windows, but should include significant streamflow events, and therefore should not be shorter for the study catchment. Furthermore, this experiment focuses on one single month, as the focus of this section is on the effects of observational errors in the forcing data. The application of the assimilation scheme to all 12 months under investigation, would not have led to an improved understanding of the effect errors in forcing data have on the assimilation scheme. The month of August 2003 was chosen, as it included two major streamflow events, and was in the southern hemisphere winter, which meant that some soil moisture dynamics had to be expected, despite the severe drought conditions in the region in 2003.

5.4.1 One Month True and Control Experiments

In this section, several different control scenarios are explored, with the true forcing data having different errors imposed on them. These scenarios are simulations with wet initial conditions, wet and dry biased forcing data, and degraded soil parameters (see Table 5.1). Errors in model predictions are therefore assumed to be solely due to the result of errors in model initial conditions, forcing data, and parameters, with no errors originating from model physics.

5.4.1.1 True Experiment

The true one-month data set is an extraction from the one year of data (Figs. 5.3 to 5.5) of the previous section. The data set comprises the days 213 to 244 (August) of the year 2003. This period was chosen for its two significant precipitation events and the subsequent soil moisture and streamflow variability.

At the beginning of the month true root zone (Fig. 5.9b) and profile (Fig. 5.9c) soil moisture were near or at the wilting point in the true run, which led to a significant dry-down of the surface soil layer (Fig. 5.9a). This was due to the internal physics of CLSM, which did not allow the two deeper layers to dry down beyond the wilting point. Consequently, as no precipitation took place and CLSM restricted the moisture exchange between the root zone and the surface soil moisture under these extreme conditions, the surface soil layer decoupled from the deeper layers and dried down until Day 223, when the first precipitation event took place. The following precipitation events introduced sufficient amounts of water for the soil layer to produce a streamflow response (Fig. 5.10). Later in the month, another precipitation event during day 236 caused a greater

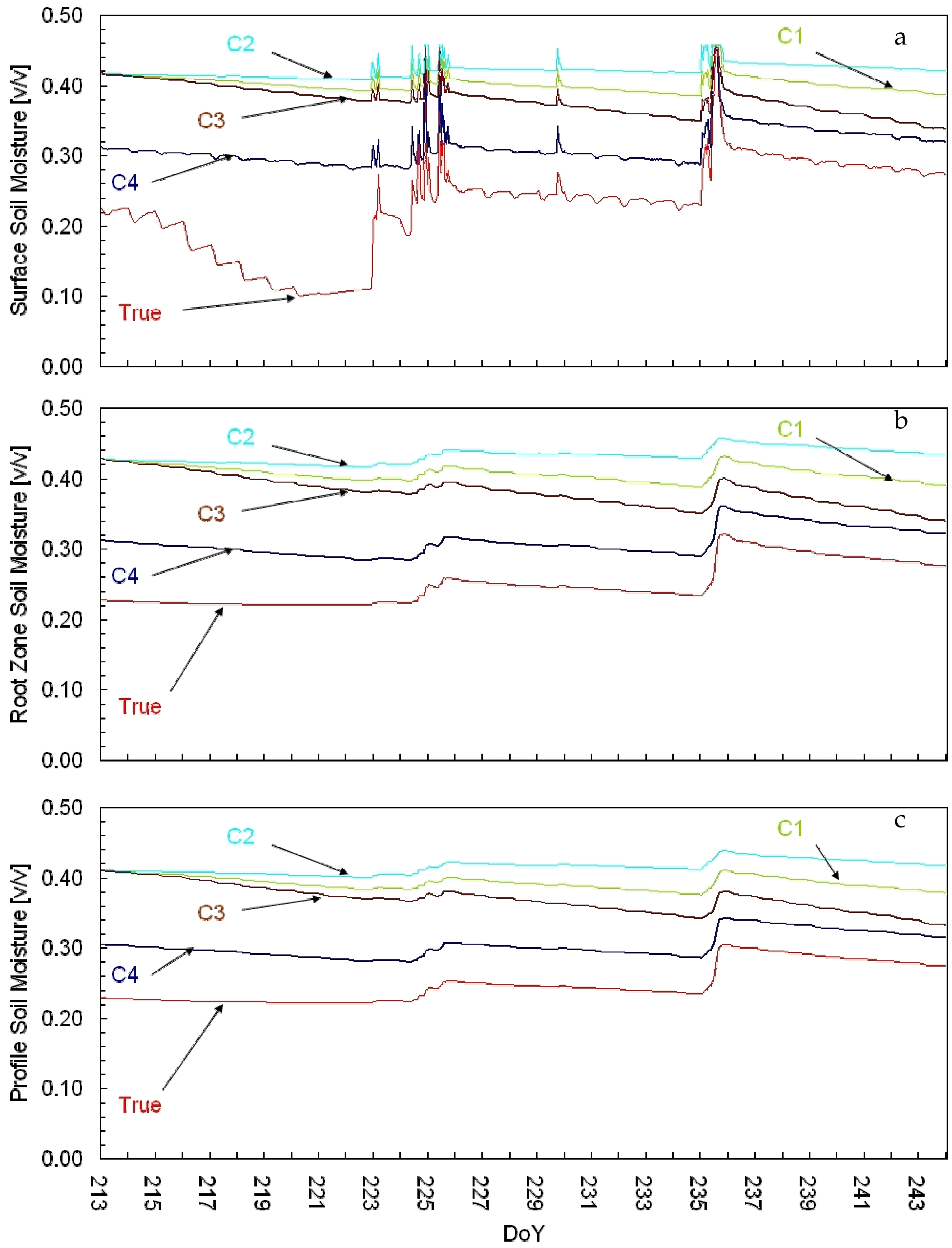

Figure 5.9. Soil moisture true observations and control runs for Catchment 2 for August 2003. a) surface soil moisture, b) root zone soil moisture, and c) profile soil moisture.

response in the river system and the soil moisture. Both rain events introduced sufficient water into the soil to avoid a later dry-down to the wilting point and therefore no dry-down of the surface soil layer similar to the beginning of the month was observed.

The sensible heat fluxes and evapotranspiration rate (Fig. 5.11) from the catchment were affected due to the soil moisture conditions

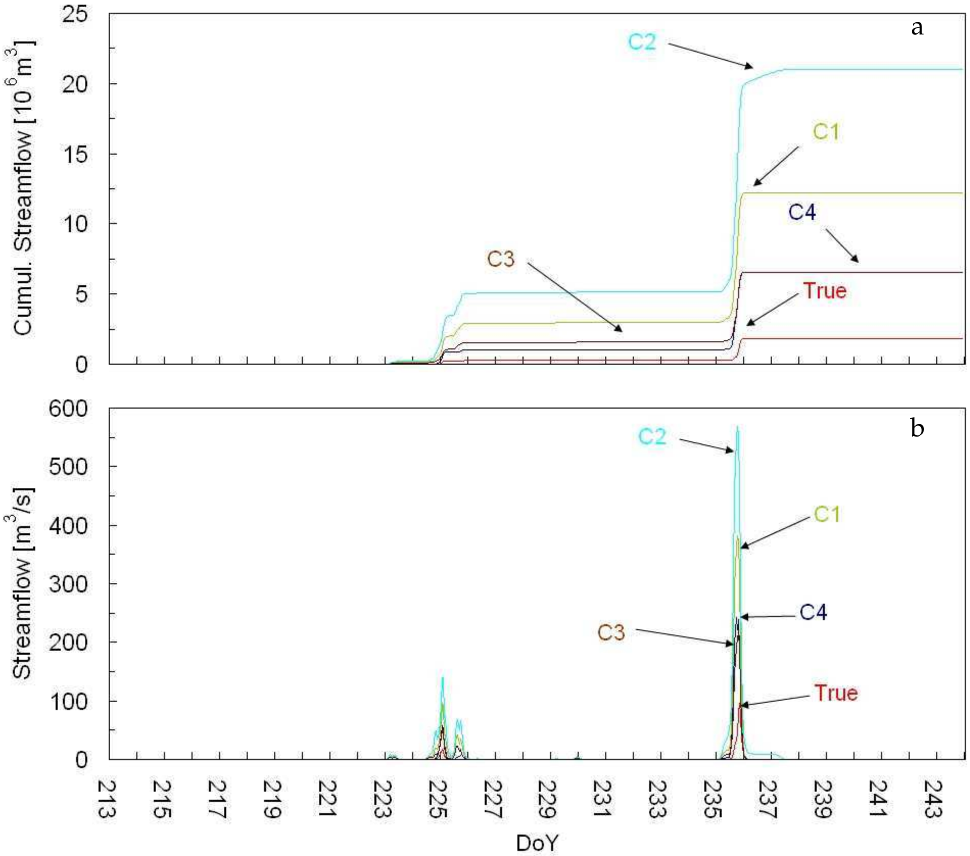

Figure 5.10. True and control run streamflow for August 2003. a) instantaneous streamflow and b) cumulative streamflow.

at the beginning of the month. Sensible heat flux (Fig. 5.11a) was higher at the beginning of the month, than towards the end, due to the lower soil moisture content, while evapotranspiration (Fig. 5.11b) was low at the beginning of the month. The latter was due to constraints following the water stress in the catchment, when soil moisture was at the wilting point and therefore evaporation and transpiration were restricted. This was changed towards the end of the month, as sufficient water had been introduced to the catchment to allow unrestricted evaporation and transpiration to take place.

5.4.1.2 Control Experiment C1

A simple degradation of the initial soil moisture states produced the first degraded control run (C1). This was achieved by setting the catchment deficit (M_D) to 50mm (ie. near saturation; the maximum possible catchment deficit for this catchment was 232mm), and

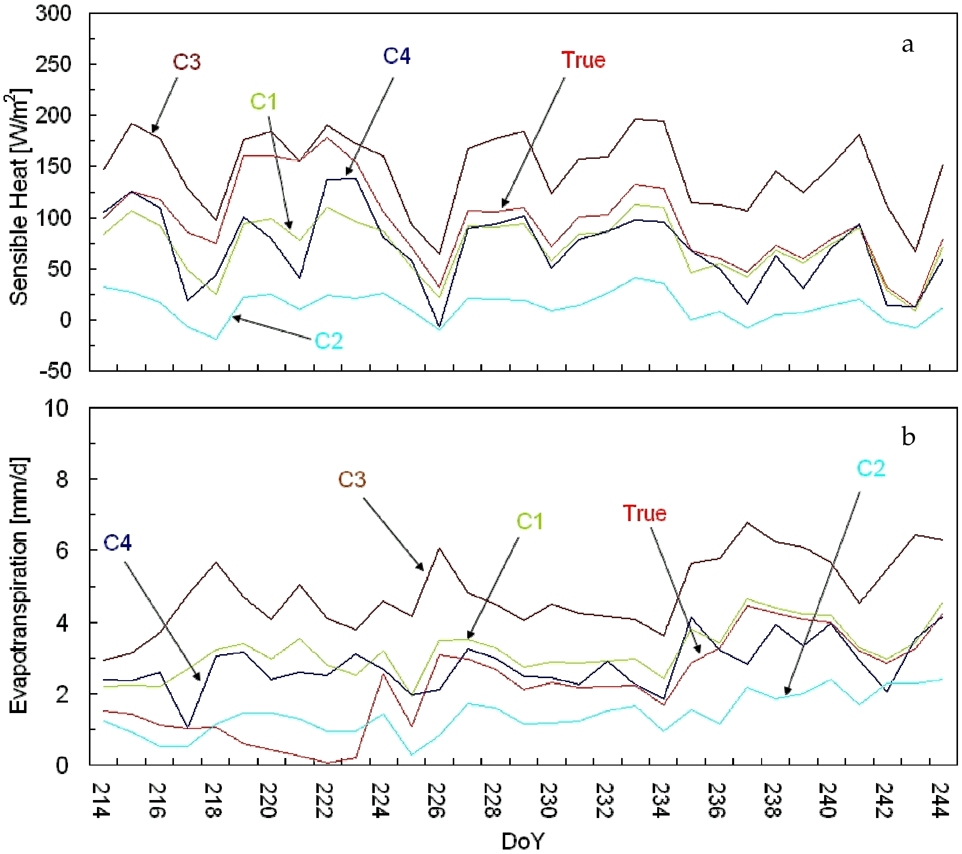

Figure 5.11. Daily averaged a) sensible heat flux and b) evapotranspiration rate for Catchment 2 in August 2003 (true observations and control runs).

surface and root zone excess to 0mm. During this control experiment both soil moisture and streamflow were overestimated throughout the entire month (Fig. 5.8 and 5.9). The true downwelling short wave radiation and air temperature, and the resulting evapotranspiration rate (Fig. 5.11b) did not suffice to dry down the catchment to similar conditions as in the control experiment. Therefore, no decoupling of surface and deeper soil moisture occurred.

The differences in streamflow are significant for the two scenarios. Even though C1 was forced with the same data as the true simulations, the wet initial conditions caused the model to produce a significantly larger amount of streamflow (Fig. 5.10). Hence, streamflow production by the model is sufficiently sensitive to changes in soil moisture that the assimilation of streamflow observations into the model is expected to yield improvements in predicted soil moisture under the same climatic conditions. In contrast to the true simulations, C1 contained sufficient soil moisture at the beginning of the month to allow evaporation and transpiration to take place throughout the whole month (Fig. 5.11b).

5.4.1.3 Control Experiment C2

To this point, the forcing data for the control runs were assumed to be correct, ie. degradation of the model predictions were solely due to initialisation errors. However, observational errors exist in forcing data due to sensor calibration and spatial representativeness of point data. In order to determine the impact of such errors on the assimilation scheme, errors were introduced to the most sensitive forcing data (precipitation and radiation).

The initial soil moisture states of C2 were set to the same wet conditions as for C1, with the addition that downwelling long wave and short wave radiation was reduced by 30% and precipitation increased by 20% for each data point. The wet initial conditions in combination with a wet bias in the forcing data led to a catchment that was almost constantly close to saturation (Fig. 5.9). As evapotranspiration was lower than in the true experiment (Fig. 5.11b), due to the low winter temperatures and the reduced downwelling long wave and short wave radiation, the model was not capable of removing the excessive soil water. This caused a significant overestimation in the streamflow during the precipitation events (Fig. 5.10), as the saturated catchment was not able to store the additional precipitation and a larger portion of the catchment contributed to the surface runoff production (see Chapter 4.3), due to its large area under saturation.

5.4.1.4 Control Experiment C3

The degraded forcing data set of C3 represents a dry bias with decreased precipitation (-20%) and increased downwelling long wave and short wave radiation (+30%). Initial soil moisture states for this control run were set to the same wet conditions of C1 (Fig. 5.9). Therefore, even with having less precipitation and increased radiation, more streamflow was generated than in the true observations (Fig. 5.10). As in the previous control runs, a large proportion of the catchment was close to saturation and therefore the runoff contributing area was still large enough to generate a larger amount of streamflow, than in the true run. Nevertheless, when comparing this data set with the previous two control runs, streamflow was reduced. While the temporal pattern of wetting and drying of the soil moisture was preserved, when compared to the other control runs, a more rapid dry-down took place during rainless periods due to the increased evapotranspiration following the increase in downwelling radiation (Fig. 5.11).

5.4.1.5 Control Experiment C4

The forcing data set for C4 consists of a more "realistic" situation than the previous scenarios, where there is both red and random noise in the forcing data. The precipitation observations received a positive bias of 20%, while no bias was applied to the radiation. Furthermore, the value of the random noise could reach values of up to ±20% of the observed precipitation and ±7.5% for the radiation (see Turner et al., 2006 for a description of the methodology). Care was taken that the average of the absolute error was 0, before the bias was applied to the precipitation. An example of the different steps of the degradation of the precipitation forcing is shown in Fig. 5.12. The reason for applying a bias to the precipitation and not the radiation is to simulate the errors originating from the spatial heterogeneity of precipitation, especially due to convectively driven precipitation rates, such as is the case in the Goulburn River catchment. On the other hand, downwelling long wave and short wave radiation were expected to be relatively homogeneous for the

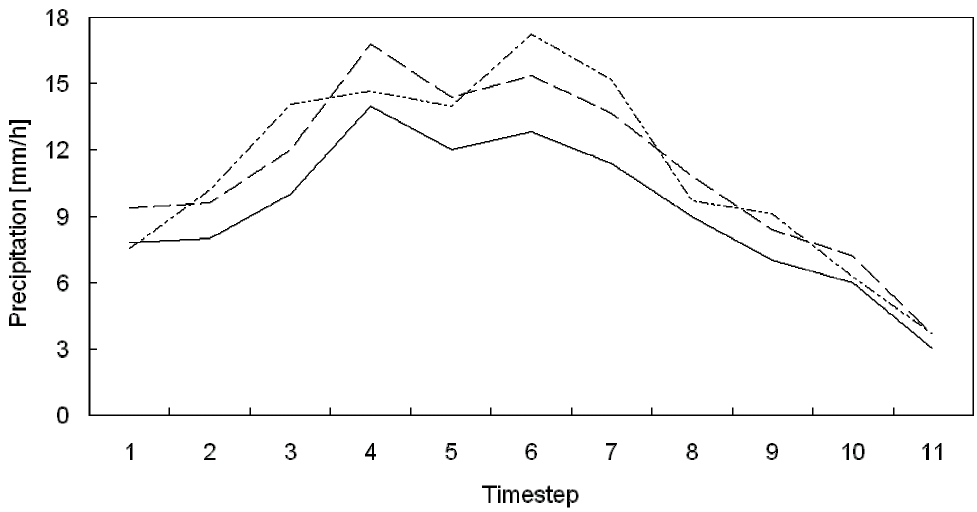

Figure 5.12. Degradation of precipitation forcing data, showing original data (solid line), biased data (dashed line), and data with random noise (dashed-dotted line).

local scales in this study, with only small variability. Unlike the other scenarios, the model was initialised with an initial guess of averaged soil moisture. An average soil moisture was used in this case, as the unrealistically wet initial condition of the previous scenarios may introduce an unrealistically large deviation from the true soil moisture simulation. Using the average of saturation and wilting halves the likely maximum initial error.

The random noise on the radiation led to an evapotranspiration rate similar to the true observations (Fig. 5.11). However, as in scenarios C1 to C3, the initialisation of the model with a high soil moisture content resulted in a higher evapotranspiration rate than the true observations at the beginning of the month.

The deeper soil moisture layers never reached wilting point. Consequently, the surface soil moisture did not show the same dry-down as in the true observations (Fig. 5.9). However, the soil moisture decay throughout the month showed an almost identical slope as the true observations. Due to the wet initialisation and bias, streamflow was overestimated (Fig. 5.10).

5.4.1.6 General Discussion

It is well understood that the over- and underestimation of streamflow produced in the control experiments would have significant impact on the prediction of floods or the allocation of water rights and would consequently have severe negative socio-economic effects. Furthermore, in the context of climate modelling an increase in riverine inputs to the ocean could adversely affect the prediction of local coastal sea surface temperatures, which in turn influence ocean circulation predictions, hence climate model predictions. This again shows the importance of a good prediction of streamflow and soil moisture.

The control runs of this section are a reference for the assimilation studies in the following sections. To avoid cluttering of the following figures, only the true observations are presented alongside the model predictions after the assimilation runs.

5.4.2 Assimilation Under Forcing Scenarios 1 to 4

The figures in this section present the true observations and the model predictions after the assimilation. The degraded model runs are not shown, as all model control experiments were improved and to avoid cluttering of the figures. The reader is referred to Figs. 5.9 to 5.11 and Table 5.4 for a comparison with the control runs.

Fig. 5.13 shows the assimilation results for the surface and root zone soil moisture prediction, while Fig. 5.14 shows the resulting streamflow prediction, and Fig. 5.15 presents the sensible heat flux and evapotranspiration prediction. The RMSE is given in Table 5.4.

5.4.2.1 Scenario R1

A significant improvement to the initial soil moisture states was observed for the surface and root zone soil moisture after the assimilation of streamflow observations under scenario 1 (R1; Fig. 5.13 and Table 5.4). These soil moisture initial states were retrieved

Table 5.4. RMSE for the volumetric soil moisture content, sensible heat flux, evapotranspiration, and the streamflow after the assimilation of streamflow only. The data in brackets is RMSE of the respective control run. The best results are in bold.

	Surface [v/v]	*Root Zone [v/v]*	*Profile [v/v]*	*Sens. Heat [W/m²]*	*ET [mm/d]*	*Streamfl. [m³/s]*
R1	**0.012** (0.184)	**0.001** (0.160)	**0.001** (0.146)	**7.013** (42.686)	**0.315** (1.933)	**0.023** (26.474)
R2	0.055 (0.200)	0.025 (0.183)	0.022 (0.168)	106.007 (110.695)	1.775 (1.768)	13.317 (43.380)
R3	0.101 (0.167)	0.065 (0.138)	0.060 (0.128)	67.845 (65.268)	3.261 (3.435)	0.689 (12.173)
R4	0.029 (0.096)	0.002 (0.062)	0.002 (0.057)	51.807 (61.454)	1.125 (1.903)	5.862 (14.777)

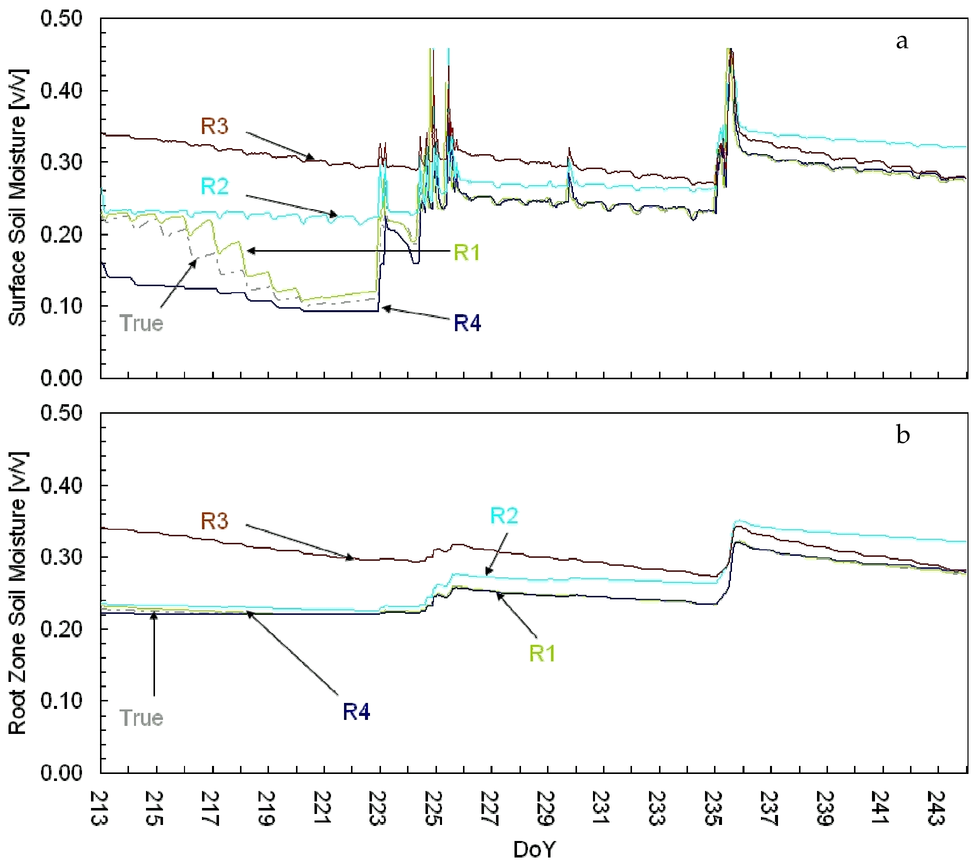

Figure 5.13. One-month assimilation window results for streamflow assimilation only. a) Surface and b) root zone soil moisture. The experiment labels are described in Table 5.2. These results are to be compared with the control run results in Fig. 5.9.

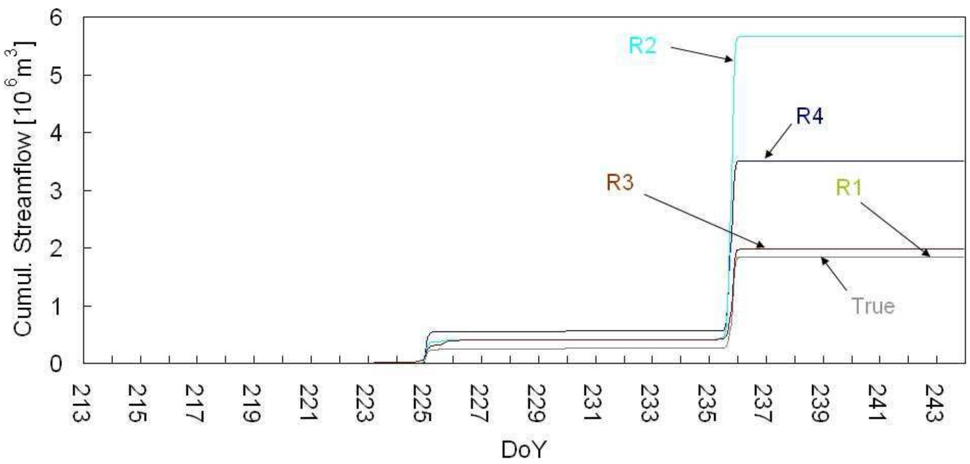

Figure 5.14. One-month assimilation window results of cumulative streamflow after streamflow assimilation only. The experiment labels are described in Table 5.2. These results are to be compared with the control run results in Fig. 5.10.

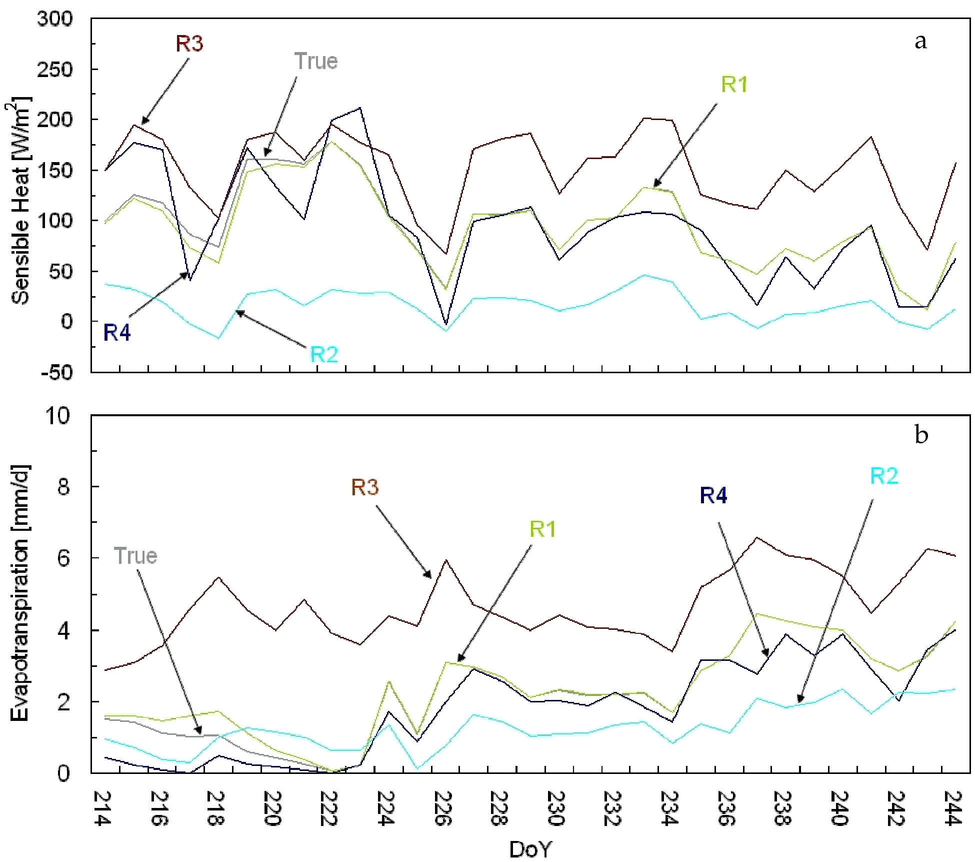

Figure 5.15. One-month assimilation window results of a) sensible heat flux and b) evapotranspiration after streamflow assimilation only. The experiment labels are described in Table 5.2. These results are to be compared with the control run results in Fig. 5.11.

to a high level of accuracy and the model response from this initialisation was almost identical to the true observations. Similarly, the streamflow was well predicted (Fig. 5.14).

Unsurprisingly, these results show that streamflow observations contain sufficient information about the upstream soil moisture conditions to allow the retrieval of initial soil moisture states, albeit within the context of a perfect model. However, as true streamflow observations were assimilated into the model from which they were obtained, retrieving the correct initial states was a simple task, with the assimilation scheme finding a near perfect fit for the root zone. Nevertheless, while the root zone soil moisture was well retrieved, a similarly good retrieval of the surface soil moisture state was not achieved. The reason for this effect was that the streamflow within the assimilation window was not sufficiently sensitive to changes in the surface soil moisture. This is an artefact of the very dry conditions in the catchment. In the present experiment, the surface soil moisture reached saturation, before any significant streamflow events took place. After the saturation of the soil, the surface soil moisture behaved like the true observation, as the root zone and profile soil moisture were correctly predicted. Because surface soil moisture plays an important role in the partitioning of the precipitated water into surface runoff and infiltration water, a wrong initialisation of the surface soil moisture impacts on the surface runoff in wet catchments. However, since no surface runoff and consequently no streamflow was produced prior to the saturation taking place, the initial surface soil moisture state can have any physically possible value, without changing the streamflow later in the month. The same effect has also been observed and briefly discussed in the previous 12-month experiment.

Due to the improved soil moisture predictions, sensible heat flux and evapotranspiration were, also, well predicted (Fig. 5.15), which is a direct consequence of the synthetic environment. However, because the surface soil moisture state was not properly retrieved, sensible heat flux and evapotranspiration started with some offset to the true observations. Nevertheless, true observations and predictions quickly converged.

5.4.2.2 Scenario R2

While the soil moisture initial states were well retrieved under a wet bias (R2), this wet bias prevented the model to predict the dry-down in the true simulation, where root zone and surface soil moisture reached the wilting point causing surface soil moisture to decouple from the root zone soil moisture. This resulted in the surface soil layer to always receive water in exchange from the root zone layer. The temporal patterns of the root zone and profile soil moisture were fairly well predicted, but tended to overestimate the soil moisture content, particularly toward the end of the assimilation window. However, the predicted streamflow was significantly improved when compared to the control experiment, with a streamflow maximum value of 243.0m^3/s as compared to 569.4m^3/s, but was still significantly overestimated as compared to the true observations (96.6m^3/s).

The overestimation of streamflow was caused by the increased precipitation and reduced evapotranspiration due to the decreased downwelling long wave and short wave radiation. The only possibility for a reduction in streamflow would have been achieved by a reduction of the soil moisture content, thus altering the partitioning between infiltration and runoff. However, the initial soil moisture content could not be reduced below the wilting point. As the true soil moisture content was already close to the wilting point in this experiment, a further reduction in initial soil moisture was not possible. Thus, the only way to achieve a better fit to the observed streamflow and hence soil moisture may be to use shorter assimilation windows. However, this could lead to having no significant streamflow event taking place within the assimilation window and consequently having an adverse effect on the assimilation. This adverse effect was shown for the 12-month experiment (section 5.2), where no streamflow occurred in one month and the assimilation scheme was displaying difficulties to retrieve the correct initial soil moisture states. Even though the soil moisture content was improved in the present assimilation, no significant improvements to the sensible heat flux and evapotranspiration were observed for R2. This shows that the evapotranspiration was not limited by soil water availability.

5.4.2.3 Scenario R3

While the RMSE of streamflow was very small (0.689m^3/s) for R3, the retrieval of the soil moisture states did not produce good results. Because of the extreme dry bias and the reduced water input (through reduced precipitation), the model required a significant overestimation of the root zone soil moisture, in order to provide sufficient water for the streamflow production to reduce the least-square error of the streamflow.

Furthermore, sensible heat flux and evapotranspiration were not improved, despite the improvement in soil moisture. This was explained with the soil never reaching wilting. Consequently, sensible heat flux and evapotranspiration were never water stressed, which would have led to an increase in sensible heat flux and a decrease in evapotranspiration.

5.4.2.4 Scenario R4

The last experiment with random noise on the radiation forcing and a wet bias in the precipitation (R4) resulted in a good improvement of the streamflow and soil moisture predictions. However, the sensible heat flux and evapotranspiration were only marginally improved at the beginning of the month. In this experiment, like in R2 (wet bias), the streamflow error could not be further reduced, as the initial soil moisture states could not be set below wilting point, in order to reduce streamflow. Furthermore, because of the retrieved initial root zone soil moisture state being at wilting point, the surface soil moisture state could not be easily retrieved. Any changes to the initial surface soil moisture did not influence the streamflow prediction of the model, as it would have required to initialise the model with soil moisture states below the wilting point. The shown initial value is therefore a random value, as the state-space for the surface soil moisture was flat, consequently the assimilation scheme could not find an optimal solution and stopped at a random value.

5.4.2.5 General Discussion

The responses of sensible heat flux and evapotranspiration show some interesting aspects of streamflow assimilation. First, an improvement to the evapotranspiration only took place at the beginning of the month, when the true observations were under water stress and the assimilation scheme was able to reduce the root zone soil moisture state to the wilting point. However, there were only small improvements during the second half of the month, when the evapotranspiration was not water limited anymore, but rather controlled by the downwelling radiation. Any influence of the changes in the initial conditions was limited, as it would have been required in most scenarios to lower the initial conditions below the wilting point. Second, some adverse effects became evident for the sensible heat flux. In particular for R4, for which the sensible heat fluxes were increased beyond the observed values at the beginning of the month. This was caused by the unchanged radiation with reduced surface soil moisture content. However, the total error decreased, because of the more significant initial underestimation of the sensible heat was reduced due to the increase at the beginning of the month. Moreover, despite a better prediction of soil moisture in R2 (wet forcing bias) and R3 (dry forcing bias), only small improvements were made to the sensible heat flux and evapotranspiration. These two cases show that extreme biases have a significant impact on the model predictions, which could not be overcome by this data assimilation scheme, as model and observation errors are not explicitly included in the formulation of the objective function. Finally, in particular R3 showed that the soil moisture values were not sufficiently constrained and could be significantly overestimated.

5.5 *Impact of Parameter Errors*

A further source of error in hydrologic modelling may stem from the model parameters (in this synthetic study, it may also be seen as a surrogate for error in the model physics). As model parameters are generally spatial averages, obtained empirically or from remote sensing platforms, they unavoidably contain errors due to the assumptions made for their estimation and/or aggregation. In particular, soil properties have a high spatial variability. However, CLSM uses only the predominant soil type within a catchment to represent the soil type for the whole catchment.

In the present study, the initial soil type was replaced with a similar soil type in terms of particle distribution (silt clay instead of clay). Consequently, the model was run with different values for porosity (0.468 instead of 0.457), wilting point (0.255 instead of 0.221), matric potential ψ_s (-0.3236m instead of -0.4677m), and the water profile shape parameter β (10.39 instead of 11.55), and *Ks(surface)*

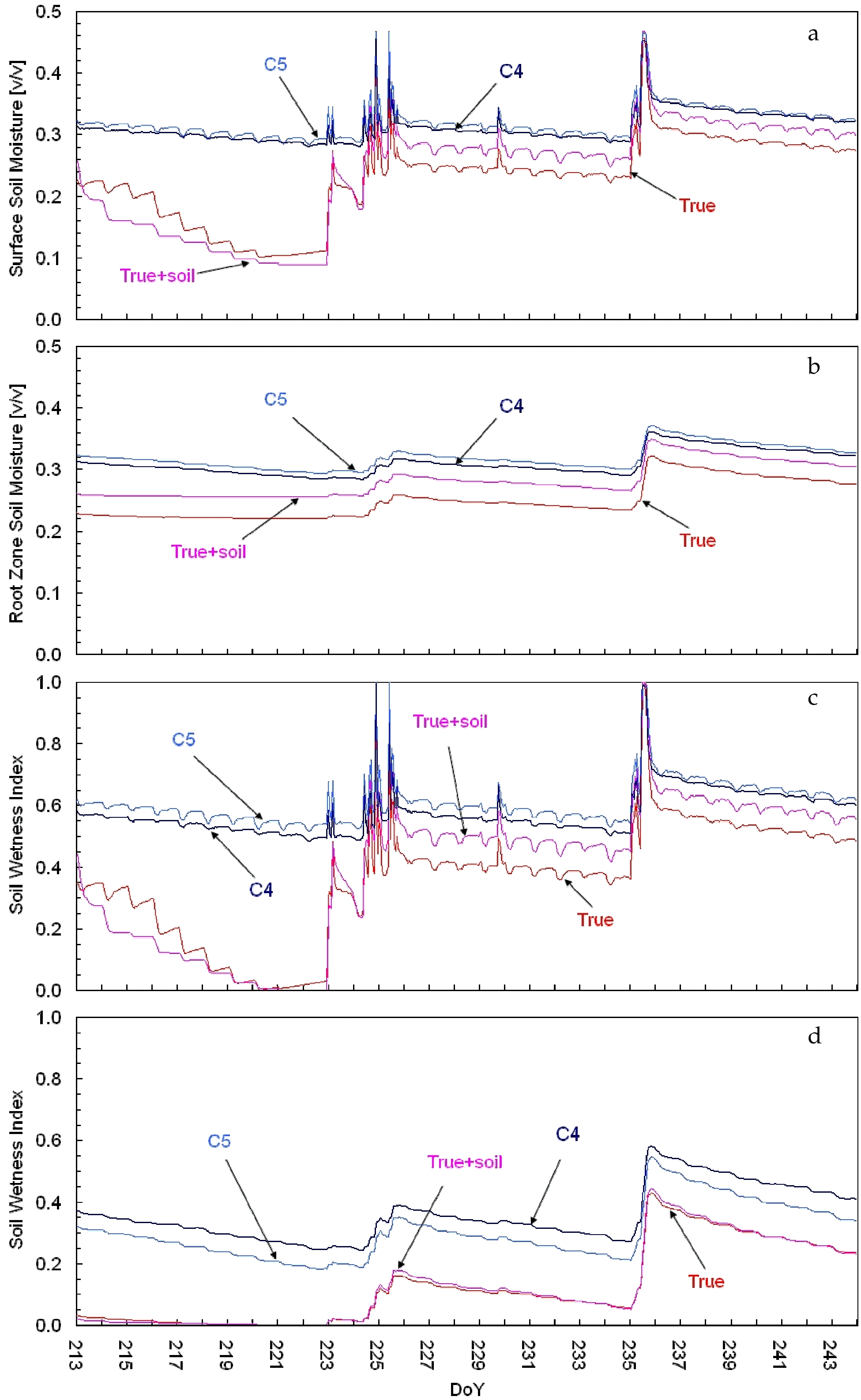

Figure 5.16. a) Surface soil moisture, b) root zone soil moisture, c) surface soil wetness index, and d) root zone soil wetness index for Catchment 2 (true and control runs).

(0.0016m/s instead of 0.0011m/s). This led to a discrepancy of the soil moisture predictions between the true experiment and the predictions of the control run (Fig. 5.16). Because the soil moisture thresholds (wilting point and saturation/porosity) of the two experiments are different, it is difficult to compare the absolute values of the model soil moisture predictions. A soil wetness index is therefore used, in order to normalise the soil moisture content. The soil wetness index (SWI) is defined as

$$SWI = \frac{\theta_{obs} - \theta_{wilt}}{\theta_{sat} - \theta_{wilt}}, \tag{5.1}$$

where θ_{obs} is the observed soil moisture content [v/v]; θ_{wilt} the soil moisture content at wilting [v/v]; and θ_{sat} the soil moisture content at soil saturation [v/v].

5.5.1 Control Run

The resetting of the soil parameters caused an offset in the soil moisture predictions, which was most significant for the period when the soil was water stressed at the beginning of the month, due to the change of the wilting point. The predictions form the true simulation for the two soil conditions had an offset of 0.04v/v (Figs. 5.16a and 5.16c). However, this did not have a significant impact on the sensible heat flux and evapotranspiration rate (Fig. 5.17), because the temporal pattern of water stressed and un-stressed periods did not change. On the other hand, streamflow was increased (Fig. 5.18) due to the reduced storage capacity of the surface which led to a quicker saturation of the surface layer and therefore to an increase in the runoff contributing area.

5.5.2 Scenario R5

The assimilation of streamflow data into the degraded model showed some improvement to the soil moisture content and the streamflow, as compared to the control run (Table 5.5, Figs. 5.19 and

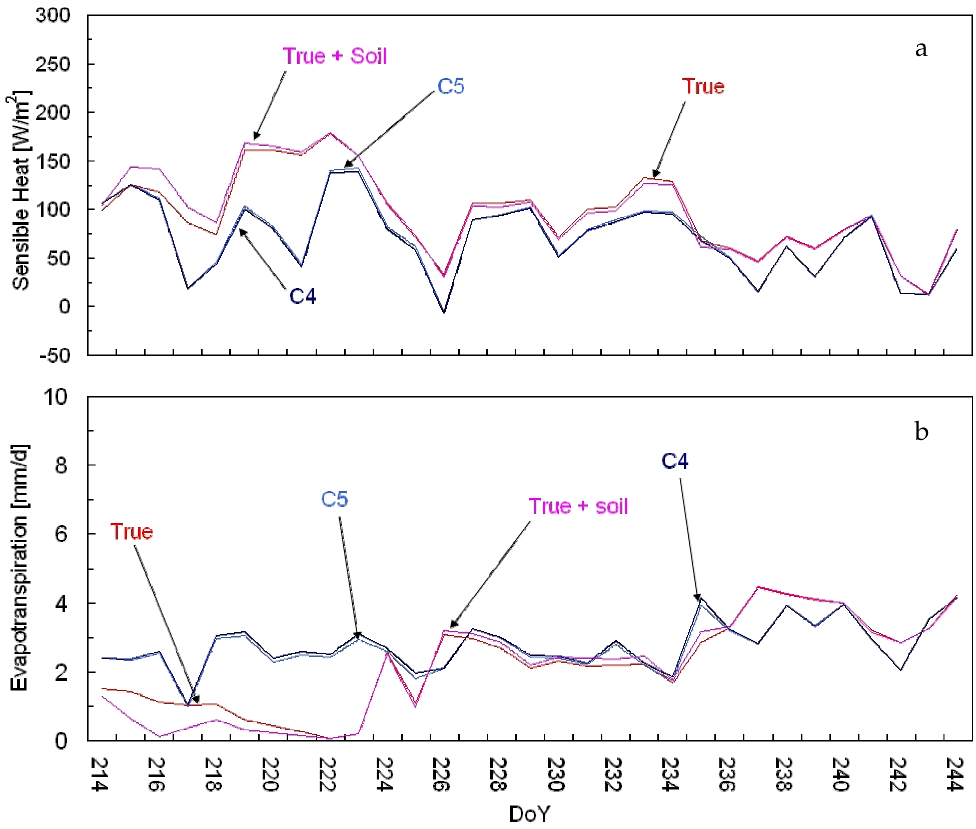

Figure 5.17. a) Sensible heat flux and b) evapotranspiration for Catchment 2 (true and control runs).

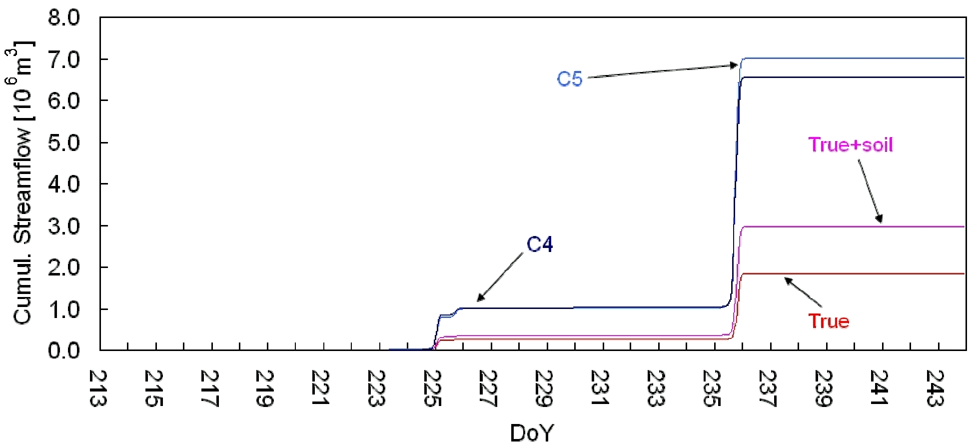

Figure 5.18. Cumulative streamflow for Catchment 2 (true and control runs).

5.20). The new soil parameters did not allow the catchment to be initialised below 0.255v/v, the new wilting point, which was higher than the original wilting point. This was the cause for some overprediction in the streamflow, as the initial soil moisture states could not be reset to the required values. Consequently, the soil

Table 5.5. RMSE for the volumetric soil moisture content, sensible heat flux, evapotranspiration, and the streamflow for the degraded soil experiment before and after streamflow assimilation (C5/R5) in absolute values and for the soil wetness index. Best RMSE values are shown in bold.

	Surface [v/v]	*Root Zone [v/v]*	*Profile [v/v]*	*Sens. Heat [W/m²]*	*ET [mm/d]*	*Streamfl. [m³/s]*
C5	0.104	0.072	0.068	59.857	1.795	16.438
R5	**0.042**	**0.033**	**0.032**	**52.653**	**1.179**	**9.919**
Soil Wetness Index						
C5	0.282	0.192	0.173	*as C5*	*as C5*	*as C5*
R5	**0.108**	**0.011**	**0.009**	*as R5*	*as R5*	*as R5*

moisture prediction was too high throughout the month, therefore resulting in a streamflow prediction, which was higher than in the true simulation, but an improvement in the control run.

As in the previous experiments, the correct surface soil moisture state was difficult to determine, because of its lack of influence on the streamflow within the assimilation window. At the end of the assimilation process, the data assimilation scheme found a value of 0.127v/v. While the absolute root zone soil moisture content after assimilation did not match the true observations there was an almost perfect match with an RMSE of 0.011 for the SWI. At the same time, the sensible heat flux and the evapotranspiration rate were improved (Fig. 5.21), in particular at the beginning of the month, where the soil moisture predictions after the assimilation were set to the wilting point.

This experiment shows that despite errors in the soil parameter set, streamflow data assimilation can still be used to improve soil moisture predictions, provided the comparison is made in terms of a soil wetness index. While the absolute values of the soil moisture predictions did not compare well, their normalised values were almost identical for the root zone, which resulted in a good

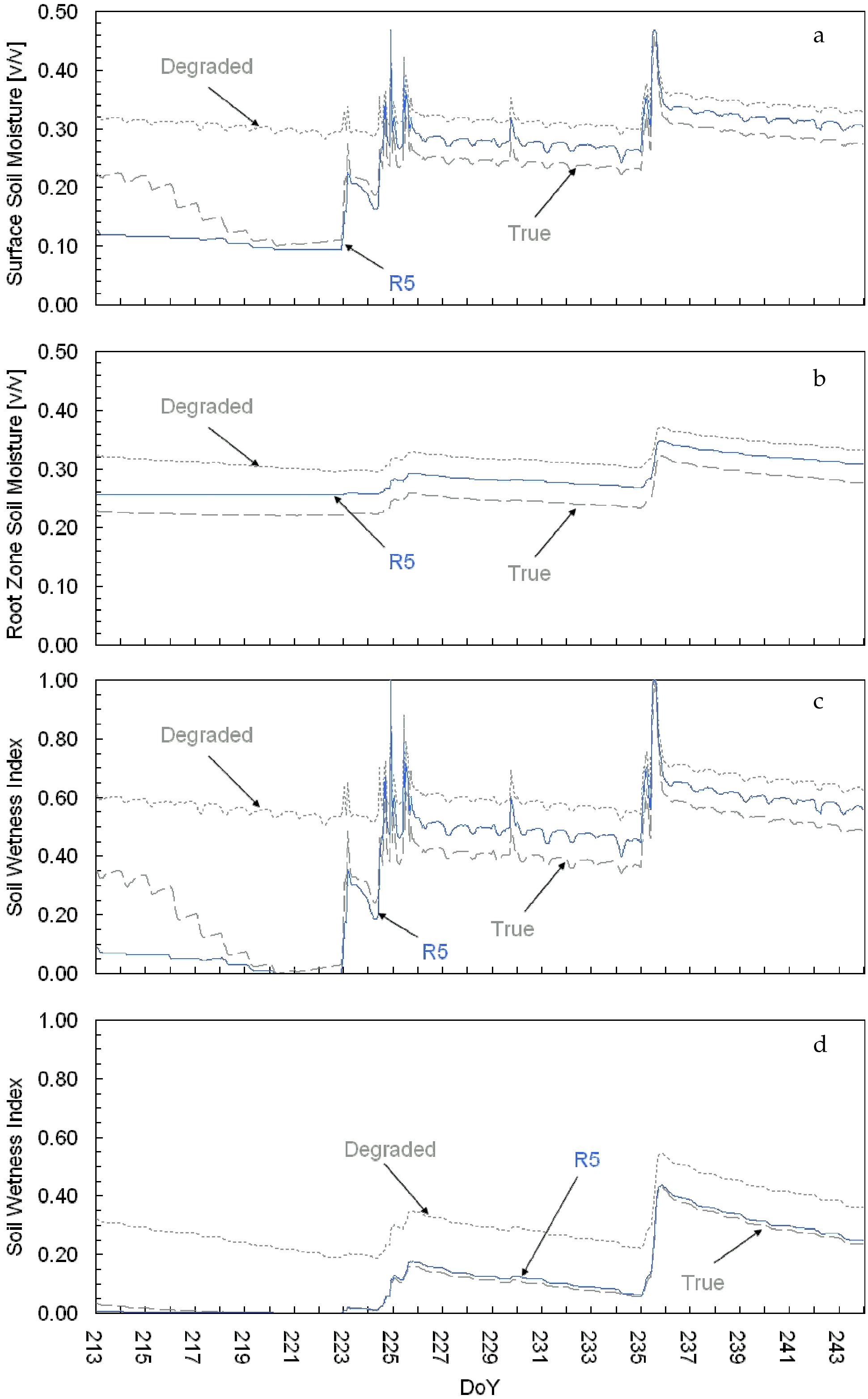

Figure 5.19. a) Surface soil moisture, b) root zone soil moisture, c) surface soil wetness index, and d) root zone soil wetness index for the Catchment 2 (after streamflow assimilation).

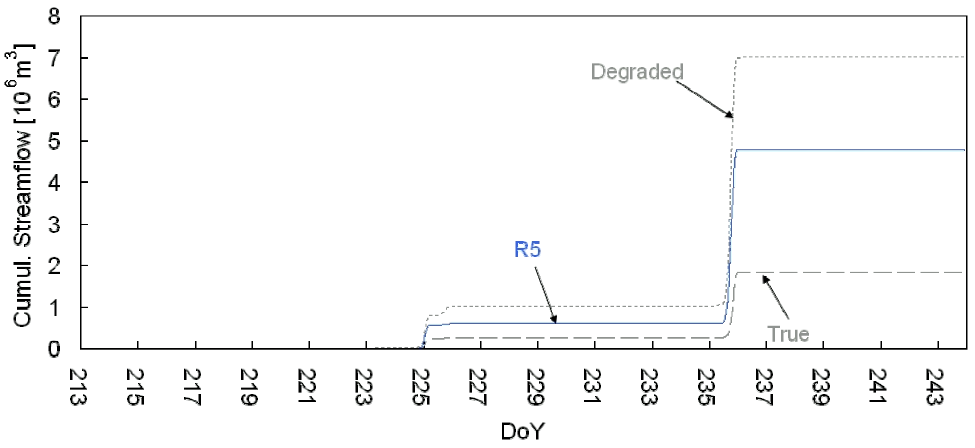

Figure 5.20. Cumulative streamflow for Catchment 2 (after streamflow assimilation).

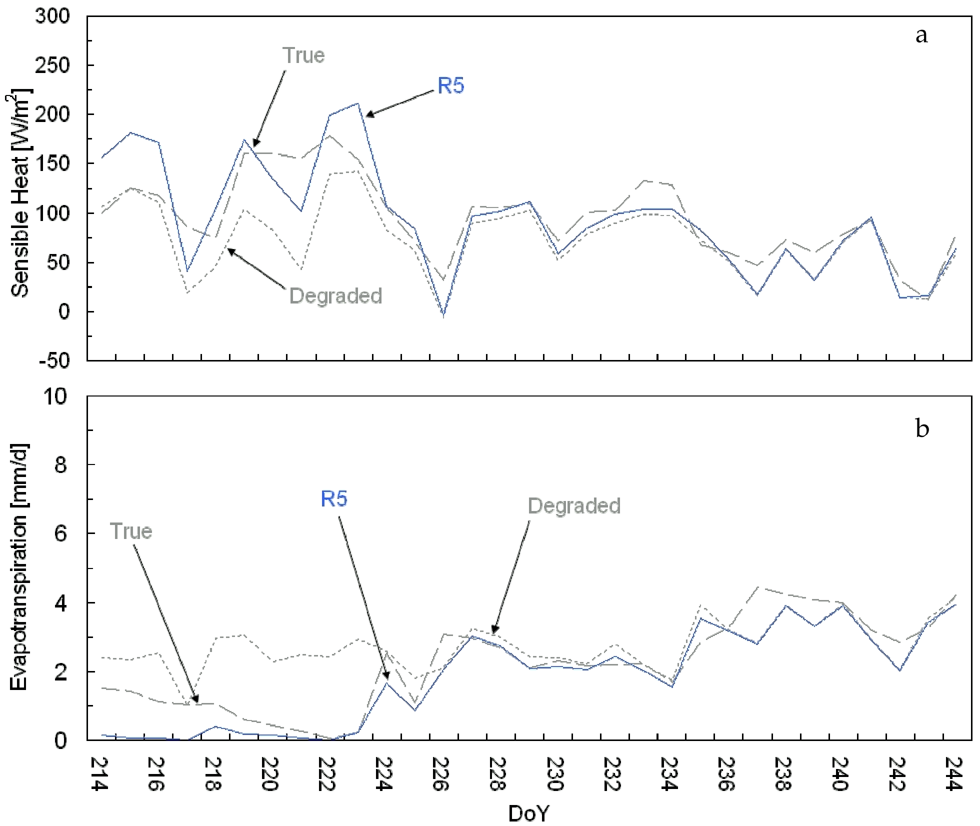

Figure 5.21. a) Sensible heat flux and b) evapotranspiration for Catchment 2 (after streamflow assimilation).

prediction of the sensible heat flux and the evapotranspiration rate.

5.6 Assimilation of Surface Soil Moisture Observations

As the aim of this thesis is the use of streamflow data assimilation where remotely sensed surface soil moisture observations are not available, this section may seem out of the scope of this thesis. However, this study explores the relative performances of streamflow and surface soil moisture assimilation and provides the basis for a potential joint assimilation, in the case that both observations become available.

In the previous sections, the model tended to produce a divergence of the true and assimilation predictions of surface and root zone soil moisture, if significant errors were present in the forcing data. This problem was kept small by reducing the length of the assimilation window to one month, as the absolute error in the mass balance was smaller over a shorter period. Nevertheless, the retrieval of the surface soil moisture states was always difficult. To further constrain the retrieval process of surface soil moisture, it is suggested to assimilate remotely sensed surface soil moisture observations and to study the effects of this approach, if and where surface soil moisture observations are available.

The present experiment is presented in two parts. First, it was assumed that no streamflow observations were available and therefore observations were limited to remotely sensed surface soil moisture observations only, which were then assimilated into the model. Then, surface soil moisture and streamflow observations were jointly assimilated into the model. The assimilation of soil moisture observations alone and the joint assimilation of streamflow and soil moisture was undertaken for the scenarios 1 to 4, with model parameter errors ignored as in the previous experiments. The

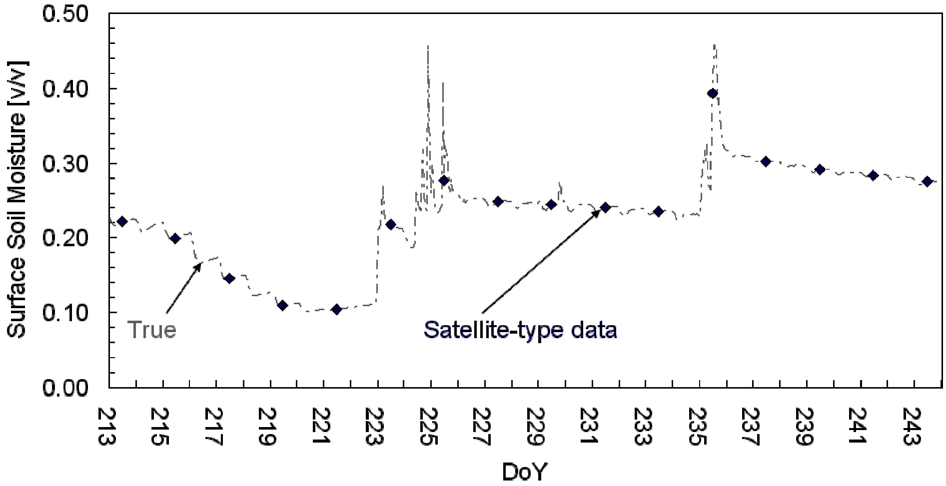

Figure 5.22. Simulated satellite overpasses. Assumed overpass rate is once every 48 hours. Presented is the surface soil moisture from the true run (dashed-dotted line) and the derived single observations (diamonds).

results from these new experiments are compared with the control runs C1 to C4 and the results from the experiments on streamflow assimilation.

5.6.1 Source of Surface Soil Moisture Observations

To simulate the use of satellite remote sensing data, only one surface (top 2cm) soil moisture observation every two days was extracted from the true surface soil moisture simulation (Fig. 5.22). This is in conformity with the satellite repeat time for instruments such as AMSR-E or the future SMOS mission at the latitudes of the Goulburn River catchment. In the past, the assimilation of surface soil moisture into hydrological land surface models was primarily undertaken to improve surface soil moisture values and hence surface heat fluxes or to predict the soil moisture profile within the soil layer, while only some studies focussed on the retrieval of surface soil moisture to improve streamflow (see Chapter 2). For the present study, true remotely sensed surface soil moisture observations were assimilated not only to improve the modelled surface soil moisture states but also to quantitatively assess the impact of their assimilation on streamflow predictions by

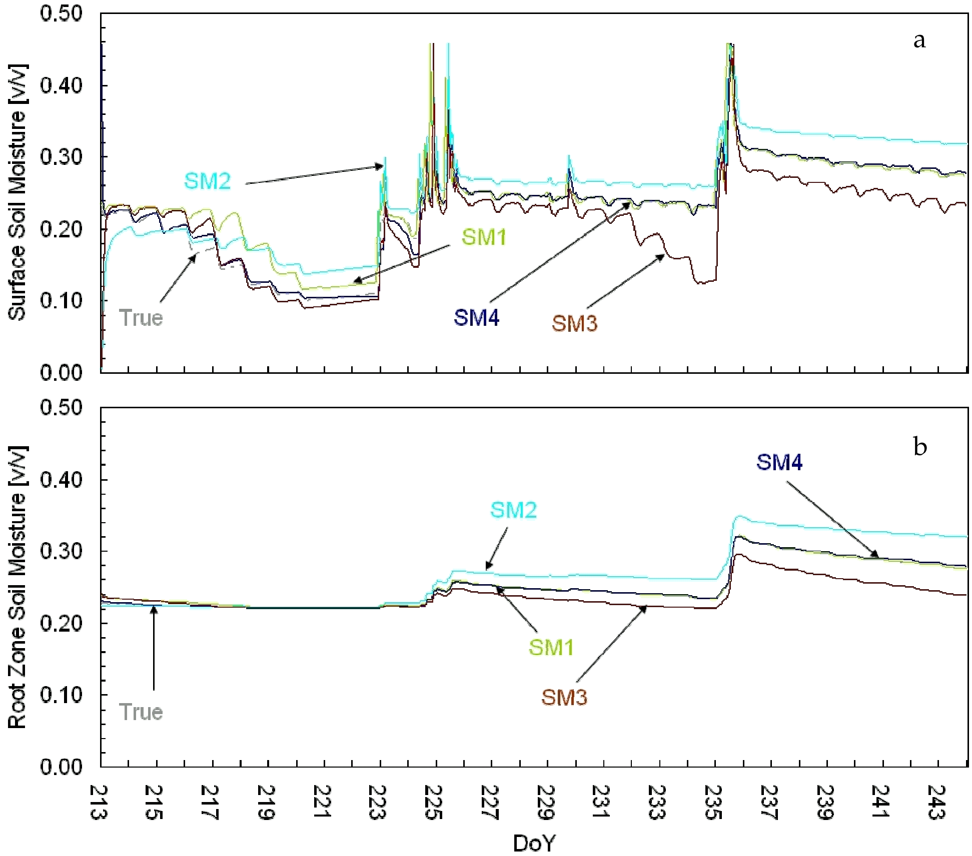

Figure 5.23. One-month assimilation window results for surface soil moisture assimilation only. a) Surface and b) root zone soil moisture. The experiment labels are described in Table 5.2. These results are to be compared with the control run results in Fig. 5.9.

comparison to streamflow observations. This experiment will provide information on whether the additional assimilation of surface soil moisture has a positive or negative impact on the streamflow predictions of a model under different conditions.

5.6.2 Assimilation of Surface Soil Moisture Observations

5.6.2.1 Scenario SM1

Unsurprisingly, the assimilation of remotely sensed surface soil moisture alone under scenario 1 (SM1) led to a good retrieval of the three prognostic soil moisture states within CLSM, and therefore the soil moisture (Fig. 5.23, Table 5.6) and streamflow prediction (Fig 5.24). However, a slight overestimation of the initial root zone soil moisture state, as compared to the true observations, affected the

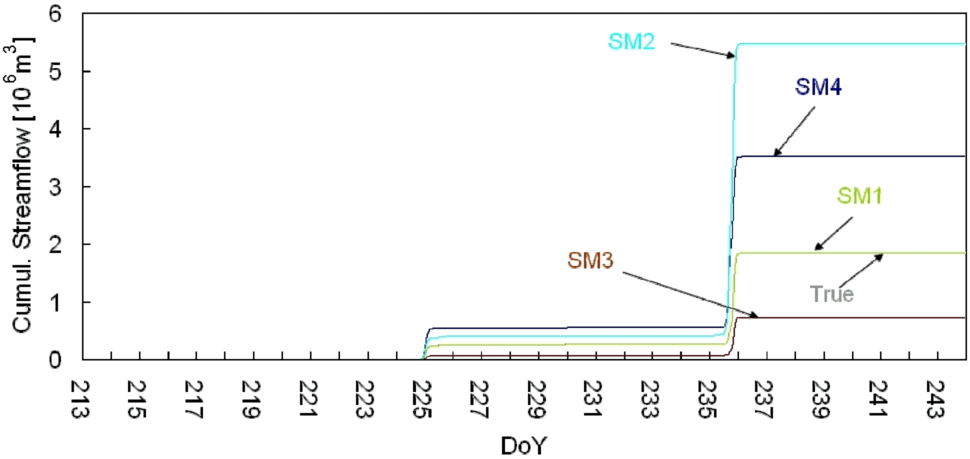

Figure 5.24. Cumulative streamflow for Catchment 2 after assimilation of remotely sensed surface soil moisture. . The experiment labels are described in Table 5.2. These results are to be compared with the control run results in Fig. 5.10.

dry-down of the surface soil layer. This was caused by the profile soil moisture (not shown) not reaching the wilting point until day 217. Nevertheless, the streamflow was well matched, as the soil moisture after the main precipitation event was correctly predicted. Sensible heat flux and evapotranspiration after assimilation of the surface soil moisture observations still had errors, caused by the small discrepancy in the retrieval of the initial surface soil moisture state (Fig. 5.25, Table 5.6). However, both predictions converged with the true observations by day 220.

Table 5.6. RMSE for the volumetric soil moisture content, evapotranspiration, sensible heat flux, and the streamflow after the assimilation of surface soil moisture. The data in brackets is RMSE of the respective control run.

	Surface [v/v]	*Root Zone [v/v]*	*Profile [v/v]*	*Sens. Heat [W/m^2]*	*ET [mm/d]*	*Streamfl. [m^3/s]*
SM1	0.021 (0.184)	0.002 (0.160)	0.002 (0.146)	11.252 (42.686)	0.508 (1.933)	0.008 (26.474)
SM2	0.033 (0.200)	0.023 (0.183)	0.020 (0.168)	100.470 (110.695)	1.772 (1.768)	12.599 (43.380)
SM3	0.035 (0.167)	0.018 (0.138)	0.016 (0.128)	103.800 (65.268)	1.339 (3.435)	3.465 (12.173)
SM4	0.011 (0.096)	0.001 (0.062)	0.001 (0.057)	48.762 (61.454)	0.952 (1.903)	5.878 (14.777)

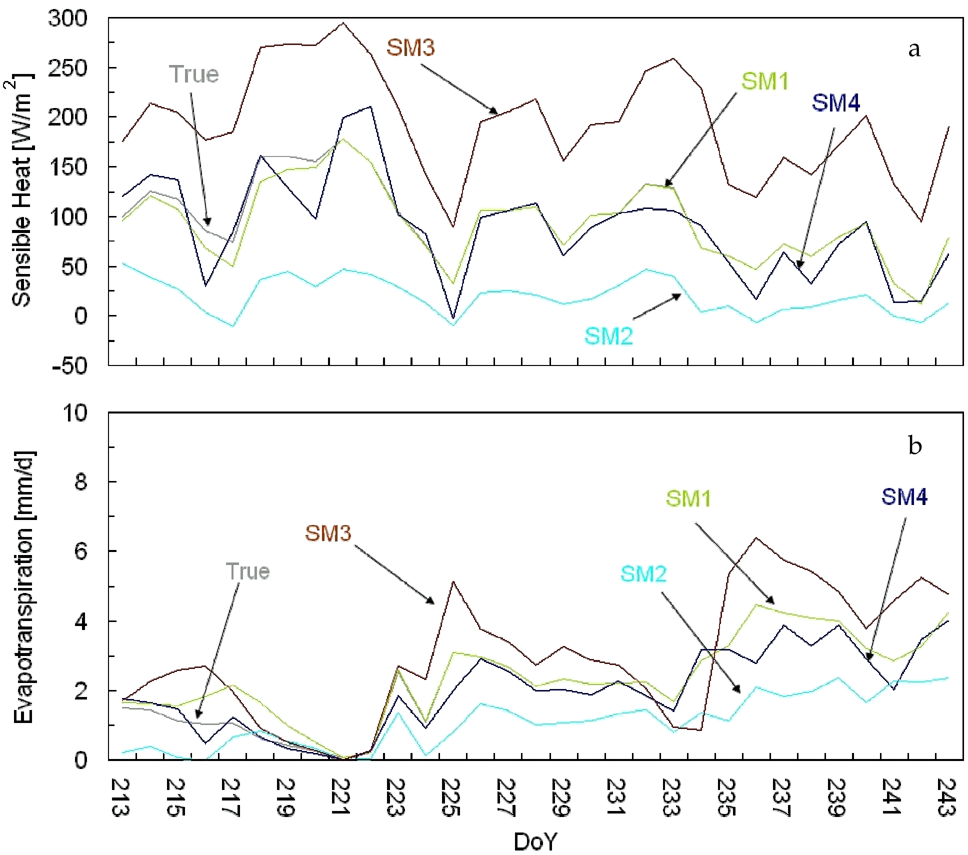

Figure 5.25. One-month assimilation window results of a) sensible heat flux and b) evapotranspiration after surface soil moisture assimilation only. The experiment labels are described in Table 5.2. These results are to be compared with the control run results in Fig. 5.11.

These results were expected, as scenario 1 is based on the true forcing data. The small inaccuracies in the retrieval of the initial soil moisture states originated from NLFIT assuming some kind of uncertainty in observations and predictions.

5.6.2.2 *Scenario SM2*

In the experiment with wet bias, the initial soil moisture states were again well retrieved (SM2; Fig. 5.23), with the root zone and surface soil moisture close to the true observation. However, the assimilation scheme attempted to create drier initial soil moisture conditions than shown, in order to accommodate the increase in soil moisture during the period of the assimilation window, due to the biased precipitation. However, the model reset any initial state to the wilting point. If the model had allowed soil moisture values below wilting point, the assimilation scheme would have set lower initial values to counter the high water input into the system. Consequently, the surface layer was not sufficiently dried down to reach true levels in response to the increased water input into the model and the reduced radiation. Furthermore, due to the wet bias in the forcing data all soil moisture values and streamflow generally diverged from the true observations towards the end of the assimilation window, as it was already found previously.

At this point, the point has to be stressed that the least-square-error approach attempted to reduce only the error for the surface soil moisture. A less significant divergence of the root zone soil moisture prediction would be achieved if the initial state of the root zone would have been higher. However, this would have increased the error in the surface soil moisture. Therefore, the result presented here is the best fit for the problem at hand.

Because of the wet bias and the generally wetter soil moisture conditions, streamflow was significantly overestimated (Fig. 5.24). This was to be expected, as no constraints were set for streamflow. The error in the sensible heat flux and the evapotranspiration rate did not change after the assimilation (Table 5.6), despite the significant changes in the soil moisture predictions. This shows that the sensible heat flux and evapotranspiration rate were dominated by temperature and radiation, and not soil moisture availability.

5.6.2.3 Scenario SM3

In contrast to the assimilation of streamflow observations into the model with dry bias (R3), the soil moisture content was well retrieved (SM3; Fig. 5.23). Due to the dry bias, the assimilation set the initial profile and root zone soil moisture values marginally higher, to avoid a premature dry down of the surface soil layer.

Towards the end of the assimilation window, a divergence of the soil moisture from the true run was observed, leading to an underestimation of the soil moisture predictions. This divergence represents the opposite effect of the soil moisture prediction under wet bias, where the soil moisture was overpredicted.

The second dry-down phase during this experiment (after day 230) was due to an increase in evapotranspiration, which caused the deeper soil moisture stores to reach wilting and therefore the surface soil layer to dry down. Because of the good fit of the soil moisture content, the streamflow production in this experiment is significantly underestimated (Fig. 5.24). This was caused by the reduced precipitation and increased downwelling long wave and short wave radiation compared to the true observations. The reason for this behaviour is the same as for the overestimation in SM2. However, the dry bias caused an under- rather than an overestimation.

The evapotranspiration rate after the assimilation was significantly improved, while the sensible heat flux prediction was degraded (Fig. 5.25). The high evapotranspiration rate from the control run was reduced, due to the lower soil moisture after the assimilation. Despite the good retrieval of the initial soil moisture states and the low error of the soil moisture within the assimilation window, the evapotranspiration rate remained the highest of all scenarios. This was due to the highest level of downwelling long wave and short wave radiation and unchanged soil moisture conditions.

It may be argued that the assimilation had to counterbalance the dry-down of the soil moisture after day 230 by overpredicting the initial soil moisture states. This was tested in a simple study, in which the initial soil moisture states were artificially augmented. However, reaching a model threshold (ie. the wilting point) in the first half of the month led to a memory loss within the model. Because of this memory loss, no more information on the changed initial soil moisture state was transferred to the model in the second half of the month. Consequently, the model performed identical to the control run, after the reaching of this threshold. Moreover, the artificial augmentation of the initial state increased the least-square error due to the degradation of the model prediction before in the first half of the month.

5.6.2.4 Scenario SM4

In the last experiment, the assimilation of surface soil moisture into C4 (SM4) resulted in a good retrieval of all soil moisture states. The streamflow was still overestimated due to the wet bias in the precipitation forcing and the subsequently increased water input. Nevertheless, streamflow was significantly improved (Fig. 5.24). The random noise in the radiation did not cause the soil moisture to deviate from the true observations, while the sensible heat flux, evapotranspiration and streamflow errors, while reduced, were still significant. The cause for these errors was the wet bias in the precipitation forcing for that particular scenario, as the fluxes were not limited by soil moisture.

5.6.2.5 General Discussion

The assimilation of surface soil moisture for all scenarios showed an improvement in the soil moisture states and the error throughout the month. In all experiments, the surface soil moisture assimilation produced well retrieved soil moisture values. This was in contrast to the streamflow data assimilation where different biases led to different soil moisture values. In particular, the difference between the wet and dry bias results was only evident in the soil moisture towards the end of the month.

The observed results were expected, as an observation directly related to the analysed state (surface and root zone soil moisture, respectively) was assimilated, rather than an observation which is only a secondary effect to the condition of the analysed states. The results also highlight that a strong link exists within CLSM between the surface soil moisture and the deeper soil moisture stores. This strong link may be exploited to use surface soil moisture assimilation to retrieve soil moisture initial states. However, the errors in the streamflow either increased (SM3) or remained the same for all scenarios, which shows that soil moisture assimilation alone does not have a better performance for streamflow predictions than the assimilation of streamflow observations. The evapotranspiration rate was improved for all scenarios, except SM2, because the soil was under a more intense water stress for a longer time in all other scenarios.

5.6.3 Joint Assimilation of Streamflow and Soil Moisture

It has been established that the respective assimilation of streamflow and surface soil moisture observations are feasible techniques for the retrieval of soil moisture. However, both techniques showed some limitations. While the assimilation of streamflow observations showed problems in accurately retrieving initial soil moisture states, particularly for the surface soil moisture, the assimilation of surface soil moisture observations alone into a model with degraded forcing data resulted in an insufficient improvement in the streamflow prediction. To increase the constraint on the model states, both observation types were jointly assimilated into CLSM in this experiment. As in the previous experiment, the joint assimilation was undertaken for the four different forcing scenarios. For this experiment, it was assumed that streamflow and remotely sensed surface soil moisture observations were available. This was only to test the potential of a joint assimilation scheme. In case of a densely vegetated catchment, this

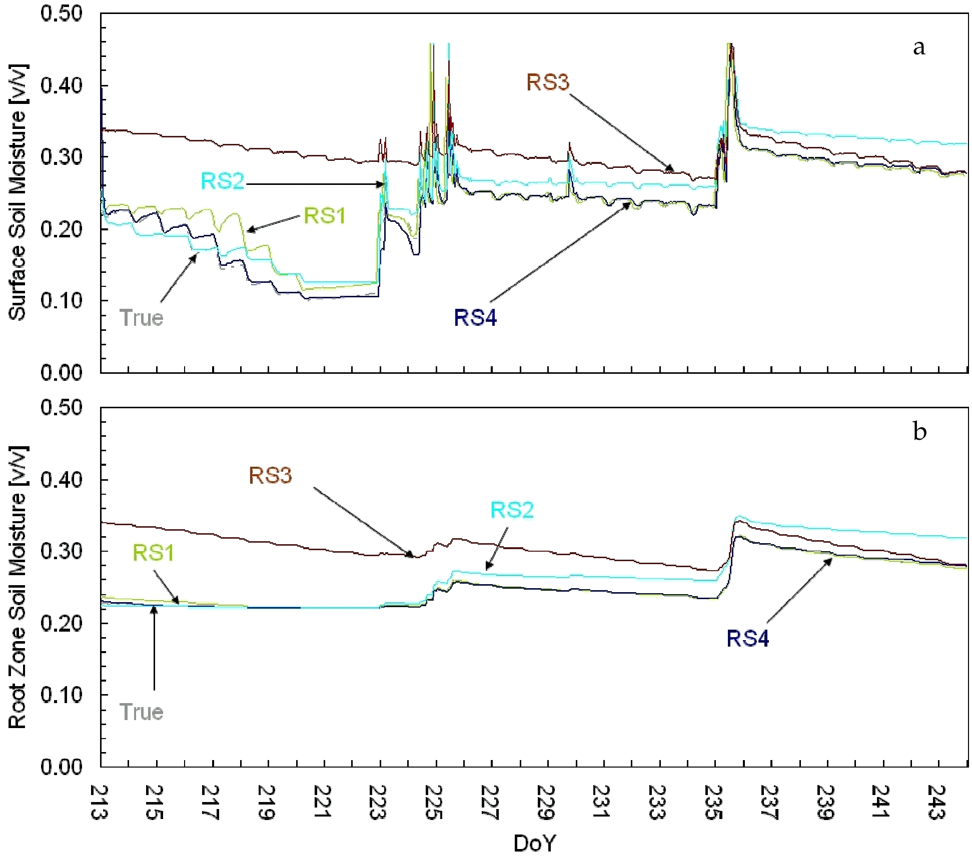

Figure 5.26. One-month assimilation window results for joint assimilation of streamflow and remotely sensed surface soil moisture. a) Surface and b) root zone soil moisture. The experiment labels are described in Table 5.2. These results are to be compared with the control run results in Fig. 5.9.

approach would not be feasible.

5.6.3.1 Scenario RS1

The assimilation of streamflow and surface soil moisture observations into scenario 1 (RS1) resulted in a good retrieval of the soil moisture states (Fig. 5.26, Table 5.7). Consequently, the streamflow output was well modelled (Fig. 5.27). This result was expected as both individual techniques showed a good retrieval of the initial states. Like in the previous studies (R1 and SM1) a small overestimation of the initial soil moisture state led to a temporal drift in the surface soil moisture predictions. This caused some discrepancy between model predictions and true observations of sensible heat flux and evapotranspiration at the beginning of the

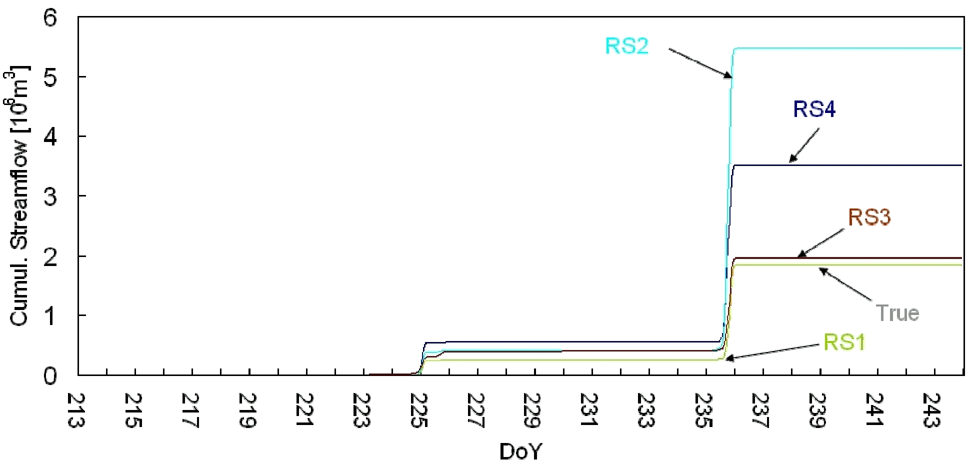

Figure 5.27. Cumulative streamflow for Catchment 2 after joint assimilation of streamflow and remotely sensed surface soil moisture. The experiment labels are described in Table 5.2. These results are to be compared with the control run results in Fig. 5.10.

Table 5.7. RMSE for the volumetric soil moisture content, sensible heat flux, evapotranspiration, and the streamflow after the joint assimilation of surface soil moisture and streamflow. The data in brackets is RMSE of the respective control run.

	Surface [v/v]	*Root Zone [v/v]*	*Profile [v/v]*	*Sens. Heat [W/m²]*	*ET [mm/d]*	*Streamflow [m³/s]*
RS1	0.019 (0.184)	0.002 (0.160)	0.002 (0.146)	11.054 (42.686)	0.499 (1.933)	0.006 (26.474)
RS2	0.027 (0.200)	0.022 (0.183)	0.020 (0.168)	100.234 (110.695)	1.752 (1.768)	12.599 (43.380)
RS3	0.100 (0.167)	0.064 (0.138)	0.059 (0.128)	67.884 (65.268)	3.259 (3.435)	0.691 (12.173)
RS4	0.009 (0.096)	0.001 (0.062)	0.001 (0.057)	48.753 (61.454)	0.952 (1.903)	5.878 (14.777)

month (Fig. 5.28). Nevertheless, true observations and model predictions converged after day 220.

5.6.3.2 Scenario RS2

The combined streamflow and surface soil moisture assimilation resulted in an improved soil moisture prediction for the scenario with wet biased forcing data (RS2), as compared to the previous studies (R2, SM2). When compared to the streamflow assimilation,

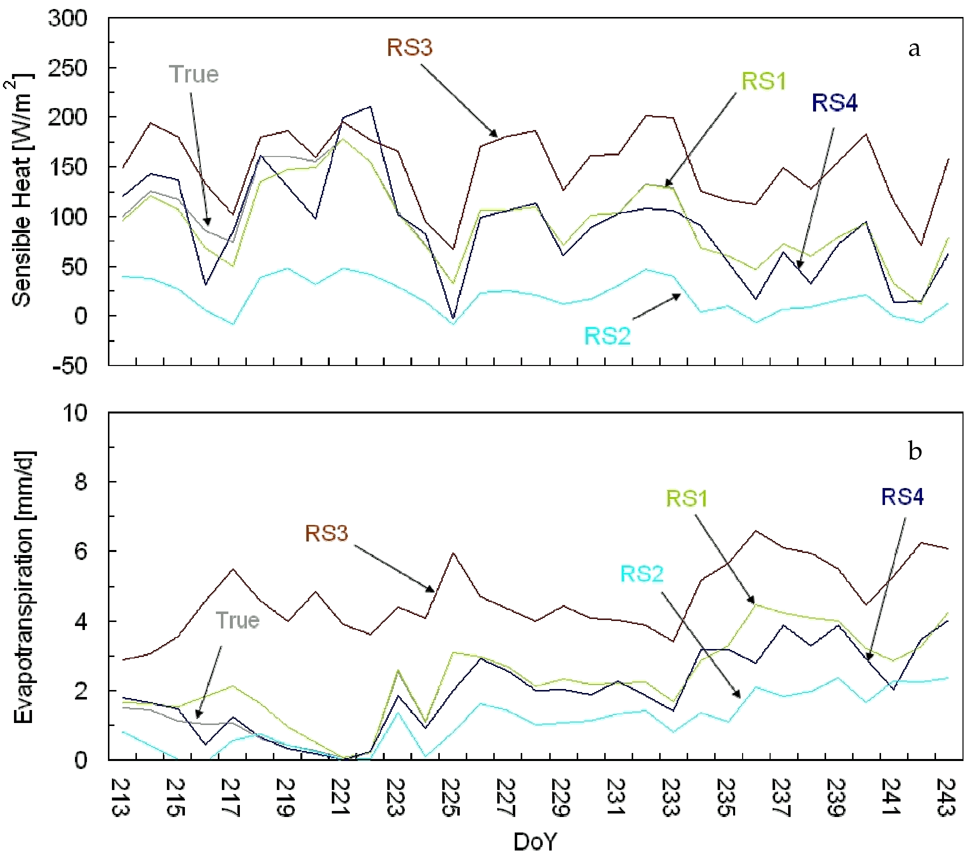

Figure 5.28. One-month assimilation window results of a) sensible heat flux and b) evapotranspiration after the joint assimilation of streamflow and remotely sensed surface soil moisture. The experiment labels are described in Table 5.2. These results are to be compared with the control run results in Fig. 5.11.

only a slight improvement of the streamflow data was observed. Similarly, the soil moisture, sensible heat and evapotranspiration were only slightly improved. Further improvements to the model predictions were not possible, because of a model threshold (wilting point) limiting the performance of the assimilation scheme.

5.6.3.3 Scenario RS3

The joint assimilation of streamflow and surface soil moisture into the simulation with dry biased forcing data (RS3) led to no significant improvement in root zone soil moisture or streamflow predictions. Moreover, it led to an increase in the error of soil moisture prediction, as compared to the assimilation of surface soil moisture alone.

This is explained with the model physics in combination with the calculation of the objective function used by the assimilation. In order to reduce the least square error of the surface soil moisture state a change in the root zone and profile soil moisture would be necessary. However, such a change significantly impacts on the streamflow output, which in turn leads to a larger change in the objective function and therefore is not performed. It was concluded from these results, that in the joint assimilation, root zone soil moisture was changed more significantly with respect to the streamflow than the surface soil moisture observations, even when the squared errors of surface soil moisture and streamflow were normalised with the standard deviation of their respective residual errors (see Chapter 4). However, the retrieved results represent an improvement to those without normalisation, as streamflow was given less precedence by NLFIT than in the previous approach with the absolute values. This means, that the ratio between residual variance and streamflow observations was not the same as for soil moisture. This is explained with the large difference between maximum and minimum streamflow rates. A solution to this is the calculation of the residual variance only with statistically significant observations. However, this would mean that the significance of every observation had to be considered for every assimilation window and observation type, after each update of the initial states. This was deemed to be infeasible for the applied assimilation scheme. However, as the calculation of the residual variance with all available data improved the performance of NLFIT, it was considered to be a valid approach.

5.6.3.4 Scenario RS4

In the last scenario (RS4), only the surface soil moisture was improved, as root zone and profile soil moisture errors were already low. The streamflow prediction was not improved, because the soil moisture states could not be further reduced, for the same reason as for RS2. However, the joint assimilation of streamflow and surface soil moisture resulted in improved predictions as compared to the streamflow assimilation alone. In particular, the surface soil moisture retrieval was significantly improved. This shows that despite the error in radiation and precipitation, the average prediction of soil moisture and streamflow correspond well with the observations.

5.6.3.5 General Discussion

Since this experiment aimed at constraining the surface soil moisture retrieval, it was concluded that the joint assimilation of streamflow and surface soil moisture is preferable to the streamflow assimilation alone. This result was expected, as the assimilation of additional and relevant observations (ie. observations that are related to the analysed states) further constrains the retrieval process. Moreover, the studies including strong biases in the forcing data (scenarios 2 and 3) showed that it is necessary to understand and quantify the errors in the forcing data. If this is not achieved, the assimilation scheme was shown not to be capable of retrieving initial states that would sufficiently correct the model performance after assimilation.

Finally, it is important to note that the most significant improvements to sensible heat flux and evapotranspiration occurred for periods when these fluxes were controlled by the soil moisture availability. Otherwise, only marginal improvements were achieved. This shows that it is particularly important to improve soil moisture for dry regions, as small changes in the soil moisture predictions have a significant impact on the sensible heat flux and evapotranspiration predictions.

5.7 Chapter Summary

A single-catchment study has shown the potential of streamflow data assimilation for the retrieval of initial soil moisture states within a hydrologic model. First, it was shown that the assimilation window length has to be short, but is required to contain at least one significant streamflow event to allow the retrieval of initial soil moisture states. Then, experiments were undertaken to study the effect of model and forcing errors. It was shown in these experiments that the use of the soil wetness index allows to compare soil moisture observations and predictions, if both are based on different porosity and wilting point parameterisations. While the retrieval of initial soil moisture states was possible for most scenarios, it remained difficult to obtain an estimate of the initial surface soil moisture state, particularly under the presence of strong forcing biases. This is a result of the strong relationship between the root zone and the surface soil moisture in CLSM. Because the model exerts a strong control on the surface soil moisture before, all chosen initial surface soil moisture state values resulted in similar streamflow. Consequently, the assimilation scheme could not detect any sensitivity of the streamflow to changes in the surface soil moisture, and fixed the initial state at a random variable. Additionally, forcing errors caused deviations of the model predictions from the observations at the end of the assimilation window, or incorrectly initialised soil moisture states. This showed that the assimilation scheme did not adequately constrain the initialisation of the soil moisture states and thus would require additional observations.

As a further constraint of the initialisation of the surface soil moisture states, surface soil moisture was jointly assimilated with the streamflow observations. The joint assimilation further improved the retrieval of the soil moisture states, as compared to the streamflow assimilation alone. However, streamflow appeared to be the dominant observation over the soil moisture observations, influencing the retrieval of the initial soil moisture much stronger.

Because the experiments of this synthetic study were undertaken for a single catchment and observations are not always available for all catchments, the next step is to test the applicability to multi-catchment networks, in which unmonitored subcatchments are present. Such a study is presented in the following chapter.

Chapter Six

6 Multi-Catchment Synthetic Study

This chapter extends the land surface assimilation scheme for climate model initialisation demonstrated in the synthetic single-catchment study of Chapter 5. Here, the assimilation scheme is applied to two synthetic multi-catchment scenarios, using the same true and degraded forcing and catchment parameter data as in the previous chapter. The two scenarios are i) the three subcatchments of the Krui River catchment within the Goulburn River Experimental catchment, and ii) an eight catchment representation of the entire Goulburn River Experimental catchment (Fig. 6.1). Through the assimilation of various observation combinations for each scenario this chapter is aiming at identifying i) the minimum number of catchments with observations required for soil moisture retrieval in a multi-catchment study, ii) the effects of errors in the forcing data on the soil moisture retrieval in the subcatchments of a multi-catchment study, and iii) the opportunities provided by a joint streamflow and surface soil moisture assimilation. This multi-catchment study is the last stepping-stone before the developed assimilation scheme is applied to, and used to interpret results from, the real data study presented in Chapter 7.

While the study in Chapter 5 focussed on the general possibility of the assimilation of streamflow and surface soil moisture into a hydrologic model, the present chapter determines the effects of the assimilation of observations into an underdetermined model (ie. less observations than subcatchments) on the prediction of streamflow and soil moisture.

6.1 Outline of Approach

First, a study with three catchments is undertaken in section 6.3. These three catchments are the subcatchments of the Krui River catchment (Fig. 6.1). The Krui catchment was chosen, because of the variability of the surface and soil conditions in the subcatchments and the use of its uppermost subcatchment in the previous chapter.

Following the study in the previous chapter, streamflow and surface soil moisture were first individually and finally jointly assimilated into the model for the different subcatchments. The forcing data were identical to those of Chapter 5. The forcing data was assumed to be spatially homogeneous, to avoid effects from forcing variability in the assimilation scheme. For all scenarios only one streamflow and one surface soil moisture observation data set were made available for assimilation purposes.

In the second part of this chapter (section 6.4), streamflow and surface soil moisture were assimilated into the model for all eight subcatchments of the Goulburn River catchment. This study was further divided into three experiments. First, only streamflow data at the catchment outlet was assimilated into the model. Next streamflow was assimilated for all subcatchments, and finally, streamflow and remotely monitored surface soil moisture were jointly assimilated for a limited number of observation points. The main difference between this study and the two preceding studies (single- and three-catchment) is the more complex catchment network of the full Goulburn River catchment than the single- and three-catchment studies Chapter 5 and section 6.3. The single-catchment study in Chapter 5, did not include a transfer of streamflow to other catchments and the stream network of the Krui River catchment only consists of three subcatchments in sequence. In contrast to the Krui River catchment with its three nested

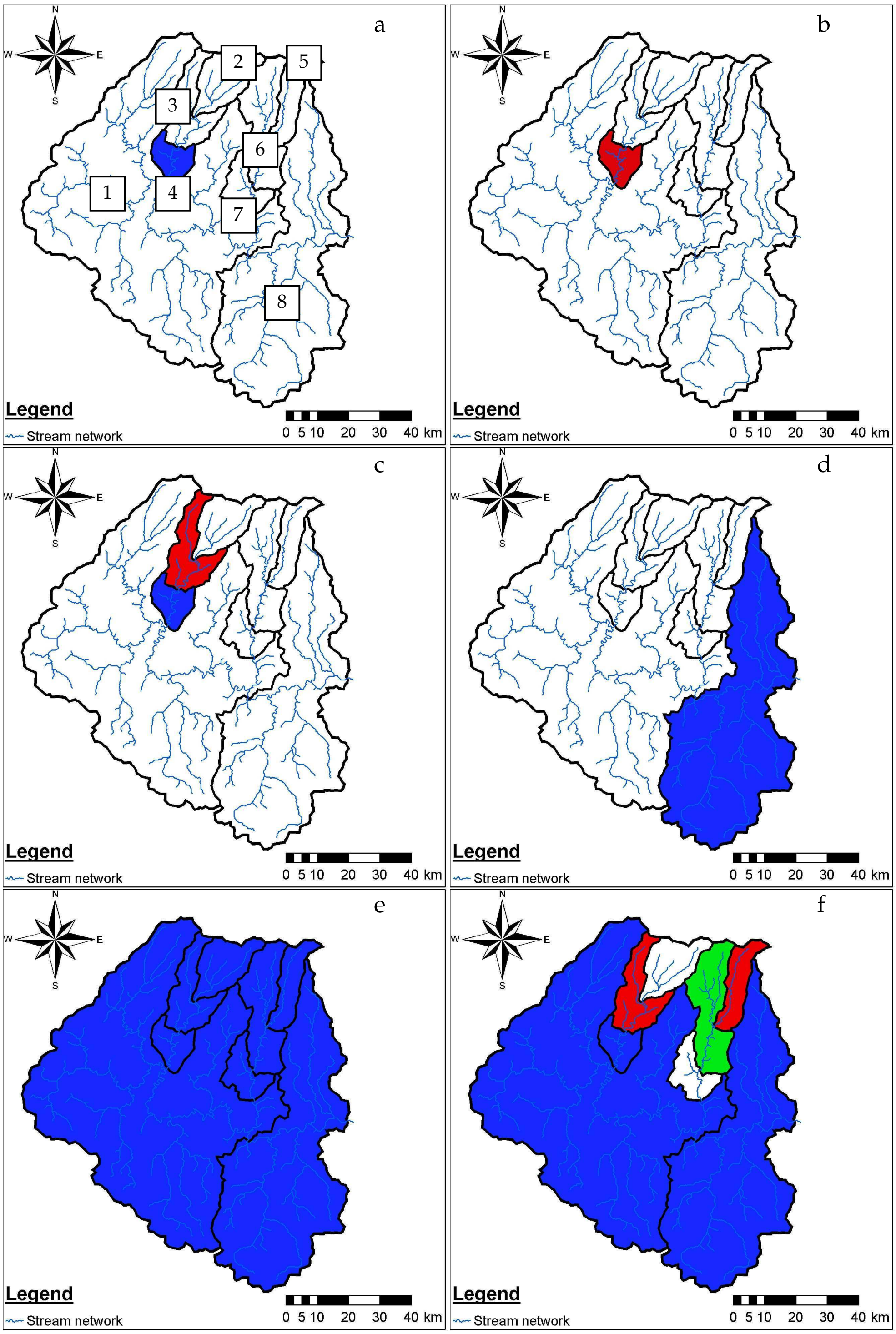

Figure 6.1. The catchments from which the assimilated observations were taken are shown. Blue: only streamflow observations are available, Red: only surface soil moisture observations are available, Green: both observations are available, and White: no observations are available. a) Streamflow at Catchment 4, b) surface soil moisture at Catchment 4, c) streamflow at Catchment 4 and surface soil moisture at Catchment 3, d) streamflow at Catchment 8, e) streamflow at all catchment outlets, f) streamflow at Catchments 1, 4, 6 and 8 and surface soil moisture at Catchments 3, 5 and 6.

subcatchments, the Goulburn River catchment consists of several parallel subcatchments, in which the streamflow is independent of the neighbouring subcatchments. The subcatchments in the following studies are only nested in terms of their streamflow (eg. the streamflow of Catchment 4 includes the streamflow produced in Catchments 2, 3, and 4), while all subcatchments were modelled as independent modelling units with different soil and vegetation parameter sets and consequently individual predictions of soil moisture, sensible heat flux and evapotranspiration. In the eight-catchment study it was determined whether the assimilation scheme is capable of retrieving the initial soil moisture states in such a network structure. The eight subcatchments of the Goulburn River catchment were created by taking the areas between existing stream gauges as subcatchments. This resulted in the subcatchment network shown in Fig. 6.1. The use of stream gauge locations as subcatchment outlets facilitated the development of the individual unit hydrograph (see section 4.4.2 for the routing model description), as real observations were used to for the calibration of the routing coefficients.

The joint assimilation of a limited number of streamflow and remotely sensed surface soil moisture observations presented in section 6.4 served as the final synthetic study before undertaking the real study in Chapter 7, as it presents the most realistic combination of observations.

Additionally, it was assessed if and how remotely sensed surface soil moisture information alone is useful in a multi-catchment study (section 6.3). In the previous chapter, it was shown that the assimilation of surface soil moisture observations resulted in the retrieval of good soil moisture values throughout the soil profile. In the present chapter, it was determined whether the assimilation of remotely sensed surface soil moisture observations would lead to the same results in a multi-catchment study as in a single catchment study. Finally, it was determined whether the assimilation of a limited number of available observations (fewer observations than subcatchments) adversely affected the retrieval process of the initial states in the remaining subcatchments.

The four degraded forcing scenarios were only applied to the three-catchment study. With the results of the single catchment and the three-catchment study, sufficient results were available to determine the effects of biases and other errors on the assimilation approach. Therefore, the eight-catchment study focused on the assimilation of different observations and not on the effects of observational biases and errors on the assimilation approach. For the latter study, only true data was assimilated in order to minimise the effects incurred by external data errors and biases so that one may focus on the effects of the stream network structure.

6.1.1 Changes to the Assimilation Process

It was shown in Chapter 5 that a strong link exists between the three soil moisture stores exists within CLSM, as the root zone and profile soil moisture generally showed the same soil moisture content and the surface soil moisture, quickly recovered despite poor initialisations. In the experiments of this chapter, the strong relationship of the catchment deficit, in particular with the root zone and surface soil moisture, allowed a reduction in the number of retrieved soil moisture states from all three to one single state (ie. only the catchment deficit). This was possible, because any differences in the model predictions of the root zone and surface soil moisture before and after the assimilation, due to incorrect initialisations, were corrected within a short time. This approach has two main advantages. Firstly, the system is less underdetermined, as fewer states have to be retrieved and secondly, the surface soil moisture is automatically constrained to be close to the root zone soil moisture content.

The results of the previous chapter showed that the physics within the model is capable to achieve equilibrium soil moisture conditions within several days, even when the excess values were set to extreme values. This was observed when the surface excess was initialised with incorrect values. Therefore, it was assumed that if the surface and root zone excess values were set to 0 (equilibrium soil moisture profile), the model would correct for this error over a short period.

The implication of such an assumption is significant, in particular for the larger catchment network structures considered later in this chapter. In the case of attempting to retrieve all three soil moisture states in each catchment, a catchment structure with three subcatchments would have a state-space of 9 dimensions, and a catchment with 8 subcatchments 24 dimensions. The reduction of the retrieved initial states leads to a significant increase in computational time, in particular for the larger catchment structure. The simplification of the assimilation scheme to retrieving one state per catchment reduces the state-space by a factor of three and any cross-correlation matrix by a factor of 9.

6.2 Synthetic Data; True and Control Runs

The forcing data and model parameters used in this chapter were the same as those from Chapter 5, representing the four different forcing scenarios (true, wet bias, dry bias, random noise; see Table 5.1). The forcing data for CLSM in this synthetic study were considered to be spatially homogeneous throughout the whole Goulburn River catchment. Spatial variability of the forcing data due to elevation or local climatic conditions was not considered in order to simplify the synthetic study and to focus on the potentials of the data assimilation scheme itself. If the data were to include spatial variability, the individual subcatchments would have shown different responses to changes in the forcing data and therefore a further level of uncertainty would have been introduced.

The modelling undertaken in this chapter was for the same one-month period as studied in Chapter 5 (August 2003). The difference between the control runs in this chapter and the control runs of Chapter 5 is the initialisation of the model runs. In the present chapter, the control runs were initialised with averaged soil moisture conditions (average of field capacity and wilting point), rather than the initialisation of the control runs with fully wet conditions. The control runs for all subcatchments are presented in Appendix A4.3. As in the previous chapter, the figures in this chapter showing the model predictions after the assimilation are presented along with the true observations only and the reader is referred to Appendix A4 for comparisons.

As described in Chapter 5, the model was spun up with the true forcing data ten times over a one-year period to obtain stable, non-changing water and energy balance conditions. The model streamflow and surface soil moisture predictions were taken as the true observations, which were then assimilated into the model. Furthermore, the true model predictions for root zone, profile soil moisture, sensible heat flux and evapotranspiration were used as validation data of the model predictions after the assimilation process.

Only a select number of subcatchments are shown in the figures of this chapter. These catchments are generally representative of the range of catchments modelled in terms of size, land cover, terrain roughness and soil type. For the three-catchment study in section

6.3, the predictions are shown for Catchment 3 only. The model predictions for the subcatchments of the eight-catchment study are not shown on figures, as the study had a different focus. Nevertheless, the RMSE for all subcatchments is presented for all studies and all subcatchments in tables in the respective sections.

6.3 Three-Catchment Study

The subcatchments of this study may be modelled as one single, large catchment. However, any retrieved initial states would be averages of the whole catchment, because of the forestation of the lower subcatchment (Catchment 4) of the Krui River catchment and its different surface and soil conditions compared to the other subcatchments. Therefore, the assumption of homogeneity in the lumped model is not valid anymore and the Krui River catchment needed to be split into smaller modelling units. Furthermore, due to these different surface and soil conditions within the Krui River catchment, a high spatial variability of soil moisture exists throughout the Krui River catchment, which is a further proof for the need of a disaggregation of the catchment into smaller modelling units. The disaggregation of the whole catchment into subcatchments allows the retrieval of soil moisture states that better account for the spatial variability of soil moisture.

In the synthetic experiments of this section, streamflow and soil moisture observations were assimilated into three subcatchments of the Krui River catchment (Catchments 2, 3 and 4). While the three subcatchments have in general different surface conditions in all aspects (slope, elevation, and vegetation), the upper two subcatchments have the same soil type.

In the first experiment, it was assumed that only streamflow observations at the outlet of the lowest of the three catchments were available (Catchment 4, Fig. 6.1a). This scenario was used to determine the potential upstream feedback of observations within a multi-catchment set up. The scenario represented a semi-distributed modelling approach, in which smaller subcatchments were treated individually within the larger catchment network.

Secondly, surface soil moisture only was assimilated into the lowest catchment (Catchment 4; Fig. 6.1b). This scenario was used to compare the differences in the performance between streamflow and surface soil moisture assimilation for the same subcatchment of a multiple catchment network.

Finally, streamflow and soil moisture observations were jointly assimilated into the model, where streamflow was assimilated at the outlet of Catchment 4 and surface soil moisture for Catchment 3 (Fig. 6.1c). For this scenario, it was assumed that streamflow observations were available for the lowest catchment and remotely sensed surface soil moisture observations for the middle catchment. No observations were available for an assimilation of data into the upper catchment.

In all scenarios, the forcing data scenarios described in the previous chapter were used.

6.3.1 Assimilation of Streamflow Observations

The assimilation of the true streamflow observations at the outlet of Catchment 4 into the LSM, was undertaken in order to retrieve the soil moisture states in the three subcatchments upstream from the stream gauge (ie. in Catchments 2, 3 and 4). This study was undertaken for all four different forcing scenarios (see Table 5.1). With these four scenarios, it was assessed whether the assimilation scheme was able to compensate for forcing data errors in a multi-catchment study. As it was mentioned previously, Catchments 2, 3 and 4 are nested, any streamflow observation at the outlet of

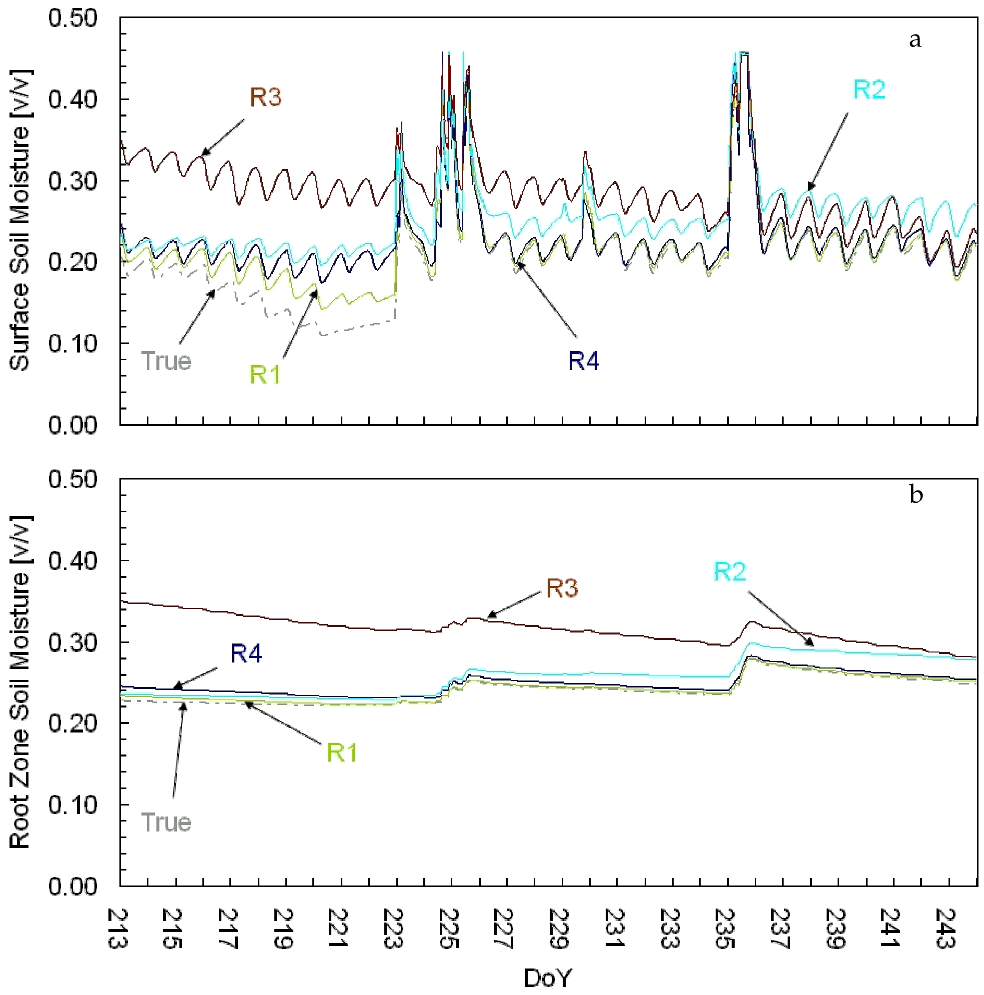

Figure 6.2. a) Surface and b) root zone soil moisture of Catchment 3 (middle catchment) for all forcing scenarios, after the assimilation of streamflow only (see Table 5.2 for the naming of the assimilation experiments).

Catchment 4 constitutes the combined streamflow contributions of those three catchments, while true, control, and assimilated soil moisture, sensible heat flux and evapotranspiration were available for all three subcatchments.

6.3.1.1 Scenario R1

The assimilation of streamflow observations into the LSM under forcing data scenario 1 at the outlet of Catchment 4 showed that the retrieval of all three profile soil moisture states was readily achievable for all three subcatchments (R1; Fig. 6.2). Consequently, the prediction of streamflow (Fig. 6.3), sensible heat flux and evapotranspiration (Fig. 6.4) was also good, with a significant

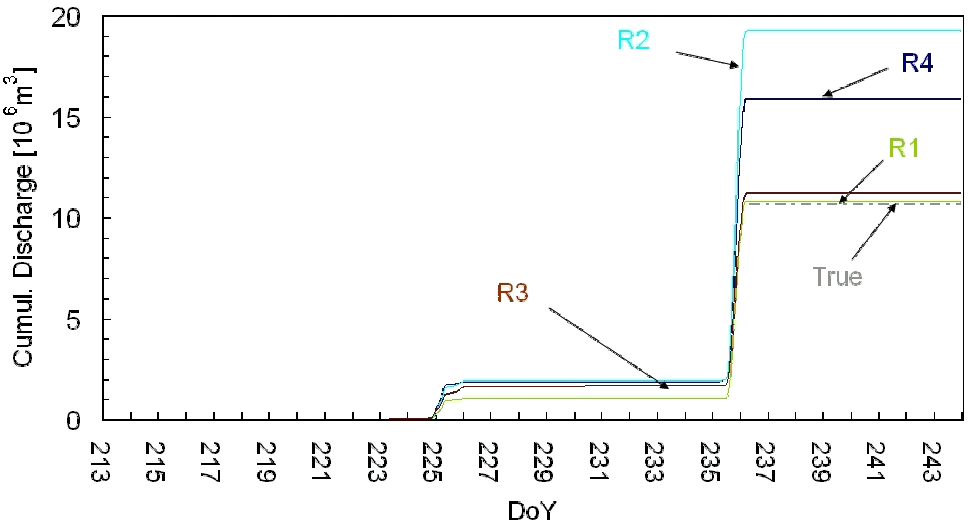

Figure 6.3. Cumulative streamflow of Catchment 3 (middle catchmet) after the assimilation of streamflow only into Catchment 4 (lower catchment).

reduction of the respective RMSE (Table 6.1), as compared with the control runs.

Some discrepancies between the true surface and root zone soil moisture and the surface and root zone soil moisture after the assimilation existed due to the assumption that the initial root zone and surface excesses were in full equilibrium with the soil moisture profile (ie. set to 0; no deviation due to dry or wet conditions). Furthermore, the assimilation scheme in the previous chapter attempted to find the minimum of the objective function for all three states, without being able to optimise for the surface soil moisture state. In the present experiment, this state is a product of the retrieved catchment water deficit, rather than being initialised with an individual value. However, these effects were minor, when compared to the inaccuracies in the retrieval of the surface soil moisture in Chapter 5. Because of this new constraint, the surface soil moisture state was more accurately retrieved than would be expected from the findings in Chapter 5, when surface soil moisture was not constrained. The new approach overestimated the surface soil moisture content and resulted in a lag in the dry-down of the

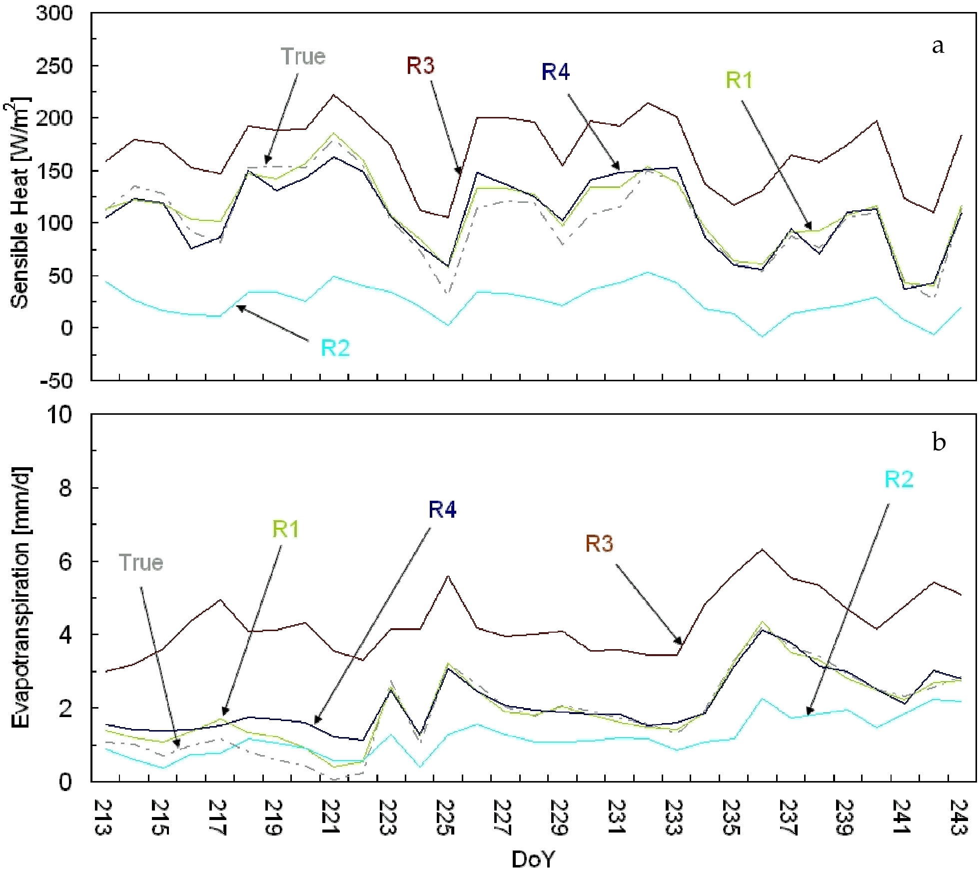

Figure 6.4. a) Sensible heat flux and b) evapotranspiration of Catchment 3 (middle catchment), after the assimilation of streamflow at Catchmnet 4 (lower catchment), only.

surface soil moisture (Fig. 6.2), while still improving the model predictions significantly.

The overestimation of the soil moisture led to a small difference between the true and assimilated sensible heat flux and evapotranspiration (Fig. 6.4) until day 222. After this day, sensible heat flux and evapotranspiration were almost identical with the true observations. The convergence of the true observations and predicted variables was due to the model physics, which was able to correct the slight overestimation of the surface and root zone soil moisture content after several days.

6.3.1.2 Scenario R2

Similarly to the results presented in the previous chapter (see section 5.3.2), the assimilation of streamflow observations into the

Table 6.1. RMSE for the volumetric soil moisture content, sensible heat flux, evapotranspiration, and the streamflow after the assimilation of streamflow only for all three subcatchments. The data in brackets is the RMSE of the respective control run, whereas the first number is calculated after the assimilation. The most accurate predictions for each catchment are in bold.

	Surface [v/v]	*Root Zone [v/v]*	*Profile [v/v]*	*Sens. Heat [W/m^2]*	*ET [mm/d]*	*Streamfl. [m^3/s]*
Catchment 2						
R1	0.015 (0.083)	0.003 (0.051)	0.003 (0.047)	20.875 (44.217)	0.884 (1.739)	**0.017** (20.148)
R2	0.038 (0.114)	0.022 (0.085)	0.020 (0.078)	84.414 (87.339)	1.605 (1.365)	12.525 (24.866)
R3	0.105 (0.074)	0.070 (0.037)	0.065 (0.035)	57.189 (73.770)	3.704 (2.947)	0.740 (2.666)
R4	**0.026** (0.082)	**0.002** (0.050)	**0.007** (0.046)	**9.751** (44.103)	**0.502** (1.738)	5.956 (27.606)
Catchment 3						
R1	**0.018** (0.114)	0.002 (0.087)	0.002 (0.081)	**8.514** (24.571)	**0.376** (1.270)	**0.279** (26.356)
R2	0.053 (0.144)	0.018 (0.107)	0.016 (0.098)	94.499 (89.231)	1.318 (0.992)	21.681 (40.930)
R3	0.099 (0.088)	0.080 (0.071)	0.075 (0.067)	56.144 (67.156)	3.091 (2.489)	1.412 (3.675)
R4	0.034 (0.112)	**0.009** (0.085)	**0.008** (0.079)	14.908 (24.620)	0.789 (1.250)	12.169 (39.023)
Catchment 4						
R1	0.004 (0.100)	0.004 (0.132)	0.003 (0.097)	**3.738** (22.784)	**0.167** (1.178)	**0.289** (30.618)
R2	0.023 (0.135)	0.017 (0.168)	0.013 (0.125)	89.602 (88.493)	1.434 (1.014)	23.108 (43.939)
R3	0.101 (0.104)	0.112 (0.118)	0.083 (0.088)	54.638 (65.278)	3.002 (2.493)	1.679 (3.807)
R4	**0.009** (0.096)	**0.007** (0.129)	**0.005** (0.095)	11.538 (22.578)	0.484 (1.159)	13.306 (44.982)

LSM under forcing scenario 2 (wet bias) resulted in initial soil moisture values at the wilting point (R2, Fig. 6.2). The wet bias in the forcing data led to a divergence of the predicted soil moisture from the true observations towards the end of the assimilation period due to the increase in precipitation and decrease in downwelling long wave and in short wave radiation (the same effect was observed in the single-catchment study of Chapter 5).

As the model physics did not allow an initial soil moisture state below the wilting point, the assimilation scheme was not capable of creating a sufficiently large moisture sink. Due to this condition, the streamflow was still overestimated (Fig. 6.3). Nevertheless, a reduction in the RMSE of the streamflow was achieved (Table 6.1). While soil moisture and streamflow predictions were improved, the resulting sensible heat flux and evapotranspiration predictions were not improved in any of the catchments, as both were not soil moisture limited, but rather controlled by radiation and temperature (Fig. 6.4; Table 6.1).

6.3.1.3 Scenario R3

As in section 5.3.2, the assimilation scheme compensated for the reduced precipitation and increased radiation of forcing data scenario 3, by an initial overestimation of the soil moisture content (Fig. 6.2). While this resulted in an improvement in streamflow (Fig. 6.3), the RMSE of soil moisture was increased (Table 6.1), as additional water had to be created to allow an improvement of the predicted streamflow. The increase in the soil moisture and the resulting increase in its overestimation led to a further degradation of the prediction of the evapotranspiration (Fig. 6.4b). In contrast, the increase in soil moisture resulted in a reduction of the RMSE of the sensible heat flux (Table 6.1), as the high sensible heat flux from the control run was reduced.

6.3.1.4 Scenario R4

Finally, the assimilation of streamflow under forcing data scenario 4 resulted in a good retrieval of the initial soil moisture states (Fig. 6.2) and an improvement to streamflow (Fig. 6.3), sensible heat flux and evapotranspiration (Fig. 6.4). As a consequence of the wet bias in the precipitation forcing of this forcing scenario, the surface soil moisture was not decoupled from the root zone and consequently did not undergo a dry-down in any of the catchments, which resulted in a larger RMSE in the surface soil moisture, than in the root zone (Table 6.1). Due to the lack of this dry-down, the sensible heat flux and evapotranspiration at the beginning of the month were not correctly predicted. The streamflow prediction exceeded the true observations, due to the same wet bias in the precipitation forcing.

6.3.1.5 General Discussion

The assimilation of streamflow under the four forcing scenarios allowed three conclusions:

i) the assimilation of streamflow observations only allowed for the retrieval of the soil moisture states in all subcatchments, located upstream of the point of observation, because the streamflow at the outlet of the lowest subcatchment contained information of all subcatchments located upstream,

ii) forcing errors negatively influence the retrieval process, as sensible heat flux and evapotranspiration were not adequately predicted, despite good prediction of the soil moisture content. This was expected, as the soil was not water-stressed for most of the period under study, and therefore, evapotranspiration was limited by the radiation and not water availability.

iii) The increase of the RMSE under forcing scenario 3 (dry bias) showed that the retrieved soil moisture states were not sufficiently constrained.

6.3.2 Assimilation of Surface Soil Moisture Observations

The assimilation of remotely sensed surface soil moisture observations in Chapter 5 showed that the retrieval of root zone and profile soil moisture led to a good retrieval of the soil moisture states

Table 6.2. RMSE for the volumetric soil moisture content, sensible heat flux, evapotranspiration, and the streamflow for all three subcatchments, after the assimilation of remotely sensed surface soil moisture only. The data in brackets is the RMSE of the respective control run, whereas the first number is calculated after the assimilation.

	Surface [v/v]	*Root Zone [v/v]*	*Profile [v/v]*	*Sens. Heat [W/m²]*	*ET [mm/d]*	*Streamfl. [m³/s]*
			Catchment 2			
SM1	0.153 (0.083)	0.124 (0.051)	0.114 (0.047)	44.644 (44.217)	2.416 (1.739)	19.724 (20.148)
			Catchment 3			
SM1	0.146 (0.114)	0.116 (0.087)	0.108 (0.081)	32.611 (24.571)	1.817 (1.270)	28.360 (26.356)
			Catchment 4			
SM1	**0.002** (0.100)	**0.001** (0.132)	**0.001** (0.097)	**0.294** (22.784)	**0.019** (1.178)	28.372 (30.618)

throughout the soil profile in the single catchment. However, these observations were limited to a small portion of a catchment network in response to vegetation cover (one subcatchment). For the experiment in this section it was assumed that only the lowest subcatchment (Catchment 4) of the Krui River catchment was sufficiently cleared of vegetation to allow surface soil moisture remote sensing, to determine the effectiveness of this approach in a multi-catchment network. It was also assumed that no streamflow observations were available in any of the three subcatchments. This scenario simulated an ungauged (or unmonitored) catchment, where only remotely sensed soil moisture data were available for a part of the catchment (Fig. 6.1b).

6.3.2.1 Scenario SM1

Under forcing data scenario 1, the assimilation of remotely sensed surface soil moisture observations into CLSM for Catchment 4 led to a good retrieval of the soil moisture content in Catchment 4 (Table 6.2), with a negligible RMSE for the root zone of 0.001v/v. In principle, there is no difference in the assimilation of this observation

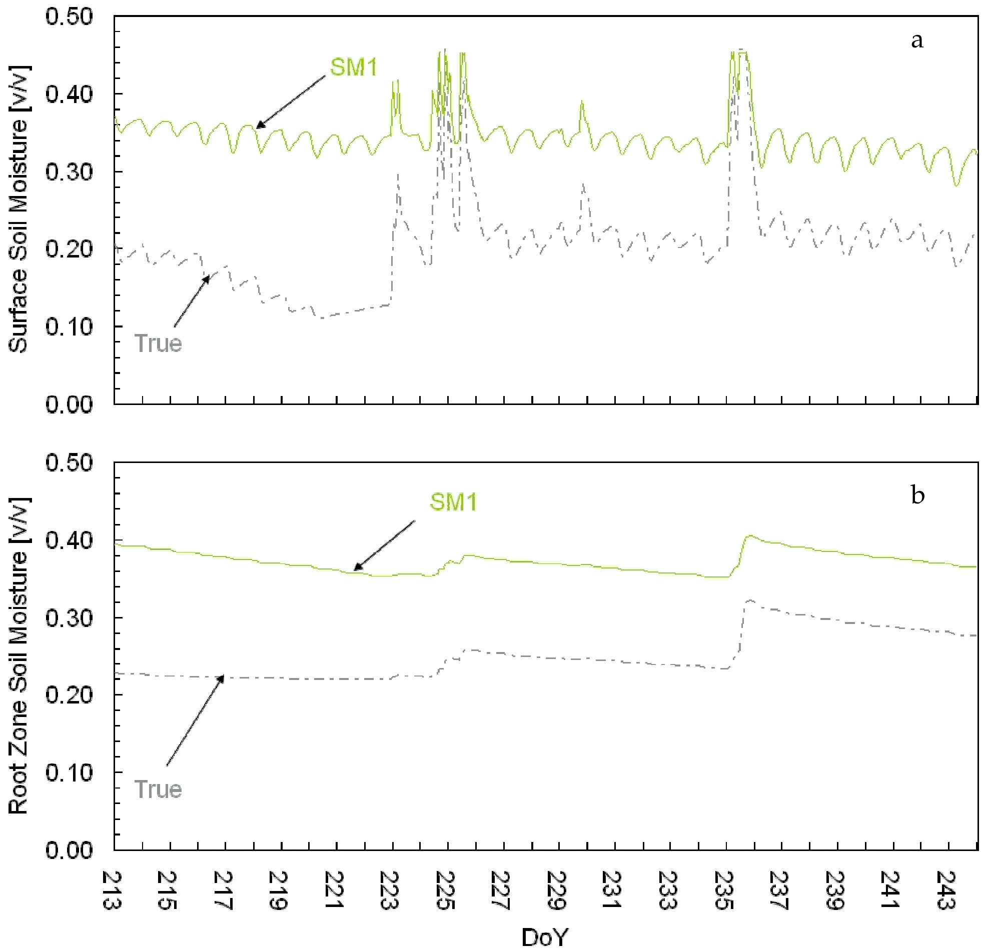

Figure 6.5. Soil moisture of Catchment 3 after the assimilation of remotely sensed surface soil moisture for Catchment 4, only. a) surface and b) root zone.

to the results presented in section 5.4 for Catchment 2, apart from the nesting with two upstream subcatchments in the present experiment. Therefore, the results for Catchment 4 are not shown here, as they show a near perfect fit with the true observations and because of their similarity with the results in Chapter 5.

Despite an accurate retrieval of soil moisture initial states in Catchment 4, there was no improvement in soil moisture content in the upstream catchments (Fig. 6.5). The assimilation scheme had a negative impact on the soil moisture content in Catchments 2 and 3 (Table 6.2), because the initial values found for Catchments 2 and 3 did not impact on the objective function of the soil moisture state in Catchment 4 and therefore could take on any physically meaningful

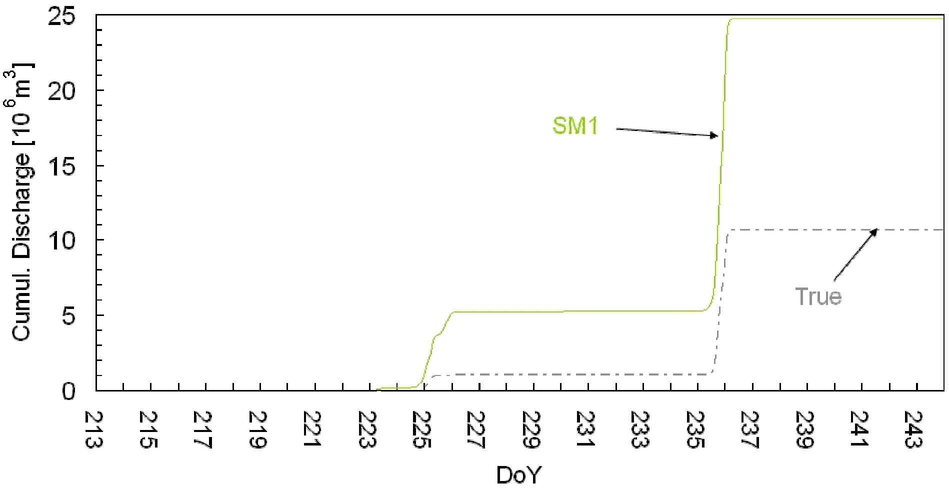

Figure 6.6. Cumulative streamflow at the outlet of Catchment 3 after assimilation of surface soil moisture into Catchment 4 only.

value (ie. between saturation and wilting). This effect was observed because soil moisture predictions in the individual catchments were uncorrelated from soil moisture predictions in other catchments in CLSM and no spatial correlation was prescribed through the assimilation scheme. Therefore, the assimilation of remotely sensed surface soil moisture content alone in a spatially uncorrelated LSM did not suffice to retrieve the respective states in the other catchments.

As the soil moisture states in the upstream catchments had been degraded through the assimilation, the streamflow was still poorly predicted at the outlet of Catchment 4 (Fig. 6.6). For the same reason, the RMSE of the sensible heat flux and the evapotranspiration from the two upstream catchments were higher than in the control run (Table 6.2; Fig. 6.7). Consequently, it was concluded that the soil moisture assimilation alone was not an adequate tool in this scenario and no further tests were undertaken with forcing data containing errors and biases.

The poor results showed that it is essential to correlate the soil moisture content in neighbouring catchments or at the least fix the predicted values from the spin-up, when assimilating only remotely

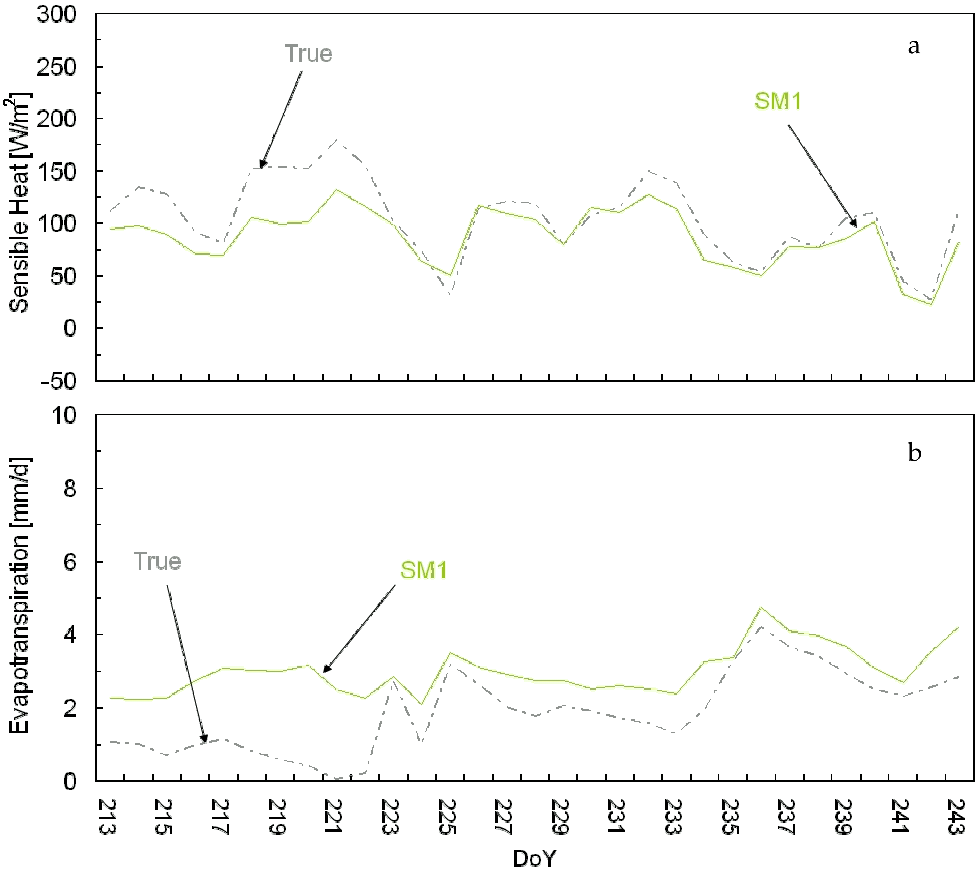

Figure 6.7. a) Sensible heat flux and b) evapotranspiration of Catchment 3 (middle catchment), after the assimilation of remotely sensed surface soil moisture for Catchment 4 (lower catchment), only.

sensed surface soil moisture in a limited number of catchments. Nevertheless, it was confirmed that remotely sensed soil moisture assimilation was capable of retrieving the full soil moisture profile accurately for a catchment.

A brief discussion about possible changes to the assimilation scheme will be presented in Chapter 8.

6.3.3 Joint Assimilation of Streamflow and Surface Soil Moisture Observations

It was shown in Chapter 5, that the joint assimilation of streamflow and surface soil moisture leads to improved model predictions, therefore, streamflow and remotely sensed soil moisture observations are jointly assimilated in this section. It was assumed for the experiments in this section, that streamflow observations were available at the outlet of the lowest subcatchment (Catchment 4) and that Catchment 3 was sufficiently cleared for remote sensing to be possible. With these experiments, the impact of assimilating different quantities (streamflow and surface soil moisture) as observed in different subcatchments was studied, where the assimilation of streamflow and remotely sensed surface soil moisture provided additional constraints on the results from their respective assimilation. All four forcing data scenarios were studied.

6.3.3.1 Scenario RS1

The joint assimilation of the true observations into the model under forcing data scenario 1 resulted in a good performance of the model for all three catchments (Fig. 6.8). This was expected, as the retrieval of the three soil moisture states with streamflow observations alone (Fig. 6.2) led to good results. However, the soil moisture initial states and the RMSE (Table 6.3) after the assimilation of streamflow alone were higher than those of the true observations, and resulted in a less significant dry-down than in the true run. This was caused by the assumption that the initial root zone and surface excesses were in equilibrium. In order to obtain the correct surface soil moisture states in Catchment 3, the initial profile soil moisture had to be decreased compared to the results of the experiment with streamflow assimilation only. However, this led to a decrease in the streamflow, which had to be compensated for in Catchments 2 and 4. Consequently, these two subcatchments had higher initial soil moisture states in order to produce sufficient streamflow. Nevertheless, these differences were minor and the overall improvement was still significant when compared to the control runs.

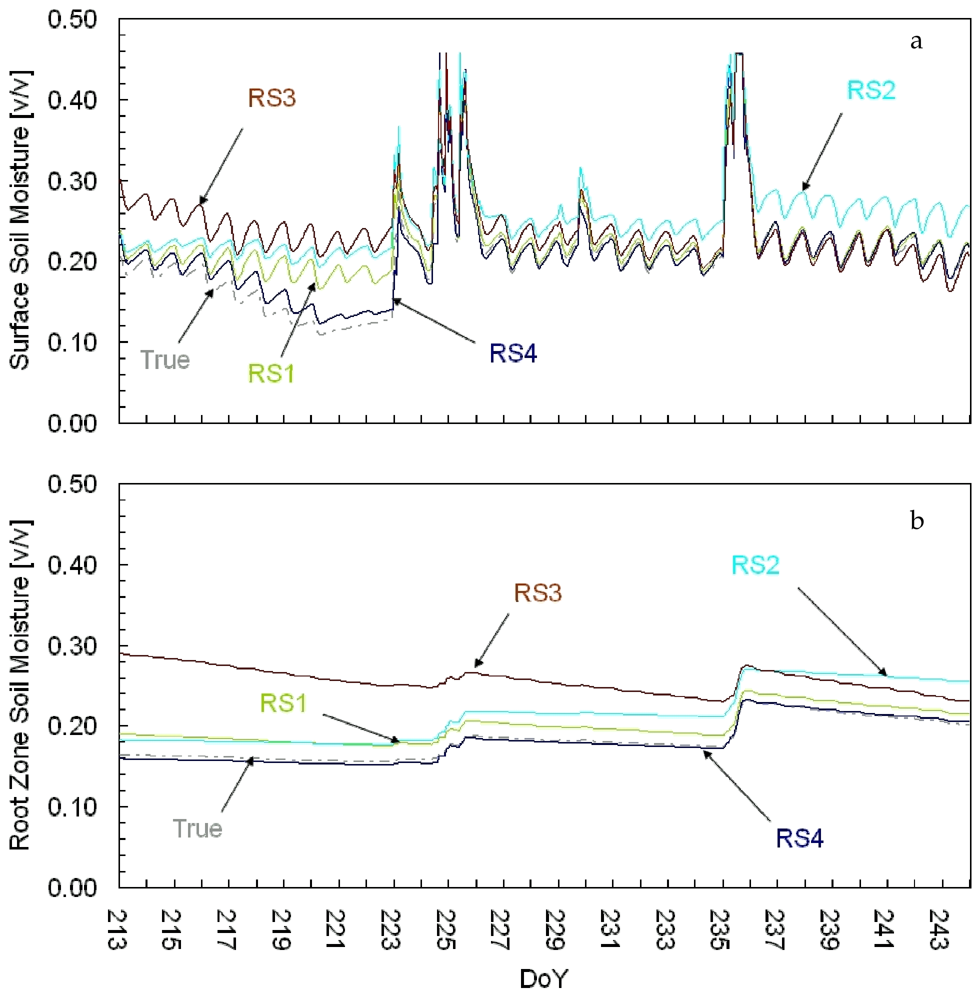

Figure 6.8. Soil moisture of Catchment 3 after the joint assimilation of streamflow at the outlet of Catchment 4 and surface soil moisture from Catchment 3 into CLSM. a) Surface and b) root zone soil moisture.

6.3.3.2 Scenario RS2

As forcing data scenario 2 forced the model to be wetter than the true observations, all catchments were expected to be near wilting point (as shown in the study in Chapter 5). However, the initial soil moisture state of Catchment 3 was more accurately retrieved than that of Catchments 2 and 4 (Table 6.3; Fig. 6.8), due to the assimilation of the remotely sensed soil moisture for Catchment 3. No significant improvement was seen for Catchment 2, when compared to the assimilation of streamflow only.

Streamflow, while improved, was overestimated (Fig. 6.9) for

Table 6.3. RMSE for the volumetric soil moisture content, sensible heat flux, evapotranspiration, and the streamflow after the joint assimilation of streamflow (Catchment 4) and remotely sensed surface soil moisture (Catchment 3). The data in brackets is the RMSE of the respective control run, whereas the first number is calculated after the assimilation. The most accurate predictions for each catchment are in bold.

	Surface [v/v]	*Root Zone [v/v]*	*Profile [v/v]*	*Sens. Heat [W/m^2]*	*ET [mm/d]*	*Streamfl. [m^3/s]*
Catchment 2						
RS1	0.044 (0.083)	0.010 (0.051)	0.009 (0.047)	36.170 (44.217)	1.519 (1.739)	**0.246** (20.148)
RS2	0.059 (0.114)	0.028 (0.085)	0.025 (0.078)	120.090 (87.339)	1.723 (1.365)	13.924 (24.866)
RS3	0.106 (0.074)	0.070 (0.037)	0.066 (0.035)	64.438 (73.770)	3.707 (2.947)	0.755 (2.666)
RS4	**0.020** (0.082)	**0.002** (0.050)	**0.002** (0.046)	**19.113** (44.103)	**0.497** (1.738)	5.974 (27.606)
Catchment 3						
RS1	0.028 (0.114)	0.005 (0.087)	0.004 (0.081)	**13.029** (24.571)	0.571 (1.270)	**0.689** (26.356)
RS2	0.051 (0.144)	0.017 (0.107)	0.015 (0.098)	116.825 (89.231)	1.319 (0.992)	22.805 (40.930)
RS3	0.053 (0.088)	0.039 (0.071)	0.037 (0.067)	72.702 (67.156)	2.615 (2.489)	4.143 (3.675)
RS4	**0.012** (0.112)	**0.001** (0.085)	**0.001** (0.079)	20.436 (24.620)	**0.434** (1.250)	11.318 (39.023)
Catchment 4						
RS1	0.017 (0.100)	0.018 (0.132)	0.013 (0.097)	**15.336** (22.784)	0.679 (1.178)	**1.047** (30.618)
RS2	0.039 (0.135)	0.034 (0.168)	0.025 (0.125)	116.456 (88.493)	1.315 (1.014)	24.479 (43.939)
RS3	0.071 (0.104)	0.080 (0.118)	0.059 (0.088)	61.655 (65.278)	2.896 (2.493)	4.844 (3.807)
RS4	**0.007** (0.096)	**0.003** (0.129)	**0.002** (0.095)	20.722 (22.578)	**0.409** (1.159)	12.555 (44.982)

forcing data scenario 2, due to the biases in the forcing data. The sensible heat flux and evapotranspiration were underestimated (Fig. 6.10), due to the wet bias in the forcing and the inevitable overprediction of soil moisture content within the catchment (sensible heat flux) and the reduced downwelling short wave and long wave radiation (evapotranspiration).

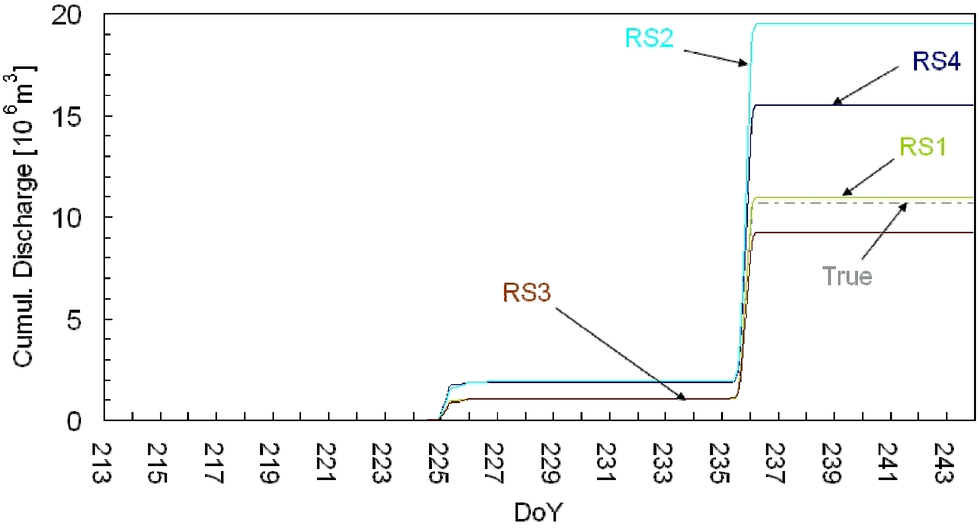

Figure 6.9. Cumulative streamflow from Catchment 3 after the joint assimilation of streamflow at the outlet of Catchment 4 and surface soil moisture from Catchment 3 into CLSM.

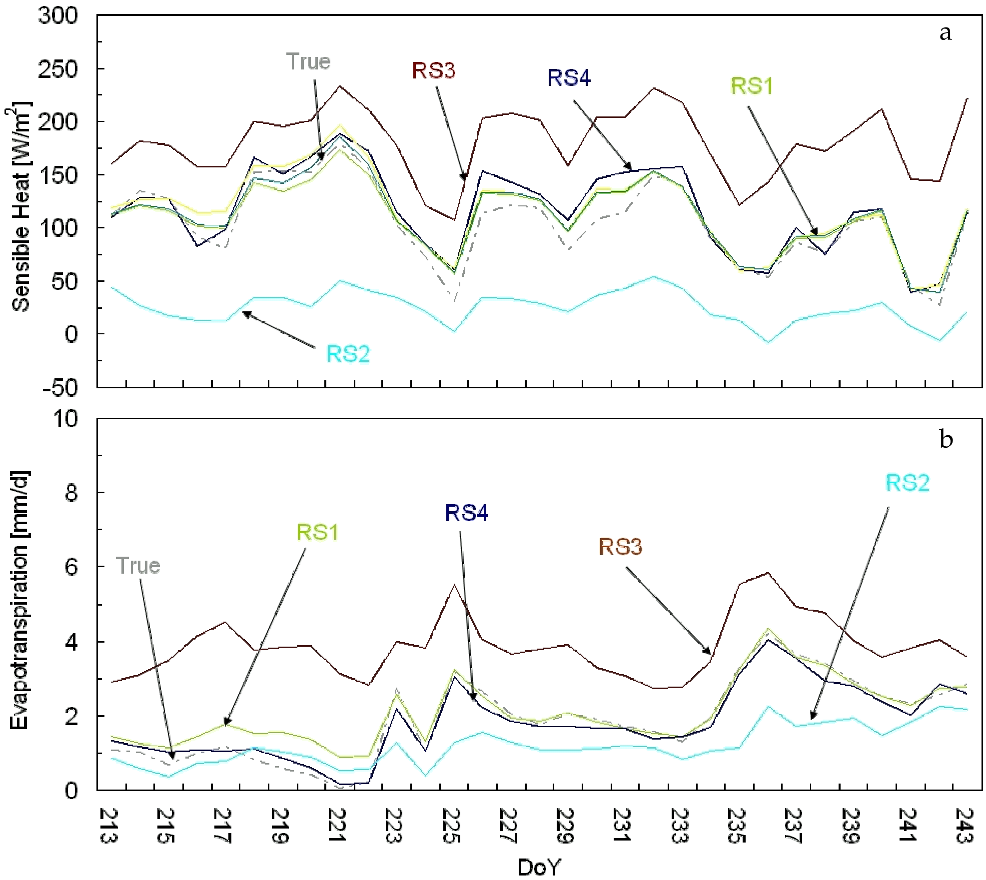

Figure 6.10. a) Sensible heat flux and b) evapotranspiration of Catchment 3 (middle catchment), after the joint assimilation of streamflow at the outlet of Catchment 4 and surface soil moisture from Catchment 3 into CLSM.

6.3.3.3 Scenario RS3

For forcing scenario 3 (dry bias), the additional assimilation of surface soil moisture state into Catchment 3 resulted in a better retrieval of the soil moisture states in that catchment compared to the assimilation of streamflow alone (Fig. 6.8). However, the soil moisture content in the upstream subcatchment (Catchment 2) was found to be wetter than Catchments 3 and 4, as the decreased runoff production from Catchment 3 had to be compensated for. This led also to a further degradation in the sensible heat flux and evapotranspiration predictions from Catchment 4. Moreover, streamflow at the outlet of Catchment 4 was still underestimated, as the decreased soil moisture in Catchment 3 led to a reduction of the streamflow from that catchment (Fig. 6.9). The change in streamflow rate could not be fully compensated for by the other two catchments, as a large change in the streamflow production of Catchment 2 and 4 would have led to an increase in the RMSE for streamflow.

6.3.3.4 Scenario RS4

The joint assimilation of streamflow and surface soil moisture for forcing scenario 4 had a positive effect on the retrieval process when compared to the assimilation of streamflow only (Fig. 6.8). In particular, Catchment 3 showed a significant improvement in the retrieval of its surface soil moisture state, due to the assimilation of surface soil moisture for this subcatchment.

In the same way as for forcing data scenario 2, the wet bias in the forcing data resulted in dry initial soil moisture states and an overestimation of the streamflow. A further improvement to the streamflow was not possible due to the physical limitations of the model, because root zone soil moisture could not be lower than the wilting point.

6.3.3.5 General Discussion

The results of this section highlight that the compensation for streamflow values which are too high or too low cannot be fully achieved, when the forcing data or the retrieval process is biased. The results of the experiments of forcing data scenarios 2 to 4 (with biased forcing data) show that errors in one subcatchment, are partly compensated for by changes in the other subcatchments (eg. streamflow is increased in one subcatchment in order to reduce the streamflow error at the point of observation). However, such changes are relatively small, because full compensation for a large error in streamflow would adversely affect the objective function, as the streamflow peaks from the other catchments are not observed at the same time at the point of observation. As a consequence the least square error would undergo a significant increase at these different points in time.

This section shows the importance of assimilating as much information into the LSM as possible, in particular in the presence of biases in the forcing data. While the assimilation of streamflow observations alone led to good results, the additional assimilation of remotely sensed surface soil moisture improved the retrieval of the subcatchment for which observations were available. Moreover, it was shown that even with a limited amount of information (three subcatchments, two observations) it was possible to retrieve adequate soil moisture states.

6.4 Assimilation of Observations into a Regional Catchment

In Chapter 5 and the preceding sections of the present chapter, it was shown that the assimilation of streamflow observations on its own and along with remotely sensed surface soil moisture observations in a joint assimilation, produced good estimates of initial soil moisture states. These experiments were undertaken for simple stream networks, first for a single catchment in Chapter 5, and then for a group of three nested subcatchment, which were aligned in a sequence. Therefore, the experiments were repeated for a more complex stream network with subcatchments feeding into the main river at different locations.

The eight catchments of the regional synthetic study, i.e. the subcatchments of the Goulburn River experimental catchment upstream from Sandy Hollow, introduce additional heterogeneity to the modelling and assimilation process as they have significantly different soil types, surface conditions and sizes. The experiment on the entire catchment provided an insight into the effects diverse soil and surface conditions have on the assimilation scheme when applied to a catchment with groups of subcatchments, which are not connected to each other, but feed into the same main river. In particular, the different sizes and soil types of the catchments resulted in significant differences in the amount of runoff produced. In this scenario it was determined whether large runoff events reduced the sensitivity of the assimilation scheme to changes in the smaller subcatchment with lower runoff production, as streamflow observations at a catchment outlet further downstream in the stream network are aggregates of the respective upstream catchments. First, the observation at the outlet of the Goulburn River catchment near Sandy Hollow was assumed to be the only available observation for the whole catchment (section 6.4.2). This observation was assimilated into CLSM to retrieve the profile soil moisture states in all eight subcatchments. In section 6.4.3 the assimilation of the streamflow observations of all eight subcatchments into CLSM is presented. This experiment served to study the possibility of a case, when a number of streamflow observations are available within a large catchment and no information on surface soil moisture is available.

The assimilation of streamflow into this larger number of subcatchments was undertaken in different steps. First, only the true streamflow observations at the outlet of Catchment 8 were assimilated (Fig. 6.1d), to obtain profile soil moisture state estimates for all eight subcatchments. Catchment 8 was chosen, as it contains the outlet of the Goulburn River catchment, at which the total streamflow from all subcatchments was observed. Second, all eight true streamflow observations were simultaneously assimilated into CLSM for the eight subcatchments of the Goulburn River catchment (Fig. 6.1e). Finally, a combination of remotely sensed surface soil moisture and streamflow observations were assimilated. In this last experiment, it was assumed that observations from stream gauges at the outlets of Catchments 1, 4, 6 and 8 were available, and that Catchments 3, 5 and 6 were sufficiently cleared to obtain remotely sensed surface soil moisture observations (Fig. 6.1f). Therefore, Catchments 2 and 7 were not providing any observations to the assimilation scheme, as they had no observations available. The subcatchments were chosen to be the same as they would be for a field study (see Chapter 7), as these subcatchments contain calibrated stream gauges (Catchments 1, 6, and 8) or AMSR-E data were available (Catchments 5 and 6). The observations of Catchments 3 and 4 were added in order to further reduce the level of freedom of the system.

The forcing data in this experiment were the true forcing (ie. homogeneous throughout the Goulburn River catchment). The soil and vegetation parameters were derived from the data sets described in Chapter 3. The implications of forcing biases and errors in a multi-catchment study were highlighted in section 6.3 and the use of these data would not have provided new insights into the assimilation of observations into a regional scale model, therefore only forcing data scenario 1 was considered in this study.

6.4.1 Assimilation of Streamflow Observations

The assimilation of one set of streamflow observations obtained for the outlet of Catchment 8 of the Goulburn River catchment with its internal subcatchments, did not lead to a good retrieval of the initial soil moisture states in the subcatchments and consequently of the respective streamflow, sensible heat flux and evapotranspiration (Table 6.4).

The RMSE for streamflow at the outlet of Catchment 8 before the assimilation was 95.520m^3/s and after the assimilation was reduced to 5.246m^3/s. The error in the streamflow prediction for Catchment 8 was caused by the errors in the streamflow of the seven upstream catchments. This showed that even though the spatial distribution of the soil moisture states was not accurately retrieved, the overall streamflow performance was significantly improved. Despite the inaccurate soil moisture pattern, seven out of eight initial soil moisture states were improved, in comparison with the control experiment.

The difficulty to retrieve the correct initial soil moisture states may be explained by noting that because of the wide range in catchment sizes, some of the catchments produced significantly more streamflow than other catchments. Therefore, streamflow from the low-yield catchments (Catchments 4 and 7) was masked by the streamflow from other catchments, making it difficult to determine the optimum soil moisture initialisation of these catchments. The assimilation of streamflow, normalised to the area of the streamflow producing subcatchment, did not significantly improve the retrieval process.

Table 6.4. RMSE of the soil moisture and streamflow predictions for all subcatchments after the assimilation of streamflow observations into CLSM at Catchment 8. The data in brackets is the RMSE of the respective control run, whereas the first number is calculated after the assimilation.

	Surface [v/v]	*Root Zone [v/v]*	*Profile [v/v]*	*Sens. Heat [W/m^2]*	*ET [mm/d]*	*Streamfl. [m^3/s]*
			Catchment 1			
R1	0.023 (0.100)	0.024 (0.126)	0.024 (0.080))	6.181 (7.263)	0.234 (0.276)	5.265 (60.244)
			Catchment 2			
R1	0.065 (0.083)	0.027 (0.051)	0.025 (0.047)	42.604 (44.217)	1.479 (1.739)	2.939 (20.148)
			Catchment 3			
R1	0.085 (0.114)	0.061 (0.087)	0.057 (0.081)	15.431 (24.571)	0.712 (1.270)	8.356 (26.356)
			Catchment 4			
R1	0.130 (0.100)	0.158 (0.132)	0.117 (0.097)	36.053 (22.784)	1.528 (1.178)	10.222 (30.618)
			Catchment 5			
R1	0.035 (0.095)	0.012 (0.075)	0.011 (0.069)	25.380 (56.231)	1.063 (2.399)	0.980 (6.070)
			Catchment 6			
R1	0.051 (0.110)	0.029 (0.083)	0.027 (0.077)	11.201 (43.563)	0.506 (1.961)	5.527 (17.995)
			Catchment 7			
R1	0.048 (0.110)	0.050 (0.126)	0.037 (0.094)	31.535 (37.908)	1.415 (1.700)	6.170 (23.016)
			Catchment 8			
R1	0.000 (0.090)	0.000 (0.116)	0.000 (0.086)	2.612 (9.121)	0.099 (0.347)	5.246 (95.520)

Due to the fixed routing times of the unit hydrograph approach of the streamflow routing model, some of the streamflow generated in Catchment 1 arrived at the outlet of Catchment 8 (ie. at the outlet of the Goulburn River experimental catchment) at the same time as the streamflow generated in Catchment 2. As a consequence, the soil moisture states of these two subcatchments were interchangeable, as the combination of different initial soil moisture states resulted in different streamflow quantities originating from these subcatchments, however the total quantity of streamflow and its

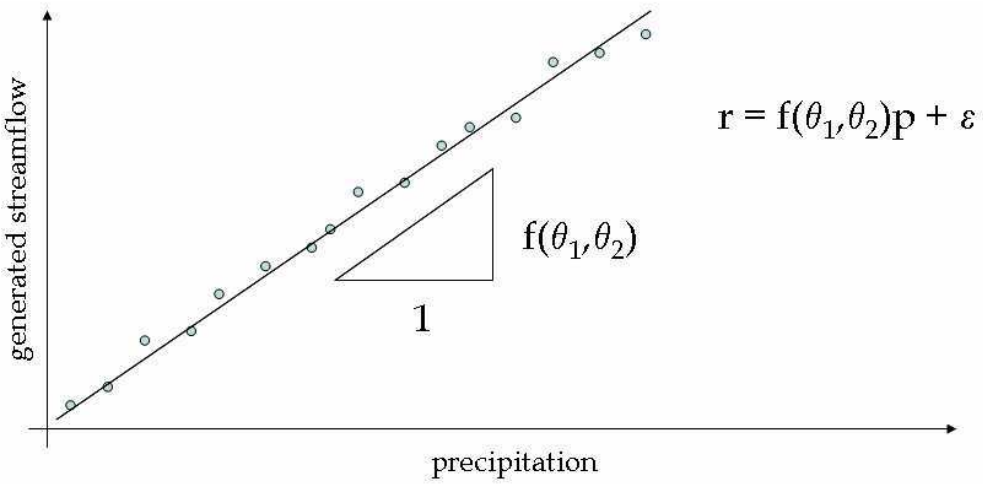

Figure 6.11. Example of a two-parameter linear fit. θ is soil moisture at a given catchment, p precipitation and ε a random error function.

temporal distribution at the outlet of Catchment 8 did not change.

In order to generate accurate streamflow at the outlet of Catchment 8, a large number of combinations of initial soil moisture states within the Catchments 1 and 2 was possible. Such a behaviour may be illustrated with a two-parameter fit to a linear data set, where an infinite number of combinations may be used to find the same solution (Fig. 6.11). In this example, a linear relationship between precipitation and streamflow in both subcatchments was assumed, while soil moisture state remained its non-linear relationship with precipitation and streamflow, and the slope of the function was assumed to be a constant function of this non-linear soil moisture relationship between the two subcatchments. This experiment showed that the system was too much underdetermined and further constraints were required, in order to obtain the true initial states.

6.4.2 Assimilation of all Eight Sets of True Streamflow Observations

The experiment presented in this section, represented the opposite extreme of the previous experiment. Here, all eight streamflow observations were assumed to be available for assimilation into the LSM. This experiment was undertaken in order to identify the implications of assimilating streamflow observations which implicitly contain the information of the upstream observations. As the subcatchments are all nested, the streamflow at the outlet of Catchment 8 contains the information about the streamflow from all eight subcatchments and the streamflow observation at the outlet of Catchment 4 contains the information of the streamflow from Catchments 2 and 3.

For this experiment, some minor adjustments had to be made to the assimilation process during the course of the experiment, as the assimilation scheme was not able to find the global optimum for all eight initial soil moisture states with the first attempt. Therefore, the assimilation scheme was repeatedly run to eliminate those subcatchments from the assimilation, in which satisfactory soil moisture and streamflow model predictions were detected. The performance of the model for these subcatchments was defined as satisfactory, when the standard deviation of the residual error of the streamflow in these subcatchments was less than 1% of the maximum observed streamflow. This iterative process reduced the number of catchments for which soil moisture initial states were searched and consequently the size of the cross-correlation matrix.

This new approach was found to behave as a "top-to-bottom" approach. The first soil moisture initial states found to be correctly retrieved were those of the upper catchments (Catchments 2 and 5; Table 6.5), which have no further upstream catchments that contribute to the observed streamflow. The subsequent assimilation runs led to the retrieval of the soil moisture initial states in subcatchments which were the downstream neighbours of the subcatchments that were previously fixed.

Eventually, the initial soil moisture states of all eight subcatchments were retrieved to within at least 0.015v/v (Table 6.5).

Table 6.5. Results from the assimilation of soil moisture states into the whole catchment. The profile soil moisture states are shown for the initial guess, the final results and the truth; the numbers in the white boxes are residual variances of the streamflow in the catchments; the numbers in the dark green boxes are profile soil moisture (top) and residual variance (bottom); X and green fields denote fixed initial states for the respective subcatchment.

	Guess	*Iter. 1*	*Iter. 2*	*Iter. 3*	*Iter. 4*	*Iter. 5*	*Final*	*True*
Cat. 1	0.263	64.11	69.85	50.22	72.85	… ...	0.168	0.182
Cat. 2	0.307	14.79	0.244 0.403	X	X	X	0.244	0.229
Cat. 3	0.332	154.3	97.71	86.57	38.46	… ...	0.231	0.229
Cat. 4	0.284	195	163.0	159.8	109.4	… ...	0.164	0.159
Cat. 5	0.328	0.230 .0025	X	X	X	X	0.230	0.229
Cat. 6	0.330	29.69	36.13	0.236 0.45	X	X	0.236	0.229
Cat. 7	0.278	36.07	39.02	16.04	0.170 1.19	X	0.170	0.159
Cat. 8	0.268	68.15	107.3	309.6	220.3	… ...	0.182	0.179

The initial soil moisture states were not retrieved to a higher accuracy, because of the assumption that root zone and surface excesses were in full equilibrium. As a consequence, streamflow, sensible heat flux and evapotranspiration contained small errors. Table 6.6 shows only the RMSE for root zone and streamflow, as an improvement of the root zone soil moisture predictions was shown in the previous experiments to coincide with improvements in the surface soil moisture, sensible heat flux and evapotranspiration, for the forcing data scenario 1 (no errors in the forcing data).

The change of the assimilation process highlighted the impact of a nested stream network on the assimilation process. Because changes in the upstream subcatchment influenced the streamflow in subcatchments located downstream, the assimilation scheme

Table 6.6. RMSE of the root zone soil moisture and streamflow predictions for all eight subcatchments after the assimilation of the streamflow observations at all subcatchment outlets into CLSM. The data in brackets is the RMSE of the respective control run, whereas the first number is calculated after the assimilation.

	Root Zone [v/v]	*Streamfl. [m^3/s]*
Catchment 1		
R1	0.001 (0.126)	0.302 (60.244)
Catchment 2		
R1	0.002 (0.051)	0.029 (20.148)
Catchment 3		
R1	0.001 (0.087)	0.056 (26.356)
Catchment 4		
R1	0.001 (0.132)	0.763 (30.618)
Catchment 5		
R1	0.001 (0.075)	0.096 (6.070)
Catchment 6		
R1	0.001 (0.083)	0.210 (17.995)
Catchment 7		
R1	0.001 (0.126)	0.247 (23.016)
Catchment 8		
R1	0.001 (0.116)	0.391 (95.520)

determined a cross-correlation of the soil moisture states within the different subcatchments, which changed with each run of the newly retrieved initial states. The elimination of the retrieved initial soil moisture states led to a gradual decrease in the complexity of the cross-correlation matrix, until a final best-fit function was found.

6.4.3 Joint Assimilation of Streamflow and Soil Moisture

The results of the experiment in the previous section showed that a fully determined system required a large number of assimilation runs before the assimilation scheme was able to find the global minimum. In order to reduce the number of these runs, the number of streamflow observations were reduced. In section 6.3, it was shown that the retrieval of the initial soil moisture states in nested stream networks, where the subcatchments were in sequence, led to a good retrieval of all upstream initial soil moisture states under forcing scenario 1 (true forcing without imposed errors), when assimilating the streamflow observations at the catchment outlet. In order to have a link to the field study of Chapter 7, only calibrated stream gauges were chosen to provide streamflow observations in this section. The stream gauge at the outlet of Catchment 4 was added, because it was used in the three-catchment studies. Furthermore, the stream gauges location at Catchment 1, 4, and 6 complied with the requirements that all upstream subcatchments were located in a sequence. As a further constraint to the assimilation process, remotely sensed surface soil moisture observations from Catchments 3, 5, and 6 were assimilated, as well (Fig. 6.1f). These subcatchments were chosen, because they are mainly cleared for agricultural purposes and were most likely to be used in a field study.

The experiment of this section was carried out to study the potential use of a limited number of observation points of different types of observations (in the present experiment streamflow and surface soil moisture) for their assimilation into the LSM of a complex stream network. To minimise the complexity of the assimilation run, this experiment was split into two parts (Fig. 6.12). At first, only the remotely sensed surface soil moisture observations for Catchments 3, 5 and 6 were assimilated into the LSM. This approach is adequate, if the remotely sensed surface soil moisture information is assumed to be accurate and there is no bias in the forcing data, which was the case for this synthetic study.

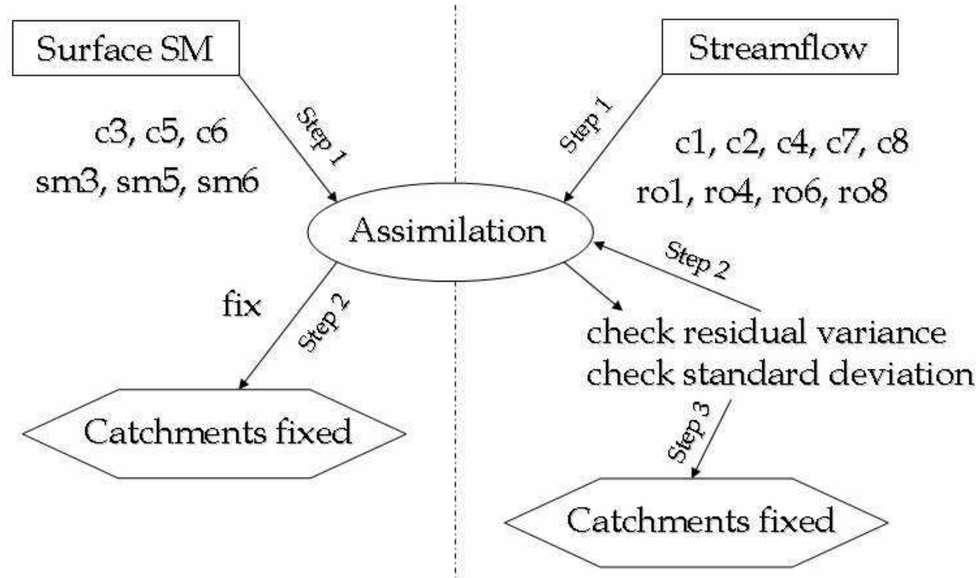

Figure 6.12. Schematic of the assimilation of different quantities. The left hand side represents the assimilation of remotely sensed surface soil moisture and the right hand side, the assimilation of streamflow observations. *c* is catchment, *sm* is soil moisture, *ro* is streamflow observation for the respective catchment. The assimilation scheme will only pass from the surface soil moisture to the streamflow assimilation, when all catchments on the left hand side are fixed. It will then continue with the remaining catchments, until the satisfy certain criteria (low residual variance and standard deviation).

This approach effectively eliminated three soil moisture states from the state-space, before the assimilation of the streamflow observations. After the three subcatchments with remotely sensed surface soil moisture observations were fixed, the remaining four streamflow observations (Catchments 1, 4, 6, and 8) were assimilated, leading to the retrieval of the initial soil moisture states in the remaining five catchments (Catchments 1, 2, 4, 7, and 8) with the "top-to-bottom" approach presented in the previous section.

In this experiment, it was shown that the initial soil moisture states were well retrieved for all eight subcatchments (Table 6.7). Consequently, streamflow, sensible heat flux and evapotranspiration were well predicted in both, gauged and ungauged catchments. The RMSEs for Catchments 3, 5 and 6, for which surface soil moisture was assimilated into CLSM, show only negligible errors for the root

Table 6.7. RMSE of the root zone soil moisture and streamflow predictions for all eight subcatchments after the joint assimilation of remotely sensed surface soil moisture and streamflow observations into CLSM. The data in brackets is the RMSE of the respective control run, whereas the first number is calculated after the assimilation.

	Root Zone [v/v]	*Streamfl. [m³/s]*
Catchment 1		
R1	0.023 (0.126)	1.39 (60.244)
Catchment 2		
R1	0.002 (0.051)	0.018 (20.148)
Catchment 3		
R1	0.000 (0.087)	0.068 (26.356)
Catchment 4		
R1	0.019 (0.132)	0.775 (30.618)
Catchment 5		
R1	0.002 (0.075)	0.086 (6.070)
Catchment 6		
R1	0.000 (0.083)	0.184 (17.995)
Catchment 7		
R1	0.004 (0.126)	0.236 (23.016)
Catchment 8		
R1	0.006 (0.116)	1.599 (95.520)

zone soil moisture predictions (below 0.002v/v). The errors in the predictions for the remaining subcatchments were only marginally larger, with RMSEs ranging from 0.004 to 0.023v/v.

As in the previous experiments, the error in the streamflow originated from the assumption that the initial soil moisture states are in equilibrium (root zone and surface excess set to 0). However, this was not the case in the true run. Therefore, CLSM produced different quantities of runoff for the true observations and the model output after the assimilation. In the present case, this led to streamflow being slightly overestimated as the soil moisture was overestimated and therefore the runoff contributing area. While the results for this experiment showed larger errors than for the previous experiment with eight streamflow observations, the computational time was significantly reduced, which is important for the application of this approach to larger scales. Furthermore, the results of this experiment were significantly better than those from the regional experiment with only one stream gauge providing observations (section 6.4.1).

With this experiment, it was shown that the joint assimilation of streamflow and remotely sensed surface soil moisture sufficiently constrained the LSM to retrieve the initial soil moisture states in all subcatchments. This was an important finding in view of the field study in the following chapter. It showed that the developed assimilation process can be applied to underdetermined situations (less points of observations than subcatchments).

6.5 Chapter Summary

In this chapter, the assimilation scheme presented in Chapter 5 for a single catchment was applied in two studies to more complex stream networks. It was shown that the joint assimilation of streamflow and remotely sensed surface soil moisture, provided only minor improvements to the retrieval of the initial soil moisture states in smaller catchments. However, for larger stream networks with a greater number of subcatchments, the combination of streamflow and remotely sensed surface soil moisture observations led to better results than the assimilation of each type of observation alone, as additional constraints were required.

The assimilation of only streamflow observations into the LSM, for large stream networks showed that subcatchments located the furthest upstream had to be fixed first, before the initial soil moisture states in the downstream catchments was retrieved ("top-to-bottom approach"). For the joint assimilation, the assimilation process had to follow a logical progression, where the remotely sensed surface soil moisture observations had to be assimilated first, in order to reduce the number of subcatchments involved in the retrieval process, before the "top-to-bottom" approach of the streamflow assimilation was applied.

Most importantly, it was shown that the full retrieval of all initial soil moisture states within the Goulburn River experimental catchment is achievable with only a limited number of observations. This was of significance for the preparation of the field study in the following chapter.

Chapter Seven

7 Field Data Study

The data assimilation scheme developed in the previous chapters was applied to a field data study, presented in this chapter. First, the forcing data and field observations used for this study are described. Next, a model verification is undertaken, showing the need for modifications to the infiltration mechanisms of the model and the level of disaggregation of the main catchment. Finally, all available streamflow data and AMSR-E soil moisture observations for two catchments are jointly assimilated into the modified model.

7.1 Outline of Approach

The synthetic studies in the previous two chapters have shown the limitations, in particular for forcing data scenarios with biases, but have also highlighted the capabilities of a streamflow assimilation scheme with and without assimilating additional observations, such as surface soil moisture. Furthermore, it was shown that the inclusion of soil moisture as an additional type of observation, in order to further constrain the assimilation process, improved the retrieval of the initial soil moisture states and consequently the soil moisture, sensible heat flux and evapotranspiration predictions. In particular the possibility to use such an assimilation scheme for larger catchments with limited observations was an important finding. However, these studies were undertaken in an environment, where errors and biases were known. To test the applicability of the developed assimilation scheme, it was applied in a field data study for the Goulburn River experimental catchment. In Chapter 5, it was shown that instead of the absolute soil moisture content, a soil wetness index (SWI) should be used, as it would facilitate the comparison of the predicted and observed soil moisture. While the necessary information (θ_{wilt} and θ_{sat}) is available for the model, detailed knowledge on the soil parameters is not available for the observations. In particular the lack of information on θ_{sat} makes it impossible to properly calculate the SWI for the observations. Therefore, the soil moisture in this chapter is given in absolute values.

In this field data study, real observations of streamflow and remotely sensed surface soil moisture observations from AMSR-E were assimilated into CLSM. In addition, the model was forced with spatially heterogeneous forcing data, unlike in Chapters 5 and 6, where forcing data were assumed to be spatially homogeneous.

Before any data were assimilated into CLSM, some model parameters and forcing data were first tuned to the streamflow and soil moisture observations of the second half of the 12-month data set. This was undertaken by comparing the observations and modelled results for the streamflow peaks, and soil moisture maxima and minima.

In the present chapter, only streamflow observations from the DIPNR stream gauges at Kerrabee and Sandy Hollow were assimilated into CLSM, while the observations at the stream gauge near Merriwa were used to verify the new model predictions. Additionally, surface soil moisture observations from AMSR-E were assimilated into the model. However, remotely sensed surface soil moisture observations were only available for Catchments 6 and 7 (Fig. 7.1).

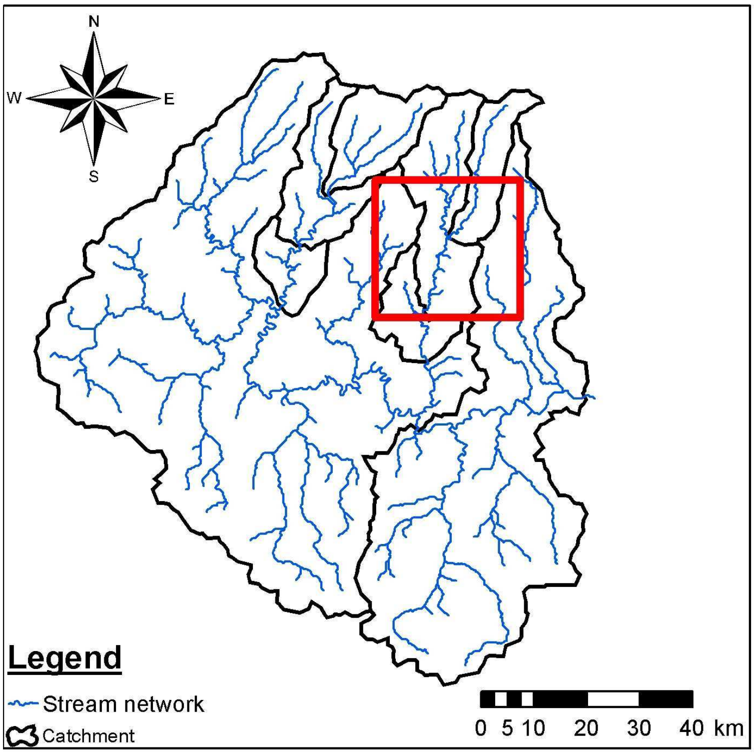

Figure 7.1. Goulburn River catchment with overlying AMSR-E-pixel (red) over Catchments 6 and 7.

7.2 *Real Forcing Data*

Unlike the multi-catchment synthetic studies in Chapter 6, the forcing data in the present study were not assumed to be spatially homogeneous throughout the catchment, but were compiled from different sources for the individual subcatchments. These sources were the two SASMAS weather stations (S2 and K6) and three weather stations at Scone (east), Mudgee (west), and Nullo Mountain (south), which are operated by the BoM (see section 3.2), and which have observations available in 20 and 60 minute time intervals, respectively. However, the weather stations operated by the BoM only provided precipitation and air temperature observations. The forcing data required by CLSM are precipitation, air temperature, atmospheric pressure, wind speed, actual vapour pressure, and downwelling long wave and short wave radiation (see the model description in Chapter 4). Consequently, the forcing data for the individual subcatchments had to be compiled from different sources.

As in the synthetic studies, all radiation data were extracted from the GDAS data set (Derber et al., 1991) for all individual subcatchments, as only a net radiometer was installed at the S2 in 2003 and 2004. The observations of atmospheric pressure, wind speed and actual vapour pressure were obtained from S2 and K6 and applied to all subcatchments within the Goulburn River experimental catchment. The forcing data for precipitation and air temperature were interpolated between the available five weather stations. To achieve this, the observations were given weights according to the distance of the weather stations to the respective subcatchments.

Finally, the observed data contained some gaps due to logger failures at the different stations. These gaps were replaced with data from other periods at the same station, which were assumed to be similar to the missing period. This was achieved by comparing the data from other stations and finding periods that were similar to each other. Fig. 7.2 shows atmospheric pressure, air temperature and precipitation data for the 12-month period for Catchment 4 (data from S2), highlighting the periods during which data had to be replaced. Overall, the data gaps accounted for less than 10% of all the data, which was assumed to introduce a negligible error.

7.3 Field Observations

7.3.1 Streamflow

The streamflow observations used in the present study for the assimilation and verification of the streamflow data were obtained from the DIPNR operated stream gauges at Kerrabee, Merriwa and Sandy Hollow. As mentioned in section 3.2, the stream gauges installed for the field observations to be used in this thesis suffered from the lack of an adequate number of streamflow events for their

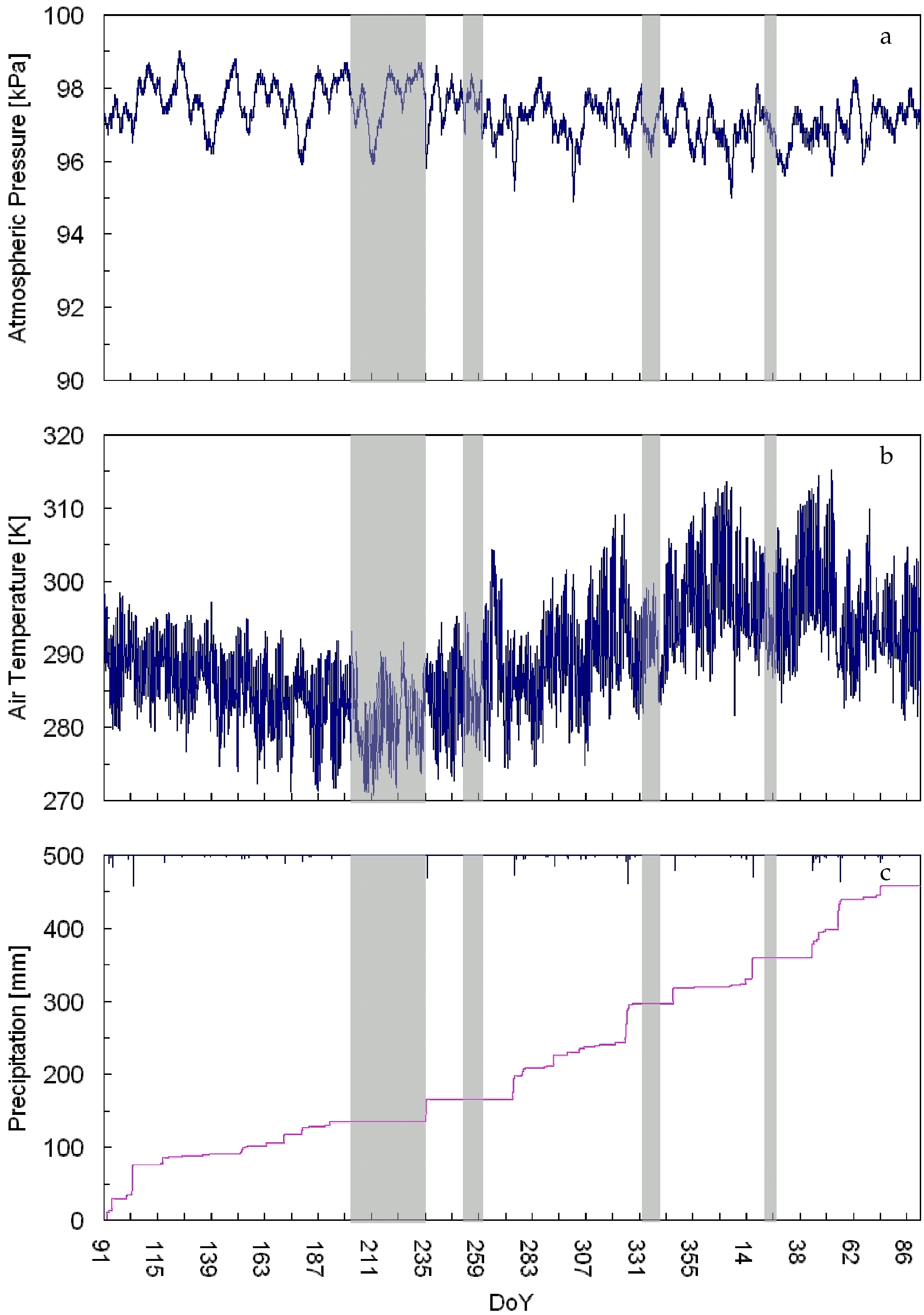

Figure 7.2. a) Atmospheric pressure, b) air temperature, and c) daily and cumulative precipitation for the 12-month period for Catchment 4 (S2). Periods with replaced data are highlighted in grey.

calibration and were therefore only used for qualitative comparisons (timing of the peak discharge), rather than quantitative (magnitude of the peak discharge and total streamflow).

7.3.2 Soil Moisture

The soil moisture observations used as verification of the root zone soil moisture in this chapter are the calibrated root zone soil moisture observations from the SASMAS soil moisture monitoring sites, which have been presented in Chapter 3. In subcatchments containing more than one soil moisture monitoring site the surface and root zone soil moisture values for the whole subcatchment were averaged from the soil moisture content observed at the soil moisture monitoring sites contained within the subcatchment. Four subcatchments (Catchments 10, 14, 15 and 16) did not contain any soil moisture monitoring sites.

It is necessary to briefly discuss the representativeness of the observed soil moisture measurements and its implications for the field study. There are two approaches that may be chosen to determine this representativeness: i) a comparison of the local CTI at the local site with the distribution of CTI within each subcatchment, and ii) the assumption of observational errors as presented in section 3.6. For the field study presented in this chapter, it was decided to follow ii). A comparison was undertaken for the CTI for all subcatchments and their respective site-specific CTI and it was found that the calculated CTI from the 250m DEM did mostly, but not always correspond with the local conditions at the site. In particular, the calculated slope played a significant role, especially in areas where large floodplains are directly adjacent to steep slopes. In these areas, a shift in the location of the site from one pixel to another significantly alters the local CTI, as the slope can undergo sudden changes from one pixel to the other. Moreover, local soil and vegetation conditions may also influence the representativeness of the site. Therefore, it was decided to use the in-situ soil moisture observations and to take the previously determined observational errors into consideration.

7.3.3 Precipitation

Several studies have shown that point measurements of precipitation have to be reduced if they are to be applied as spatial averages to a catchment (eg. Pilgrim, 1987; Sivapalan and Blöschl, 1998). The principle behind such a reduction factor is that precipitation events rarely show the same intensity over the whole catchment and therefore, the observation of precipitation at a single rain gauge within a catchment is not representative of the whole catchment. In principle, this should have been overcome with the interpolation of the precipitation data from the five weather stations. However, preliminary model runs showed a significant overestimation of the streamflow, compared to the field observations (not shown).

Chapman (1963) and McMahon (1964) showed for the Goulburn River catchment that a strong correlation between topography and rainfall intensity existed for the monitoring sites. In their studies, they derived correction factors for locations at a certain distance and elevation difference from a weather station in the western part of the catchment. Both authors showed that high elevation sites within the catchment had a significantly higher amount of annual precipitation than sites located in the lower parts of the catchment. Since the weather station used as a base station in Chapman (1963) and McMahon (1964) has long been decommissioned, a new correction factor for the Goulburn would have been required to be derived. Such work is beyond the scope of this thesis. Therefore, a more general approach was adopted.

Using the water balance equation

$$P = ET + R + \Delta SM \ , \tag{7.1}$$

where P is precipitation [mm]; ET is evapotranspiration [mm]; R is streamflow at the catchment outlet [mm]; and ΔSM is the change in the soil moisture storage [mm], a catchment wide rainfall reduction factor (*RRF*) was determined by

$$\frac{ET + R + \Delta SM}{P} = RRF\ . \qquad (7.2)$$

The precipitation represents the amount of water falling onto the catchment, while the streamflow observations represent the water being extracted from the catchment through lateral surface water movement, the difference in soil moisture was assumed to be the additional storage or loss of water within the catchment, and evapotranspiration was assumed to be the water removed from the catchment due to bare soil evaporation and transpiration from vegetation. This *RRF* allowed to reduce the errors introduced to the precipitation forcing data by averaging over a large spatial domain with sites from different elevations, by either increasing or reducing the precipitation.

To assess the validity of the assumption of being able to correct the streamflow events through manipulating the precipitation, two periods within the 12 months under investigation were analysed and an *RRF* calculated. The two periods covered winter (Julian day 235 to 253) and summer (Julian day 32 to 60) events (Fig. 7.3). To obtain the *RRF*, observed cumulative streamflow (at the Goulburn River catchment outlet at Sandy Hollow), precipitation (for the whole Goulburn River catchment), evapotranspiration (calculated for all subcatchments using the observed net radiation at S2), and changes in soil moisture storage (from all 26 monitoring sites) were compiled.

Potential evapotranspiration was calculated by using the Penman-Monteith equation (Smith, 1991). Since this equation produces the evapotranspiration rate for a saturated soil, the obtained values had to be adjusted, as the evapotranspiration rate is reduced with lower soil moisture content. This reduction was achieved by using the soil

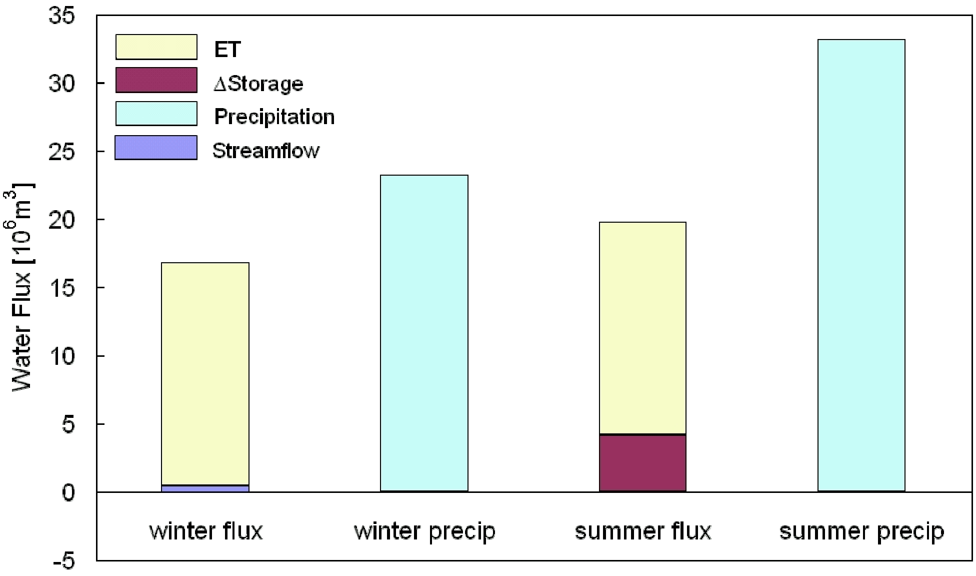

Figure 7.3. Water fluxes in the Goulburn River catchment for a winter 2003 and a summer 2004 event. The left column in a pair is the aggregate of soil moisture storage change (ΔStorage), Streamflow and evapotranspiration (ET). The right hand column is the catchment-wide precipitation derived from the real forcing data.

moisture stress index by Kalma et al. (1995)

$$SI = \left(\frac{\theta}{\Phi}\right)_{\text{total depth}}, \qquad (7.3)$$

where SI is the dimensionless stress index; θ is the soil moisture content [v/v] over the whole soil depth; and Φ is the porosity [v/v] over the whole soil depth, so that

$$ET_a = SI * ET_p, \qquad (7.4)$$

where ET_a and ET_p are the actual and potential evapotranspiration, respectively. Eqs. (7.3) and (7.4) allow the interpolation between the potential evapotranspiration and the minimum evapotranspiration, according to the level of the hydric stress in the soil. This results in a smooth transition of the evapotranspiration between the different levels of soil moisture content. Eqs. (7.3) and (7.4) represent only an empirical model for the calculation of evapotranspiration. Consequently, this approach may introduce an unknown level of error to the calculation of the water balance. Because the water balance within the Goulburn River catchment has been shown to be dominated by evapotranspiration this error may be significant. However, for the purpose of this study, it was assumed that the RRF reduced this error.

The change in the water storage within a subcatchment was calculated by averaging the differences in soil moisture storage from the monitoring stations within the respective subcatchments and then multiplying with the area of the subcatchment to obtain the total change in cubic metres. The ratio of extracted water from the catchment to the observed precipitation was the estimate of the *RRF* (eq. 7.2). The *RRF* for the winter period was 0.71 and for the summer period 0.59 (Fig. 7.3). While there is a difference between the two values an average *RRF* of 0.7 was assumed for all precipitation events. The explanation for the choice of this value over an average value between the two events is fourfold. First, McMahon (1964) showed that the observational error in smaller streamflow events at Sandy Hollow was high, which could lead to a relatively large error in the calculation of the *RRF* for the summer period. Second, all observations introduced a certain level of uncertainty, and this uncertainty could not be adequately quantified. Third, a lower *RRF* caused some small streamflow events not to occur anymore during the simulation, which was regarded as an unsatisfactory situation. Fourth, the determined *RRF* was assumed to be constant throughout time, representing the average *RRF* for the period. As shown with the differences in the *RRF* between the summer and winter period, the assumption that the *RRF* is constant throughout time is not correct. However, a more accurate temporally variant factor can not be determined. The calculation of such a temporally variant factor would require the exact knowledge of the time of travel of each water particle from its point of origin to the catchment outlet at any given time.

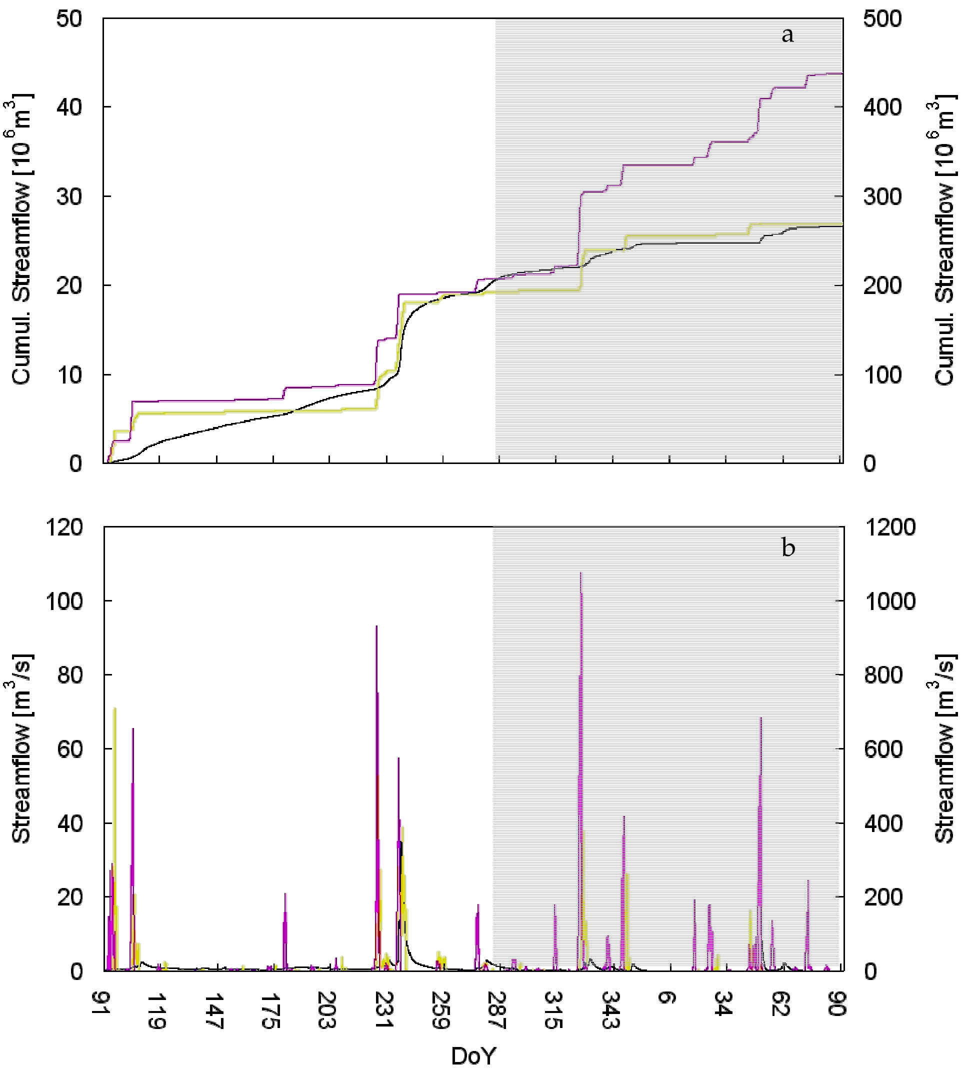

Figure 7.4. a) Cumulative and b) instantaneous streamflow at Sandy Hollow for the full 12 months of the study data. Blue are the streamflow field observations, pink the results of the original model and yellow the results of the modified model. The left hand axis is the scale for field observations and the results of the modified model, the right hand axis is the scale for the original model results. The shaded area represents the period used for the calibration of the model.

The reduction of the catchment-wide precipitation intensity showed a significant decrease in the streamflow magnitude, showing that an *RRF* was required. However, the cumulative streamflow for the one year was still largely overestimated by a factor of 16.5 (Fig. 7.4). This suggested that other factors were contributing to the misrepresentation of the streamflow quantities within the model.

7.4 Model Verification and Modification

The comparison of the simulated and observed streamflow at the outlet of the Goulburn River catchment at Sandy Hollow showed a significant discrepancy between model and observations (Fig. 7.4), after the model spin up with real forcing data and generic model parameters. In particular streamflow was significantly overestimated and the assimilation of the observed streamflow did not result in a satisfactory improvement of the modelled streamflow, because of the significant differences between model prediction and observation. Therefore, some model parameters had to be adjusted and the representation of several physical processes had to be modified.

These adjustments were undertaken by comparing soil moisture and streamflow field observations with modelled soil moisture and streamflow predictions, and the soil parameters determined in the laboratory. After each adjustment, CLSM was spun up ten times over the one year period and the performance of the model in the last six months was used as verification to the field observations. The modifications of CLSM were performed by changing the subcatchment delineation, a change to the wilting point and porosity values of the soil parameters, a change to the infiltration capacity and the surface runoff production of the model. Changes to ponding were considered, as well, however did not show any satisfactory improvements. The modifications of the model were limited to the parameters presented in the following sections. No further model adjustments or parameter tuning was undertaken. The reason for this limited number of modifications is that detailed tuning is not always possible and this thesis will present a near-operational case.

Fig. 7.4 shows the streamflow from the generic model, the observations and the modified model (all for the catchment outlet at

Sandy Hollow). The changes after the individual modifications are not presented in figures.

7.4.1 Subcatchment Delineation

For the synthetic studies in Chapters 5 and 6, and the assimilation of field streamflow observations into the generic model (see section 7.5.1), the subcatchment delineation followed the location of the stream gauges installed throughout the Goulburn River catchment. However, this resulted in two large subcatchments (Catchments 1 and 8; Fig. 3.19a), which then included clayey soils (in the north) and sandy soils (in the south) in the same subcatchment. Consequently, a large part of the Goulburn River catchment was not properly represented in terms of its vegetation and soil types. To further improve the subcatchment structure these two larger subcatchments were further disaggregated, in order to better represent the heterogeneity of the soil and surface conditions. For that purpose, all river reaches that are tributaries to the Goulburn River were defined as individual subcatchments (Fig. 3.22b), with their own soil properties.

The disaggregation of the Goulburn River catchment and the following changes to the forcing data in some of the subcatchments led to a significant reduction in the modelled streamflow. However, further improvements were necessary, as streamflow was still overestimated.

7.4.2 Wilting Point and Porosity

The comparison of the modelled soil moisture values and the real observations showed that the dry-down of the model predictions quickly reached the lower model threshold, beyond which no further dry down was possible (Fig. 7.5a). However, this dry-down continued for the real observations. Furthermore, the soil moisture content in sandy soils was significantly overestimated (Fig. 7.5b).

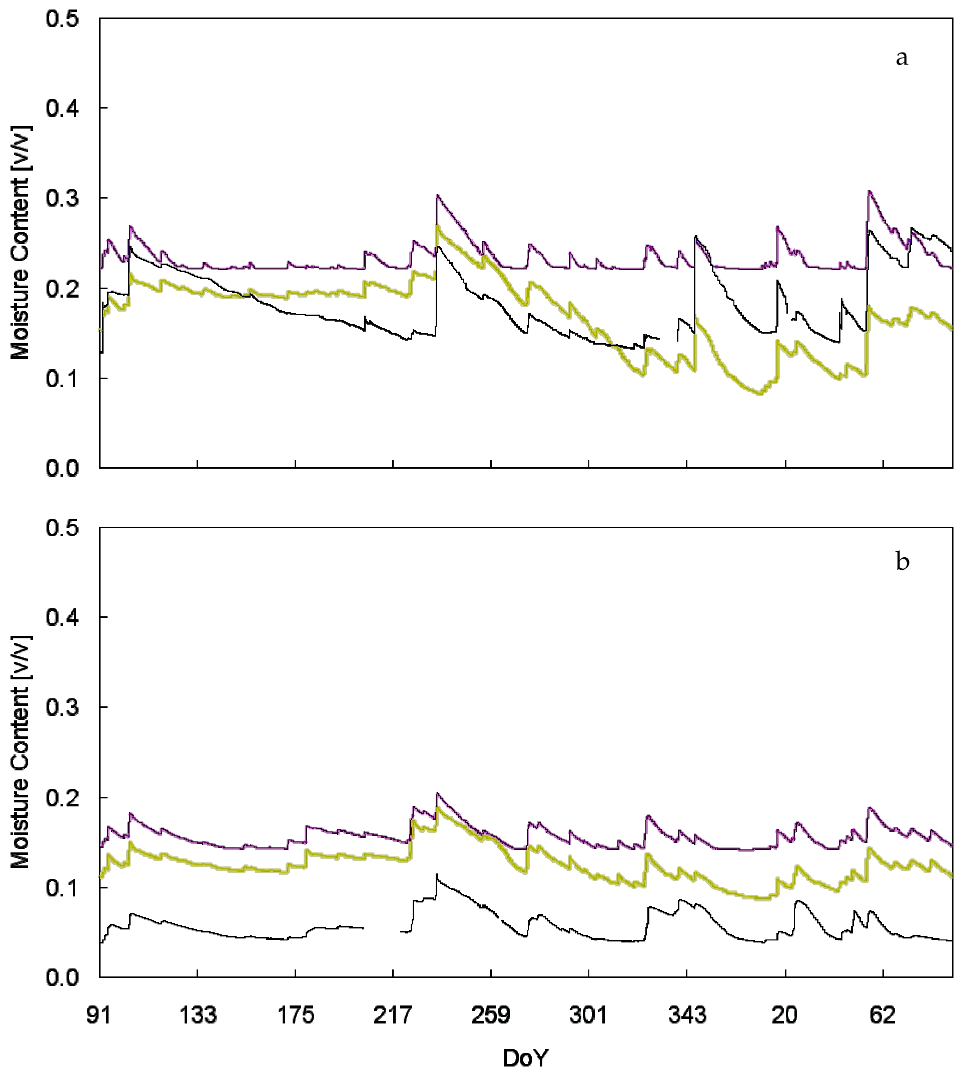

Figure 7.5. Root zone soil moisture for a) Catchment 2 and b) Catchment 7. Blue are the soil moisture field observations, pink the results of original model and yellow the results of the modified model.

Therefore, it was concluded that the wilting point (one of the generic model parameters) was not correct and had to be decreased.

Using the observations of the installed soil moisture sensors for the different monitoring sites, the soil parameters were redefined. As the lower limit (wilting point) for the model, the average minimum soil moisture content values from the monitoring sites located within the respective subcatchments were chosen. The upper limit (saturation) was defined as the average of the observed maximum soil moisture content.

This adjustment had two effects. First, due to the reduction of the wilting point, in some cases to nearly 50% of the original values, the modelled soil moisture was significantly lower within the subcatchments, compared to the previous model runs. Second, as the lower soil moisture limit was reduced, the total storage capacity of the soil was increased, more water was able to infiltrate into the soil, leading to longer periods when evapotranspiration was possible, and consequently reducing the total streamflow.

7.4.3 Infiltration Capacity

In CLSM all precipitation water falling at a rate exceeding the infiltration capacity of the soil is instantaneously transferred into surface runoff. However, the comparison of precipitation and streamflow events observed in the Goulburn River catchment suggested that not all intensive precipitation events resulted in surface runoff. Moreover, less intensive, but longer precipitation events following other events, and therefore a previous wetting of the soil, resulted in more streamflow than the preceding more intensive precipitation events. This is in accordance with the findings of Chapman (1963) for the same catchment. In his study, Chapman (1963) found that the relationship between storm precipitation and streamflow depended on the antecedent soil moisture ("surface catchment dryness index", which describes the dryness and therefore the level of cracking of the soil) and precipitation conditions ("antecedent precipitation index", which quantifies the water input into the soil changing the "surface catchment dryness index") within the catchment, where wetter soils caused larger streamflow events even with less precipitation.

In order to develop an approach that allowed to influence the streamflow production within the LSM in those terms, it was necessary to change the processes of infiltration and streamflow

Figure 7.6. Example of a black cracking clay. (image courtesy of the Upper Parramatta River Catchment Trust).

production of the LSM. For the present study, it was suggested to define a certain threshold below or above which different physical processes are dominant.

From an analysis of the origins of the modelled streamflow it was concluded that the majority of the streamflow was produced in the northern subcatchments, as precipitation in those clayey subcatchments quickly exceeded the infiltration capacity of the soil. The soil in these subcatchments are mainly basalt-derived soils (see section 3.1), which are known in the region as "black cracking clays". These soils tend to display large cracks during periods of low or no precipitation events (Fig. 7.6). Consequently, any precipitation falling on these cracking soils directly infiltrates the soil, without producing noticeable surface runoff. The drying and wetting of the soils result in their cracking and swelling. When the cracks eventually close, surface runoff is produced during subsequent precipitation events.

To allow for changing infiltration capacities due to the described soil cracking, the surface runoff production within the LSM was modified in two steps. First, the area contributing to surface runoff was set to 0% of the total area for catchment deficit values exceeding a certain threshold. This ensured that all precipitated water was available for infiltration into the soil under antecedent dry conditions. Second, it was assumed that the infiltration capacity of the soil is increased due to its cracking. As for the previously described runoff production, another threshold of the catchment deficit had to be defined at which the infiltration capacity of the soil was changed. The described assumptions still allowed runoff to be produced for extreme precipitation events which exceeded the increased maximum infiltration capacity of the soil. The catchment deficit is the prognostic variable that describes the dryness of the soil and therefore allowed to define a threshold between wet and dry soil conditions.

The tuning of the thresholds resulted in a value of 75% of the catchment deficit for both, infiltration capacity and surface runoff production. Above this threshold, the soil was defined as dry (and therefore suffering from cracking) or wet when the catchment deficit was below 75%. This threshold led to the decrease of streamflow events occurring after a long period of dry weather and a significant change in the dynamics of the modelled root zone and soil moisture states. Furthermore, the optimum multiplication factor to increase the infiltration capacity in case of cracked soils, was found to be 1.5.

Recently, the swelling and shrinking of soils and their subsequent changes to the soil parameters was modelled by Camporese et al. (2006). Similarly to the approach chosen in this thesis, they developed a relationship between moisture content and soil conditions. With their model, they showed good results in representing the parameter changes. However, their study focussed on peatlands, only, and results for other soils were not presented.

7.4.4 Soil Depth and Conductivity

A sensitivity study was undertaken, in order to determine the effect of uncertainty in soil depth on baseflow and subsequently streamflow production within the model. For that purpose, the soil depth was changed to 50% and 200% of the original soil depth, determined for the study in this thesis. However, no significant effect was observed. This is a result of the extremely dry conditions within the catchment, which resulted in water table depths below bedrock for all soil depth scenarios and consequently no baseflow production due to the model physics.

A further approach was pursued to adjust certain soil parameters, in particular for the calculation of the conductivity. However, the calculation of the conductivity is based on various parameter sets and internally calculated within CLSM (Ducharne et al., 2000). Consequently, the adjustment of only certain parameters may result in inconsistencies within the model parameters and eventually in the model states, with the possibility of undesired effects in the simulations. Therefore, it was decided to assume the calculation of these parameters provided by CLSM as correct.

7.4.5 Ponding

In a final adjustment to CLSM, it was assessed whether the inclusion of ponding of the precipitation water on the soil surface merited to be included into the model.

As described above and in section 4.2, any precipitation water in excess of the infiltration capacity within a modelling time step is instantaneously transferred into surface runoff. However, this does not allow for potential ponding of water on the soil surface and a later infiltration. Such modelled ponding was achieved in the proposed approach by redistributing the precipitation over several time steps. In the present study, the forcing data were provided in

20 minute time steps. In particular during intensive precipitation events, the infiltration capacity of the soil during these 20 minutes was regularly exceeded. In order to simulate ponding, the precipitation of each 20 minute time step was evenly distributed over three time steps (ie. one hour; the original time step and the subsequent two) following the event.

However, the introduced ponding scheme did not allow to relate the changes in the streamflow and soil moisture to the modification made to the precipitation. The modifications to the precipitation led to significant changes in the streamflow, with smaller precipitation events not producing any streamflow events and larger events reduced too significantly. However, ponding may play an important role, in particular in semi-arid or arid regions, in such regions of low topography, as excess water may settle on the soil surface. In such cases, the ponded water on the surface will then partially evaporate while the infiltration into the soil continues.

7.4.6 Spin-up of Final Model

Fig. 7.4 shows the observed and modelled streamflow for Sandy Hollow, and Fig. 7.5 the root zone soil moisture for Catchments 2 and 7 within the Goulburn River catchment, after the modifications to the model and precipitation forcing data as described above. The RMSE for all catchments are presented in Table 7.1.

The spin-up of the final modified version of CLSM still produced unexpected streamflow events, in particular in the first month of the simulation, but still led to a significant reduction of the RMSE of the streamflow at the three stream gauges (Table 7.1). The severe overestimation of the streamflow events at the beginning of the 12-month period were due to a) precipitation exceeding the infiltration capacity of the soil and b) the initialisation of the model with wetter initial states than the soil moisture observations would suggest. The

Table 7.1. Subcatchment specific RMSE of soil moisture and streamflow [m^3/s] for the generic and the modified model., as compared with the field observations. Streamflow was only observed at three locations, and four subcatchments (of the 16 subcatchments after delineation) did not contain a soil moisture monitoring site. The catchment number in brackets represents the numbering system before further delineation of the catchment.

	Generic Model		*Modified Model*	
	Soil Moisture [v/v]	*Streamflow [m^3/s]*	*Soil Moisture [v/v]*	*Streamflow [m^3/s]*
1 (1)	0.035	---	0.019	---
2	0.045	---	0.027	---
3	0.106	---	0.245	---
4	0.055	---	0.040	---
5	0.044	---	0.111	---
6	0.068	15.086	0.049	2.402
7	0.105	---	0.045	---
8 (1)	0.035	---	0.195	---
9 (1)	0.035	---	0.074	---
10 (1)	0.035	46.448	---	3.350
11 (1)	0.035	---	0.129	---
12 (8)	0.020	---	0.039	---
13 (8)	0.020	---	0.155	---
14 (8)	0.020	---	---	---
15 (1)	0.035	---	---	---
16 (8)	0.020	61.946	---	4.313

explanation for these wetter soil moisture states was that more precipitation fell during the last two months of the 12-month period of the simulation (February and March 2004) than the two months preceding the simulation (February and March 2003). As a consequence, the restart parameters of the simulation contained a wet bias.

This situation could not be avoided and is in the nature of spinning up models. In the present case, the reason for the distinctively different weather conditions in the months of February and March of the two years was the severe drought conditions in the region during the southern hemisphere summer of 2002/2003, which caused a dry-down of the area. While precipitation during the summer of 2003/2004 was below the long-term average of these months, as well, it was still wetter than during the previous summer and therefore did not lead to such an extreme dry-down of the soil.

The results on Fig. 7.5 showed that the model modifications now allowed the root zone predictions to undergo a greater variability over time than it was previously possible. Despite the changes to the model and the improved soil moisture dynamics in the root zone layer, the extreme values still show a difference of up to 0.07v/v. However, a more accurate model output was difficult to achieve, due to the dry conditions within the catchment during the period under investigation. Chiew and McMahon (1993) and Chiew et al. (2002) showed that it is difficult to model streamflow adequately under such climate conditions, because absolute errors in the observations become relatively large. The total observed runoff from the catchment at Sandy Hollow for the 12-month period was 4.1mm. This value is less than 1% of the observed annual precipitation. Consequently, small errors in the forcing data or model led to large relative errors in the modelled streamflow output.

The RMSE of the soil moisture showed that the new parameterisation led to a decrease of the soil moisture RMSE for the majority of the subcatchments, but also to an increase for some subcatchments (Table 7.1). These results are explained in two different ways. First, the Catchments 3 and 5 are subcatchments, which consist of two distinct soil types (derived from basalt and sandstone). The original model prediction was drier than the observations and the new parameterisation of the model physics led to a further dry-down. The observations were taken in a soil, that did not allow such a significant dry-down and consequently, the RMSE increased. Second, it was shown in Chapter 3, that the reduction of monitoring sites per catchment decreases the representativeness of the observation for the catchment. The original Catchment 1 contained five monitoring sites. Therefore, the averaged soil moisture observed at these sites included a smaller error for the large Catchment 1, than for the six subcatchments created after the further disaggregation, with a maximum of one monitoring site each.

7.5 Assimilation of Field Observations into the Generic and Modified Model

The “wrong” initial soil moisture states due to the spinning up of the model show the importance of finding the correct initial states of models in another way than a model spin up. In the following sections it is assessed whether the developed assimilation scheme is capable of retrieving better initial states and therefore, to improve the general model performance.

The observed streamflow data from the DIPNR stream gauges at Kerrabee and Sandy Hollow were assimilated into CLSM, leaving the stream gauge at Merriwa as a point of verification of the model. Furthermore, surface soil moisture observations were obtained from the AMSR-E soil moisture product for Catchments 6 and 7. These observations were assimilated into the model alone (section 7.5.3) and jointly (section 7.5.4) with the streamflow observations.

The assimilation of the available observations followed the conclusions of Chapters 5 and 6. Therefore, the assimilation of the assimilation window length was set to one month, surface soil moisture observations were assimilated before the streamflow observations, to reduce the level of freedom of the system and the remaining streamflow observations were assimilated in the top-to-bottom approach of Chapter 6.

7.5.1 Assimilation of Streamflow into the Generic Model

In a first step the streamflow observations at Kerrabee and Sandy Hollow were assimilated into the generic model for August 2003 with the same subcatchment set up of 8 subcatchments as for the synthetic studies in Chapters 5 and 6. Furthermore, all generic soil and vegetation specific parameters within CLSM were assumed to be correct, as it is generally not possible to verify these parameters in the field. August 2003 was chosen as a first test, as the most significant streamflow events of the 12-month period were observed during that month and to allow a comparison of the results from the assimilation of the field observations to those of the synthetic studies, which mainly focussed on this month. This experiment was undertaken to determine whether the assimilation of streamflow into an uncalibrated model leads to an improvement of the model performance.

The assimilation was undertaken as a top-to-bottom approach, as suggested in Chapter 6. First, the observations at Kerrabee were assimilated in order to retrieve the soil moisture values in Catchments 1-7 (the generic model has only 8 subcatchments; see section 7.4.2) and then the observations at Sandy Hollow were assimilated into CLSM to retrieve the soil moisture states in Catchment 8.

The results after the assimilation showed that the modelled streamflow, while improved, was still significantly overestimated and that the results were not better than the modified model itself (therefore, the results are not shown here). This situation was similar to the synthetic studies presented in sections 6.3 and 6.4, where the wet bias in the data caused the model to produce excessive streamflow. Such an overestimation in the streamflow led to a significant underestimation of the soil moisture values, as presented in sections 6.3 and 6.4, because the assimilation scheme reduced the soil moisture content to reduce the runoff-contributing areas and to the water stored in the soil. A further improvement of the streamflow was not possible as the initial soil moisture states were at a minimum.

While this result was similar to those presented in sections 6.3 and 6.4, the present overestimation in streamflow was not caused by a wet bias in the soil moisture data, as the modelled soil moisture did not show a divergence from the observations. Therefore, the overestimation was the result of a bias in the model itself, which made modifications to the model necessary (see section 7.4) and showed that the assimilation scheme is not an effective tool for the present situation.

7.5.2 Assimilation of Streamflow into the Modified Model

Streamflow observations were first assimilated into the modified model at Kerrabee (for catchments 1-11 and 15) and then at Sandy Hollow (for catchments 12-14 and 16), using one-month assimilation windows. The streamflow observations near Merriwa were used as a verification of how well soil moisture states, and consequently streamflow, may be retrieved in upstream catchments.

Table 7.2 shows the RMSE for the 6 months (April to September) of streamflow for the calibrated model and the model after the assimilation of the streamflow observations. For all three stream gauges, an improvement in the streamflow predictions was observed, compared to the simulated streamflow from the modified model. In particular the stream gauge near Merriwa (Catchment 6) showed a significant improvement for the 6 months under investigation, despite not having been part of the assimilation process. However, the RMSEs were high compared to the average streamflow at those stream gauges (Merriwa – 0.051m^3/s; Kerrabee – 0.593m^3/s; Sandy Hollow 1.202m^3/s; see Table 7.2).

To identify the months, which most contributed to the high RMSE, the RMSE for streamflow for each one-month assimilation window was calculated. The RMSE values in Table 7.3 show that two months had significant RMSE values (April and August). However, there were different causes for the high RMSE values during these two months. The high RMSE in April was caused by the misrepresented streamflow, even after the assimilation, when excessive precipitation caused surface runoff due to some remaining bias in the model (Fig. 7.7, see also section 7.4.5), where streamflow was produced in the model, while there was almost no observed streamflow in the rivers. This suggested, that the model modifications achieved by tuning the model to the second half of the 12-month period were not fully representative of the first 6 months, or that there was still a bias in the precipitation forcing data. The high RMSE in August was mainly caused by the shift of the flood peaks, due to the static routing model, which assigned the same unit hydrograph to all flow conditions. Therefore, larger streamflow events occurred earlier than

Table 7.2. Subcatchment specific RMSE [m^3/s] of streamflow for the modified model (April to September) without assimilation, after the assimilation of streamflow only (R) and after the joint assimilation of streamflow and remotely sensed surface soil moisture (RS). No streamflow observations were available for Catchments 1-5, 7-9 and 11-15, as no calibrated stream gauges were operational at the outlets of these subcatchments).

	Modified Model	*R*	*RS*
6 (Merriwa)	2.402	1.391	1.255
10 (Kerrabee)	3.350	3.248	3.035
16 (Sandy H.)	4.313	3.767	3.464

Table 7.3. Subcatchment specific RMSE [m^3/s] of streamflow for the modified model (April to September) without assimilation, after the assimilation of streamflow only (R) and after the joint assimilation of streamflow and remotely sensed surface soil moisture (RS). The values in brackets show the average observed streamflow in that month at the different stream gauges and values in bold highlight the best result for the individual month. No streamflow observations were available for Catchments 1-5, 7-9 and 11-15, as no calibrated stream gauges were operational at the outlets of these subcatchments).

		6 (Merriwa)	*10 (Kerrabee)*	*16 (Sandy H.)*
April	*Streamflow*	(0.001)	(0.429)	(0.952)
	Model	3.588	7.405	7.329
	R	3.323	7.373	7.296
	RS	**3.078**	**6.494**	**6.428**
May	*Streamflow*	(0.003)	(0.301)	(0.665)
	Model	0.033	0.283	0.642
	R	0.059	**0.260**	**0.566**
	RS	**0.004**	0.264	0.593
June	*Streamflow*	(0.016)	(0.191)	(0.514)
	Model	**0.021**	0.228	0.505
	R	0.299	**0.214**	**0.490**
	RS	0.081	0.222	0.608
July	*Streamflow*	(0.035)	(0.186)	(0.835)
	Model	0.040	0.368	0.861
	R	0.040	**0.178**	**0.781**
	RS	**0.036**	0.185	0.796
August	*Streamflow*	(0.188)	(1.950)	(3.361)
	Model	4.645	3.508	7.406
	R	0.798	**3.028**	5.479
	RS	**0.329**	3.621	**5.331**
September	*Streamflow*	(0.061)	(0.503)	(0.884)
	Model	0.186	0.789	1.277
	R	**0.084**	**0.561**	**1.046**
	RS	0.095	0.573	1.061

smaller events due to the different velocities in the stream at different stages. However, the magnitudes of modelled peaks were not influenced by the biases in the observations or the model and showed a good agreement with the field observations (Fig. 7.7a). Fig. 7.7b shows that the cumulative streamflow had been decreased below the observed streamflow. The reason is that the modified

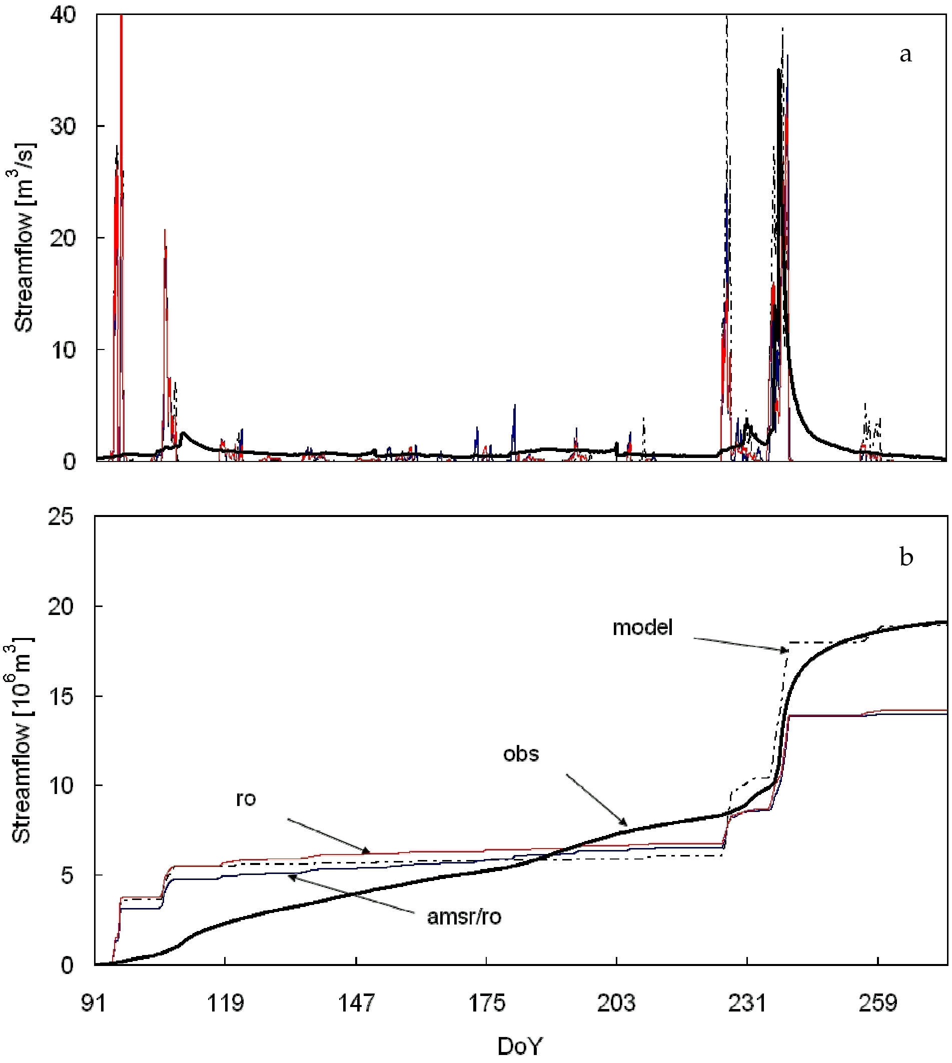

Figure 7.7. a) Instantaneous and b) cumulative streamflow for (i) the streamgauge at the outlet of the Goulburn River catchment at Sandy Hollow (obs, thick black), (ii) streamflow from the modified model (model, dash-dotted black), after streamflow assimilation (ro, red), (iv) joint assimilation of streamflow and remotely sensed surface soil moisture (blue).

model fitted well the cumulative observed streamflow, while still overestimating the peak events. The assimilation had caused a decrease of these peak events, as they were the major factor for the high RMSE values. As no additional streamflow was produced between the major streamflow events, this led to an improvement in the peak streamflow, but to an underestimation of the cumulative streamflow.

The cause of the larger error of streamflow for the streamgauge

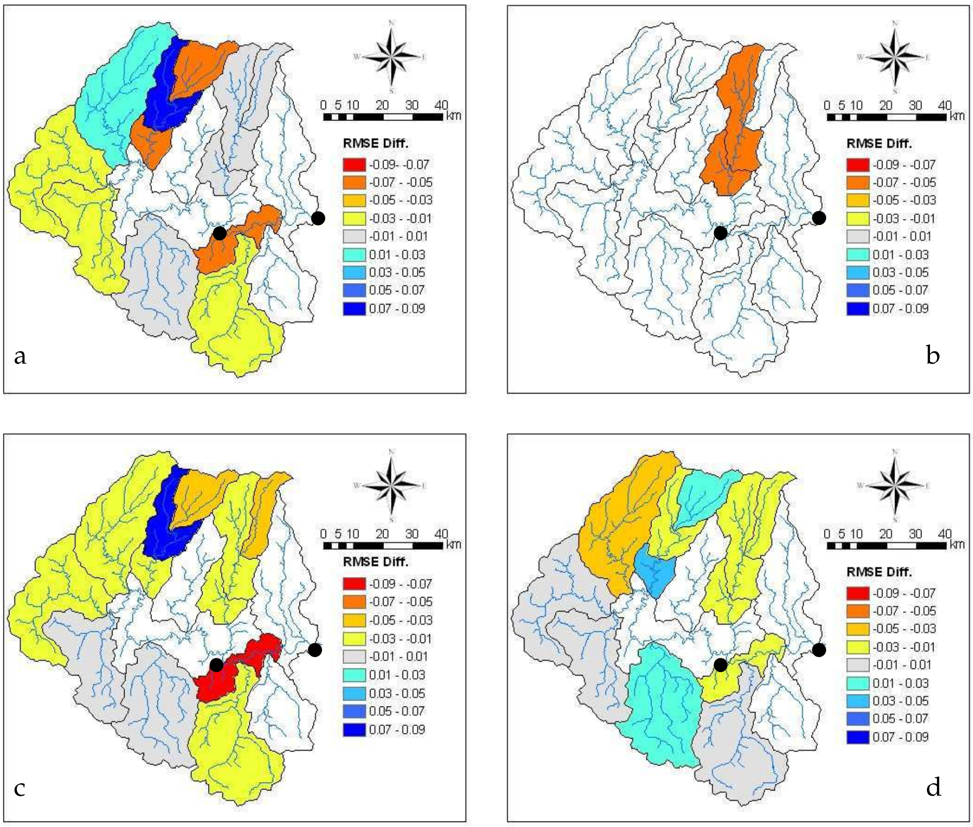

Figure 7.8. Differences in the RMSE of the modified model (with new delineation of the 16 subcatchments) to a) model after streamflow assimilation, b) surface soil moisture assimilation, c) after assimilation of streamflow and surface soil moisture, and d) difference in RMSE between (a) and (c). Negative values denote negative impact on the RMSE and positive values an improvement in the RMSE. The Black circles show the location of the streamgauges from which streamflow observations were assimilated.

near Merriwa in June after the assimilation is not clear. It is assumed that retrieving only one prognostic variable (catchment deficit) rather than all three (surface excess, root zone excess and catchment deficit) introduced some bias in the streamflow production of the model, as the initial values of the root zone and surface excesses were set to equilibrium conditions, while they may have not been in equilibrium, potentially causing a small wet or dry bias.

The RMSE for soil moisture in the subcatchments (Fig. 7.8, Table 7.4) did not provide a basis for conclusive results. An improvement of the soil moisture predictions was achieved for catchments, which

Table 7.4. Subcatchment specific RMSE [v/v] of soil moisture (surface and root zone) for the modified model (April to September) without assimilation, after the assimilation of streamflow only (R) and after the joint assimilation of streamflow and remotely sensed surface soil moisture (RS). No soil moisture observations were available for Catchments 10, 14, 15 and 16, as no monitoring sites are located in those catchments). The values in bold highlight the best results.

		Modified Model	*R*	*RS*
1	*Surface*	**0.044**	0.053	0.062
	RZ	**0.019**	0.036	0.039
2	*Surface*	**0.046**	0.094	0.079
	RZ	**0.027**	0.136	0.108
3	*Surface*	0.203	**0.122**	0.130
	RZ	0.245	**0.149**	0.160
4	*Surface*	**0.030**	0.111	0.085
	RZ	**0.040**	0.092	0.060
5	*Surface*	**0.114**	0.123	0.138
	RZ	**0.111**	0.133	0.162
6	*Surface*	**0.036**	0.045	0.045
	RZ	**0.049**	0.049	0.068
7	*Surface*	**0.038**	0.058	0.046
	RZ	0.045	**0.039**	0.056
8	*Surface*	0.191	**0.170**	0.200
	RZ	0.195	**0.171**	0.207
9	*Surface*	**0.072**	0.083	0.080
	RZ	**0.074**	0.086	0.078
11	*Surface*	0.163	0.157	**0.148**
	RZ	0.129	0.130	**0.119**
12	*Surface*	**0.042**	0.099	0.113
	RZ	**0.039**	0.108	0.125
13	*Surface*	**0.039**	0.056	0.055
	RZ	**0.155**	0.171	0.170

had wetter soil moisture observations (Catchment 3 and 8). However, catchments, in which soil moisture was adequately predicted did not show an improvement in soil moisture, and in some cases showed degraded soil moisture conditions (Catchments 2, 4 and 12).

Interestingly, the average soil moisture for the whole Goulburn River catchment was improved (Fig. 7.9). The situation of better

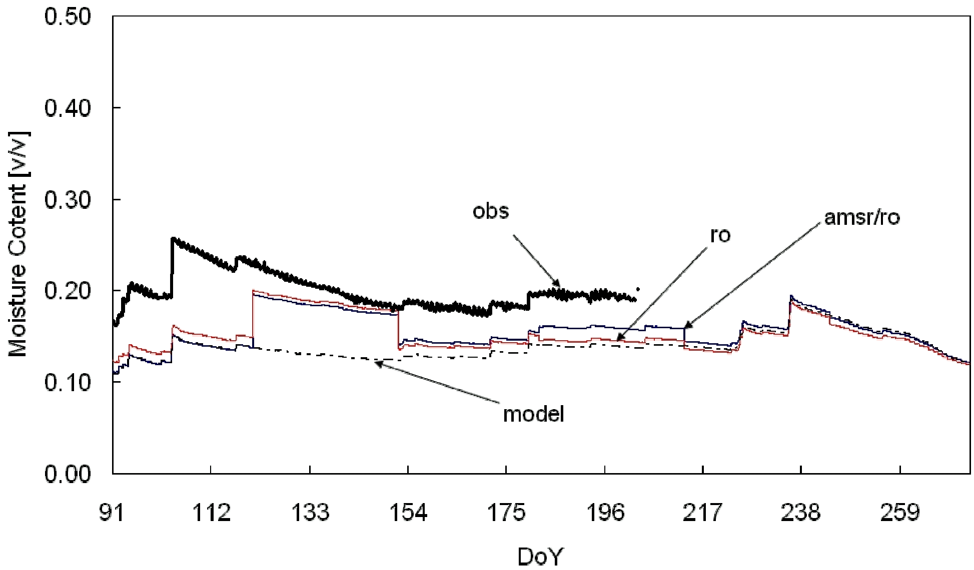

Figure 7.9. Average root zone soil moisture for the Goulburn River catchment, calculated with weighted averages from the 16 subcatchments using (i) all available soil moisture observations (obs, thick black), (ii) the modified model output (model, dash-dotted black), iii) after streamflow assimilation (ro, red), and (iv) joint assimilation of streamflow and remotely sensed surface soil moisture (blue).

results for the whole catchment, while having results with larger errors in the individual subcatchments, was already discussed for the differences between the generic and the modified model, where some subcatchments showed an increase in RMSE after the modifications. Similarly, a single observation in a subcatchment does not provide a representative soil moisture observation for the subcatchment in which it is located.

The results of the soil moisture predictions after the assimilation may be explained in several ways. First, the use of streamflow observations may not be adequate to retrieve soil moisture in catchments under real conditions, even though the synthetic studies in Chapter 5 and 6 have shown that it can indeed be a useful tool. Second, in section 6.4.1 it was shown that a single observation was not sufficient in a synthetic study to adequately retrieve all eight upstream soil moisture states. In the present field study there are 12 subcatchments located upstream from the stream gauge at Kerrabee

(Fig. 7.8), which may limit the retrieval abilities of the assimilation scheme. Furthermore, the retrieved initial soil moisture states, and the soil moisture predictions following from these initial states, were counterbalanced by the temporal drift in the streamflow peaks and therefore improved the RMSE of the streamflow and were thus found to produce the best fit to the observations. Most importantly, however, is that the assimilation scheme in its current configuration did not allow observational and model errors to be included in the assimilation process. The quantification of errors should allow a better retrieval of the soil moisture states.

7.5.3 Assimilation of Surface Soil Moisture

The soil moisture product from AMSR-E shows a significantly dry bias (even for a catchment under drought conditions) with only a little response to precipitation events. This is due to the algorithm used for obtaining soil moisture information from the observed brightness temperatures, which essentially optimises the parameters of the radiative transfer model to best fit model and satellite observations. Because of this indirect approach and its problematic results, the focus of current research is on the assimilation of the brightness temperatures into LSMs (Balsamo et al., 2006; J.-C. Calvet and J.-F. Mahfouf, M. Drusch and E. Anderson, personal communication). However, this approach requires a radiative transfer model between the LSM and the assimilation scheme, which could not be undertaken within the scope of this thesis. Alternatively, the soil moisture observations (from model and satellite) may be normalised in order to enable the assimilation scheme to at least assimilate the seasonal dynamics of the soil moisture (R. de Jeu, personal communication). However, this resulted in an exaggeration of the soil moisture observed by the satellites around days 145 and 175. It was therefore decided to only use the available soil moisture product.

The assimilation of remotely sensed surface soil moisture observations into the model was undertaken for Catchments 6 and 7, only. No data from the southern subcatchments were included as the dense vegetation cover made the satellite observations unreliable due to the signal attenuation of the microwave signal (see Chapter 2). Furthermore, some of the northern subcatchments showed significantly different soil moisture observations at the soil moisture monitoring sites than the satellite observations, and more confidence was given to the soil moisture observations on the ground, than the satellite based measurements. This decision was made, in particular because the soil moisture retrieval algorithm of AMSR-E uses the 10.7GHz band and its observations therefore relate only to the top few millimetres of the soil.

The model was already showing a dry bias in the soil moisture data during wet events (Fig. 7.10), compared to the soil moisture field observations. This bias was increased as the assimilation scheme further reduced the initial soil moisture states of Catchment 6 and 7, due to even drier AMSR-E surface soil moisture observations. This led to an increase in the RMSE of soil moisture in those subcatchments (Table 7.5a). However, the RMSE between remotely sensed surface soil moisture and modelled surface soil moisture was improved following the assimilation process, as the differences between model and observations decreased (Table 7.5b).

The assimilation of the AMSR-E surface soil moisture observations into CLSM resulted in a significant improvement of the streamflow (Table 7.5a). This was caused by the reduced soil moisture throughout the months and the subsequent reduction in streamflow production.

As in section 6.3.2 the assimilation of surface soil moisture alone did not have any impact on the soil moisture conditions in the

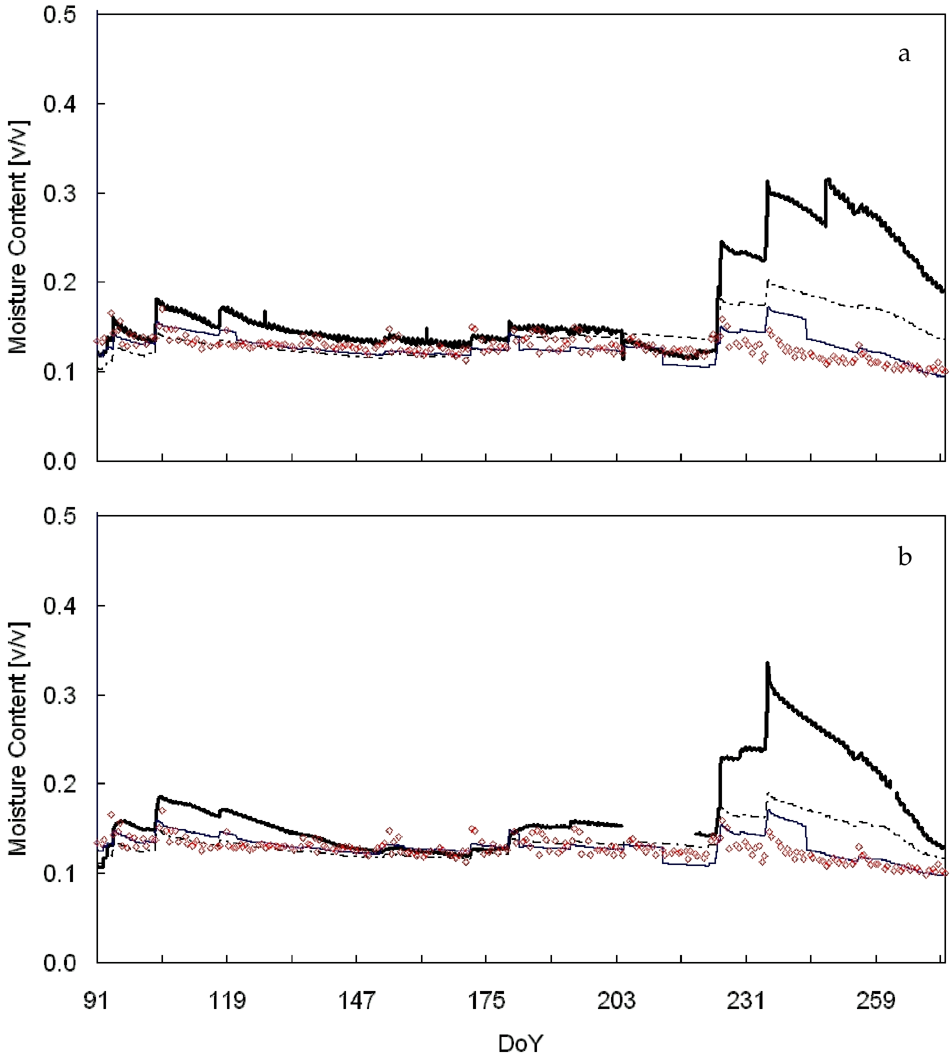

Figure 7.10. Root zone soil moisture for Catchments a) 6 and b) 7, showing the (i) average observed root zone soil moisture (thick black), (ii) modelled root zone soil moisture (dash-dotted), (iii) AMSR-E observations, (iv) modelled soil moisture after surface soil moisture assimilation (blue).

catchments for which no observations were assimilated. This was due to the assumption that no correlation between the soil moisture in neighbouring catchments existed, by not allowing the assimilation scheme to determine a correlation between the model predictions.

7.5.4 Joint Assimilation of Streamflow and Soil Moisture

The joint assimilation of the previously described streamflow and remotely sensed surface soil moisture observations showed an improvement to some soil moisture states and a further

Table 7.5a. Subcatchment specific RMSE for the period of April to September for in-situ and modelled surface and root zone soil moisture [v/v] and streamflow [m^3/s] observations.

		Modified Model	*SM*
6	*Surface*	**0.036**	0.046
	RZ	**0.049**	0.068
	Streamflow	2.402	**0.177**
7	*Surface*	**0.038**	0.041
	RZ	**0.045**	0.058

Table 7.5b. Subcatchment specific RMSE for the period of April to September for remotely sensed and modelled surface soil moisture [v/v] observations.

		Modified Model	*SM*
6	*Surface*	0.065	**0.022**
7	*Surface*	0.053	**0.015**

improvement to the modelled streamflow (Tables 7.2 and 7.3). While the RMSE for soil moisture for Catchment 6 was degraded (due to the drier observations of ASMR-E), the streamflow prediction was significantly improved, in consequence of the drier soil moisture conditions in the subcatchment and the resulting reduced streamflow production. However, as in section 7.5, there was no conclusive evidence that the joint assimilation of streamflow and surface soil moisture observations was capable of improving the model states in all subcatchments. The decrease and increase in the RMSE for the individual catchments did not show any preferential patterns (Fig. 7.8c). The difference in RMSE between the streamflow and the joint assimilation shows, that the soil moisture in six subcatchments was degraded, and improved only in three (a further three remained almost unchanged).

These results are far from encouraging. However, it is assumed that the semi-arid conditions of the catchment were the cause for problems in the accurate representation of the streamflow and soil moisture, as the observed and modelled streamflow are both less than 1% of the total precipitation within the Goulburn River catchment and small errors in the forcing data have relatively large effects on the streamflow. Furthermore, the limited number of observations (two streamflow and two remotely sensed soil moisture observations) may not have been sufficient for a catchment with a large number of subcatchments, however it was shown in sections 6.3 and 6.4, that it is possible to retrieve the soil moisture states with a number of observations which is smaller than the total of the subcatchments (admittedly under more favourable conditions). Therefore, an increase in the number of sites from which observations are obtained may increase the accuracy of the assimilation approach.

Finally, the comparison of the observations at one soil moisture monitoring site with the lumped soil moisture of the LSM is not adequate. As it was shown in Chapter 3 and discussed previously, the average error of using just one monitoring site to represent a full subcatchment is in the order of 0.08v/v for the stations in the Goulburn River experimental catchment. Therefore, the results of this field data study have to be considered against this background.

7.6 Evapotranspiration

Neither the assimilation of streamflow alone nor the joint assimilation of streamflow and surface soil moisture into the model showed a satisfactory improvement for the majority of the subcatchments, when compared to the soil moisture conditions before the assimilation process. Similarly, modelled evapotranspiration was not expected to have improved.

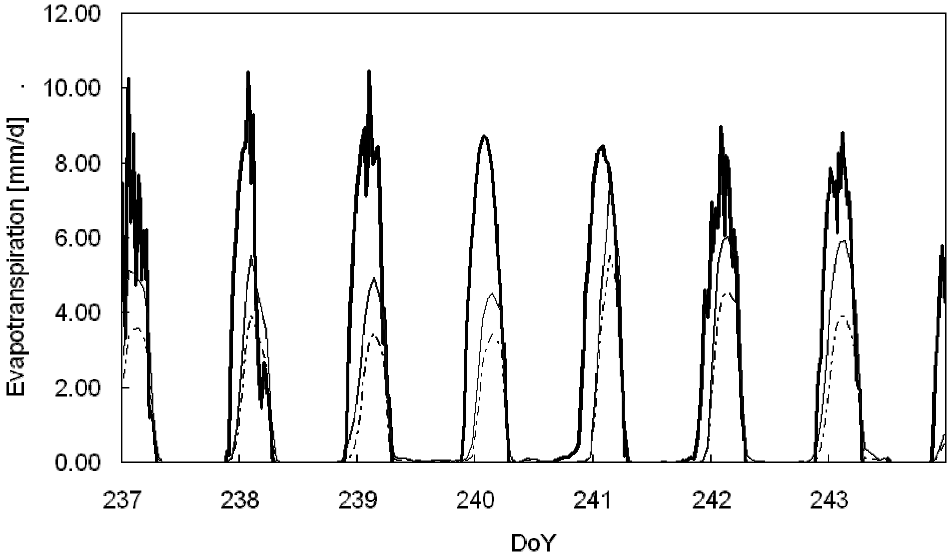

Figure 7.11. Comparison of the evapotranspiration rate for Catchment 4 from (i) field observations (solid thick line), (ii) modified model prediction (dashed line), and (iii) modified model prediction after joint assimilation of streamflow and surface soil moisture (solid thin line).

Evapotranspiration was calculated using the Penman-Monteith equation (Smith, 1991) and the stress index (Kalma et al, 1995), as described in section 7.3.3. The only observation of net radiation required for the calculation of evapotranspiration was available for S2, which is located in Catchment 4, the predicted and calculated evapotranspiration in Fig. 7.11 are shown for eight days from this subcatchment. Fig. 7.11 shows that the prediction of the evapotranspiration was improved in the case of an improvement of the modelled soil moisture states through the assimilation of observations (thin solid line), because the soil moisture of Catchment 4 was one of the few which were improved. The RMSE of the model predicted evapotranspiration was 2.674mm/d and after the joint assimilation 2.481mm/d.

An analysis of the change in the evapotranspiration of other subcatchments was not undertaken, as the only net-radiometer was located at site S2, which in turn was located in Catchment 4. Nevertheless, the degradation of the soil moisture prediction after the assimilation as shown in the previous sections was likely to have led to a degradation of the evapotranspiration as these are directly linked.

As for the comparison of soil moisture point observations with the lumped model results, the evapotranspiration calculated from the observations at S2 was only representative for this particular site and did not represent the whole subcatchment.

7.7 Chapter Summary

In this chapter, real streamflow and remotely sensed surface soil moisture observations were assimilated into a model forced with distributed forcing data. Several shortfalls of CLSM were discovered in this study, which made some changes necessary. The catchment was further disaggregated into smaller modelling units, and wilting point and porosity were adjusted. Moreover, the model itself had to be modified. A simple threshold separating the model processes under dry and wet conditions was defined (75% of the maximum catchment deficit). These changes resulted in improved streamflow and soil moisture prediction within the model.

The joint assimilation of streamflow and remotely sensed surface soil moisture into the modified model did not show any conclusive results to allow for a statement about the viability of the approach under real conditions. While the soil moisture conditions in 2 of the 12 monitored subcatchments were improved, 10 subcatchments showed degraded soil moisture conditions. Because of the high uncertainty in the representativeness of one point of observation in one catchment, the degradation of the model predictions has to be considered against this background, without invalidating the improvements made to the model through the modifications in sections 7.3 and 7.4.

Chapter Eight

8 Conclusions and Future Directions

8.1 Thesis Conclusions

This thesis has developed and tested an assimilation scheme for soil moisture retrieval using streamflow (and remotely sensed surface soil moisture) observations. The approach taken was a brute-force variational-type assimilation scheme, so that the time delay between runoff generation at the hillslope and its subsequent observation impact on downstream streamflow and the time of concentration of the runoff water within the catchment could be accounted for. Moreover, the brute-force approach allowed to retrieve the initial states without the need for deriving an adjoint. It was necessary to apply a variational-type assimilation scheme, as the retrieval of soil moisture states in complex stream networks is not feasible using sequential assimilation schemes. This new streamflow assimilation approach for soil moisture retrieval was developed through a series of synthetic experiments and then tested using field data from the Goulburn River Experimental Catchment.

In the first experiment, it was determined that the length of the assimilation window plays a significant role in this variational-type assimilation scheme. In particular, when biases and errors were present in the forcing data, longer assimilation windows led to a larger error in the initial soil moisture states and the model predictions. The reason for this is that the assimilation scheme corrected the model and observational inadequacies by changing the initial conditions so that the following simulation had a best fit with the observations. When the forcing data was biased this was counter-balanced with an increase or decrease in the initial soil moisture states to either reduce or increase streamflow. Therefore, the longer the assimilation window were, the larger were the discrepancies between the initial model states and the observations. In general, this limitation may be solved by decreasing the length of the assimilation window. However, in the present case, care had to be taken not to reduce the length of the assimilation window to less than the time of concentration in the catchments. The reason for this limitation is that the lumped soil moisture state is the governing factor of the quantity of streamflow within the model and streamflow is the integrated result from the runoff production during the time of concentration. Were the assimilation window shorter than the response time or time of concentration, the cause of the event (precipitation) would be separated from its response (streamflow), and the assimilation scheme would not be able to assign a soil moisture state to some of the runoff events. It has also to be observed that the length of the assimilation window is not shortened to such an extent as to exclude any streamflow events (in particular in dry regions). Though it may be argued that no-flow conditions are still streamflow observation, these conditions do not allow an adequate definition of the upstream soil moisture states. During no-flow conditions, the only constraint to the soil moisture states is that they are below the threshold which is needed to allow the production of surface runoff to take place. However, this definition is not a satisfactory constraint, as the soil may be drier than the threshold value.

In the experiments of the different studies, the soil moisture predictions reached either their upper (saturation) or lower (wilting point) boundaries, which led to a loss of any knowledge of the changes in the initial soil moisture states. This effect was apparent in the one-year assimilation window, where the assimilated model output and the degraded control run show the same performance after the model runs have reached the wilting point. Similarly, surface soil moisture conditions appeared unaffected by the initial soil moisture states after the time, when saturation due to strong rain events took place. This loss of prior knowledge of the initial state in the event of extreme events is a further support for choosing shorter assimilation windows, as it is more likely to have an extreme event, the longer the assimilation window is.

The use of shorter assimilation windows led to an improvement in the retrieval of root zone and profile soil moisture. However, the accuracy of the retrieval of the surface soil moisture states was not affected by the assimilation window length. It was found that streamflow assimilation alone was unable to retrieve well the surface soil moisture, especially when strong errors in the forcing data were present, even though a significant improvement of the streamflow prediction was still achieved. In order to improve the retrieval of surface soil moisture, it was tested whether the assimilation of observed surface soil moisture introduces a sufficient constraint on the retrieval of the surface soil moisture states. The assimilation of remotely sensed surface soil moisture observations alone led to an improved retrieval of all initial soil moisture states, however, streamflow generation was not improved. This was a consequence of the fact that streamflow was not considered in the determination of the objective function, when surface soil moisture only was assimilated. Therefore, it was concluded that streamflow and surface soil moisture should be jointly assimilated, when both are available.

The joint assimilation of streamflow and remotely sensed surface soil moisture observations resulted in an improvement of the retrieval of the soil moisture states. However, first results showed that streamflow observations had precedence over surface soil moisture observation in the assimilation. This was due to differences of scale in the soil moisture (fractions) and streamflow (m^3/s) on the objective function, requiring both streamflow and surface soil moisture observations to be normalised. Normalisation was achieved by scaling the observations with their respective residual variances. This resulted in normalised values, which facilitated the joint assimilation of these different quantities. However, while the normalisation resulted in improved results, the streamflow observations continued to dominate the retrieval process, particularly during the extreme streamflow events, because the more significant dynamics of the streamflow observations could not be fully removed by the normalisation.

The results to this point, were found for a single catchment, with one or two types of observations. In order to assess the required number of points of observations (be it streamflow or soil moisture) for an accurate retrieval of the initial soil moisture states, two experiments were undertaken with increasingly complex nested subcatchment networks. The first experiment included three nested catchments of the Krui River, while the second experiment consisted of eight catchments of the Goulburn River and its tributaries. For both multi-catchment studies, it was shown that the retrieval of soil moisture states within a catchment is possible, even with a limited number of available observations, and therefore ungauged (no stream gauges) or unobservable (vegetation masking the soil moisture signal) subcatchments within the main catchment. This may have important implications for prediction in ungauged basins (PUB), as it is now possible to obtain soil moisture information from catchments, from which this information was not previously available. While, one observation location was sufficient in the three-catchment study, the assimilation of streamflow observations from one point into the larger and more complex catchment network did not prove to be sufficient. More points of observation were required to achieve the same level of accuracy in the larger and more complex catchment structure. The availability of eight streamflow observations for all eight catchments did not result in a direct retrieval of the initial soil moisture states in all catchments. The process of retrieval process was found to occur in a top-to-bottom approach, in which the initial soil moisture states of the most upstream catchments were found first and the states of the catchment at the outlet were found last.

The additional observations required to constrain the retrieval process could be obtained from either more streamflow observation locations, or the inclusion of near-surface soil moisture observations. However, the assimilation of surface soil moisture alone into one of the catchments only improved the soil moisture retrieval in the catchment for which these observations were available. The remaining catchments were not affected by the assimilation. This shows that, in order to be effective in large catchments, soil moisture needs to be jointly assimilated with streamflow observations. It was found that the joint assimilation of streamflow and surface soil moisture for the multi-catchment studies had to be undertaken in two steps. First, the initial soil moisture states of the catchments with surface soil moisture observations were retrieved and fixed, which would then be followed by the assimilation of the streamflow observations with the top-to-bottom approach described above.

Throughout the different experiments it was found that profile and root zone soil moisture were almost identical. Furthermore, errors in the surface soil moisture were generally corrected for within several days. These findings were used in order to reduce the number of retrieved initial states, which significantly reduce the computational costs and more importantly, led to a better retrieval of the soil moisture, as the state space was reduced, which simplified the optimisation procedure. Moreover, the optimisation procedure was further improved with informed decisions on the initial guess and a limitation of the range of possible values of the model states. These decisions were based on the knowledge of the maximum catchment deficit, to estimate the initial guess, and the preceding forcing data, to preset a certain range of the possible initial states.

In a final synthetic study, the impact of wrong parameters was assessed, by changing the soil type in the model. An inaccurate parameterisation of the model was found to lead to problems within the assimilation scheme, as absolute soil moisture values could not be compared anymore. It was shown that the calculation of a soil wetness index, which normalises the soil moisture values is a good tool to overcome the differences in the absolute values. However, this was only shown for the synthetic studies and could not be applied to the field study, as insufficient information on the real soil moisture at saturation and wilting were available.

For all synthetic studies of the development phase, it was shown that evapotranspiration and sensible heat fluxes were particularly well improved, when the model was water-stressed. This was the case for all different forcing scenarios. The overestimation of evapotranspiration and the sensible heat flux due to the biases was corrected for, as the soil moisture predictions in the catchments were improved.

The above conclusions were all obtained through several single- and multi-catchment synthetic studies, for which model parameters and more importantly forcing data were degraded, in order to simulate uncertainties in the these data. While the results of these studies showed good results after the assimilation of the streamflow observations, it has to be acknowledged at this point, that the model conditions in these studies were either assumed perfect or their level of uncertainty was known, which is not the case in a real environment. Perfect or well known model conditions facilitate the interpretation of the results. However, it is important to understand the impact of uncertainties in the model or its forcing data for the assimilation scheme, as this newly gained knowledge can then be applied to a field study.

8.2 Field Study

The methodology developed in the synthetic studies, was finally tested and evaluated in a field study. It was found that streamflow assimilation alone could not correct for the extreme overestimation of the predicted streamflow using the default model and globally derived parameters. Consequently, the model and its input parameters were modified based on an understanding of the variability of the forcing data throughout the catchment and changes in the physical conditions of the soil. The introduced modifications included i) precipitation corrections for orography, ii) cracking soils impact on infiltration capacity and iii) soil porosity and wilting point, and iv) disaggregation of the Goulburn River catchment into 16 rather than 8 subcatchments to better represent the soil variability. However, the inclusion of more catchments resulted in four subcatchments that had no soil moisture or streamflow observations for verification purposes. These results show, that an assimilation scheme requires a well calibrated model and that the assimilation of even high quality observations does not overcome shortcomings in the LSM.

The assimilation of the streamflow observations led to some improvement of all streamflow prediction, due to changed soil moisture states. However, the resultant soil moisture states did not agree well with the soil moisture observations, showing RMSE values of 0.039 to 0.171v/v. The streamflow assimilation led to the improvement of soil moisture predictions in only two subcatchments (out of 12 subcatchments with in-situ observations), when compared to the control, while the remaining ten subcatchments showed degraded soil moisture conditions. While the assimilation methodolgy developed in this thesis did not lead to good results in the field study, it has shown some promising results in the synthetic studies. In order to achieve similarly good results in field applications as in the synthetic studies, some problems have to be solved. In particular, the model has to be a reasonable approximation of the system to be modelled, forcing data must be unbiased and observations reliable (ie. bias free), or fully known. Furthermore, most catchments contained only one soil moisture observations site. It was shown in Chapter 3 that the representativeness of one site for a catchment sizes as those of the field study is not guaranteed and that the sites may include large errors (up to 0.20v/v) as compared to the catchment average soil moisture. The RMSEs found for the different catchments after the assimilation have to be interpreted with this knowledge in mind.

The explanation for the lower level of performance of the assimilation in the field study as compared to the synthetic studies lies in the high uncertainty in the model parameters, the streamflow observations, and the representativeness of the in-situ soil moisture observations. While the synthetic studies showed that the assimilation scheme is indeed capable of retrieving the initial soil moisture states to within a good accuracy, those studies were conducted under well controlled model conditions, which was not the case in the field study. This leads to the conclusion, that a well calibrated model, or at least a model with well known parameter uncertainties, is required to obtain good results with this streamflow assimilation scheme.

The field study highlighted the requirement of well parameterised models for the streamflow assimilation scheme to work correctly. A first attempt was made to adapt the LSM used in this thesis to the particular environmental conditions in south-eastern Australia during the study period. It was shown that the introduction of a variable infiltration rate and surface runoff production significantly improved the model performance in both streamflow and soil moisture prediction. However, most operational LSMs apply the same physics amd/or soil type to the entire world. It is therefore essential, that these models be improved so that streamflow observations can be assimilated.

As a final comment it must to be acknowledged that all the presented results and conclusions are drawn from studies using a particular (brute force) assimilation scheme and a lumped land surface model. It is likely, that the use of a different model or assimilation scheme would lead to different conclusions.

8.3 Recommendations for Future Work

8.3.1 Application to Humid Catchments

In this thesis, only streamflow from a catchment under severe drought conditions during the study period was considered for assimilation. The intermittent streamflow events have as a consequence that only soil moisture information from a short time window preceding the streamflow event can be adequately obtained. This leaves certain periods for which soil moisture predictions are less certain, as it was shown in the synthetic studies, when no streamflow observations were available and the initial soil moisture states were incorrectly estimated. However, the streamflow from a humid catchment should provide continuous observations and therefore continuous information on the soil moisture states.

8.3.2 Model Modifications

As shown in the field study, an improvement to LSMs is necessary for a good performance of the streamflow assimilation scheme. As a first step, CLSM was adapted to better suit the dominant environmental conditions in south-eastern Australia, introducing a new infiltration and surface runoff scheme. These modification showed a significant improvement in the prediction of streamflow, but also soil moisture. However, these modifications with their associated set of parameters may only be valid for this particular region in the world and may have to be redefined for other regions. Moreover, other regions of the world are likely to require different changes to the physical behaviour of the model, to suit their particular environmental conditions.

It is suggested to develop models (or model extensions) that allow for these different model requirements. Nevertheless, these modifications should not lead to a further increase in the complexity of the LSMs. The introduction of the variable infiltration capacity and surface runoff production uses information already available within the original model, which did not result in an increase in computational cost. Any new "regionalisation" of LSMs should endeavour to use a similar approach.

8.3.3 Routing Model

Only a simple linear routing model based on a combination of the unit hydrograph and source-to-sink methods was applied to the runoff generation of the LSM used in the research of this thesis. However, real streamflow hardly displays a linear behaviour. The linear model was chosen to simplify the assimilation scheme, by eliminating a further nonlinearity. This decision resulted in some error in the assimilation of streamflow, in particular for the regional scale model set up.

The unit hydrograph method assumes that the timing of the flood wave within a river system is a constant and that only the magnitude changes. However, in real river systems, an increase in the magnitude of the streamflow causes an increase in the flow velocity and consequently a shift in the timing of the streamflow peak. Therefore, due to the changing time-lags in the real streamflow, the least square error may be significantly different, as the observed streamflow peak may be earlier or later than the predicted peak. An assimilation scheme linked to a linear model can only change the least square error by increasing or decreasing the magnitude of the streamflow and does not lead to a temporal shift in the streamflow peak, which may lead to erroneous initial soil moisture states. However, changes to the magnitude of the streamflow event would lead to shift in the timing of the peak of a non-linear routing model and therefore affect the cost function. This would result in a more realistic retrieval of the initial soil moisture states.

8.3.4 Parameter Analysis

It was shown that the assimilation scheme has difficulties to retrieve the initial soil moisture states correctly (in particular the surface soil moisture states), when errors and biases in the model or the forcing data are present. However, the assimilation scheme may be used to detect and correct these errors and biases. In particular the parameters used to correct for the effects described in Chapter 7 (orographic effects on precipitation and cracking of soils) may be retrieved simultaneously with the soil moisture states. Moreover, it may be studied whether the assimilation scheme can be used to retrieve catchment specific rainfall parameters (such as the *RRF*), which would lead the study towards retrieval of the patchiness of the precipitation throughout the full catchment. Additionally, this approach may also be extended to allow the optimisation of the model parameters in each of the subcatchments, themselves.

Alternatively, the variational data assimilation scheme may be augmented to explicitly include model and observational errors. While the current assimilation scheme implicitly calculates the error covariances and cross-correlations, these may be predefined through sensitivity studies and analyses of the observations, which should essentially improve the quality of the streamflow data assimilation.

8.3.5 Sliding or Event-based Assimilation Windows

Possible solutions to further improve the performance of the streamflow assimilation at this point are event-based or sliding assimilation windows. Event-based assimilation windows are of variable length, with a minimum length of the catchment response, in order to contain all catchment information. The assimilation process is started when a new event is available, rather than having a fixed window with no events (see the period of day of year 152-181 in section 5.3.3), as such a period does not transfer any knowledge to the assimilation scheme. Nevertheless, event-based assimilation windows would become large in areas with extended dry conditions.

Sliding windows are overlapping, fixed-length assimilation windows, unlike the sequential technique presented in this thesis. The advantage of this approach is that the assimilation process is not paused for a fixed period (like the one month in this thesis), as this is counterproductive to operational weather forecasting, which requires updated information at a significantly higher frequency. However, sliding assimilation windows are limited to brute force approaches, such as the assimilation scheme presented here. Sliding assimilation windows would cause a sub-optimality with assimilation schemes utilising explicit background and observation errors. In such assimilation schemes, the model output would be forced to increasingly tend towards the observations, despite observational errors, because too much weight would be given to the observations.

8.3.6 Use of Cross-Correlations

In the presented studies, the assimilation of surface soil moisture observations was undertaken only for the catchment for which observations were available, without affecting the soil moisture state retrieval in adjacent catchments. However, assuming that soil moisture in adjacent catchments are correlated, the updating of the soil moisture in one catchment may be used to extrapolate changes in its adjacent catchments. For example, precipitation indeces may be used to derive correlations between the dynamics of the soil moisture conditions in the respective catchments. Nevertheless, it has to be considered that such indeces are only crude approximations of the spatial patterns and could only be used to derive tendencies in the soil moisture behaviour in the catchments.

The retrieval of the initial soil moisture states in the three-catchment study showed that only one streamflow observation was needed to retrieve the initial root zone soil moisture in all upstream catchments. However, this would not be the case for two parallel catchments. In two parallel catchments, the moisture would be interchangeable, as an infinite number of moisture combinations may produce the same streamflow. This problem may be solved by applying the potential correlation of the soil moisture states, as described above.

8.3.7 Catchment (Dis-)Aggregation

It was shown that the soil moisture initial states from catchments that are in sequence to each other may be retrieved relatively well, when only one streamflow observation is available (section 6.3.1). While it is important to disaggregate the catchments in terms of their land cover and soil conditions, in order to retrieve the accurate soil moisture states, this increases the number of states to be retrieved from a limited number of observations, which was shown to be problematic. To avoid this problem, subcatchments may be grouped into clusters, for which first the lumped soil moisture content is predicted to allow for the predictions of the streamflow from each cluster. This streamflow can then be used to retrieve the individual soil moisture in each subcatchment of the cluster. In the Goulburn River catchment assimilation such clusters are the Krui River catchment (Catchments 2, 3 and 4) and the Merriwa River (Catchments 5, 6 and 7).

"If we shadows have offended,
Think but this, and all is mended,
That you have but slumber'd here
While these visions did appear.
And this weak and idle theme,
No more yielding but a dream,
Gentles, do not reprehend:
If you pardon, we will mend:
And, as I am an honest Puck,
If we have unearned luck
Now to 'scape the serpent's tongue,
We will make amends ere long;
Else the Puck a liar call;
So, good night unto you all.
Give me your hands, if we be friends,
And Robin shall restore amends."

William Shakespeare
A Midsummer Night's Dream
Act 5, Scene I

The End

References

A

Ács, F. (2003). A comparative analysis of transpiration and bare soil evaporation. *Bound.-Layer Meteorol.*, **109 (2)**, 139-162.

Ajami, N.K., Gupta, H., Wagener, T., and S. Sorooshian (2004). Calibration of a semi-distributed hydrologic model for streamflow estimation along a river system. *J. Hydrol.*, **298**, 112-135.

Arnell, N.W. (1999). A simple water balance model for the simulation of streamflow over a large geographic domain. *J. Hydrol.*, **217**, 314-335.

Arrigo, J.A.S and G.D. Salvucci (2005). Investigation hydrologic scaling: Observed effects of heterogeneity and nonlocal processes across hillslope, watershed, and regional scales. *Water Resour. Res.*, **41 (11)**, 11417.

Askne, J., Santoro, M., Smith, G., and J.E.S. Fransson (2003). Multitemporal repeat-pass SAR interferometry of boreal forests. *Geosci. Remote Sens.*, **41 (7)**, doi: 10.1109/TGRS.2003.813397

Atkinson, S.E., Sivapalan, M., Viney, N. R., and R. A. Woods (2003). Predicting space–time variability of hourly streamflow and the role of climate seasonality: Mahurangi Catchment, New Zealand. *Hydrol. Proc.*, **17**, 2171-2193.

Atkinson, W. (1966). *A Review of the Land Systems of the Hunter Valley, N.S.W*, The Hunter Valley Research Foundation, Newcastle, Australia.

Aubert, D., Loumagne, C., and L. Oudin (2003). Sequential assimilation of soil moisture and streamflow data in a conceptual rainfall–runoff model. *J. Hydrol.*, **280**, 145-161.

Australian Bureau of Meteorology (1988). *Climatic Atlas of Australia*. Australian Government Printing Service, Canberra, Australia, 67pp.

Australian Surveying and Land Information Group (2001). *GEODATA 9 second DEM Version 2*, Belconnen, ACT, Australia.

Awwad, H.M., Valdes, J.B., and P.J. Restrepo (1994). Streamflow forecasting for Han River basin, Korea. *J. Water Resour. Plan. & Management*, **120 (5)**, 651-673.

B

Baker, J.M. and R.J. Lascano (1989). The spatial sensitivity of time-domain reflectometry. *Soil Sci.*, **147 (5)**, 378–384.

Balsamo, G., Bouyssel, F., and J. Noilhan (2004). A simplified bi-dimensional variational analysis of soil moisture from screen-level observations in a mesoscale numerical weather-prediction model. *Quart. J. Roy. Meteor. Soc.*, **130**, 895-915.

Balsamo, G., Mahfouf, J.-F., Bélair, S., and G. Deblonde (2006). A global root-zone soil moisture analysis using simulated L-band brightness temperature in preparation for the Hydros satellite mission. *J. Hydromet.*, **7**, 1126-1146.

Barnes, H.B. (1967). Roughness characteristics of natural channels. *U.S. Geological Survey, Water Supply Paper 1849*. United States Government Printing Office, Washington, USA. 219pp.

Beljaars, A.C.M., Viterbo, P., Miller, M.J., and A.K. Betts (1996). The anomalous rainfall over the United States during July 1993: Sensitivity to land surface parameterization and soil moisture anomalies. *Mon. Wea. Rev.,* **124,** 362–383.

Berendes, T.A., Berendes, D.A., Welch, R.M., Dutton, E.G., Uttal, T., and E.E. Clothiaux (2003). Cloud cover comparisons of the MODIS daytime cloud mask with surface instruments at the North Slope of Alaska ARM site. *Geosci. Remote Sens.*, **42 (11)**, doi: 10.1109/TGRS.2004.835226.

Berg, A.A., Famiglietti, J.S., Walker, J.P., and P.R. Houser (2003). Impact of bias correction to reanalysis products on simulations of North American soil moisture and hydrological fluxes. *J. Geophys. Res.*, **108 (D16)**, doi:10.1029/2002JD003334.

Betts, A.K., Ball, J.H., Beljaars, A.C.M., Miller, M.J., and P.A. Viterbo (1996). The land surface-atmosphere interaction: A review based on observational and global modeling perspectives. *J. Geophys. Res.*, **101 (D3)**, 7209-7225.

Beven, K.J. and M.J. Kirkby (1979). A physically-based variable contributing area model of basin hydrology. *Hydrol. Sci. Bull.*, **24**, 43-69.

Beven, K. (2004). Robert E. Horton's perceptual model of infiltration processes. *Hydrol. Proc.*, **18**, 3447-3460.

Bos, M.G., (Ed.). Working Group on Small Hydraulic Structures (1976). Discharge Measurement Structures. *International Institute for Land Reclamation and Improvement Publication 20*. Wagenigen, The Netherlands. 464pp.

Boulet, G., Kalma, J.D., Braud, I., and M. Vauclin (1999). An assessment of effective land surface parameterisation in regional-scale water balance studies. *J. Hydrol.*, **217**, 225-238.

Box, G.E.P. and O.R. Cox (1964). The analysis of transformations. *J. Roy. Statist. Soc. Series B*, **26 (2)**, 211-252.

Box, G.E.P. and G.M. Jenkins (1976). *Time series analysis: Forecasting and control*. Holden-Day, San Francisco, California, USA.

Bridgman, H.A. (1984) *Climatic Atlas of the Hunter Valle*y. Dept of Geography, University of Newcastle, Callaghan NSW, Australia.

Brunsell, N.A. and R.R. Gillies (2003). Scale issues in land-atmosphere interactions: implications for remote sensing of the surface energy balance. *Agric. Forest Meteorol.*, **117**, 203-221.

C

Calvet, J.C. (2000). Investigating soil and atmospheric plant water stress using physiological and micrometeorological data. *Agric. Forest Meteorol.*, **103**, 229-247.

Calvet, J.C. and J. Noilhan (2000). From near-surface to root-zone soil moisture using year-round data. *J. Hydromet.*, **1**, 393-411.

Calvet, J.C., Rivalland, V., Picon-Cochard, C., and J.-M. Guehl (2004). Modelling forest transpiration and CO2 fluxes – response to soil moisture stress. *Agric. Forest Meteorol.*, **124**, 143-156.

Campbell Scientific Inc. (2002). *CS616 Water Content Reflectometer Instruction Manual*. Campbell Scientific Inc., Logan, USA, 33pp.

Camporese, M., Ferraris, S., Putti, M, Salandin, P., and P. Teatini (2006). Hydrological modeling in swelling/shrinking peat soils. *Water Resour. Res.*, **42 (6)**, W06420, doi: 10.1029/2005WR004495.

Carpenter, T.M., Georgakakos, K.P., and J.A. Sperfslage (2001). On the parametric and NEXRAD-radar sensitivities of a distributed hydrologic model suitable for operational use. *J. Hydrol.*, **254**, 169–193.

Castillo, V.M., Gomez-Plaza, A., and M. Martinez-Mena (2003). The role of antecedent soil water content in the runoff response of semiarid catchments: a simulation approach. *J. Hydrol.*, **284**, 114-130.

Chapman, T.G. (1963). Rainfall-runoff relations in the Upper Goulburn River Catchment, N.S.W. *Trans. Inst. Eng. Aust. Civ. Eng.*, CE 5 (1), 25-35.

Chiew, F.H.S. and T.A. McMahon (1993). Assessing the adequacy of catchment streamflow yield estimates. *Aust. J. Soil Res.*, **31**, 665-680.

Chiew, F.H.S., Whetton, P.H., McMahon, T.A., and A.B. Pittock (1995). Simulaiton of the impacts of climate change on runoff and soil moisture in Australian catchments. *J. Hydrol.*, **167**, 121-147.

Chiew, F.H.S and T.A. McMahon (2002). Global ENSO-streamflow teleconnection, streamflow forecasting and interannual variability. *Hydrol. Sci. J.*, **47**, 505-522.

Chiew, F.H.S., Peel, M.C., and A.W. Western (2002). Application and testing of the simple rainfall-runoff model SIMHYD. In: Singh, V.P., and D. Frevert (eds.), *Mathematical models of small watershed hydrology and applications*, Water Resources Publ., Littleton, Colorao, USA, pp. 335-367.

Choudhury, B.J., Schmugge, T.J., Chang, A.T.C., and R.W. Newton (1979). Effect of surface roughness on the microwave emission from soils. *J. Geophys. Res.*, **84**, 5699-5705.

Clapp, R. B. and G. M. Hornberger (1978). Empirical Equations for Some Soil Hydraulic Properties. *Water Resour. Res.*, **14 (4)**, 601-604.

Cohen, W.B., Maiersperger, T.K., Yang, Z., Gower, S.T., Turner, D.P., Ritts, W.D., Berterretche, M., and S.W. Running (2003). Comparisons of land cover and LAI estimates derived from ETM+ and MODIS for four sites in North America: a quality assessment of 2000/2001 provisional MODIS products. *Remote Sens. Environ.*, **88**, 233-255.

Cosby, R.B., Hornberger, G.M., Clapp, R.B., and T.R., Ginn (1984). A statistical exploration of the relationships of soil moisture characteristics to the physical properties of soils. *Water Resour. Res.*, **14**, 682-690.

Courtier, P., Andersson, E, Heckley, W., Pailleux, J., Vasiljevic, D., Hamrud, M., et al. (1998). The ECMWF implementation of three dimensional variational assimilation (3D-Var). Part 1: formulation. *Quart. J. Roy. Meteor. Soc.*, **124 (550B)**, 1783-1807.

Cowan, W.L. (1956). Estimating hydraulic coefficients. *Agric. Eng.*, **37 (7)**, 473-475.

Crosson, W.L., Laymon, C.A., Inguva, R., and M.P. Schamschula (2002). Assimilating remote sensing data in a surface flux–soil moisture model. Hydrol. Process., **16 (8)**, 1645-1662.

Crow, W.T., Wood, E.F., and M. Pan (2003). Multiobjective calibration of land surface model evapotranspiration predictions using streamflow observations and spaceborne surface radiometric temperature retrievals. *J. Geophys. Res.*, **108 (D23)**, 4725, doi:10.1029/2002JD003292.

Crow, W.T. and E.F. Wood (2003). The assimilation of remotely sensed soil brightness temperature imagery into a land surface model using Ensemble Kalman filtering: a case study based on ESTAR measurements during SGP97. *Adv. Water Res.*, **26**, 137-149.

D

Delworth, T.L. and S. Manabe (1988). The influence of potential evaporation on the variabilities of simulated soil wetness and climate. *J. Climate*, **1**, 523-547.

Delworth, T.L. and S. Manabe (1989). The influence of soil wetness on near-surface atmospheric variability. *J. Climate*, **2**, 1447-1462.

Derber, J.C., Parrish, D.F., and S.J. Lord (1991). The new global operational analysis system at the National Meteorological Center. *Wea. Forecasting*, **6**, 538-547.

Descroix, L., Nouvelot, J.-F., and M. Vauclin (2002). Evaluation of an antecedent precipitation index to model runoff yield in the western Sierra Madre (North-west Mexico). *J. Hydrol.*, **263**, 114-130.

Dirmeyer, P.A., Dolman, A.J., and N. Sabo (1999). The pilot phase of the global soil wetness project. *Bull. Am. Meteorol. Soc.*, **80**, 851-878.

Dirmeyer, P.A., Zeng, F.J., Ducharne, A., Morrill, J.C., and R.D. Koster (2000). The Sensitivity of Surface Fluxes to Soil Water Content in Three Land Surface Schemes. *J. Hydromet.*, **1**, 121-134.

Dirmeyer, P., Gao, X., and T. Oki (2002). GSWP-2: The second global soil wetness project science and implementation plan. *IGPO Publication Series No. 37*, 65pp.

Douville, H. (2003). Assessing the influence of soil moisture on seasonal climate variability with AGCMs. *J. Hydromet.*, **4**, 1044-1066.

Du, Y., Ulaby, F.T., and M.C. Dobson (2000). Sensitivity to soil moisture by active and passive microwave sensors. *Geosci. Remote Sens.*, **38 (1)**, 105-114.

Duan, Q., Sorooshian, S., and V. Gupta (1992). Effective and efficient global optimisation for conceptual rainfall-runoff models. *Water Resour. Res.*, **28 (4)**, 1015-1031.

Duan, Q., Sorooshian, S., and V. Gupta (1994). Optimal use of the SCE-UA global optimization method for calibrating watershed models. *J. Hydrol.*, **158**, 265-284.

Ducharne, A., Koster, R.D., Suarez, M.J., Stieglitz, M., and P. Kumar (2000). A catchment-based approach to modeling land surface processes in a general circulation model. 2. Parameter estimation and model demonstration. *J. Geophys. Res.*, **105 (D20)**, 24823-24838.

Ducharne, A., Golaz, C., Leblois, E., Laval, K., Polcher, J., Ledoux, E., and G. de Marsily (2003). Development of a high resolution runoff routing model, calibration and application to assess runoff from the LMD GCM. *J. Hydrol.*, **280**, 207-228.

Dunne, T. and R.D. Black (1970). Partial area contributions to storm runoff in a small New England watershed. *Water Resour. Res.*, **6**, 1296-1311.

E

Engman, E.T. and N. Chauhan (1995). Status of microwave soil moisture measurements with remote sensing. *Remote Sens. Environ.*, **51**, 198-198.

Entekhabi, D. and P.S. Eagleson (1989). Land surface hydrology parameterization for atmospheric general circulation models and including subgrid scale spatial variability. *J. Climate*, **2**, 816-831.

Entekhabi, D., Nakamura, H., and E.G. Njoku (1994). Solving the Inverse problem for soil moisture and temperature profiles by sequential assimilation of multifrequency remotely sensed observations. *IEEE Trans. Geosci. Rem. Sens.*, **32 (2)**, 438-448.

Entekhabi, D., Rodriguez-Iturbe, I., and F. Castelli (1996). Mutual interaction of soil moisture and atmospheric processes. *J. Hydrol.*, **184**, 3-17.

Enting, I.G. and G.I. Pearman (1987). Description of a one-dimensional carbon cycle model calibrated using techniques of constrained inversion. *Tellus B*, **39**, 459-476.

Evensen, G., (1994). Sequential data assimilation with a nonlinear quasi-geostrophic model using Monte Carlo methods to forecast error statistics. *J. Geophys. Res.*, **99 (C5)**, 10143–10162.

F

Fitzjohn, C., Ternan, J.L., and A.G. Williams (1998). Soil moisture variability in a semi-arid gully catchment: implications for runoff and erosion control. *CATENA*, **32**, 55-70.

François, C., Quesnay, A., and C. Ottlé (2003). Sequential Assimilation of *ERS-1* SAR Data into a Coupled Land Surface–Hydrological Model Using an Extended Kalman Filter. *J. Hydromet.*, 4 (2), 473-487.

French, A.N., Jacob, F., Anderson, M.C., Kustas, W.P., Timmermans, W., Gieske, A., Su, Z., Su, H., McCabe, M.F., Li, F., Prueger, J., and N. Brunsell (2005). Surface energy fluxes with the Advanced Spaceborne Thermal Emission and Reflection radiometer (ASTER) at the Iowa 2002 SMACEX site (USA). *Remote Sens. Environ.*, **99**, 55-65.

G

Gelb, A. (1974). *Applied Opimal Estimation*. MIT Press, Cambridge, USA.

Georgakakos, K.P. and R.L. Bras (1982). Real-time, statistically linearized, adaptive flood routing. *Water Resour. Res.*, **18 (3)**, 513-524.

Georgakakos, K.P. and G.F. Smith (1990). On improved hydrologic forecasting: results from a WMO real-time forecasting experiment. *J. Hydrol.,* **114**, 17-45.

Georgakakos, K.P., Bae, D.H., and D.R. Cayan (1995). Hydroclimatology of continental watersheds, Part 1: Temporal analysis. *Water Resour. Res.*, **31**, 655-675.

Gessler, P.E., Moore, I.D., McKenzie, N.J., and P.J. Ryan (1995). Soil-landscape modelling and spatial prediction of soil attributes. *Int. J. Geog. Inform. Sys.*, **9**, 421-432.

Gloersen, P. and F.T. Barath (1977). A scanning multichannel microwave radiometer for Nimbus-G and SeaSat-A. *J. Ocean. Eng.*, **2**, 172-178.

Gong, Y., Cao, Q., and Z. Sun (2003). The effects of soil bulk density, clay content and temperature on soil water content measurement using time-domain reflectometry. *Hydrol. Process.*, **17**, 3601-3614.

Grayson, R.B. and A.W. Western (1998). Towards areal estimation of soil water content from point measurements: time and space stability of mean response. *J. Hydrol.*, **207**, 68-82.

Guha, A., Jacobs, J.M., Jackson, T.J., Cush, M.H., Hsu., E.C., and J. Judge (2003). Soil moisture mapping using ESTAR nder dry conditions from the Southern Great Plains experiment (SGP99). *Geosci. Remote Sens.*, **41 (10)**, 2392-2397.

H

Hay, L.E. and M.P. Clark (2003). Use of statistically and dynamically downscaled atmospheric model output for hydrologic simulations in three mountainous basins in the western United States. *J. Hydrol.*, **282**, 56-75.

Heathman, G.C., Starks, P.J., Ahuja, L.R., and T.J. Jackson (2003). Assimilation of surface soil moisture to estimate profile soil water content. J. Hydrol., **279**, 1-17.

Hemakumara, H.M., Kalma, J.D., Walker, J.P., and G.R. Willgoose. Validation and downscaling of low resolution passive microwave soil moisture observations. *J. Hydromet.*, in review.

Henderson-Sellers, A., Yang, Z.L., and R.E. Dickinson (1993). The Project for Intercomparison of Land-surface Parameterization Schemes (PILPS). *Bull. Amer. Meteor. Soc.*, **74**, 1335-1349.

Hogue, T.S., Bastidas, L.A., Gupta, H.V., and S. Sorooshian (2006). Evaluating model performance and parameter behavior for varying levels of land surface model complexity. *Water Resour. Res.*, **42**, doi:10.1029/2005WR004440.

Holland, J.H. (1975). *Adaptation in natural and artificial systems*. University of Michigan Press, Ann Arbor, USA.

Horton, R.E. (1933). The role of infiltration in the hydrologic cycle. *AGU Transactions, EOS*, **14**, 446-460.

Horton, R.E. (1940). An approach toward a physical interpretation of infiltration capacity. *Sci. Soc. Am.*, **5**, 399-417.

Houser, P.R., Shuttleworth, W.J., Famiglietti, J.S., Gupta, H.V., Syed, K.H., and D.C. Goodrich (1998). Integration of soil moisture remote sensing and hydrologic modeling using data assimilation, *Water Resour. Res.*, **34 (12)**, 3405-3420.

Houser, P.R., Rodell, M., Jambor, U., Gottschalck, J., Cosgrove, B., Radakovich, J., Arsenault, K., Bosilovich, M., Entin, J.K., Walker, J.P., Mitchell, K., Pan, H.L., and C.-J. Meng. (2001). The Global Land Data Assimilation System, *GEWEX News*, **11 (2)**, 11-13.

J

Jackson, T.J. (1980). Profile Soil Moisture from Surface Measurements. *J. Irrigation Drainage Div., Proc. ASCE,* **106 (IR2)**, 81-92.

Jackson, T.J., Schmugge, T.J., Nicks, A.D., Coleman, G.A. and E.T. Engman (1981). Soil moisture updating and microwave remote sensing for hydrological simulation. *Hydrol. Sci. Bull.*, **26 (3)**, 305-319.

Jackson, T.J. (1982). Passive microwave sensing of soil moisture under vegetation canopies. *Water Resour. Res.*, **18 (4)**, 1137-1142.

Jackson, T.J., Le Vine, D.M., Hsu, A.Y., Oldak, A., Starks, P.J., Swift, C.T., Isham, J.D., and M. Haken (1999). Soil moisture mapping at regional scales using microwave radiometry: the Southern Great Plains Hydrology Experiment. *Geosci. Remote Sens.*, **37 (5)**, 2136-2151.

Jakeman, A.J., Littlewood, I.G., and P.G. Whitehead (1990). Computation of the instantaneous unit hydrograph and identifiable component flow with application to two small upland catchments. *J. Hydrol.*, **117**, 275–300.

Jakeman, A.J. and G.M. Hornberger (1993). How much complexity is warranted in a rainfall-runoff model? *Water Resour. Res.*, **29 (8)**, 2637–2649.

Jin, M., Shepherd, J.M., and M.D. King (2005). Urban aerosols and their variations with clouds and rainfall: A case study of New York and Houston. *J. Geophys. Res.*, **110**, doi:10.1029/2004JD005081.

K

Kalma, J.D., Bates, B.C., and R.A. Woods (1995). Predicting catchment scale soil moisture status with limited field measurements. *Hydrol. Processes*, **9**, 445-467.

Kalman, R.E. (1960). A new approach to linear filtering and prediction problems. *J. Basic Eng.*, **82 (D)**, 35-45.

Kerr, Y.H., Waldteufel, P., Wigneron, J.P., Font, J., and M. Berger (2001). Soil moisture retrieval from space: The Soil Moisture and Ocean Salinity (SMOS) mission. *Geosci. Remote Sens.*, **39 (8)**, 1729-1735.

Kim, K.C., and C.H. Benson (2002). *Water Content Reflectometer calibrations for final cover soils*. University of Wisconsin-Madison, Madison.

Koster, R.D. and M.J. Suarez (1992). Modeling the land surface boundary in climate as a composite of independent vegetation stands. *J. Geophys. Res.*, **97**, 2697-2715.

Koster, R.D. and M.J. Suarez (1996). Energy and water balance calculations in the Mosaic LSM. In: M.J. Suarez (ed.), *Technical Report Series on Global Modeling and Data Assimilation, NASA Technical Memorandum 104606, Vol. 9*, 68pp.

Koster, R.D., Suarez, M.J., and M. Heiser (2000a). Variance and predictability of precipitation at seasonal-to-interannual timescales. *J. Hydromet.*, **1**, 26-46.

Koster, R.D., Suarez, M.J., Ducharne, A., Stieglitz, M., and P. Kumar (2000b). A catchment-based approach to modeling land surface processes in a general circulation model. 1. Model structure. *J. Geophys. Res.*, **105 (D20)**, 24809-24822.

Koster, R.D. and M.J. Suarez (2001). Soil moisture memory in climate models. *J. Hydromet.*, **2**, 558-570.

Koster, R.D. and M.J. Suarez (2003). Impact of land surface initialization on seasonal precipitation and temperature prediction. *J. Hydromet.*, **4**, 408-423.

Koster, R.D., Dirmeyer, P.A., Guo, Z., Bonan, G., Chan, E., Cox, P., et al. (2004). Regions of strong coupling between soil moisture and precipitation. Science, **305**, 1138-1140.

Kuczera, G. (1983a). Improved parameter inference in catchment models, 1. Evaluating parameter uncertainty. *Water Resour. Res.*, **19 (5)**, 1151-1162.

Kuczera, G. (1983b). Improved parameter inference in catchment models, 1. Combining different kinds of hydrologic data and testing their compatibility. *Water Resour. Res.*, **19 (5)**, 1163-1172.

Kuczera, G. (1994). *NLFIT: A Bayesian Nonlinear Regression Program Suite.* Department of Civil Engineering and Surveying, The University of Newcastle, Australia. 148pp.

L

Lakshmi, V. and J. Susskind (2001). Utilization of satellite data in land surface hydrology: sensitivity and assimilation. *Hydrol. Process.*, **15 (5)**, 877-892.

Le Dimet, F.X. and O. Talagrand (1986). Variational algorithms fr analysis and assimilation of meteorological observations. *Tellus A*, **38**, 97-110.

Lettenmaier, D.P. (2001). Macroscale Hydrology: Challenges and opportunities, present and future of modeling global environmental change: toward integrated modelling. *In: Matsuno, T. and H. Kida (eds.), Terra Scientific Publishing*, Tokyo, Japan, pp. 111-136.

Li, L., Njoku, E.G., Im, E., Chang, P.S., and K. St. Germain (2004). A preliminary survey of radio-frequency interference over the U.S. in Aqua AMSR-E data. *Geosci. Remote Sens.*, **42 (2)**, 380-390.

Liang, X. and D.P. Lettenmaier (1994). A simple hydrologically based model of land surface water and energy fluxes for general circulation models. *J. Geophys. Res.*, **99 (D7)**, 14415-14428.

Lohmann, D., Nolte-Holube, R., and E. Raschke (1996). A large-scale horizontal routing model to be coupled to land surface parametrization schemes. *Tellus A*, **48 (5)**, 708-721.

Lohmann, D., Lettenmaier, D.P., Liang, X., Wood, E.F., Boone, A., Chang, S., et al. (1998). The Project for Intercomparison of Land-surface Parameterization Schemes (PILPS) phase 2(c) Red-Arkansas River basin experiment: 3. Spatial and temporal analysis of water fluxes. *Global Planet. Change*, **19 (1-4)**, 161-179.

Loveday, J. (ed.) (1974). Methods for analysis of irrigated soils. Commonwealth Agricultural Bureau. *Technical communication of the Commonwealth Bureau of Soils, no.54*. Slough, England.

M

Madsen, H. and C. Skotner (2005). Adaptive state updating in real-time river flow forecasting—a combined filtering and error forecasting procedure. *J. Hydrol.*, **308**, 302-312.

Magagi, R.D. and Y.H. Kerr (1997). Retrieval of soil moisture and vegetation characteristics bu use of ERS-1 wind scatterometer over arid and semi-arid areas. *J. Hydrol.*, **188-189**, 361-384.

Mahanama, S.P.P. and R.D. Koster (2003). Intercomparison of Soil Moisture Memory in Two Land Surface Models. *J. Hydromet.*, **4**, 1134-1146.

Mahanama, S.P.P. and R.D. Koster (2005). AGCM biases in evaporation regime: Impacts on soil moisture memory and land-atmosphere feedback. *J. Hydromet.*, **6**, 656-669.

Mahfouf, J.-F. (1991). Analysis of soil moisture from near-surface parameters: A feasibility study. *J. Appl. Meteor.*, **30**, 1534–1547.

Manabe, S. (1969). Climate and the ocean circulation: 1, the atmospheric circulation and the hydrology of the Earth's surface. *Mon. Weather Rev.*, **97**, 739–805.

Martinez, C. (2004). *Geomorphic and hydrologic scaling properties of the Merriwa basalt catchments*. Honours thesis, The University of Newcastle, Callaghan, Australia.

Maurer, E.P., O'Donnell, G.M., Lettenmaier, D.P., and J.O. Roads (2001). Evaluation of the land surface water budget in NCEP/NCAR and NCEP/DOE reanalyses using an off-line hydrologic model, *J. Geophys. Res.*, **106**, 17,841– 17,862.

McMahon, T.A. (1964) *Hydrologic Features of the Hunter Valley, N.S.W*, The Hunter Valley Research Foundation, Newcastle, Australia.

Merlin, O., Chehbouni, A.G., Kerr, Y.H., Njoku, E.G., and D. Entekhabi (2005). A combined modeling and multipectral/multiresolution remote sensing approach for disaggregation of surface soil moisture: Application to SMOS configuration. *Geosci. Remote Sens.*, **43 (9)**, 2036-2050.

Mo, T., Choudhury, B.J., Schmugge, T.J., Wang, J.R., and T.J. Jackson (1982). Passive microwave sensing of soil moisture under vegetation canopies. *Water Resour. Res.*, **18**, 1137-1142.

Montaldo, N. and J.D. Albertson (2003). Multi-scale assimilation of surface soil moisture data for robust root zone moisture predictions. *Adv. Water Res.*, **26**, 33-44.

Moore, I.D. and R.B. Grayson (1991). Terrain based prediction of runoff with vector elevation data. *Water Resour. Res.*, **27 (6)**, 1177–1191.

Moran, M.S., Vidal, A., Troufleau, D., Inoue, Y., and T.A. Mitchell (1998). Ku- and C-band SAR for discriminating agricultural crop and soil conditions. *Geosci. Remote Sens.*, **36 (1)**, 265-272.

𝒩

Naden, P.S. (1993). A routing model for continental-scale hydrology, inMacroscale Modeling of the Hydrosphere. *Proceedings of the Yokohama Symposium*, *July 1993*, *IAHS Publ.*, **214**, 67–79, 1993.

Nash, J. E. and J.V. Sutcliffe (1970). River flow forecasting through conceptual models. Part I: A discussion of principles. *J. Hydrol.*, **10 (3)**, 282-290.

Nelder, J.A. and R. Mead (1965). A simplex method for function minimization. *Comput. J.*, **7 (4)**, 308-313.

Ni-Meister, W., Houser, P.R., and J.P. Walker (2006). Soil moisture initialization for climate prediction: Assimilation of SMMR soil moisture data into a land surface model. *J. Geophys. Res.*, **111**, D20102, doi:10.1029/2006JD007190.

Nijssen, B., Lettenmaier, D.P., Liang, X., Wetzel, S.W., and E.F. Wood (1997). Streamflow simulation for continental-scale river basins. *Water Resour. Res.*, **33 (4)**, 711-724.

Njoku, E.G. and D. Entekhabi (1996). Passive microwave remote sensing of soil moisture. *J. Hydrol.*, **184**, 101-129.

Njoku, E.G., Jackson, T.J., Lakshmi, V., Chan, T.K., and S.V. Nghiem (2003). Soil moisture retrieval from AMSR-E. *Geosci. Remote Sens.*, **41 (2)**, 215-229.

Njoku, E.G., Lakshmi, V., and P.E. O'Neill (2004). Soil moisture field experiment special issue. *Rem. Sens. Environ.*, **92**, 425-426.

Njoku, E.G., Ashcroft, P., Chan, T.K., and L. Li (2005). Global survey and statistics of radio-frequency interference in AMSR-E land observations. *Geosci. Remote Sens.*, **43 (5)**, 938-947.

Njoku, E.G. and S.K. Chan (2006). Vegetation and surface roughness effects on AMSR-E land observations. *Rem. Sens. Environ.*, **100**, 190-199.

Noilhan, J., and S. Planton (1989). A simple parameterization of land surface processes for meteorological models. *Mon. Wea. Rev.*, **117**, 536-549.

Northcote, K.H. (1960). *Atlas of Australian Soils*, Sheet 3, CSIRO and Melbourne University Press.

Northcote, K. H. (1979). *A Factual Key for the Recognition of Australian Soils*, 4th Ed., Rellim Technical Publications, Glenside, South Australia, 123pp.

O

Oldak, A., Jackson, T.J., Starks, P., and R. Elliott (2003). Mapping near-surface soil moisture on regional scale using ERS-2 SAR data. *Int. J. Remote Sens.*, **24 (22)**, 4579-4598.

Olivera, F., Famiglietti, J. and K. Asante (2000). Global-scale flow routing using a source-to-sink algorithm. *Water Resour. Res.*, **36 (8)**, 2197-2207.

Owe, M., de Jeu, R., and J. Walker (2001). A methodology for surface soil moisture and vegetation optical depth retrieval using the Microwave Polarisation Difference Index. *Geosci. Remote Sens.*, **39 (8)**, 1643-1654.

P

Pauwels, V.R.N., Hoeben, R., Verhoest, N.E.C., and F.P. de Troch (2001). The importance of the spatial patterns of remotely sensed soil moisture in the improvement of discharge predictions for small-scale basins through data assimilation. *J. Hydrol.*, **251 (1-2)**, 88-102.

Pauwels, V.R.N., Hoeben, R., Verhoest, N.E.C., de Troch, F.P., and P.A. Troch (2002). Improvement of TOPLATS-based discharge predictions through assimilation of ERS-based remotely sensed soil moisture values. *Hydrol. Proc.*, **16 (5)**, 995-1013.

Pauwels, V.R.N. and G.J.M. de Lannoy (2006). Improvement of modeled soil wetness conditions and turbulent fluxes through the assimilation of observed discharge. *J. Hydromet.*, **7**, 458-477.

Press, W.H., Flannery, B.P., Teukolsky, S.A., and W.T. Vetterling (1986). *Numerical recipes: The art of scientific computing*. Cambridge University Press, Cambridge, UK. 818pp.

Price, W.L. (1987). Global optimization methods for CAD workstation. *J. Optim. Theory Appl.*, **55 (1)**, 133-146.

Philip, J.R. (1957). Evaporation, and moisture and heat fields in the soil. *J. Meteorol.*, **14**, 354–366.

Pilgrim, D.H. (Edt., 1987). *Australian Rainfall and Runoff: A guide to flood estimation, 3rd Edition*. Institution of Engineers Australia, Canberra, A.C.T., 1987.

Pitman, A.J. (2003). The evolution of, and revolution in, land surface schemes designed for climate models. *Int. J. Climatol.*, **23**, 479-510.

Q

Quinones, H., Ruelle, P., and I. Nemeth (2003). Comparison of three calibration procedures for TDR soil moisture sensors. *Irrig. and Drain.*, **52**, 203-217.

R

Rabier, F., Courtier, P., and O. Talagrand (1992). Application of adjoint models to sensitivity analysis. *Beitr. Phys. Atmosph.*, **65 (3)**, 177-192.

Ragab, R. (1995). Towards a continuous operational system to estimate the root-zone soil moisture from intermittent remotely sensed surface moisture. *J. Hydrol.*, **173**, 1-25.

Reichle, R., Entekhabi, D., and D. McLaughlin (2001a). Variational data assimilation of microwave radiobrightness observations for land surface hydrology applications. *Geosci. Remote Sens.*, **39**, 1708-1718.

Reichle, R., Entekhabi, D., and D. McLaughlin (2001b). Downscaling of radiobrightness measurements for soil moisture estimation: A four-dimensional variational data assimilation approach. *Water Resour. Res.*, **37,** 2353–2364.

Reichle, R.H., Walker, J.P., Koster, R.D., and P.R. Houser (2002a). Extended versus Ensemble Kalman Filtering for land data assimilation. *J. Hydromet.*, **3**, 728-740.

Reichle, R.H., McLaughlin, D.B., and D. Entekhabi (2002b). Hydrologic data assimilation with the ensemble Kalman filter. *Mon. Wea. Rev.*, **130 (1)**, 103-114.

Richards, L.A. (1931). Capillary conduction of liquids through porous mediums. *Physics*, **1,** 318–333.

Robock, A., Vinnikov, K.Y., Srinivasan, G., Entin, J.K., Hollinger, S. E., Speranskaya, N.A., Liu, S., and A. Namkhai (2000). The global soil moisture data bank, *Bull. Am. Meteorol. Soc.*, **81**, 1281– 1299.

Rodell, M. and J.S. Famiglietti (2001). Terrestrial water storage variations over Illinois: Analysis of observations and implications for GRACE. *Water Resour. Res.*, **37 (5)**, 1327-1340.

Rodriguez-Iturbe, I., Porporato, A., Laio, F., and L. Ridolfi (2001). Intensive or extensive use of soil moisture: plant strategies to cope with stochastic water availability. *Geophys. Res. Lett.*, **28 (23)**, 4495-4497.

S

Saleh, K., Wigneron, J.P., de Rosnay, P., Calvet, J.C., Escorihuela, M.J., Kerr, Y., and P. Waldteufel (2006). Impact of rain interception by vegetation and mulch on the L-band emission of natural grass. *Remote Sens. Env.*, **101**, 127-139.

Schmugge, T.J., Gloersen, P., Wilheit, T., and F. Geiger (1974). Remote sensing of soil moisture with microwave radiometers. *J. Geophys. Res.*, **79 (2)**, 317-323.

Schmugge, T.J., Jackson, T.J., and H.L. McKim (1980). Survey of methods for soil moisture determination. *Water Resour. Res.,* **16 (6)**: 961-979.

Schmugge, T.J. Kustas, W.P., Ritchie, J.C., Jackson, T.J., and A. Rango (2003). Remote sensing in hydrology. *Adv. Water Resour.*, **25**, 1367-1385.

Schreider, S.Y., Young, P.C., and A.J. Jakeman (2001). An application of the Kalman filtering technique for streamflow forecasting in the Upper Murray Basin. *Mathematical and Computer Modelling*, **33 (6-7)**, 733-743.

Sellers, P.J., Dickinson, R.E., Randall, D.A., Betts, A.K., Hall, F.G., Berry, J.A., Collatz, G.J., Denning, A.S., Mooney, H.A., Nobre, C.A., Sato, N., Field, C.B., and A. Henderson-Sellers (1997). Modelling the exchanges of energy, water and carbon between continents and the atmosphere. *Science*, **275**, 502–509.

Seo, D.J., Koren, V., and N. Cajina (2003). Real-time variational assimilation of hydrologic and hydrometeorological data into operational hydrologic forecasting. *J. Hydromet.*, **4 (3)**, 627-641.

Seyfried, M.S. and M.D. Murdock (2001). Response of a new soil water sensor to variable soil, water content, and temperature. *Soil Science Society of America Journal*, **65**, 28-34.

Shinoda, M. and Y. Yamaguchi (2003). Influence of Soil Moisture Anomaly on Temperature in the Sahel: A Comparison between Wet and Dry Decades. *J. Hydromet.*, **4**, 437-447.

Shuttleworth. W.J. (1991). The Modellion concept. *Rev. Geophys.*, **29**, 585-606.

Sivapalan, M. and G. Blöschl (1998). Transformation of point rainfall to areal rainfall: Intensity-duration-frequency curves. *J. Hydrol.*, 204, 150-167.

Sivapalan, M. (2003). Prediction in ungauged basins: a grand challenge for theoretical hydrology. *Hydrol. Process.*, **17 (15)**, 3163-3170.

Smith, M. (1991). *Report on the expert consultation on revision of FAO methodologies for crop water requirements.* Land and Water Development Division Food and Agriculture Organization of the United Nations, 54pp.

Sorooshian, S., Gao, X., Hsu, K., Maddox, R.A., Hong, Y., Gupta, H.V., and B. Imam, (2002). Diurnal Variability of Tropical Rainfall Retrieved from Combined GOES and TRMM Satellite Information. *J. Climate*, **15 (9)**, 983–1001.

St-Hilaire, A., Ouarda, T.B.M.J., Lachance, M., Bobée, B., Gaudet, J., and C. Gignac (2003). Assessment of the impact of meteorological network density on the estimation of basin precipitation and runoff: a case study. *Hydrol. Proc.*, **17**, 3561-3580.

Stern, H., de Hoedt, G., and J. Ernst (2000). *Objective classification of Australian Climates*. Bureau of Meteorology, Australia at http://www.bom.gov.au [last accessed August, 2004].

Stewart, M.D., Bates, P.D., Anderson, M.G., Price, D.A., and T.P. Burt (1999). Modelling floods in hydrologically complex lowland river reaches. *J. Hydrol.*, **223 (1-2)**, 85-106.

Story, R., Galloway, R.W., van de Graaff, R.H.M. and A.D. Tweedie (1963). *General Report on the Lands of the Hunter Valley*. Land Research Series No. 8, Commonwealth Scientific and Industrial Research Organization, Australia, Melbourne, Australia.

Su, Z., Yacob, A., Wen, J., Roerink, G., He, Y., Gao, B., Boogaard, H., and C. van Dieppen (2002). Assessing relative soil moisture with remote sensing data: theory, experimental validation, and application to drought monitoring over the North China Plain. *Phys. Chem. Earth*, **28**, 89-101.

Sun, C., Walker, J.P., and P.R. Houser (2004). A methodology for snow data assimilation in a land surface model. *J. Geophys. Res.*, **109**, doi:10.1029/2003/JD003765.

Suojala-Ahlfors, T. and T. Salo (2005). Growth yield of pickling cucumber in different soil moisture circumstances. *Sci. Horticult.*, **107**, 11-16.

T

Talagrand, O. and P. Courtier (1987). Variational assimilation of meteorological observations with the adjoint vorticity equation. I: Theory. *Quart. J. Roy. Meteor. Soc.*, **113**, 1311-1328.

Turner, M.R.J., Walker, J.P., and P.R. Oke (2006). Ensemble member generation for sequential data assimilation. *Remote Sens. Environ.*, in press.

U

Uitdewilligen, D.C.A., W.P. Kustas, and P.J. van Oevelen, Estimating surface soil moistures with the scanning microwave radiometer (SLFMR) during the Southern Great Plains 1997 (SGP97) hydrology experiment, *Phys. Chem. Earth*, **28**, 41-51, 2003.

Ulaby, F.T., Batliva, P.P., and M.C. Dobson (1978). Microwave backscatter dependence on surface roughness, soil moisture and soil texture; Part 1—bare soil. *Geosci. Electr.*, **GE-16 (4)**, 286–295.

Ulaby, F.T., Moor, R.K., and A.K. Fung (1986). Microwave remote sensing: Active and Passive, Vol. III, From Theory to Application, Artec House, Norwood (MA), USA.

U.S. Geological Survey. *Surface-water field techniques*. Internet: http://wwwrcamnl.wr.usgs.gov/sws/fieldmethods/Indirects/nvalues/ (last accessed: 23 January 2006)

V

Vrugt, J.A., Gupta, H.V., Bouten, W., and S. Sorooshian (2003). A Shuffled Complex Evolution Metropolis algorithm for optimization and uncertainty assessment of hydrologic model parameters. *Water Resour. Res.*, **39 (8)**, doi:10.1029/2002WR001642

W

Wagner, W., Lemoine, G., and H. Rott (1999). A method for estimating soil moisture ERS scatterometer and soil data. *Remote Sens. Environ.*, **70**, 191-207.

Walker, J.P. (1999). *Estimating Soil moisture profile dynamics from near-surface soil moisture measurements and standard meteorological data*. Ph.D. thesis, Dept. of Civil, Surveying and Environmental Engineering, Univ. of Newcastle, Callaghan, Australia.

Walker, J.P. and P.R. Houser (2001). A methodology for initializing soil moisture in a global climate model: Assimilation of near-surface soil moisture observations, *J. Geophys. Res.*, **106 (D11)**, 11,761–11,774.

Walker, J.P., Willgoose, G.R., and J.D. Kalma (2001). One-dimensional soil moisture profile retrieval by assimilation of near-surface measurements: A simplified soil moisture and field application. *J. Hydromet.*, **2 (4)**, 356-373.

Walker, J.P., Willgoose, G.R., and J.D. Kalma (2002). Three-dimensional soil moisture profile retrieval by assimilation of near-surface measurements: Simplified Kalman filter covariance forecasting and field application. *Water Resour. Res.*, **38 (12)**, doi:10.1029/2002WR001545.

Walker, J.P. and P.R. Houser (2004). Requirements of a global near-surface soil moisture satellite mission: Accuracy repeat time, and spatial resolution. *Adv. Water Resour.*, **27**, 785-801.

Walker, J.P., Houser, P.R., and G.R. Willgoose (2004a). Active microwave remote sensing for soil moisture measurement: a field evaluation using ERS-2. *Hydrol. Process.*, **18 (11)**, 1975-1997.

Walker, J.P., Willgoose, G.R., and J.D. Kalma (2004b). In-situ measurement of soil moisture: a comparison of techniques. *J. Hydrol.*, **293**, 85-99.

Walker, J.P. and P.R. Houser (2005). *Hydrologic Data Assimilation*, In: A. Aswathanarayana (Ed.), Advances in Water Science Methodologies. A.A. Balkema, The Netherlands, 230pp.

Walker, J.P., Hacker, J.M., Kalma, J.D., Kim, E.J. and Panciera, R. (2005). National Airborne Field Experiments for Prediction in Ungauged Basins. In A. Zerger and R. M. Argent (Eds), *MODSIM 2005 International Congress on Modelling and Simulation*. Modelling and Simulation Society of Australia and New Zealand, December 2005, 2974-2980.

Wang, J.R. and T.J. Schmugge (1980). An empirical model for the complex dielectric permittivity of soils as a function of water content. *Geosci. Rem. Sens.*, **GE-18 (4)**, 288-295.

Wang, J.R., O'Neill, P.E., Jackson, T.J., and E.T. Engman (1983). Multifrequency measurements of the effects of soil moisture, soil texture, and surface roughness. *Geosci. Remote Sens.*, **GE-21 (1)**, 44-51.

Wen, J., and Z. Su (2004). An analytical algorithm for the determination of vegetation Leaf Area Index from TRMM/TMI data. *Int. J. Remote Sensing*, **25 (6)**, 1223-1234.

Western, A.W., Sadek, T., Grayson, R.B., and H.N. Turral (2004). On the ability of AirSAR to measure patterns of dielectric constant at the hillslope scale. *J. Hydrol.*, **289**, 9-22.

Western, A.W. and M.S. Seyfried (2005). A calibration and temperature correction procedure for the water content reflectometer. *Hydrol. Process.*, **19**, 3785-3793.

Wetzel, J.P. and J.T. Chang (1987). Concerning the relationship between evapotranspiration and soil moisture. *J. Clim. Appl. Meteorol.*, **26**, 18-27.

Wetzel, P.J., Liang, X., Irannejad, P., Boone, A., Noilhan, J., Shao, Y., Skelly, C., Xue, Y., and Z.L. Yang (1996). Modeling vadose zone liquid water fluxes: Infiltration, runoff, drainage, interflow. *Global Planet. Change*, **13 (1-4)**, 57-71.

Wigneron, J.P., Chanzy, A., Calvet, J.C., and N. Bruguier (1995). A simple algorithm to retrieve soil moisture and vegetation biomass using passive microwave measurements over crop fields. *Remote Sens. Environ.*, **51**, 331-341.

Wigneron, J.P., Kerr, Y., Waldteufel, P., Saleh, K., Escorihuela, M.J., Richaume, P., et al. (2007). L-band Microwave of the Biosphere (L-MEB) model: Results from calibration against experimental data sets over crop fields. *Remote Sens. Environ.*, **107**, 639-655.

Wilheit, T.T. (1978). Radiative transfer in a plane stratified dielectric. *IEEE Trans. Geosci. Rem. Sens.*, **16**, 138-143.

Wood, E.F., Lettenmaier, D.P., and V.G. Zartarian (1992). A land-surface hydrology parameterization with subgrid variability for General Circulation Models. *J. Geophys. Res.*, **97 (D3)**, 2717-2728.

Wooldridge, S., Kalma, J., and G. Kuczera (2001). Parameterisation of a simple semi-distributed model for assessing the impact of land-use on hydrologic response. *J. Hydrol.*, **254 (1-4)**, 16-32.

Y

Yoo, C. (2001). Sampling of soil moisture fields and related errors: implications to the optimal sampling design. *Adv. Water Resour.*, **24 (5)**, 521-530.

Z

Zhan, X., Houser, P.R., Walker, J.P., and W. Crow (2006). A method for retrieving high resolution surface soil moisture from Hydros L-band radiometer and radar observations. *Geosci. Remote Sens.*, **44 (6)**, 1534-1544.

Zribi, M., Le Hégarat-Mascle, S., Ottlé, C., Kammoun, B., and C. Guerin (2003). Surface soil moisture estimation from the synergistic use of the (multi-incidence and multi-resolution) active microwave ERS Wind Scatterometer and SAR data. *Remote Sens. Environ.*, **86**, 30-41.

Zribi, M., Baghdadi, N., Holah, N., and O. Fafin (2005). New methodology for soil surface moisture estimation and its application to ENVISAT-ASAR multi-incidence data inversion. *Remote Sens. Environ.*, **96**, 485-496.

empty page

Appendix A1

A1 Monitoring Stations

A1.1 General

This appendix presents the different weather, soil moisture, and streamflow monitoring stations installed for the SASMAS project. For all stations, detailed information on locations[1], station type, and calibration data are given. Furthermore, the coordinates for the BoM weather stations and DIPNR stream gauges are provided.

Table A1-1. Summary of the monitoring stations throughout the Krui River subcatchment. AWS – automated weather station, SM – soil moisture monitoring site, STR – streamflow monitoring site.

Catchment / ID		*Type of Site*	*Elev. [m]*	*Latitude [deg,min,sec]*	*Longitude [deg,min,sec]*
Krui	K1	SM	400	32° 8′ 55″S	150° 4′ 12″E
	K2	SM	424	32° 9′ 38″S	150° 8′46″E
	K3	SM	408	32° 2′ 22″S	150° 8′ 17″E
	K4	SM	376	31° 58′ 54″S	150° 10′ 48″E
	K5	SM	475*	31° 55′ 59″S	150° 8′ 1″E
	K6	AWS, SM	739	31° 51′ 52″S	150° 12′ 22″E
	S1	SM	329	32° 5′ 32″S	150° 7′ 28″E
	S2	AWS, SM	376	32° 5′ 44″S	150° 8′ 13″E
	S3	SM	412	32° 5′ 44″S	150° 8′ 22″E
	S4	SM	454	32° 5′ 42″S	150° 8′ 33″E
	S5	SM	373	32° 5′ 47″S	150° 8′ 2″E
	S6	SM	397	32° 5′ 55″S	150° 8′ 4″E
	S7	SM	439	32° 6′ 1″S	150° 8′ 7″E
	KP	STR	357	32° 0′ 27″S	150° 9′ 59″E
	SF	STR	322	32° 5′ 36″S	150° 7′ 17″E
	KB	STR	308	32° 5′ 46″S	150° 7′ 5″E
	KN	STR	230	32° 11′ 58″S	150° 5′ 6″E

[1] Site elevations marked with an asterisk (*) were derived from a 25m DEM.

Table A1-2. Summary of the monitoring stations throughout the Merriwa River subcatchment. SM – soil moisture monitoring site, STR – streamflow monitoring site.

Catchment		*Type of Site*	*Elev. [m]*	*Latitude [deg,min,sec]*	*Longitude [deg,min,sec]*
Merriwa	M1	SM	242*	32° 14′ 30″S	150° 18′ 41″E
	M2	SM	282*	32° 9′ 28″S	150° 20′ 1″E
	M3	SM	305*	32° 6′ 42″S	150° 22′ 29″E
	M4	SM	327	32° 2′ 31″S	150° 23′ 47″E
	M5	SM	357*	32° 1′ 20″S	150° 21′ 4″E
	M6	SM	394	31° 56′ 49″S	150° 25′ 54″E
	M7	SM	471	31° 51′ 31″S	150° 28′ 2″E
	MU	STR	253	32° 5′ 10″S	150° 22′ 12″E
	ML	STR	224	32° 12′ 31″S	150° 19′ 28″E

Table A1-3. Summary of the monitoring stations throughout the larger Goulburn River subcatchment. SM – soil moisture monitoring site.

Catchment		*Type of Site*	*Elev. [m]*	*Latitude [deg,min,sec]*	*Longitude [deg,min,sec]*
Goul-burn	G1	SM	175*	32° 22′ 58″S	150° 29′ 22″E
	G2	SM	189*	32° 31′ 33″S	150° 21′ 33″E
	G3	SM	448*	32° 33′ 36″S	150° 5′ 15″E
	G4	SM	455*	32° 24′ 22″S	149° 52′ 56″E
	G5	SM	449*	32° 18′ 33″S	149° 44′ 14″E
	G6	SM	511	32° 1′ 15″S	150° 0′ 41″E

A1.2 Automated Weather Stations

A1.2.1 S2 (Stanley)

Elevation	376m
Latitude	32° 5′ 44′′S
Longitude	150° 8′ 13′′E
Aspect	n/a
Slope	n/a
Instruments	1 Young wind sentry (3m), 1 pyranometer (3m), 1 air temperature (2m), 1 barometric pressure (2m), 1 relative humidity (2m), 1 4-way radiometer (1m), 1 rain gauge (0.5m), 2 heat flux plates (-0.025m)

A1.2.2 K6 (Spring Hill)

Elevation	739m
Latitude	31° 51′ 52′′S
Longitude	150° 12′ 22′′E
Aspect	90°
Slope	10°
Instruments	1 wind anemometer (3m), 1 1 air temperature (2m), 1 relative humidity (2m), 1 rain gauge (0.5m)

A1.2.3 Bureau of Meteorology (BoM) (Mudgee, Nullo Mt., Scone)

Table A1-4. Summary of the BoM AWSs.

Site (BoM ID)	*Elev. [m]*	*Latitude [deg,min,sec]*	*Longitude [deg,min,sec]*	*Avail. Data*
Mudgee (62101)	471	32° 33′ 36′′S	149° 36′ 36′′E	Precip, Air Temp.
Nullo Mt. (62100)	1080	32° 43′ 48′′S	150° 13′ 48′′E	Precip, Air Temp.
Scone (61363)	223	32° 2′ 24′′S	150° 49′ 48′′E	Precip, Air Temp.

A1.3 Soil Moisture Monitoring

A1.3.1 K1 (Illogan)

Elevation	400m
Latitude	32° 8′ 55′′S
Longitude	150° 4′ 12′′E
Aspect	1°
Slope	0°
Soil Depth	>900mm
Instruments	3xCS616, 3xTDR, 1xT107
Soil Type (0-300mm)[2,3]	Silt Loam (23/51/26%)
Soil Type (300-600mm)	(Silt Loam)
Soil Type (600-900mm)	(Silt Loam)
$P_{0.4}$ (0-300mm)	n/a
$P_{0.4}$ (300-600mm)	n/a
$P_{0.4}$ (600-900mm)	n/a
Salinity[4]	0.516dS/m

A1.3.2 K2 (Roscommon)

Elevation	424m
Latitude	32° 9′ 38′′S
Longitude	150° 8′ 46′′E
Aspect	250°
Slope	5°
Soil Depth	>900mm
Instruments	3xCS616, 3xTDR, 1xT107
Soil Type (0-300mm)	Loamy Sand (6.5/8.5/85%)
Soil Type (300-600mm)	(Loamy Sand)
Soil Type (600-900mm)	(Loamy Sand)
$P_{0.4}$ (0-300mm)	30.40978μs
$P_{0.4}$ (300-600mm)	(30.40978μs)
$P_{0.4}$ (600-900mm)	29.93062μs
Salinity	0.008dS/m

[2] The percentage of the particle fractions; given in the order clay, silt and sand.

[3] Names for soil types and $P_{0.4}$ values in brackets are estimations, based on the amplitude of P_{obs}.

[4] The salinity was determined with a 5:1 solution (AS 1289) and multiplied with an empirical equation (determined for Australian soils only), in order to obtain values equivalent to those of a paste extract (Loveday, 1974).

A1.3.3 K3 (Pembroke South)

Elevation	408m
Latitude	32° 2′ 22′′S
Longitude	150° 8′ 17′′E
Aspect	274°
Slope	1°
Soil Depth	>900mm
Instruments	3xCS616, 3xTDR, 1xT107
Soil Type (0-300mm)	Clay (71/23/6%)
Soil Type (300-600mm)	(Clay)
Soil Type (600-900mm)	(Clay)
$P_{0.4}$ (0-300mm)	40.3067μs
$P_{0.4}$ (300-600mm)	(40.3067μs)
$P_{0.4}$ (600-900mm)	(40.3067μs)
Salinity	0.472dS/m

A1.3.4 K4 (Pembroke North)

Elevation	376m
Latitude	31° 58′ 54′′S
Longitude	150° 10′ 48′′E
Aspect	70°
Slope	0°
Soil Depth	>900mm
Instruments	3xCS616, 3xTDR, 1xT107
Soil Type (0-300mm)	Clay (54/36/10%)
Soil Type (300-600mm)	(Clay)
Soil Type (600-900mm)	(Clay)
$P_{0.4}$ (0-300mm)	(39.3054μs)
$P_{0.4}$ (300-600mm)	(39.3054μs)
$P_{0.4}$ (600-900mm)	(39.3054μs)
Salinity	0.308dS/m

A1.3.5 K5 (Burnbrae)

Elevation	475m*
Latitude	31° 55′ 59′′S
Longitude	150° 8′ 1′′E
Aspect	n/a
Slope	n/a
Soil Depth	>900mm
Instruments	3xCS616, 3xTDR, 1xT107
Soil Type (0-300mm)	Clay (62/26/12%)
Soil Type (300-600mm)	(Clay)
Soil Type (600-900mm)	(Clay)
$P_{0.4}$ (0-300mm)	37.0723µs
$P_{0.4}$ (300-600mm)	(37.0723µs)
$P_{0.4}$ (600-900mm)	(37.0723µs)
Salinity	0.368dS/m

A1.3.6 K6 (Spring Hill)

Elevation	739m
Latitude	31° 51′ 52′′S
Longitude	150° 12′ 22′′E
Aspect	90°
Slope	10°
Soil Depth	>900mm
Instruments	3xCS616, 3xTDR, 1xT107
Soil Type (0-300mm)	Clay Loam (35/44/21%)
Soil Type (300-600mm)	(Clay Loam)
Soil Type (600-900mm)	(Clay Loam)
$P_{0.4}$ (0-300mm)	44.7094µs
$P_{0.4}$ (300-600mm)	(44.7094µs)
$P_{0.4}$ (600-900mm)	(44.7094µs)
Salinity	4.454dS/m

A1.3.7 S1 (Stanley)

Elevation	329m
Latitude	32° 5′ 32′′S
Longitude	150° 7′ 28′′E
Aspect	0°
Slope	2°
Soil Depth	>900mm
Instruments	3xCS616, 3xTDR, 1xT107
Soil Type (0-300mm)	Clay (54/40/6%)
Soil Type (300-600mm)	(Clay)
Soil Type (600-900mm)	(Clay)
$P_{0.4}$ (0-300mm)	38.6011µs
$P_{0.4}$ (300-600mm)	(38.6011µs)
$P_{0.4}$ (600-900mm)	(38.6011µs)
Salinity	0.170dS/m

A1.3.8 S2 (Stanley)

Elevation	376m
Latitude	32° 5′ 44′′S
Longitude	150° 8′ 13′′E
Aspect	n/a
Slope	n/a
Soil Depth	>900mm
Instruments	3xCS616, 3xTDR, 8xT107
Soil Type (0-300mm)	Clay Loam (39/35/26%)
Soil Type (300-600mm)	(Clay Loam)
Soil Type (600-900mm)	(Clay Loam)
$P_{0.4}$ (0-300mm)	37.8775µs
$P_{0.4}$ (300-600mm)	(37.8775µs)
$P_{0.4}$ (600-900mm)	(37.8775µs)
Salinity	0.126dS/m

A1.3.9 S3 (Stanley)

Elevation	412m
Latitude	32° 5′ 44′′S
Longitude	150° 8′ 22′′E
Aspect	218°
Slope	5°
Soil Depth	<900mm
Instruments	2xCS616, 2xTDR, 1xT107
Soil Type (0-300mm)	(Clay Loam)
Soil Type (300-600mm)	(Clay Loam)
Soil Type (600-900mm)	---
$P_{0.4}$ (0-300mm)	38.4282μs
$P_{0.4}$ (300-600mm)	(38.4282μs)
$P_{0.4}$ (600-900mm)	---
Salinity	0.288dS/m

A1.3.10 S4 (Stanley)

Elevation	454m
Latitude	32° 5′ 42′′S
Longitude	150° 8′ 33′′E
Aspect	245°
Slope	8°
Soil Depth	<600mm
Instruments	1xCS616, 1xTDR, 1xT107
Soil Type (0-300mm)	(Clay Loam)
Soil Type (300-600mm)	---
Soil Type (600-900mm)	---
$P_{0.4}$ (0-300mm)	36.3024μs
$P_{0.4}$ (300-600mm)	---
$P_{0.4}$ (600-900mm)	---
Salinity	0.891dS/m

A1.3.11 S5 (Stanley)

Elevation	373m
Latitude	32° 5′ 47′′S
Longitude	150° 8′ 2′′E
Aspect	n/a
Slope	n/a
Soil Depth	>900mm
Instruments	3xCS616, 3xTDR, 1xT107
Soil Type (0-300mm)	Silty Clay (46/42/12%)
Soil Type (300-600mm)	(Silty Clay)
Soil Type (600-900mm)	(Silty Clay)
$P_{0.4}$ (0-300mm)	(33.9663μs)
$P_{0.4}$ (300-600mm)	(33.9663μs)
$P_{0.4}$ (600-900mm)	(33.9663μs)
Salinity	n/a

A1.3.12 S6 (Stanley)

Elevation	397m
Latitude	32° 5′ 55′′S
Longitude	150° 8′ 4′′E
Aspect	n/a
Slope	n/a
Soil Depth	<900mm
Instruments	2xCS616, 2xTDR, 1xT107
Soil Type (0-300mm)	Clay (41/28/31%)
Soil Type (300-600mm)	(Clay)
Soil Type (600-900mm)	---
$P_{0.4}$ (0-300mm)	37.0558μs
$P_{0.4}$ (300-600mm)	(37.0558μs)
$P_{0.4}$ (600-900mm)	---
Salinity	n/a

A1.3.13 S7 (Stanley)

Elevation	439m
Latitude	32° 6′ 1′′S
Longitude	150° 8′ 7′′E
Aspect	n/a
Slope	n/a
Soil Depth	<600mm
Instruments	1xCS616, 1xTDR, 1xT107
Soil Type (0-300mm)	Silt Loam (16/52/32%)
Soil Type (300-600mm)	---
Soil Type (600-900mm)	---
$P_{0.4}$ (0-300mm)	(33.9663μs)
$P_{0.4}$ (300-600mm)	---
$P_{0.4}$ (600-900mm)	---
Salinity	n/a

A1.3.14 M1 (Maram Park)

Elevation	242m*
Latitude	32° 14′ 30′′S
Longitude	150° 18′ 41′′E
Aspect	n/a
Slope	n/a
Soil Depth	<900mm
Instruments	2xCS616, 2xTDR, 1xT107
Soil Type (0-300mm)	Sandy Loam (6.5/21.5/72%)
Soil Type (300-600mm)	(Sandy Loam)
Soil Type (600-900mm)	---
$P_{0.4}$ (0-300mm)	27.9364μs
$P_{0.4}$ (300-600mm)	(27.9364μs)
$P_{0.4}$ (600-900mm)	---
Salinity	0.021dS/m

A1.3.15 M2 (Cullingral)

Elevation	282m*
Latitude	32° 9′ 28′′S
Longitude	150° 20′ 1′′E
Aspect	n/a
Slope	n/a
Soil Depth	>900mm
Instruments	3xCS616, 3xTDR, 1xT107
Soil Type (0-300mm)	Sand (0/6/94%)
Soil Type (300-600mm)	(Sand)
Soil Type (600-900mm)	(Sand)
$P_{0.4}$ (0-300mm)	27.2195µs
$P_{0.4}$ (300-600mm)	(27.2195µs)
$P_{0.4}$ (600-900mm)	(27.2195µs)
Salinity	0.141dS/m

A1.3.16 M3 (Merriwa Park)

Elevation	305m*
Latitude	32° 6′ 42′′E
Longitude	150° 22′ 29′′E
Aspect	n/a
Slope	n/a
Soil Depth	<900mm
Instruments	2xCS616, 2xTDR, 1xT107
Soil Type (0-300mm)	Clay Loam (36/43/21%)
Soil Type (300-600mm)	(Clay Loam)
Soil Type (600-900mm)	---
$P_{0.4}$ (0-300mm)	37.1620µs
$P_{0.4}$ (300-600mm)	(37.1620µs)
$P_{0.4}$ (600-900mm)	---
Salinity	0.290dS/m

A1.3.17 M4 (Kilwirrin)

Elevation	327m
Latitude	32° 2′ 31′′S
Longitude	150° 23′ 47′′E
Aspect	60°
Slope	5°
Soil Depth	<600mm
Instruments	1xCS616, 1xTDR, 1xT107
Soil Type (0-300mm)	Loam (25/49.5/25.5%)
Soil Type (300-600mm)	---
Soil Type (600-900mm)	---
$P_{0.4}$ (0-300mm)	40.3563µs
$P_{0.4}$ (300-600mm)	---
$P_{0.4}$ (600-900mm)	---
Salinity	0.129dS/m

A1.3.18 M5 (Midlothian)

Elevation	357m*
Latitude	32° 1′ 20′′S
Longitude	150° 21′ 4′′E
Aspect	n/a
Slope	n/a
Soil Depth	<900mm
Instruments	2xCS616, 2xTDR, 1xT107
Soil Type (0-300mm)	Clay (69/21/10%)
Soil Type (300-600mm)	(Clay)
Soil Type (600-900mm)	---
$P_{0.4}$ (0-300mm)	40.8890µs
$P_{0.4}$ (300-600mm)	(40.8890µs)
$P_{0.4}$ (600-900mm)	---
Salinity	0.545dS/m

A1.3.19 M6 (Dales)

Elevation	394m
Latitude	31° 56′ 49′′S
Longitude	150° 25′ 54′′E
Aspect	100°
Slope	6°
Soil Depth	<900mm
Instruments	2xCS616, 2xTDR, 1xT107
Soil Type (0-300mm)	Clay (51/17.5/31.5%)
Soil Type (300-600mm)	(Clay)
Soil Type (600-900mm)	---
$P_{0.4}$ (0-300mm)	39.7318μs
$P_{0.4}$ (300-600mm)	(39.7318μs)
$P_{0.4}$ (600-900mm)	---
Salinity	0.135dS/m

A1.3.20 M7 (The Echo)

Elevation	471m
Latitude	31° 51′ 31′′S
Longitude	150° 28′ 2′′E
Aspect	115°
Slope	12°
Soil Depth	>900mm
Instruments	3xCS616, 3xTDR, 1xT107
Soil Type (0-300mm)	Clay Loam (35/40/25%)
Soil Type (300-600mm)	(Clay Loam)
Soil Type (600-900mm)	(Clay Loam)
$P_{0.4}$ (0-300mm)	41.8521μs
$P_{0.4}$ (300-600mm)	(41.8521μs)
$P_{0.4}$ (600-900mm)	38.6910μs
Salinity	0.398dS/m

A1.3.21 G1 (Blue Wren Park)

Elevation	175m*
Latitude	32° 22′ 58′′S
Longitude	150° 29′ 22′′E
Aspect	n/a
Slope	n/a
Soil Depth	>900mm
Instruments	3xCS616, 3xTDR, 1xT107
Soil Type (0-300mm)	Sandy Loam (8/15/77%)
Soil Type (300-600mm)	(Sandy Loam)
Soil Type (600-900mm)	(Sandy Loam)
$P_{0.4}$ (0-300mm)	(30.9944µs)
$P_{0.4}$ (300-600mm)	30.9944µs
$P_{0.4}$ (600-900mm)	28.8232µs
Salinity	0.044dS/m

A1.3.22 G2 (Widden Stud)

Elevation	189m*
Latitude	32° 31′ 33′′S
Longitude	150° 21′ 33′′E
Aspect	0°
Slope	0°
Soil Depth	>900mm
Instruments	3xCS616, 3xTDR, 1xT107
Soil Type (0-300mm)	Silty Loam (21/56/23%)
Soil Type (300-600mm)	(Silty Loam)
Soil Type (600-900mm)	(Silty Loam)
$P_{0.4}$ (0-300mm)	33.0761µs
$P_{0.4}$ (300-600mm)	(33.0761µs)
$P_{0.4}$ (600-900mm)	(33.0761µs)
Salinity	0.225dS/m

A1.3.23 G3 (Talooby)

Elevation	448m*
Latitude	32° 33′ 36′′S
Longitude	150° 5′ 15′′E
Aspect	n/a
Slope	n/a
Soil Depth	>900mm
Instruments	3xCS616, 3xTDR, 1xT107
Soil Type (0-300mm)	Clay (64/25/11%)
Soil Type (300-600mm)	(Clay)
Soil Type (600-900mm)	(Clay)
$P_{0.4}$ (0-300mm)	40.1388µs
$P_{0.4}$ (300-600mm)	(40.1388µs)
$P_{0.4}$ (600-900mm)	(40.1388µs)
Salinity	0.304dS/m

A1.3.24 G4 (Cumbo)

Elevation	455m*
Latitude	32° 24′ 22′′S
Longitude	149° 52′ 56′′E
Aspect	n/a
Slope	n/a
Soil Depth	<900mm
Instruments	2xCS616, 2xTDR, 1xT107
Soil Type (0-300mm)	Sandy Loam (11/13/76%)
Soil Type (300-600mm)	(Sandy Loam)
Soil Type (600-900mm)	---
$P_{0.4}$ (0-300mm)	(26.6669µs)
$P_{0.4}$ (300-600mm)	26.6669µs
$P_{0.4}$ (600-900mm)	---
Salinity	0.012dS/m

A1.3.25 G5 (Glenmoor)

Elevation	449m*
Latitude	32° 18′ 33′′S
Longitude	149° 44′ 14′′E
Aspect	n/a
Slope	n/a
Soil Depth	>900mm
Instruments	3xCS616, 3xTDR, 1xT107
Soil Type (0-300mm)	Sandy Loam (9/17/74%)
Soil Type (300-600mm)	(Sandy Loam)
Soil Type (600-900mm)	(Sandy Loam)
$P_{0.4}$ (0-300mm)	27.5468µs
$P_{0.4}$ (300-600mm)	(27.5468µs)
$P_{0.4}$ (600-900mm)	(27.5468µs)
Salinity	0.046dS/m

A1.3.26 G6 (Nagolli)

Elevation	511m
Latitude	32° 1′ 15′′S
Longitude	150° 0′ 41′′E
Aspect	310°
Slope	6°
Soil Depth	<600mm
Instruments	1xCS616, 1xTDR, 1xT107
Soil Type (0-300mm)	Clay Loam (33/35/32%)
Soil Type (300-600mm)	---
Soil Type (600-900mm)	---
$P_{0.4}$ (0-300mm)	39.6832µs
$P_{0.4}$ (300-600mm)	---
$P_{0.4}$ (600-900mm)	---
Salinity	0.201dS/m

A1.4 Streamflow Monitoring

The depth-streamflow conversions given in this section are estimates, calculated with Manning's equation and an estimated roughness coefficient (*n*, see section 3.2.2). Due to the persistent drought in the region and the ensuing low- or no-flow conditions, only a limited number of streamflow measurements were possible, which did not suffice for a validation of the rating curves, developed from the depth-streamflow conversions.

A1.4.1 KP (Krui Pembroke)

Elevation	357m
Latitude	32° 0′ 27′′S
Longitude	150° 9′ 59′′E
In-flow slope	1.1°
Instrument	Solinst Model 3001 Levelogger
Depth-Streamflow Conversion	Q=15.30067*$d^{2.62274}$

A1.4.2 SF (Stanley Flume)

Elevation	322m
Latitude	32° 5′ 36′′S
Longitude	150° 7′ 17′′E
In-flow slope	1.5°
Instruments	Partial 1′6′′ (46cm) Parshall Flume Innovonics MD4W Water Level Logger (until March 2005) Solinst Model 3001 Levelogger (from March 2005)
Depth-Streamflow Conversion	*See Bos (1976)*

A1.4.3 KB (Krui Bridge)

Elevation	308m
Latitude	32° 5′ 46′′S
Longitude	150° 7′ 5′′E
In-flow slope	0.9°
Instrument	Solinst Model 3001 Levelogger
Depth-Streamflow Conversion	Q=27.27203*$d^{2.46468}$

A1.4.4 KN (Krui Neverfail)

Elevation	230m
Latitude	32° 11′ 58′′S
Longitude	150° 5′ 6′′E
In-flow slope	0.6°
Instrument	Solinst Model 3001 Levelogger
Depth-Streamflow Conversion	Q=11.43815*$d^{2.11433}$

A1.4.5 MU (Upper Merriwa)

Elevation	253m
Latitude	32° 5′ 10′′S
Longitude	150° 22′ 12′′E
In-flow slope	0.5°
Instrument	Solinst Model 3001 Levelogger
Depth-Streamflow Conversion	Q=9.48900*$d^{2.00715}$

A1.4.6 ML (Lower Merriwa)

Elevation	224m
Latitude	32° 12′ 31′′S
Longitude	150° 19′ 28′′E
In-flow slope	0.4°
Instrument	Solinst Model 3001 Levelogger
Depth-Streamflow Conversion	Q=4.91953*$d^{2.31886}$

A1.4.7 Merriwa River (210066[5])

Elevation	n/a
Latitude	32° 12′ 21″S
Longitude	150° 19′ 41″E
In-flow slope	n/a
Instrument	Greenspan PS1200 pressure sensor

A1.4.8 Goulburn River (210016)

Elevation	n/a
Latitude	32° 24′ 31″S
Longitude	150° 18′ 55″E
In-flow slope	n/a
Instrument	Min2100 pressure sensor / DP chart recorder

A1.4.9 Goulburn River (210033)

Elevation	n/a
Latitude	32° 21′ 12″S
Longitude	150° 36′ 1″E
In-flow slope	n/a
Instrument	Honeywell pressure sensor

[5] No calibration data is available for DIPNR sites

Appendix A2

A2 Stream Gauge Calibration

A2.1 General

This appendix includes the information about the stream gauges operated within the SASMAS project and their preliminary calibrations.

For the development of the rating curves, Manning's equation was assumed to describe the streamflow at the stream gauging sites accurately

$$Q = \frac{S^{\frac{1}{2}} R^{\frac{2}{3}} A}{n}, \qquad \text{(A1-1)}$$

where Q is the streamflow [m^3/s]; S is the slope in flow direction [m/m]; R is the hydraulic radius [m]; A is the cross sectional area of the flow [m^2]; and n is Manning's roughness coefficient. The hydraulic radius is defined as

$$R = \frac{A}{P}, \qquad \text{(A1-2)}$$

where P is the wetted perimeter of the flow [m].

The respective geometrical values (S, A and P) were determined from site surveys. n was estimated following Cowan's (1956) method that takes into consideration adjustment factors for the conditions of the bed (eg. obstructions and roughness), the vegetation, any surface irregularities and the variations in the cross section of the flow.

A2.2 SASMAS Stream Gauges

A2.2.1 Krui Pembroke (KP)

The streamgauge on Pembroke is located at an altitude of 357m (32° 0′ 27′′S, 150° 9′ 59′′E), on a straight stretch, approximately 60m upstream of a bend, between two steep bank slopes. Flow is uninhibited unless debris located before the bend leads to a build up of water in the channel (Fig. A2-1). n is set to 0.04.

A2.2.2 Krui Bridge (KB)

The logger is located at a road bridge across the Krui (Fig. A2-2) at an altitude of 308m (32° 5′ 46′′S, 150° 7′ 5′′E). Two possible channels have formed under the bridge (left of the logger). A gravel bank has been accumulated on both sides possibly leading to standing water and deviating the water form a straight flowpath. The logger is mounted onto the middle pylon of the bridge on the downstream side. Apart from the gravel bank, some debris can be observed and plant growth occurs in the centre of the stream. n is set to 0.065.

A2.2.3 Krui Neverfail (KN)

The logger is situated on a straight stretch of the channel, lined with small floodplains and steep banks on each side of the stream (Fig. A2-3), at an altitude of 230m (32° 11′ 58′′S, 150° 5′ 6′′E). The logger is sufficiently far away located from the gravel bank (inclusive some plant growth) further upstream of the logger, so that this obstacle should not interfere with the measurements at the actual site. n is set to 0.065.

A2.2.4 Stanley Flume (SF)

A flume has been installed to observe the local runoff on the property “Stanley” (see Chapter 3) near the Krui Bridge (Fig. A2-4). The flume is located in a small gully in the lower part of the microcatchment. No calibration is required for the flume, as the flume has been built following standardised dimensions of a 1ft6in partial Parshall flume (the reader is referred to Bos (197x) and Walker (1999), for the original calibration and verification of the flume).

A2.2.5 Merriwa Upper (MU)

The site is located halfway between the bends of the river (approximately 50 to 60m each way; Fig. A2-5) at an altitude of 253m (32° 5′ 10′′S, 150° 22′ 12′′E). Some debris is found after the upstream bend that might inhibit the flow of water, but is unlikely to influence the measurements of the logger. There is no discernible slope in the stream bed at the location of the logger. n is set to 0.04.

A2.2.6 Merriwa Lower (ML)

The station is located in the lower Merriwa reaches at an altitude of 224m (32° 12′ 31′′S, 150° 19′ 28′′E). In general, the logger is located on the right bank of the channel (Fig. A2-6), where the channel consists of a steep bank on the left side and an extensive floodplain on the right side. The channel section is sufficiently straight in this part of the stream to allow uninhibited flow conditions. n is set to 0.04.

A2.3DIPNR Stream Gauges

While streamflow observations were provided by DIPNR, neither the cross sectional geometry nor the calibration data were made available.

A2.3.1 Merriwa River (210066)

The DIPNR stream gauge in the Merriwa River is located near the town of Merriwa (32° 12′ 21′′S, 150° 19′ 41′′E). The surrounding section of the river is located in a gully, bordered by steep banks (Fig. A2-7a).

A2.3.2 Goulburn River (210016)

The DIPNR stream gauge in the Goulburn River near Kerrabee is located in the upper part of the fluvial flood plain near the outlet of the catchment (32° 24′ 31′′S, 150° 18′ 55′′E). The river has extensive flood plains on each sides, bordered by steep banks (Fig. A2-7b).

A2.3.3 Goulburn River (210031)

The DIPNR stream gauge in the Goulburn River near Sandy Hollow is located in the lower part of the fluvial flood plain near the confluence of the Goulburn River and the Hunter River (32° 24′ 31′′S, 150° 18′ 55′′E). The river is bordered by steep banks on each side (Fig. A2-7c).

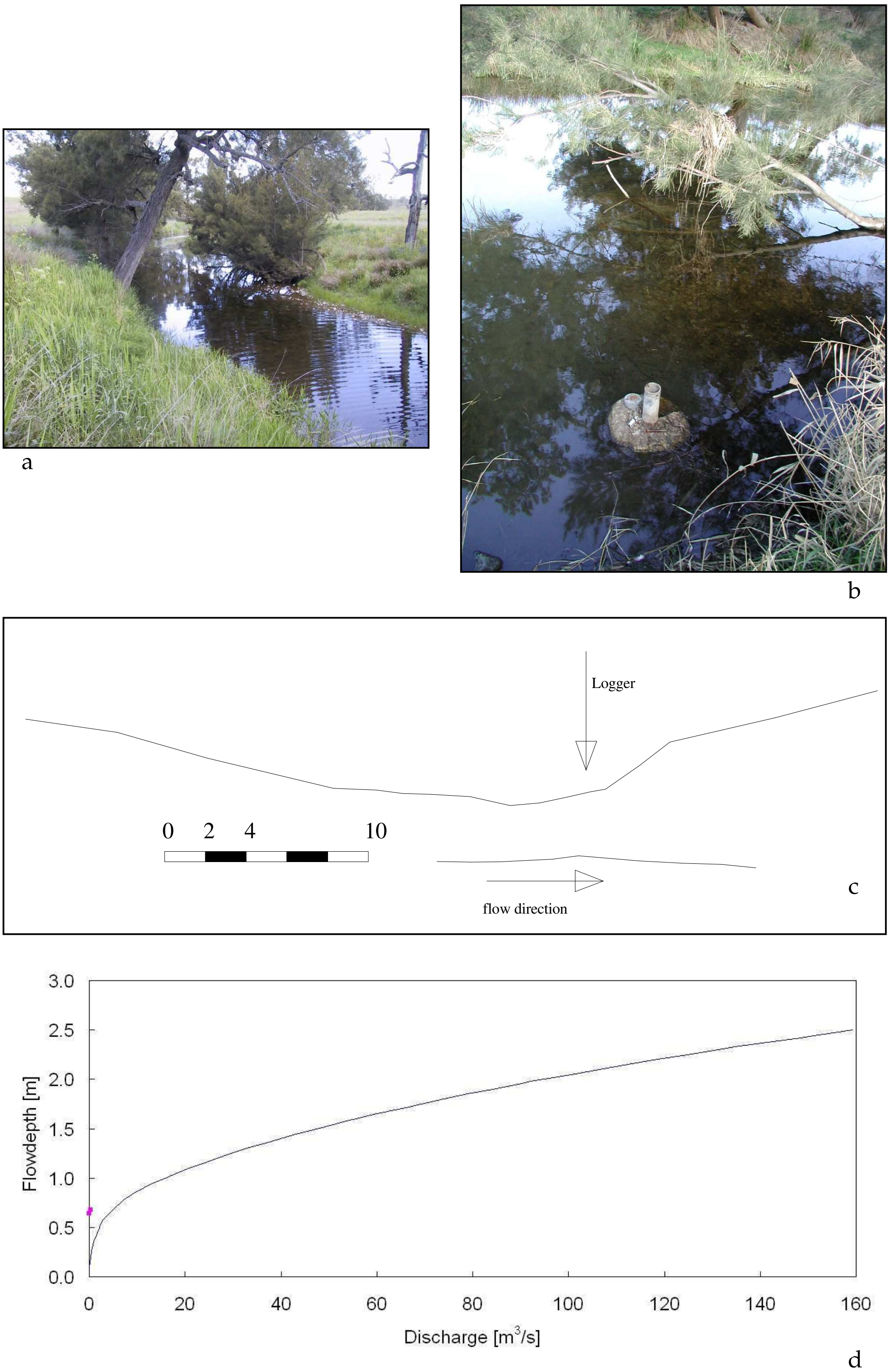

Figure A2-1. Krui River at Pembroke a) in flow direction, b) instrument location, c) cross section and slope, d) preliminary rating curve with two flow velocity measurements.

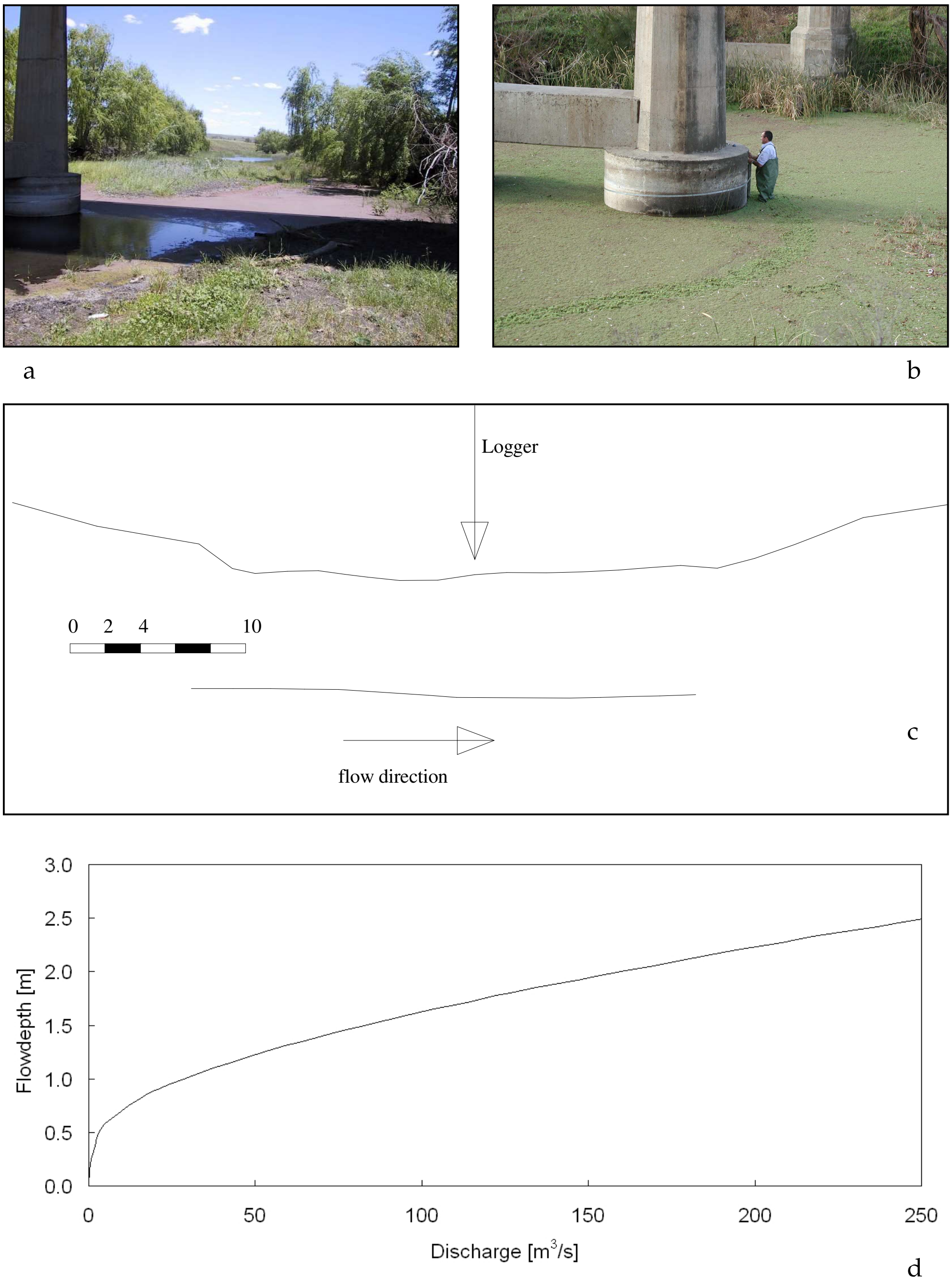

Figure A2-2. Krui River at Krui Bridge a) in flow direction, b) instrument location, c) cross section and slope, d) preliminary rating curve.

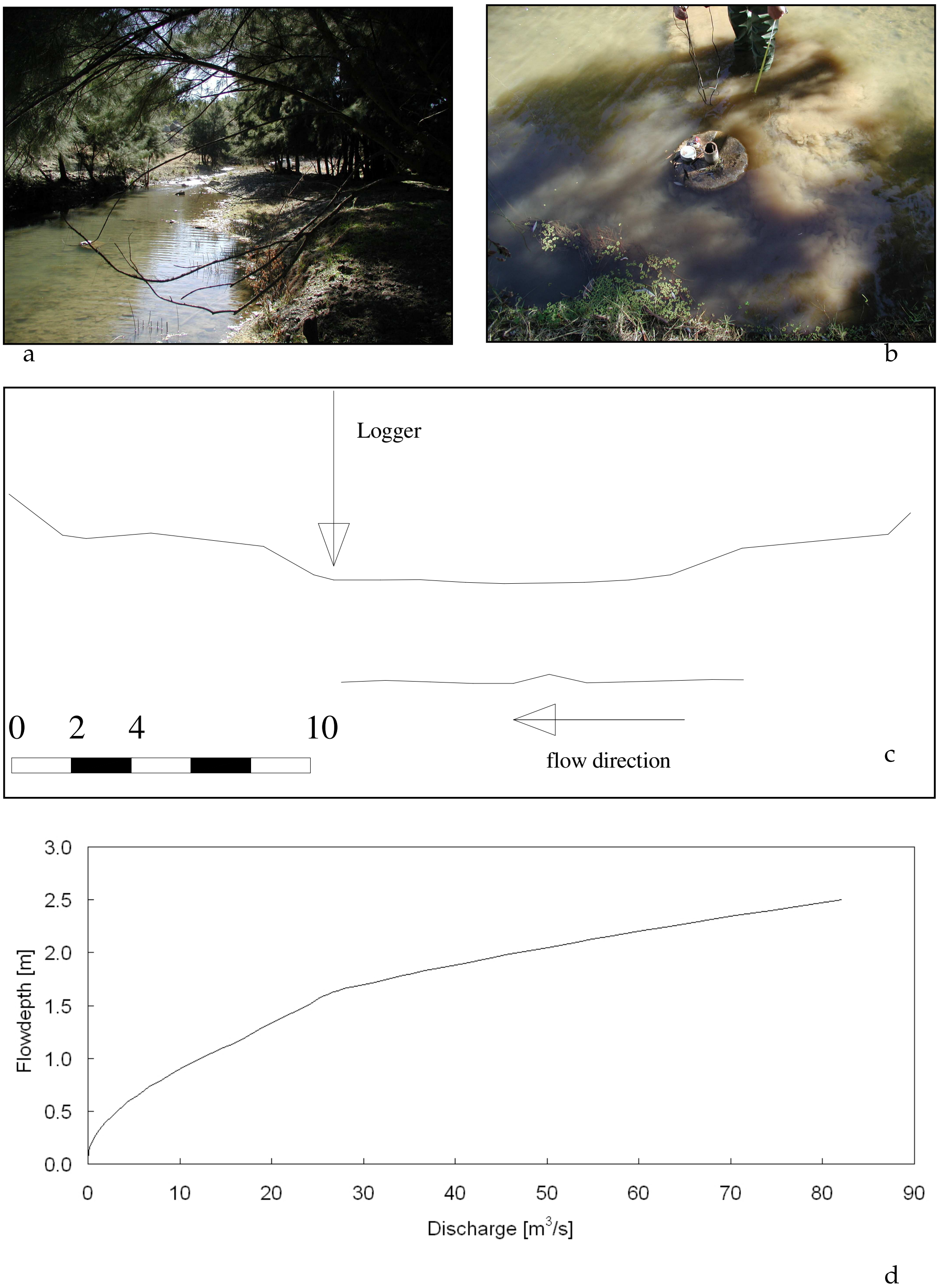

Figure A2-3. Krui River at Neverfail a) in flow direction, b) instrument location, c) cross section and slope, d) preliminary rating curve.

a

b

c

Figure A2-4. Parshall flume on "Stanley". a) Upstream view of the gully, b) detailed view of the flume, and c) full view.

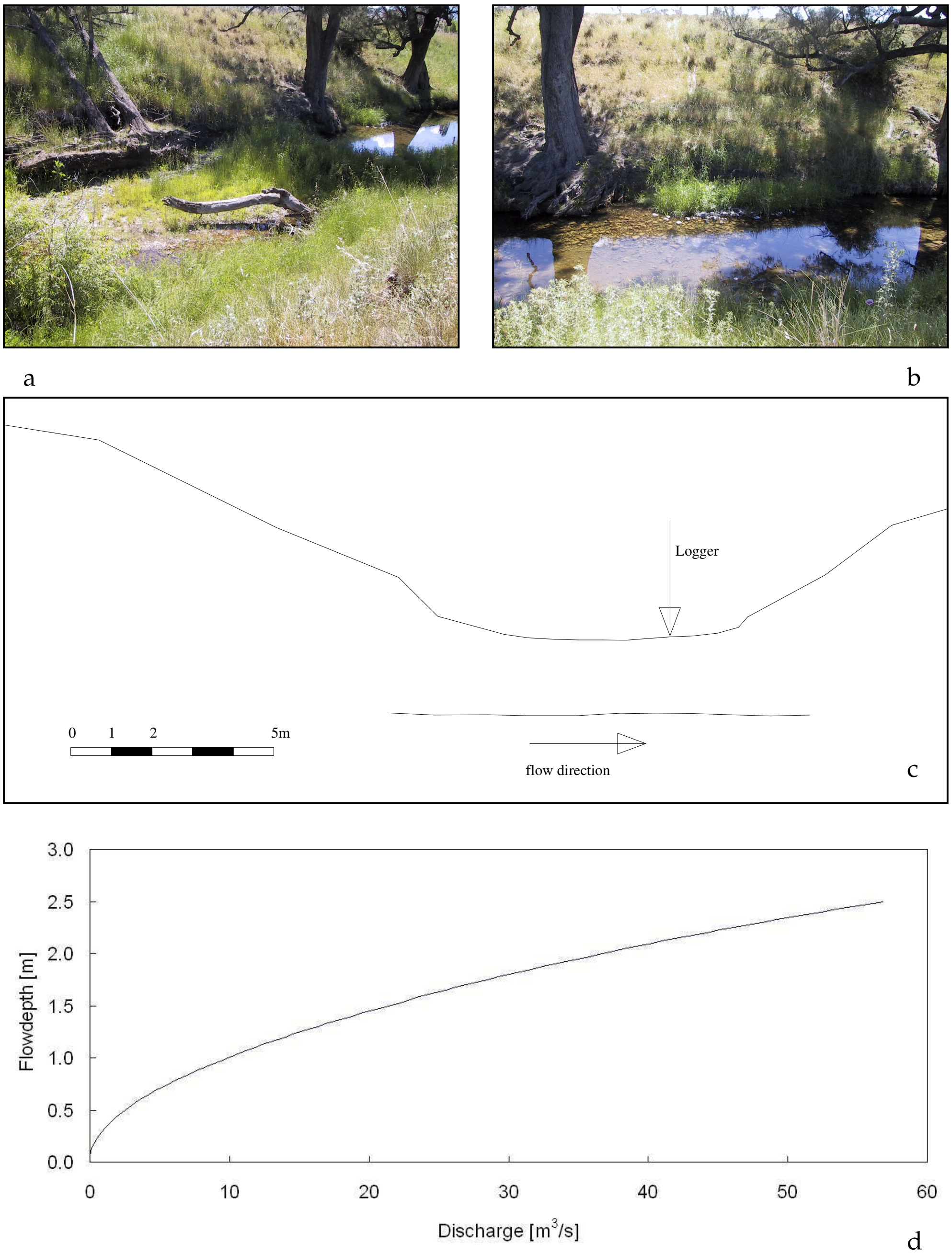

Figure A2-5. Merriwa River in the upper reaches a) in flow direction, b) instrument location, c) cross section and slope, d) preliminary rating curve.

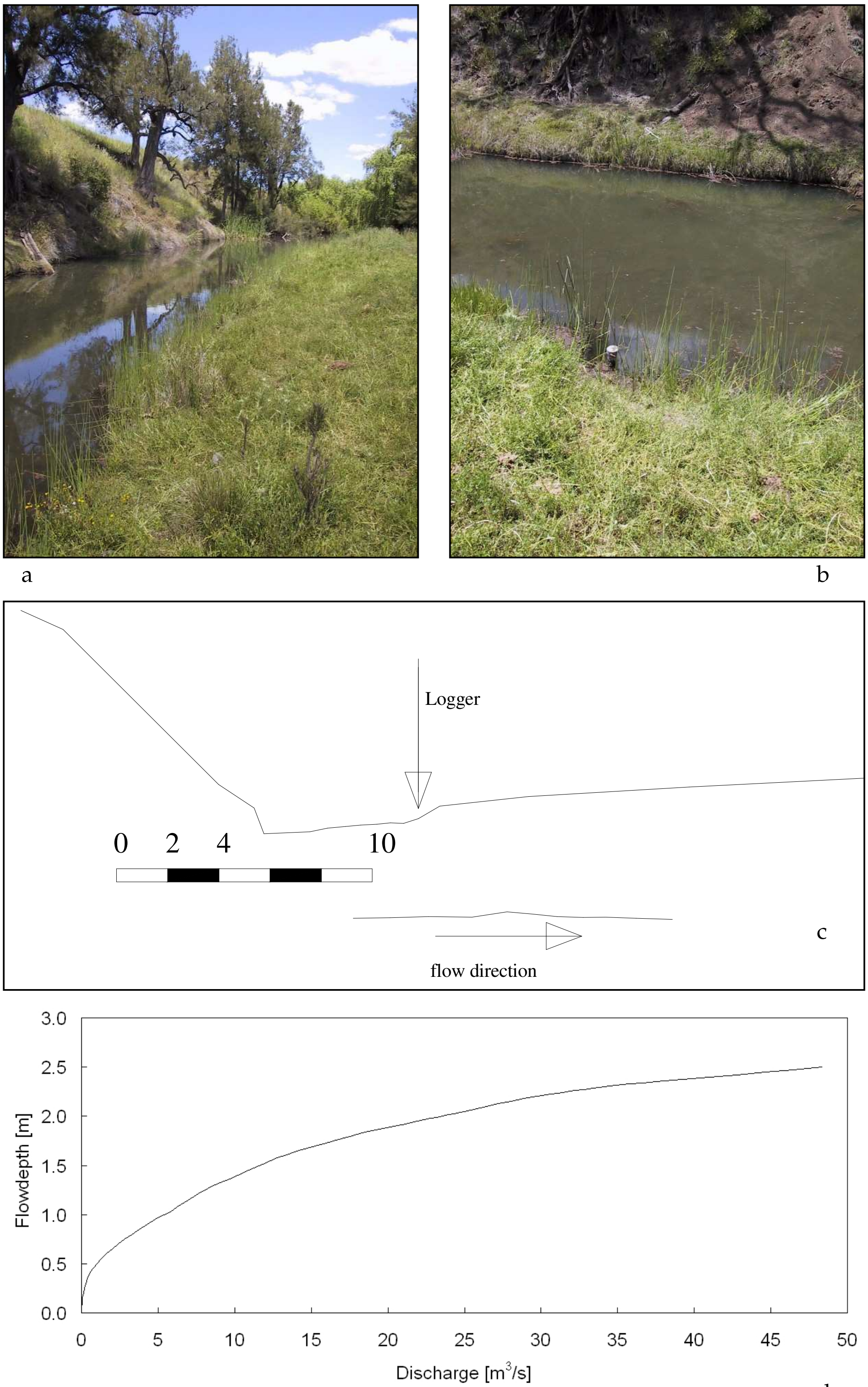

Figure A2-6. Merriwa River in the lower reaches a) in flow direction, b) instrument location, c) cross section and slope, d) preliminary rating curve.

a b c

Figure A2-7. DIPNR stream gauge locations in the a) Merriwa River, b) Goulburn River near Kerrabee, and c) Goulburn River near Sandy Hollow.

Appendix A3

A1 Routing Model

A1.1 General

In this appendix the routing model conceptually described in Chapter 4 is presented with its main equations and an example.

As a first assumption, surface sheet flow, subsurface flow and streamflow is described with a variation of Manning's equation,

$$V_{i,f} = \frac{5}{3} c_{r,i,f} S_i^{1/2} , \qquad \text{(A3-1)}$$

where $V_{i,f}$ is the flow velocity, with f denoting the type of flow and i the cell index; $c_{r,i,f}$ is a routing coefficient; and S_i is the slope of the grid cell [m/m], with the assumption that the subsurface water table is parallel to the surface slope; the factor $\frac{5}{3}$ is included to allow for the kinematic wave propagation in the flow velocity calculations.

Using ArcGIS, slope, orientation, and hence the internal flow length, and the flow length from each individual pixel to the outlet of a DEM within the catchment are determined. In order to distinguish between river and surface flow, the number of contributing upstream pixels is determined and a threshold defined from when a pixel is defined as river (in the present case this value was about 1% of the total number of pixels within a catchment). Using the results for $V_{i,f}$ a weighting function is applied to the individual flow length function, the flow time of each pixel to the outlet is calculated with

$$FT_{j,f} = \sum_{i=j}^{n} FL_i \times V_{i,f}^{-1} , \qquad \text{(A3-2)}$$

where $FT_{j,f}$ is the flow time to the outlet; j is the upstream pixel; n is any number of pixels in the downstream flow path from j; FL_i is the pixel flow length.

Plotting the distribution of the contributing cells at any time gives a hydrograph. This is then translated into a unit hydrograph by normalising the numbers of contributing pixels,

$$R_{t1,t2} = \frac{\sum_{i=t1}^{t2} N_{cp,i}}{N_{cp,all}}, \tag{A3-3}$$

where $R_{t1,t2}$ is the normalised number of pixels for a given time step i=[$t1$,$t2$]; $N_{cp,i}$ and $N_{cp,all}$ are the numbers for contributing pixels for a given time step and all contributing pixels within a catchment, respectively.

Throughout the previous equations no units are prescribed for the variables, as they may be set according to the needs of the application. In the studies presented in this thesis, the hydrologic land surface model provides runoff values in [kg/(m^2*d)] for each time step, therefore these values have to be converted into [m^3/s]

$$Q_{conv,i,k} = Q_{CLSM,i,k} \times \frac{1}{h(\Delta t)} \times A_c \times \frac{1}{\rho} \times \frac{1}{3600 \times 24}, \tag{A3-4}$$

which is equivalent to the following unit transformation

$$\frac{L^3}{T_s} = \frac{M}{L^2 T_{day}} \times \frac{1}{T} \times L^2 \times \frac{1}{M/L^3} \times \frac{1}{T_s/T_h \times T_h/T_{day}}, \tag{A3-5}$$

hence the observed runoff within any given time step i is then defined as

$$Q_{out,i,k} = Q_{conv,i,k} \times R_i, \tag{A3-6}$$

where Q is the runoff [m^3/s]; the subscripts denote "at the outlet" (out), converted runoff values ($conv$) [m^3/s]; the time step of the observation (i); and an identifier for the rain event (k).

As individual rain events may produce runoffs that are within the maximum catchment response times (max($FT_{j,f}$)) of the previous event, simple redistribution of the runoff is not sufficient. The accumulation of the individual runoff events is simply undertaken by adding the runoff matrices at the outlet

$$Q_{tot,i} = \sum_{k=1}^{n} \begin{bmatrix} Q_{out,i,k} \\ \cdots \\ Q_{out,w,k} \end{bmatrix}_k , \tag{A3-7}$$

with w being the sum of the time length of the assimilation and $\max(FT_{j,f})$, where the values for $Q_{tot,i}$ for $i=[w-FT_{j,f}+1,w]$ are transferred to the following time window for the time step $i=[1,FT_{j,f}]$.

Inter-catchment routing is achieved by routing the water inflow with the routing coefficient in the river section, ie. introducing a time-lag before it can produce runoff at the outlet

$$Q_{tot,i,lower}^{comb} = Q_{tot,i+lag,upper} + Q_{tot,i,lower} , \tag{A3-8}$$

with $Q_{tot,i,lower}^{comb}$ being the combined runoff production of the catchments upstream of the observed outlet at a given time step i.

A1.2 Example Application to Catchment 2

The DEM for Catchment 2 (see Chapter 3) is used for the following application of the routing model described above.

a) From the DEM the local slope for each individual pixel is derived (Fig. A3-1a), at the same time the values are converted from [m/deg] into [m/m].

b) The local flow direction within the pixels is derived from the DEM, as well, producing 8 individual flowdirections (Fig. A3-1b).

c) Using the flowaccumulation tool in ArcGIS the contributing upstream pixels can be determined and quantified for each individual pixel. This allows to distinguish between surface and stream runoff conditions. In the present case the minimum number of contributing pixels to define a river is set to 50; for any number

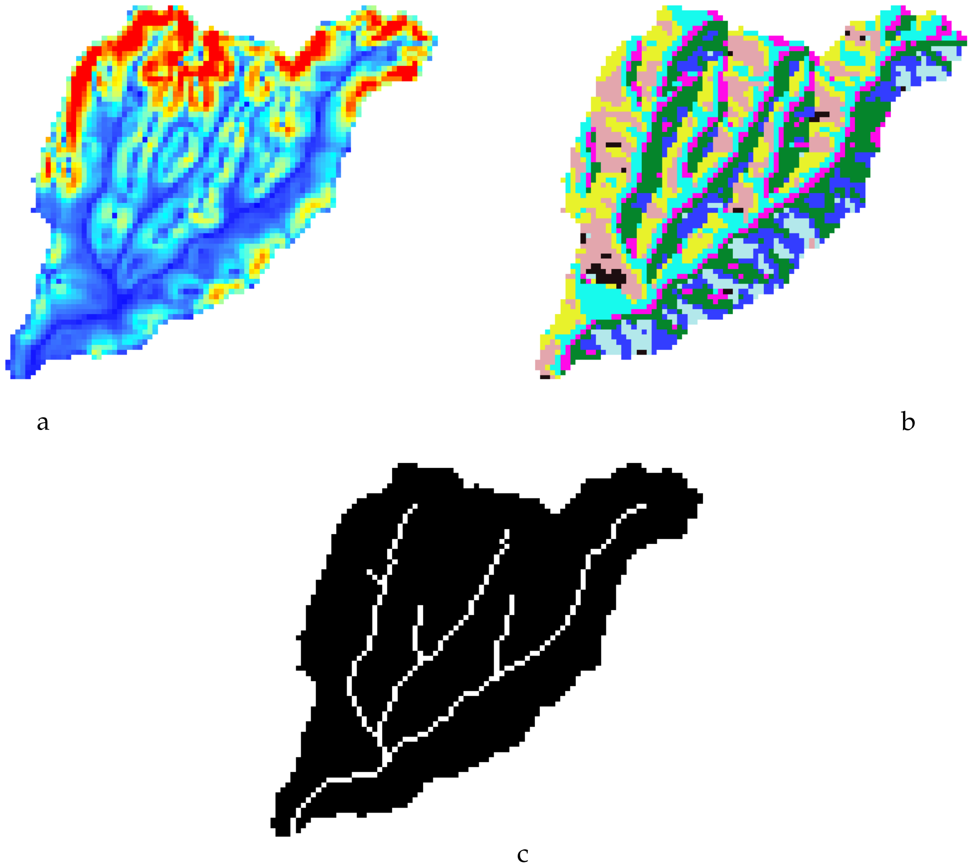

Figure A3-1. a) Local slope and b) flowdirections as derived from the DEM, c) different flow conditions as derived from the flowaccumulation.

below this threshold sheetflow and baseflow are assumed to take place, 50 and above represents stream flow only. Areas of different flow conditions are derived from these results (Fig. A3-1c).

d) The routing coefficients are then assigned to the areas, assuming that each of the two areas has homogeneous conditions (Fig. A3-1c). These values are adjusted to fit real runoff observations at the outlet, qualitatively. For catchments without observations these values are set in accordance with other catchments with similar topography and vegetation.

e) Eq. (A3-1) allows the calculation of the local flow velocities (Fig. A3-2a)

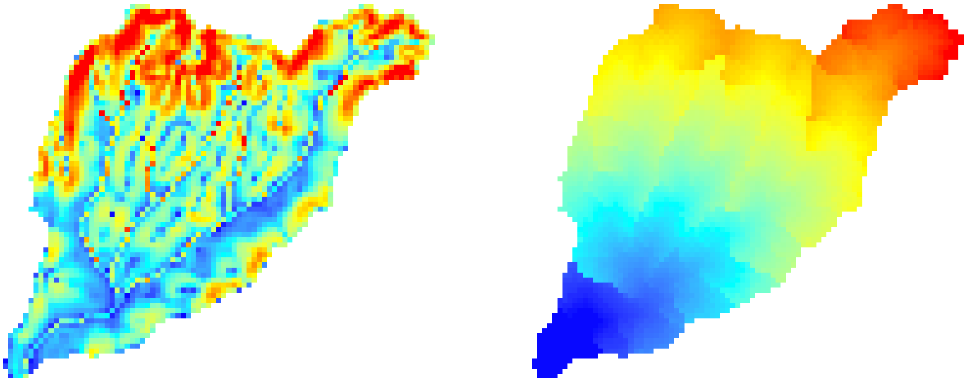

a b

Figure A3-2. a) Local flow velocities and b) flow time for each individual pixel within Catchment 2.

f) To obtain the flowtime, determine the flowlength from each pixel and multiply with the inverse of the velocity function, in order to represent a weighting function to the flowlength calculations (Fig. A3-2b). Note: Some DEM may be in degrees rather than metres. A conversion factor has to be applied to obtain two compatible functions for flowlength and velocity. Furthermore, a DEM in degrees leads to grid distortions that may affect the flow direction.

g) Summarising the number of contributing pixels to each time step and normalising their number to the total number of pixel within the catchment produces the catchment hydrograph (Fig. A3-3)

An example of the application of the presented routing model is shown in Table A3-1. The data presents one runoff event (DoY 235 and 236) from the multi catchment study in Chapter 6. The first two columns represent the day of year (DoY) and time of day (ToD), respectively. Columns 3 and 4 show the runoff in [kg/m^2] for Catchments 2 and 3 as predicted by CLSM. Columns 5 and 6 show the runoff in [m^3/s] for the same catchments and precipitation event after the time delay of the routing model has been applied. The changes in the runoff concentration are apparent. Furthermore, the

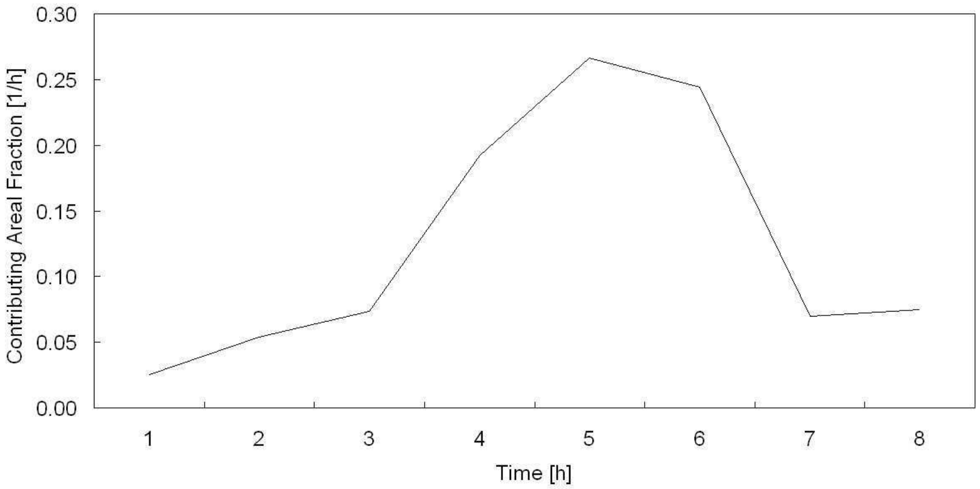

Figure A3-3. Hydrograph for hourly runoff production from Catchment 2.

runoff from Catchment 2 is seen to exit Catchment 3 five hours after leaving Catchment 2.

Table A3-1. Comparison of instantaneous CLSM runoff and routed runoff.

		CLSM			*CLSM & Routing*	
DoY	*ToD*	*Catchment 2*	*Catchment 3*		*Catchment 2*	*Catchment 3*
235	0	0.00000	0.00000		0.00000	0.00000
235	1	0.05575	0.05191		0.00306	0.00349
235	2	0.10524	0.09408		0.01260	0.01921
235	3	0.09631	0.07484		0.02873	0.04392
235	4	0.16897	0.12437		0.06730	0.07193
235	5	0.13240	0.09301		0.13296	0.10391
235	6	0.27145	0.18921		0.21226	0.13930
235	7	0.22843	0.15727		0.28888	0.19344
235	8	0.08041	0.05544		0.34883	0.23835
235	9	0.05698	0.03995		0.41491	0.29207
235	10	0.40264	0.28623		0.46548	0.37961
235	11	1.00393	42.24759		0.52980	3.34425
235	12	14.41315	146.87824		1.28964	20.93471
235	13	3.23757	173.69144		2.50747	61.38930
235	14	3.74970	138.44634		4.17297	110.72994
235	15	32.07460	175.44605		10.57253	157.75653
235	16	110.07359	164.68640		22.50744	203.55823
235	17	4.23402	9.94362		32.65693	234.03235
235	18	1.32144	0.25067		44.02251	230.08286
235	19	1.91647	0.39544		80.25196	212.21433
235	20	1.12284	0.24758		96.60646	207.33630
235	21	0.00000	0.00000		77.25107	221.46639
235	22	0.00000	0.00000		32.51368	216.64191
235	23	0.00000	0.00000		26.43206	200.28049
236	0	0.00000	0.00000		3.04327	211.45569
236	1	0.13201	0.03723		1.33026	193.87105
236	2	0.00000	0.00000		0.63366	122.94357
236	3	0.00000	0.00000		0.25976	40.53513
236	4	0.00000	0.00000		0.06226	27.01817
236	5	0.00000	0.00000		0.08795	3.22630
236	6	0.00000	0.00000		0.07955	1.40837
236	7	0.00000	0.00000		0.02550	0.64940
236	8	0.00000	0.00000		0.02760	0.26582
236	9	0.00000	0.00000		0.00000	0.07091
236	10	0.00000	0.00000		0.00000	0.09953
236	11	0.00000	0.00000		0.00000	0.08779
236	12	0.00000	0.00000		0.00000	0.02676
236	13	0.00000	0.00000		0.00000	0.02760
236	14	0.00000	0.00000		0.00000	0.00000
236	15	0.00000	0.00000		0.00000	0.00000

Appendix A4

A4 True and Control Runs

In this thesis, control runs are labelled according to the following scheme:

C – Control run

True forcing data – 1

Forcing data with wet bias – 2

Forcing data with dry bias – 3

Forcing data with wet bias and white noise – 4

For example:

C2 – Control run with wet bias in the forcing data

A4.1 Single-Catchment Study

A4.1.1 General

In the single catchment study only Catchment 2 is investigated. The control runs 1, 2 and 3, were initialised with soil moisture states near saturation, control run 4 with averaged values between saturation and wilting point (for further descriptions see Chapter 4.6).

The one year control run is only initialised with average soil moisture values and run with forcing data with wet bias and white noise (C4). Finally, the control runs of the multi-catchment study are all initialised with averaged values.

A4.1.2 Year-long Assimilation Window

A4.1.2.1 Soil Moisture

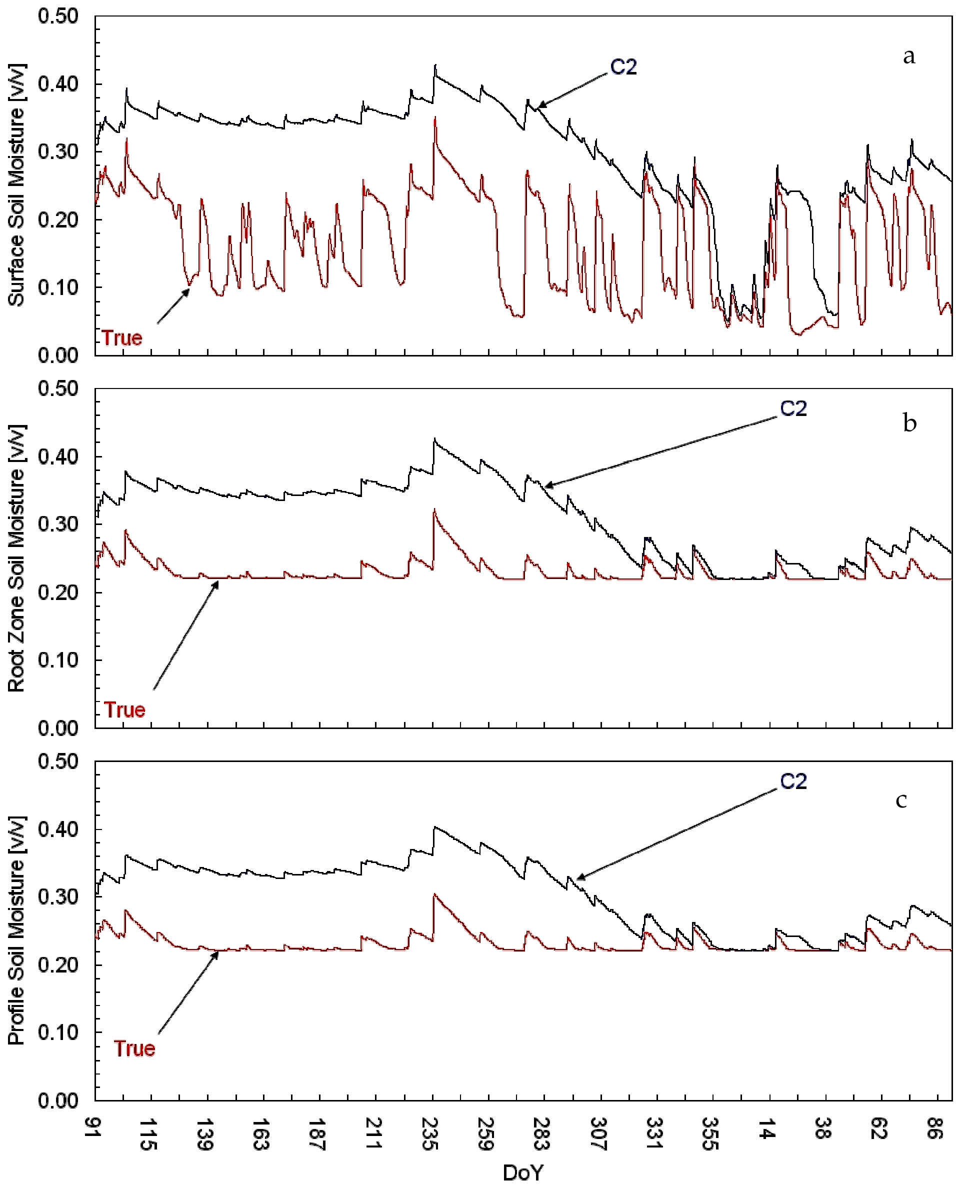

Figure A4.1. Annual soil moisture for Catchment 2. a) surface soil moisture, b) root zone soil moisture and c) profile soil moisture.

A4.1.2.2 Streamflow

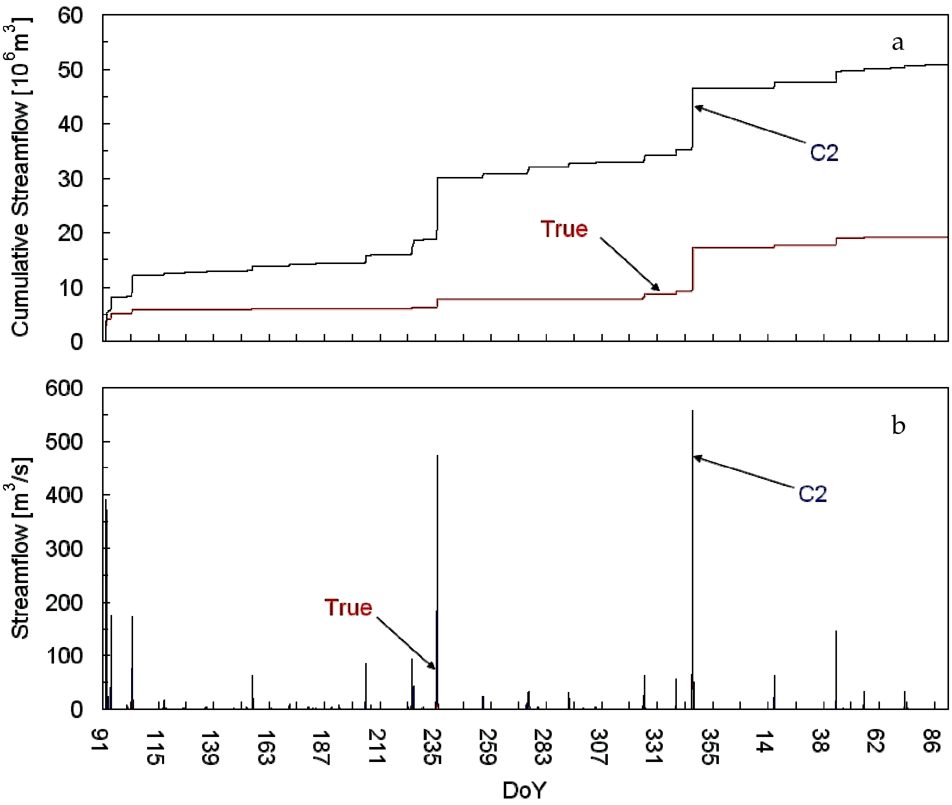

Figure A4.2. Annual a) cumulative and b) instantaneous streamflow for Catchment 2.

A4.1.2.3 Sensible Heat Flux and Evapotranspiration

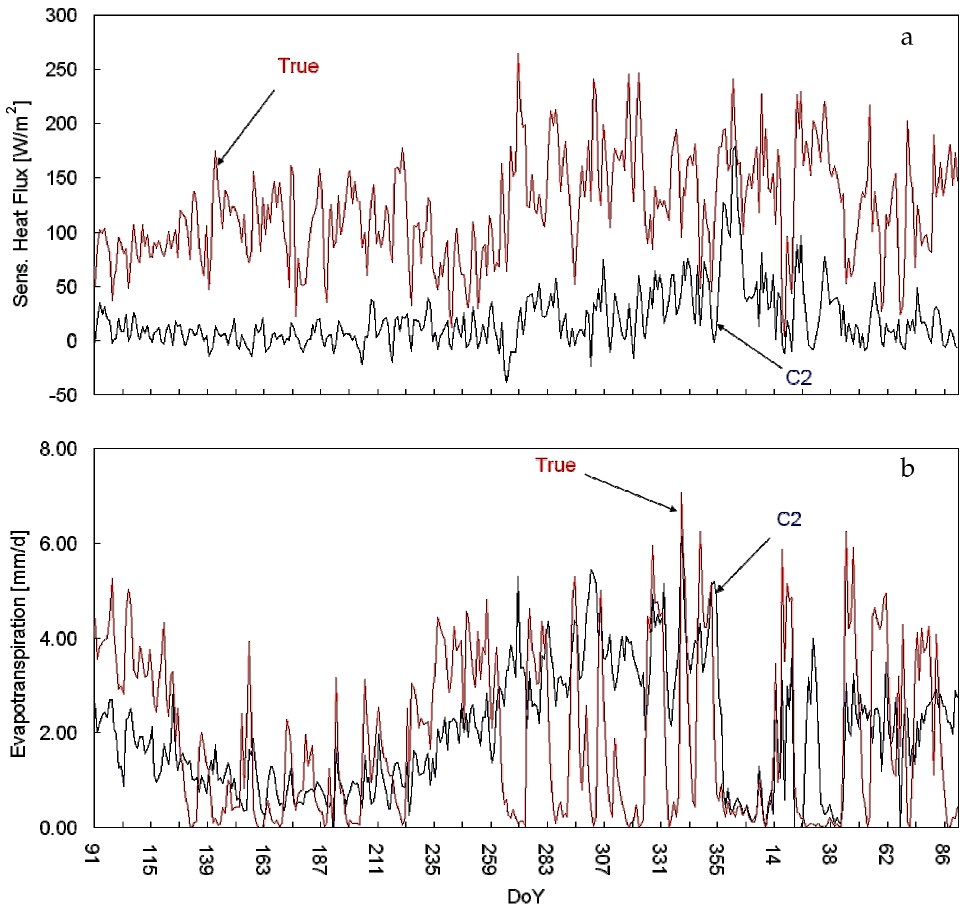

Figure A4.3. Control runs for degraded soil parameters a) sensible heat flux and b) evapotranspiration.

A4.1.3 Month-long Assimilation Window

A4.1.3.1 Soil Moisture

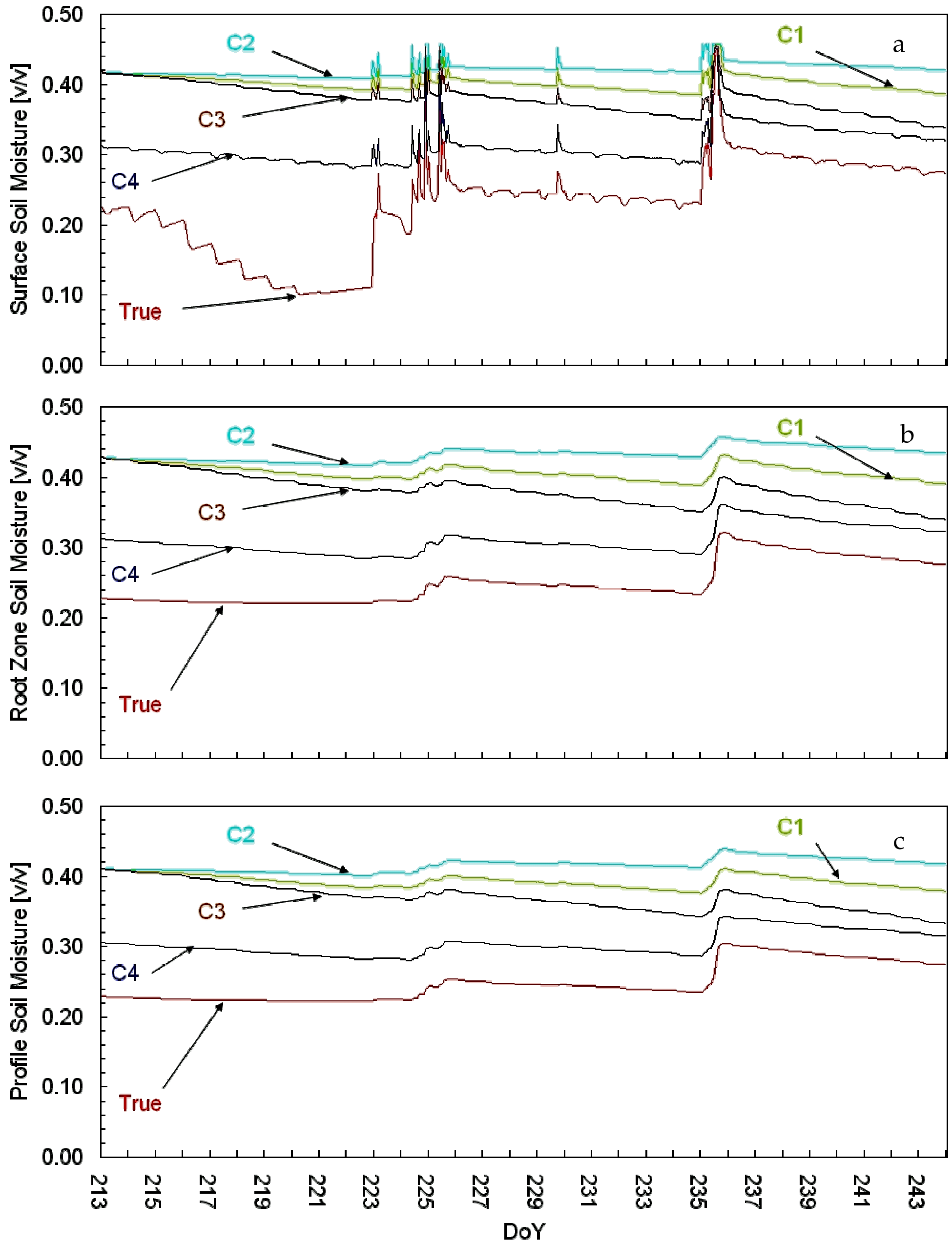

Figure A4.4. Soil moisture control runs for Catchment 2 for August 2003. a) surface soil moisture, b) root zone soil moisture and c) profile soil moisture. The numbering is explained in Table 2 of Chapter 4.6.

A4.1.3.2 Streamflow

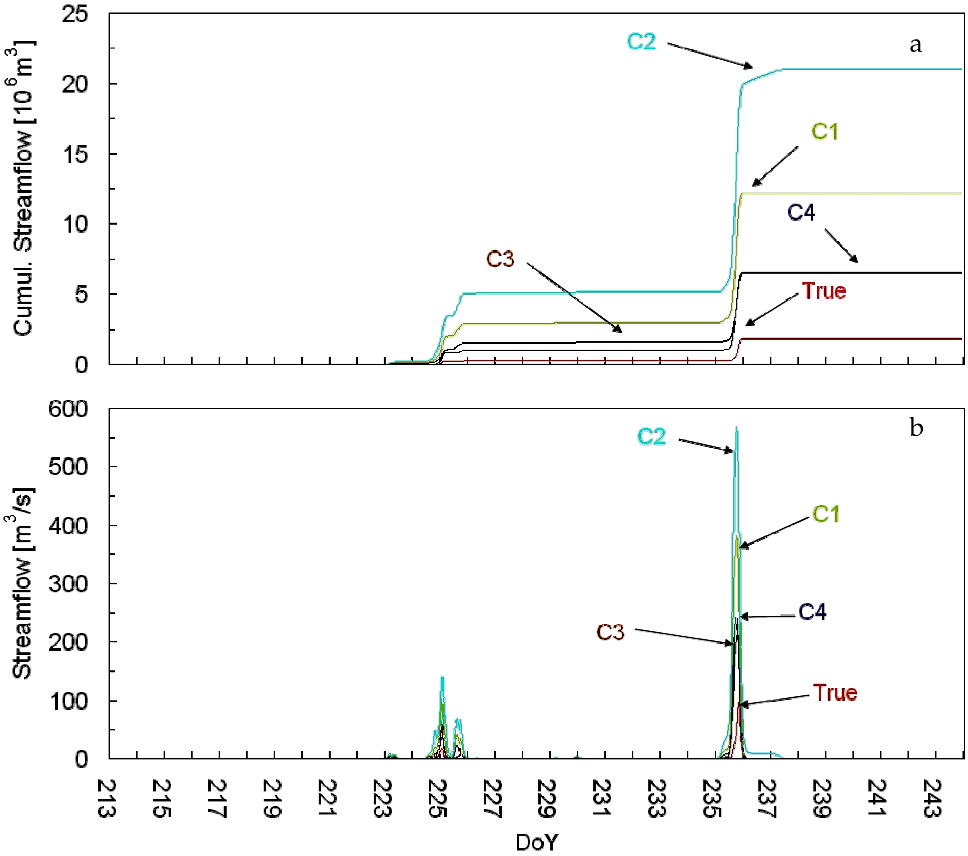

Figure A4.5. a) Cumulative and b) instantaneous streamflow from Catchment 2.

A4.1.3.3 Sensible Heat Flux and Evapotranspiration

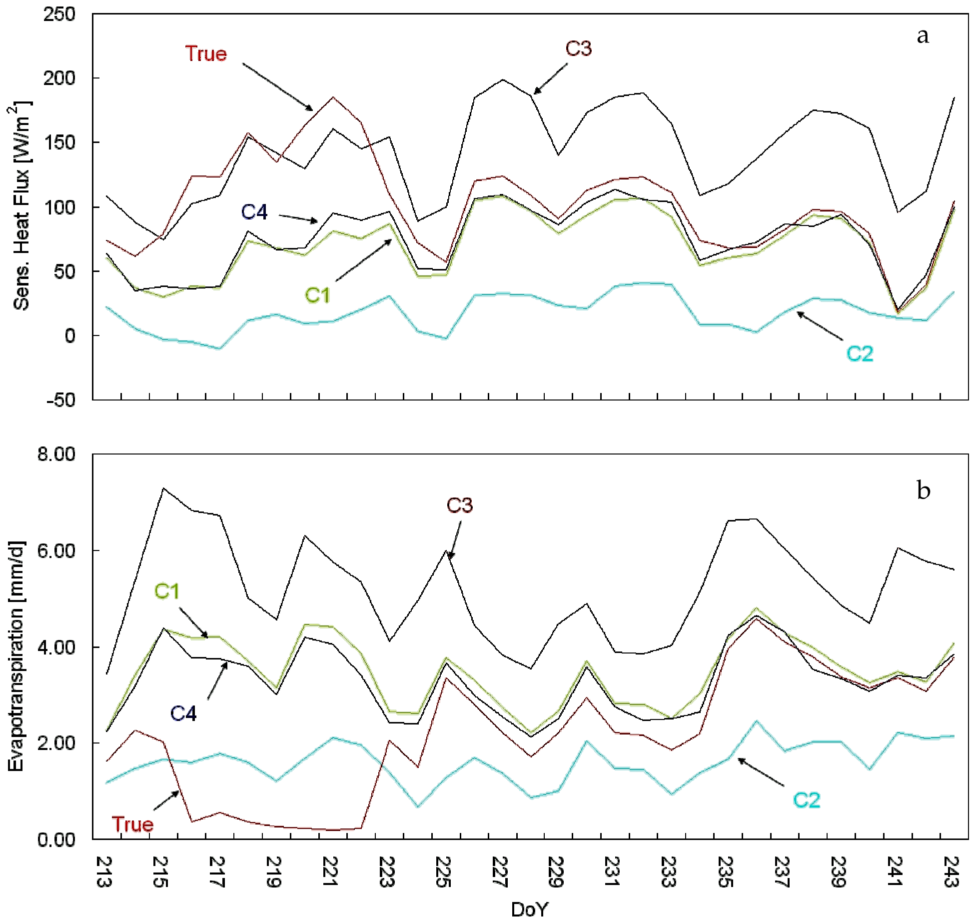

Figure A4.6. a) Sensible heat flux and b) evapotranspiration for Catchment 2.

A4.1.4 Degraded Soil Parameters

A4.1.4.1 Soil Moisture

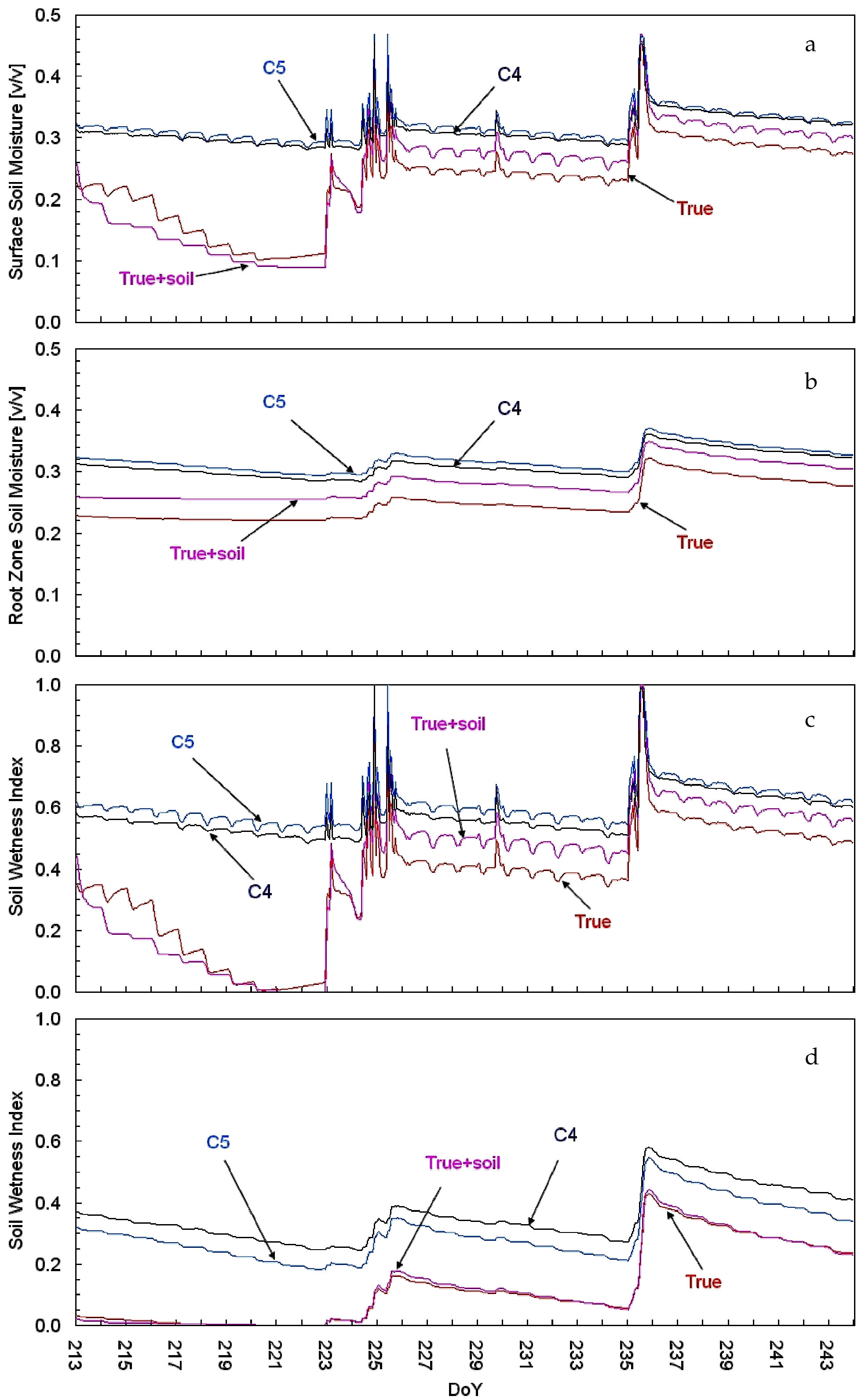

Figure A4.7. Soil moisture and soil wetness index for Catchment 2. Absolute a) surface and b) root zone soil moisture, and soil wetness index for c) surface and d) root zone.

A4.1.4.2 Streamflow

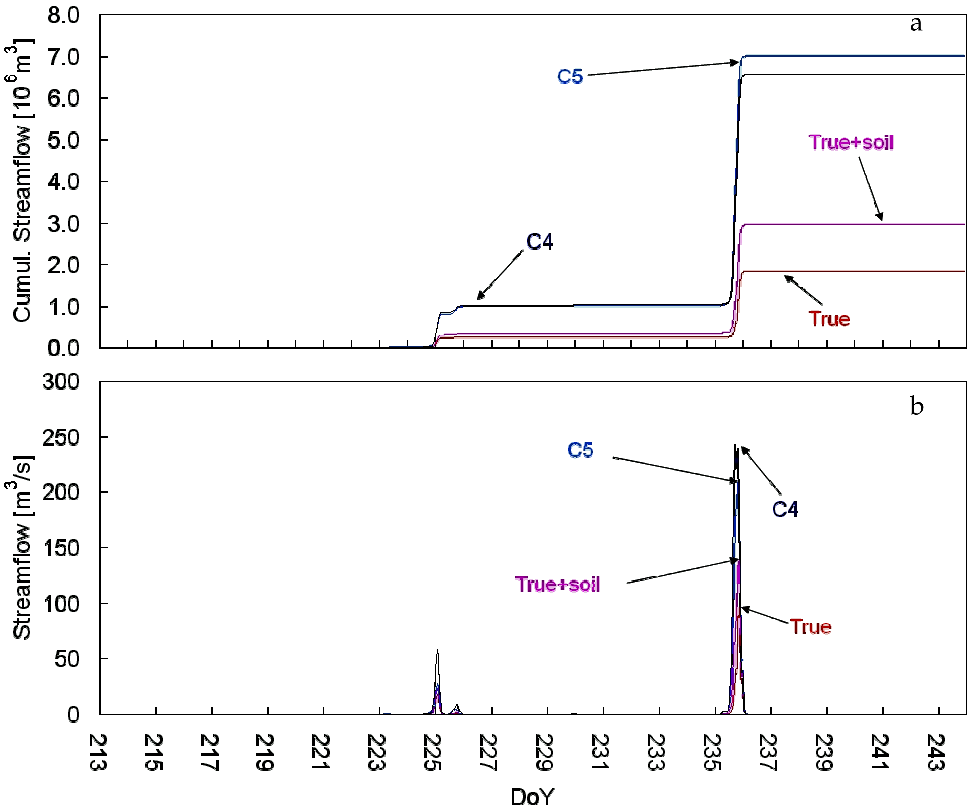

Figure A4.8. a) Cumulative and b) instantaneous streamflow from Catchment 2.

A4.1.4.3 Sensible Heat Flux and Evapotranspiration

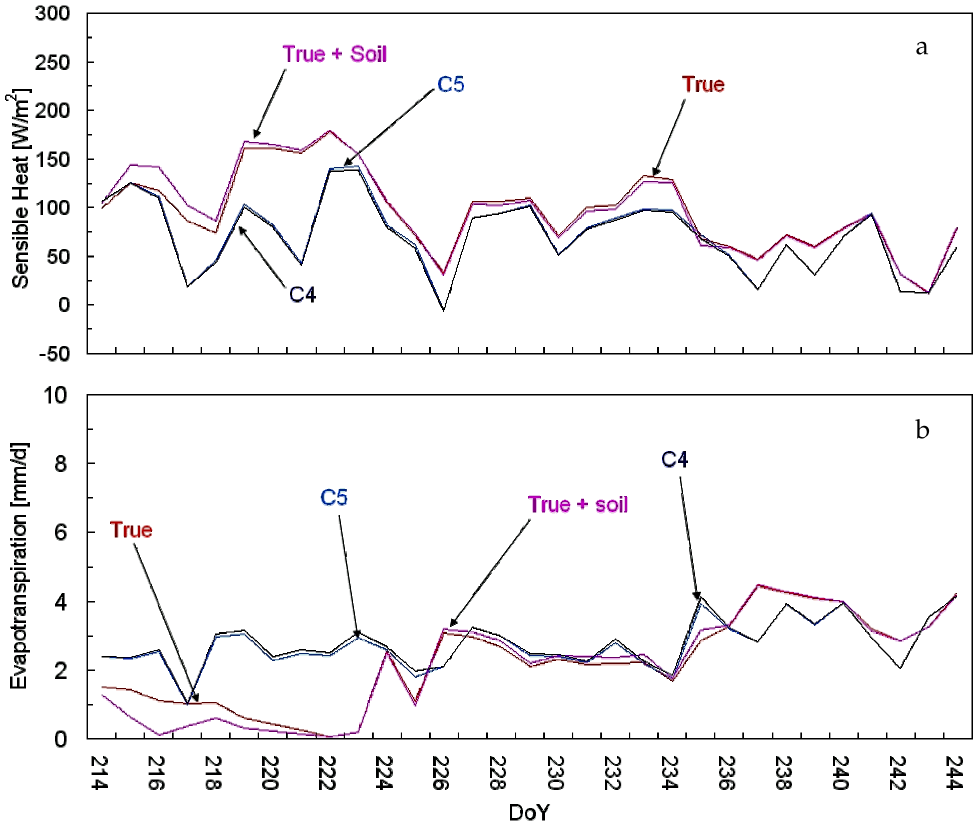

Figure A4.9. Control runs for degraded soil parameters a) sensible heat flux and b) evapotranspiration.

A4.2 Multi-Catchment Study

A4.2.1 Soil Moisture

A4.2.1.1 Catchment 1

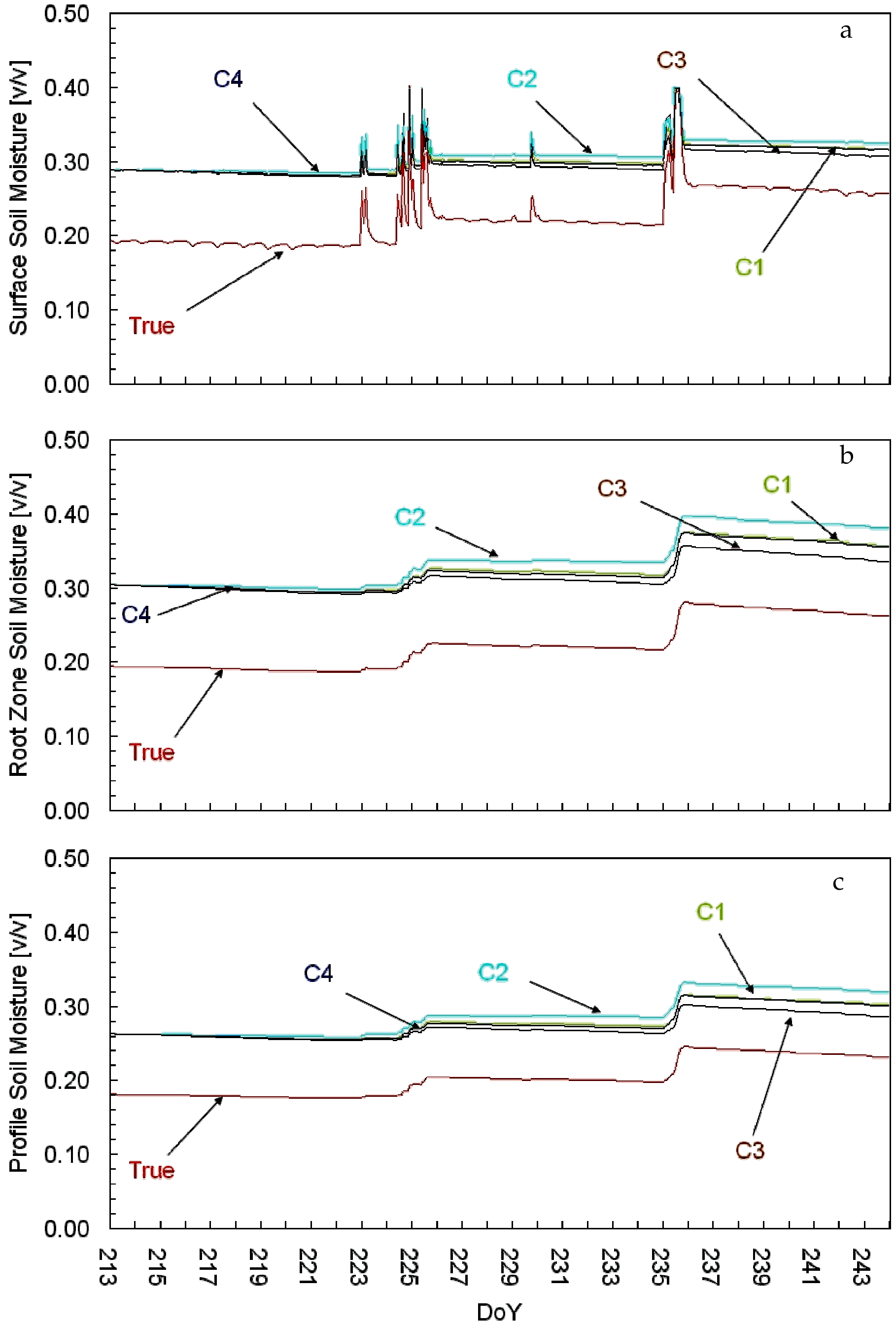

Figure A4.10. Soil moisture control runs for Catchment 1 for August 2003. a) Surface soil moisture, b) root zone soil moisture and c) profile soil moisture. The numbering is explained in Table 5.1.

A4.2.1.2 Catchment 2

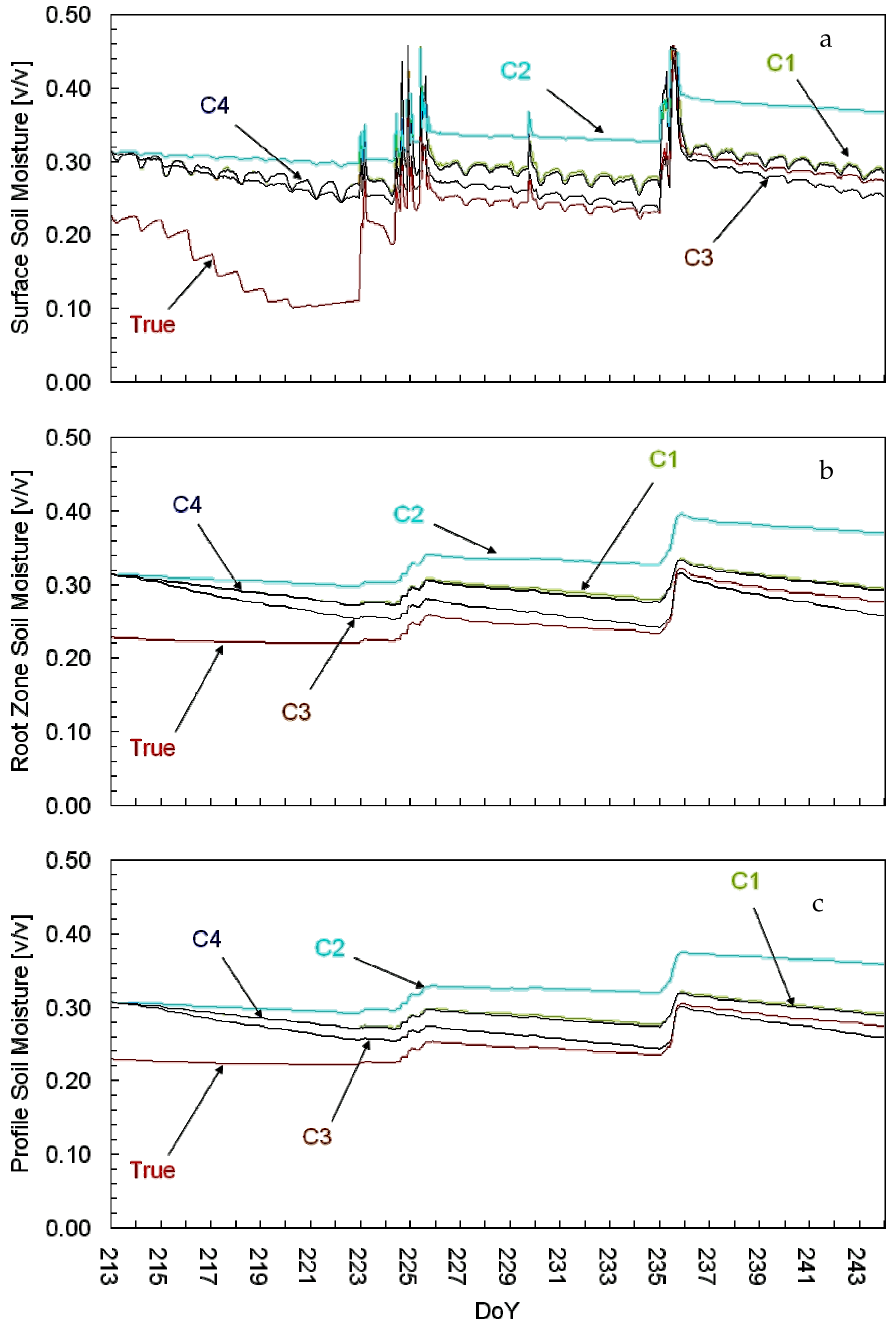

Figure A4.11. Soil moisture control runs for Catchment 2 for August 2003. a) Surface soil moisture, b) root zone soil moisture and c) profile soil moisture. The numbering is explained in Table 5.1.

A4.2.1.3 Catchment 3

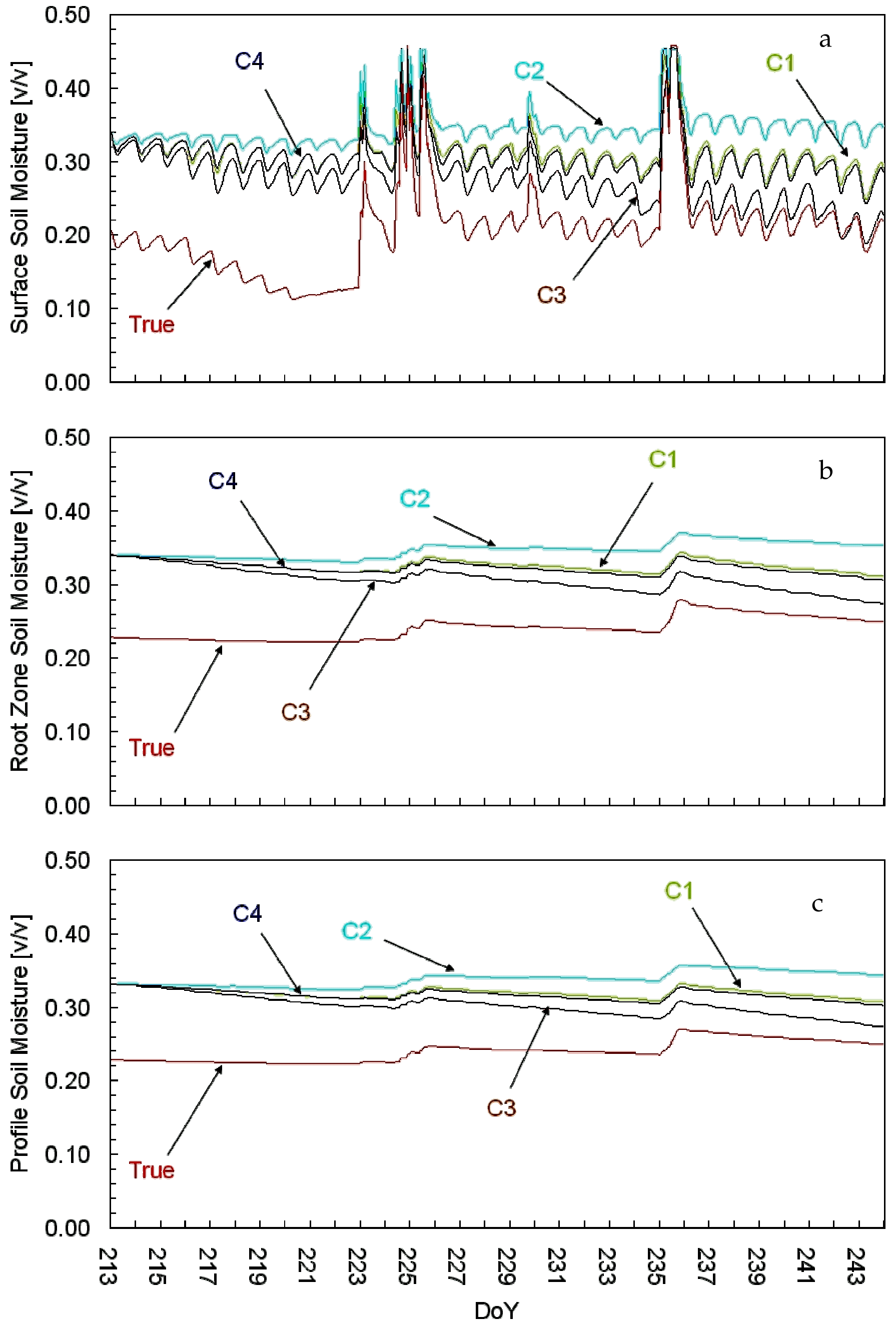

Figure A4.12. Soil moisture control runs for Catchment 3 for August 2003. a) Surface soil moisture, b) root zone soil moisture and c) profile soil moisture. The numbering is explained in Table 5.1.

A4.2.1.4 Catchment 4

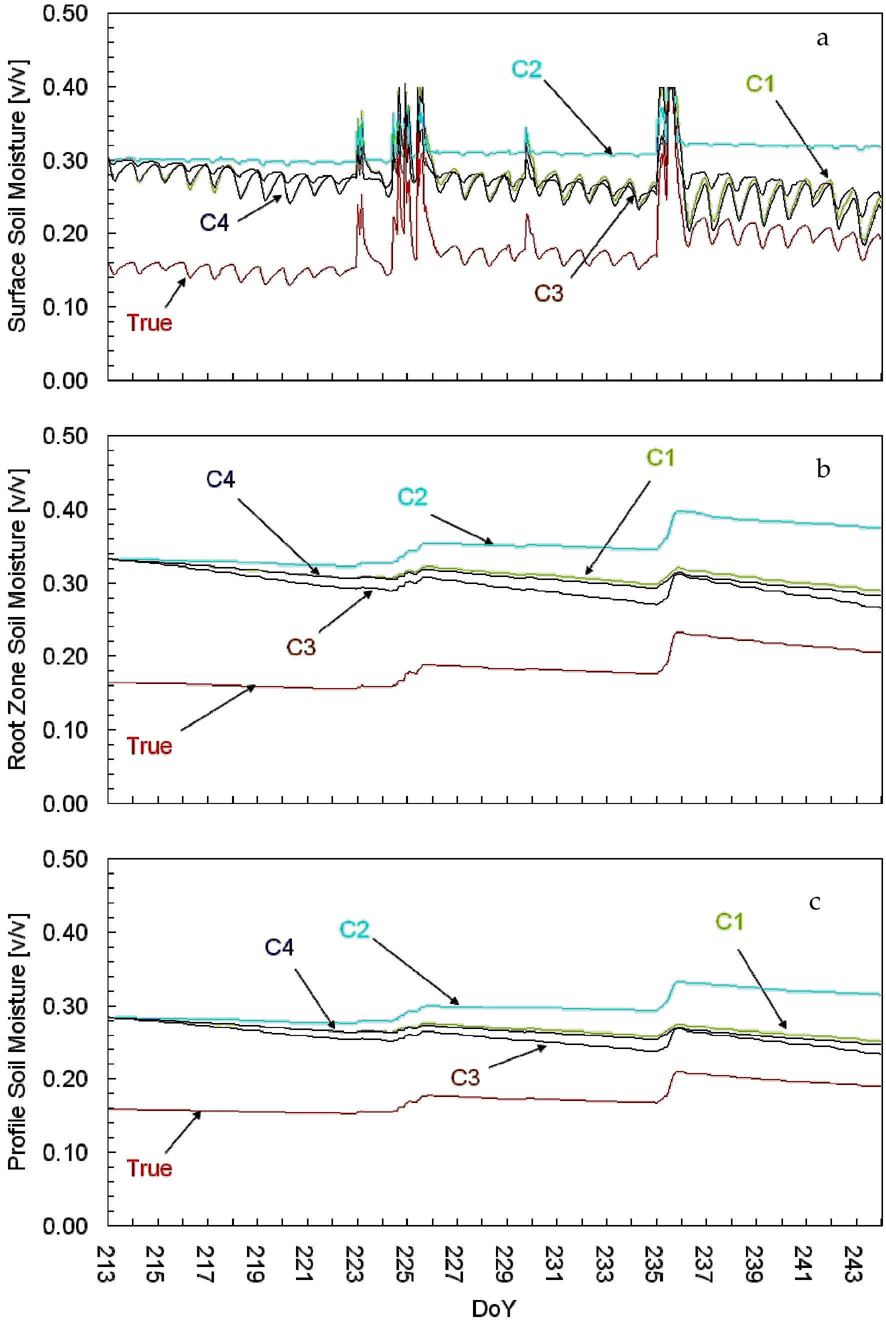

Figure A4.13. Soil moisture control runs for Catchment 4 for August 2003. a) Surface soil moisture, b) root zone soil moisture and c) profile soil moisture. The numbering is explained in Table 5.1.

A4.2.1.5 Catchment 5

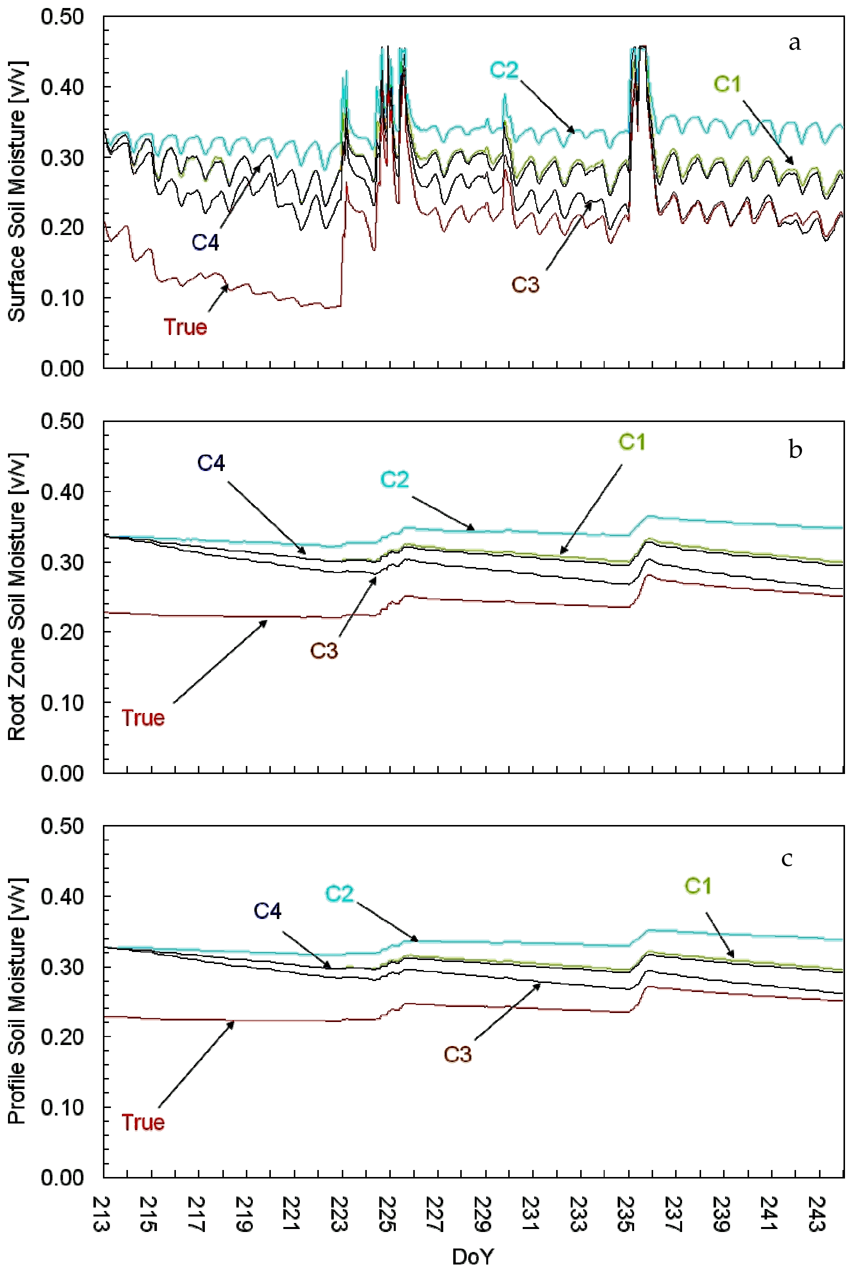

Figure A4.14. Soil moisture control runs for Catchment 5 for August 2003. a) Surface soil moisture, b) root zone soil moisture and c) profile soil moisture. The numbering is explained in Table 5.1.

A4.2.1.6 Catchment 6

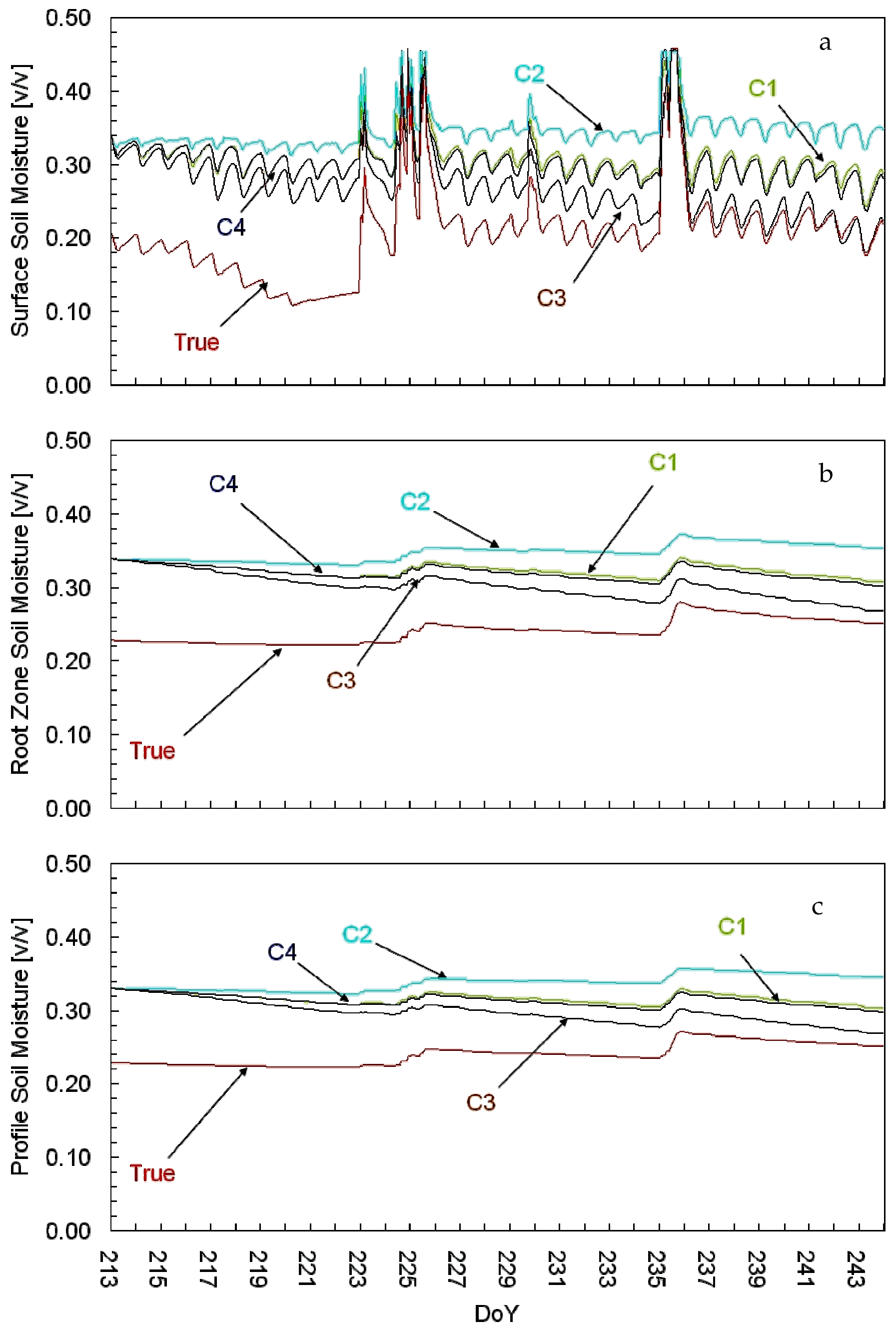

Figure A4.15. Soil moisture control runs for Catchment 6 for August 2003. a) Surface soil moisture, b) root zone soil moisture and c) profile soil moisture. The numbering is explained in Table 5.1.

A4.2.1.7 Catchment 7

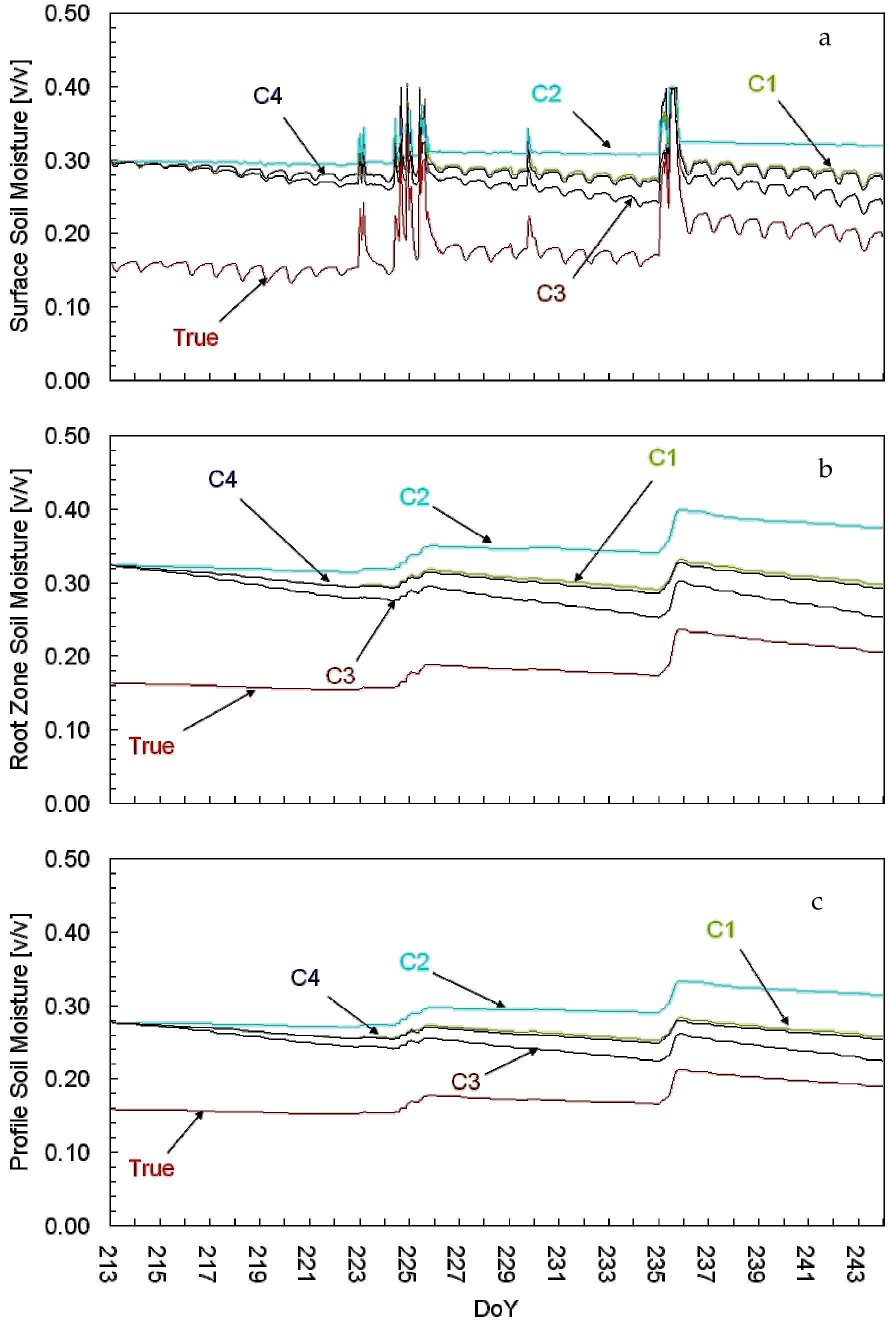

Figure A4.16. Soil moisture control runs for Catchment 7 for August 2003. a) Surface soil moisture, b) root zone soil moisture and c) profile soil moisture. The numbering is explained in Table 5.1.

A4.2.1.8 Catchment 8

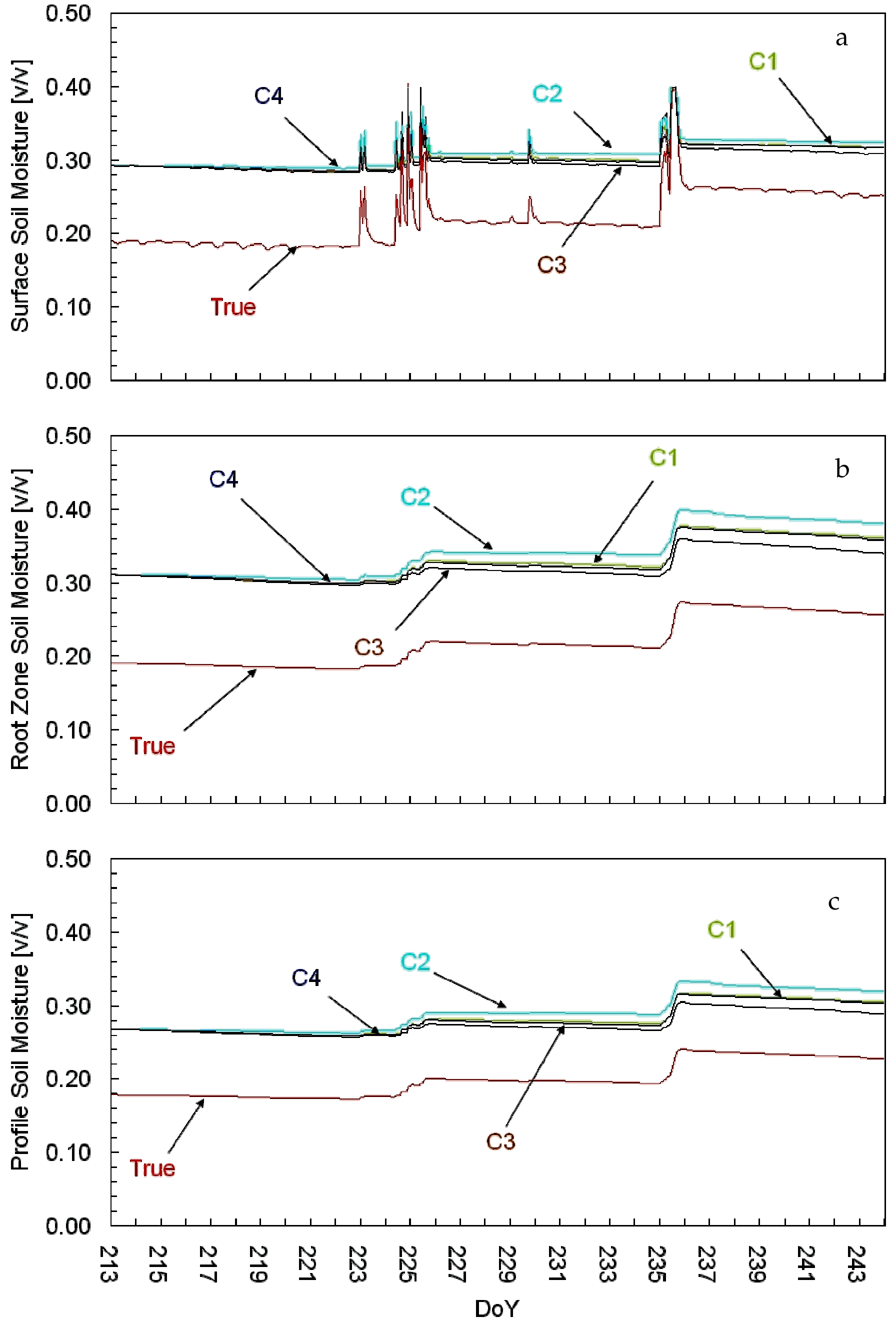

Figure A4.17. Soil moisture control runs for Catchment 8 for August 2003. a) Surface soil moisture, b) root zone soil moisture and c) profile soil moisture. The numbering is explained in Table 5.1.

A4.2.2 Streamflow

A4.2.2.1 Catchment 1

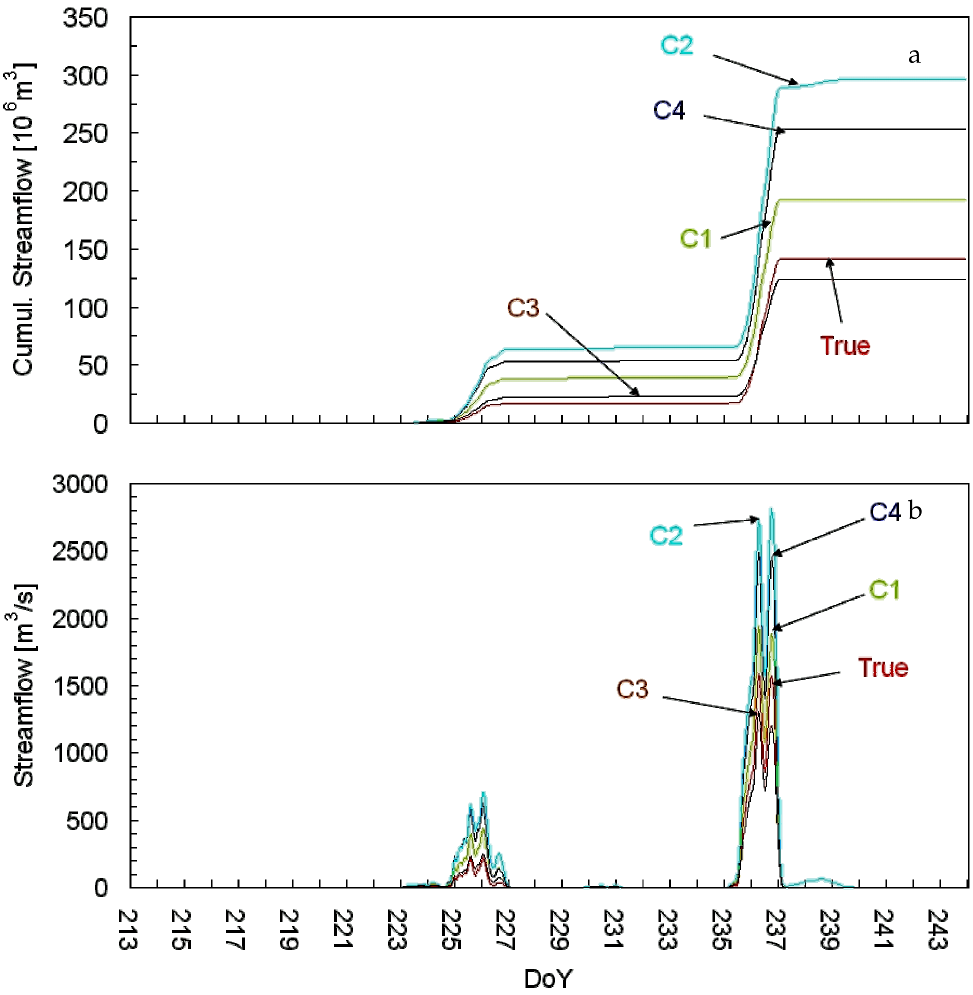

Figure A4.18. Streamflow control runs for Catchment 1 for August 2003. a) Cumulative streamflow and b) instantaneous streamflow. The numbering is explained in Table 5.1.

A4.2.2.2 Catchment 2

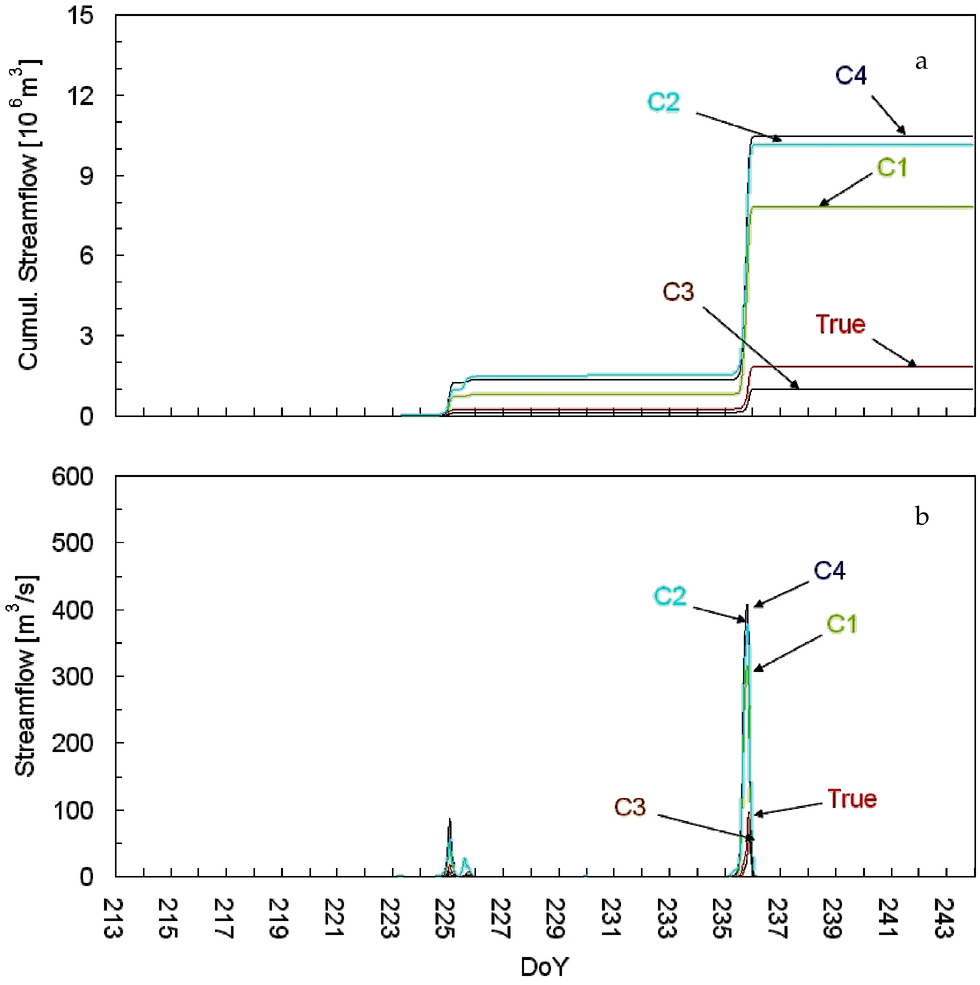

Figure A4.19. Streamflow control runs for Catchment 2 for August 2003. a) Cumulative streamflow and b) instantaneous streamflow. The numbering is explained in Table 5.1.

A4.2.2.3 Catchment 3

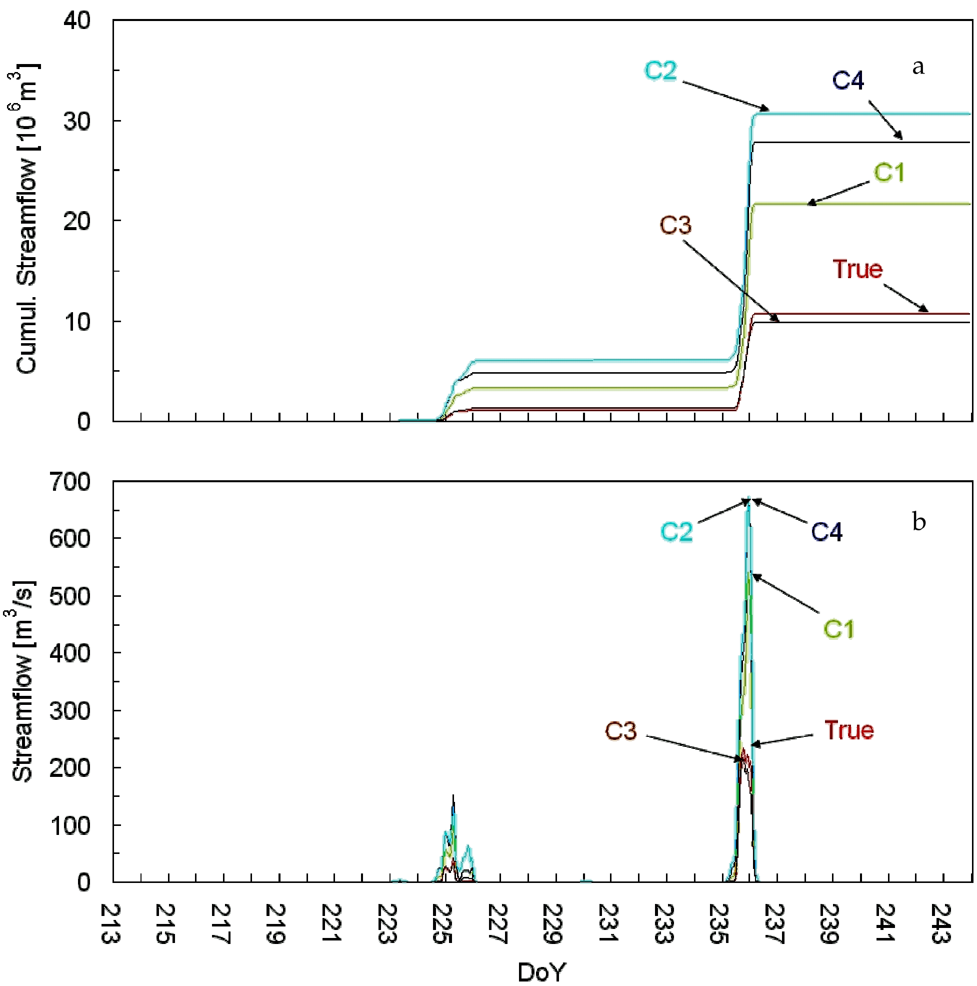

Figure A4.20. Streamflow control runs for Catchment 3 for August 2003. a) Cumulative streamflow and b) instantaneous streamflow. The numbering is explained in Table 5.1.

A4.2.2.4 Catchment 4

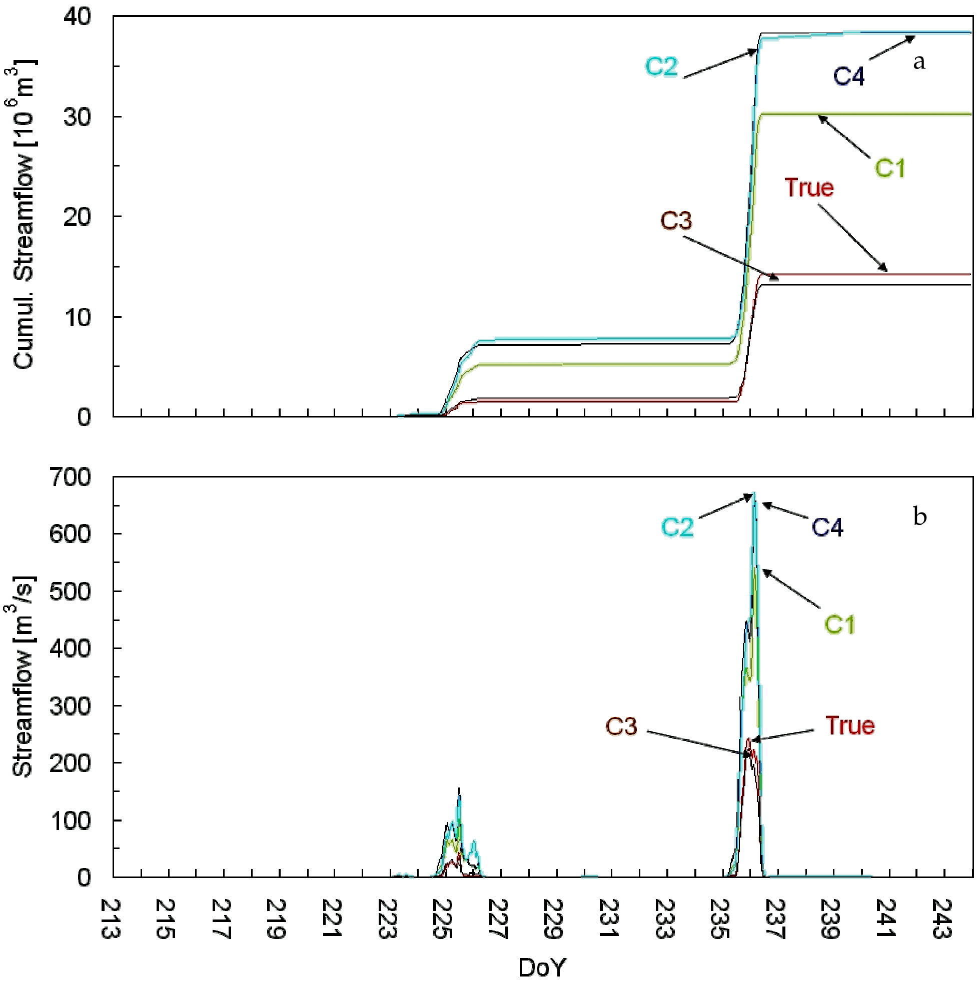

Figure A4.21. Streamflow control runs for Catchment 4 for August 2003. a) Cumulative streamflow and b) instantaneous streamflow. The numbering is explained in Table 5.1.

A4.2.2.5 Catchment 5

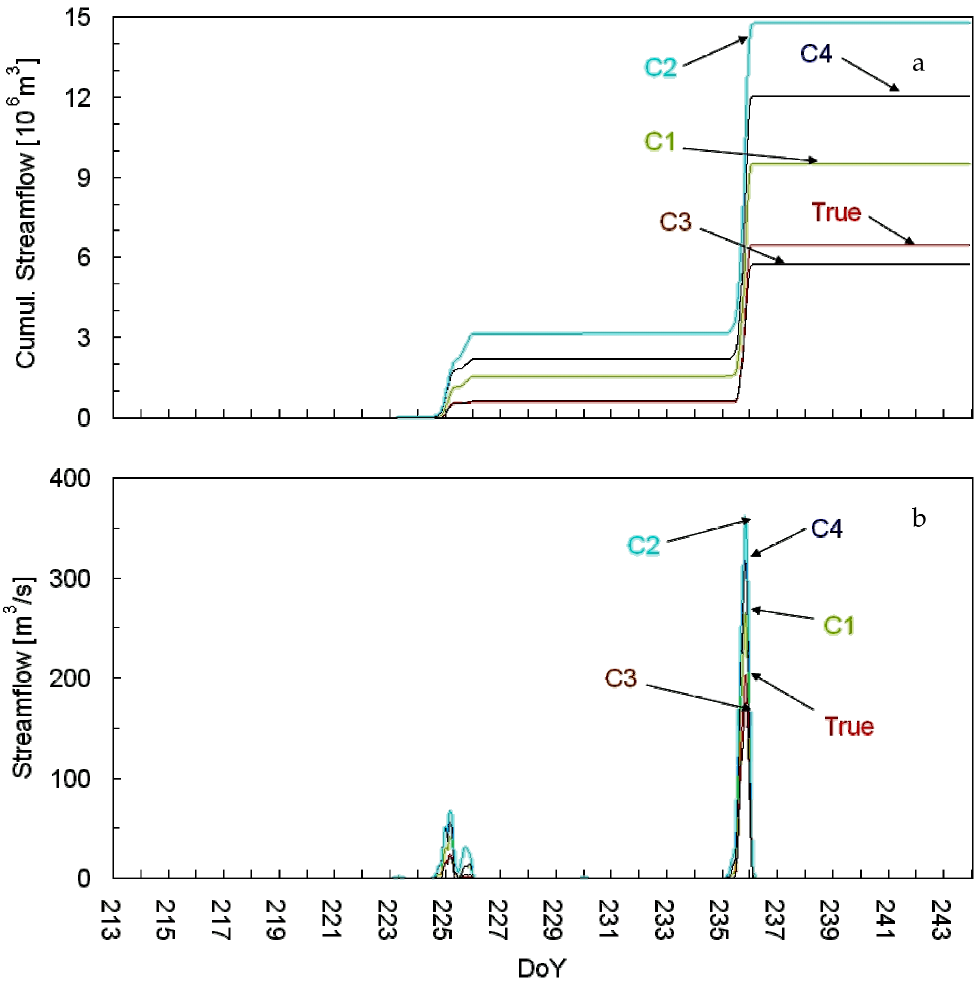

Figure A4.22. Streamflow control runs for Catchment 5 for August 2003. a) Cumulative streamflow and b) instantaneous streamflow. The numbering is explained in Table 5.1.

A4.2.2.6 Catchment 6

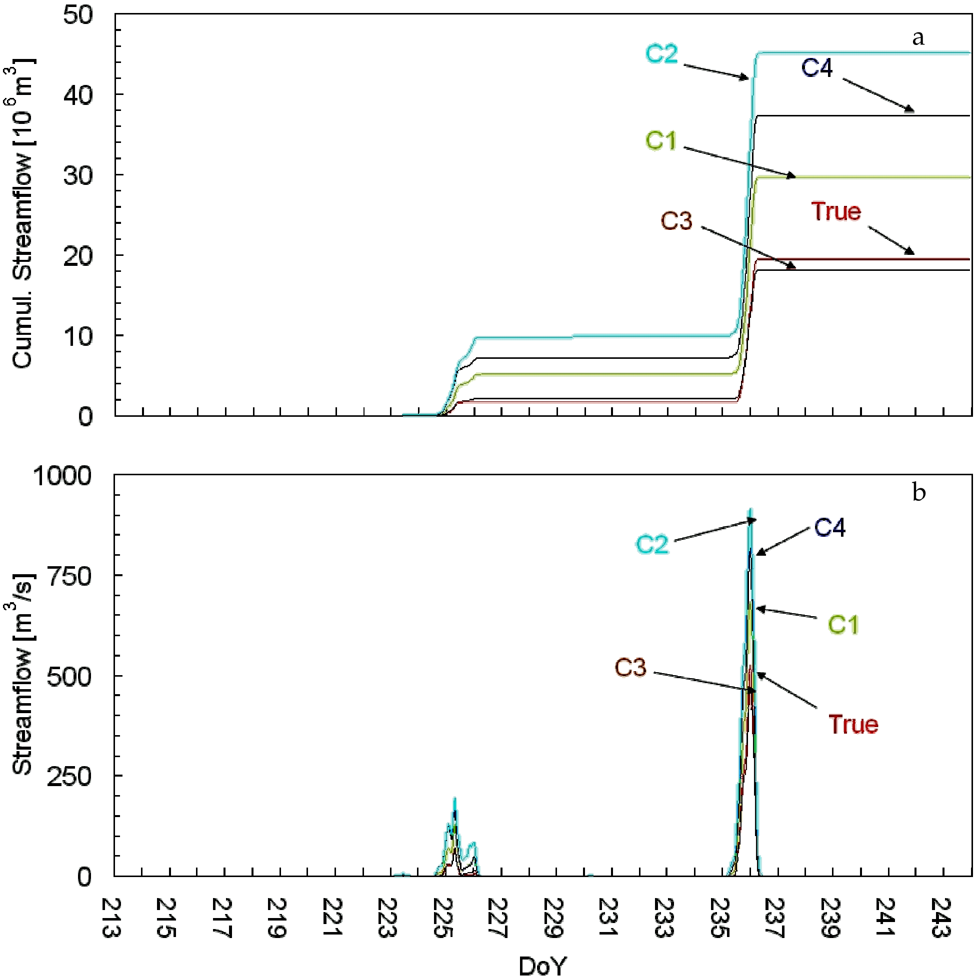

Figure A4.23. Streamflow control runs for Catchment 6 for August 2003. a) Cumulative streamflow and b) instantaneous streamflow. The numbering is explained in Table 5.1.

A4.2.2.7 Catchment 7

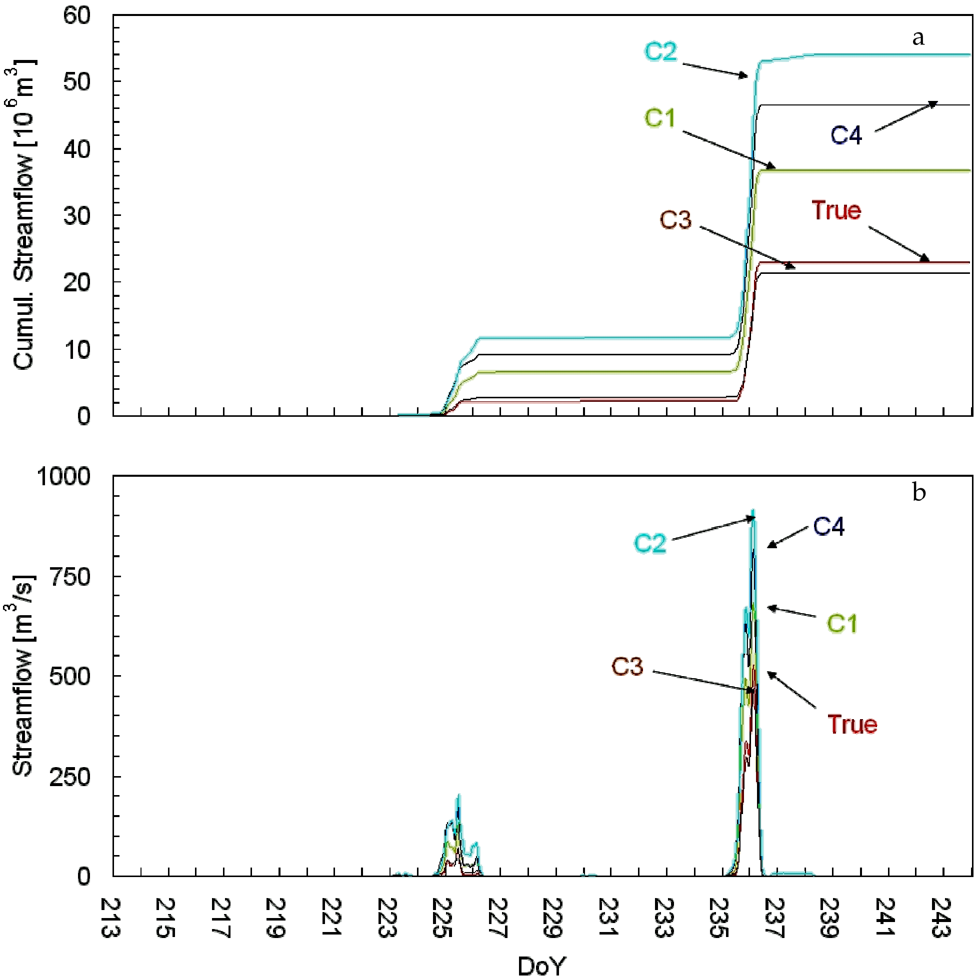

Figure A4.24. Streamflow control runs for Catchment 7 for August 2003. a) Cumulative streamflow and b) instantaneous streamflow. The numbering is explained in Table 5.1.

A4.2.2.8 Catchment 8

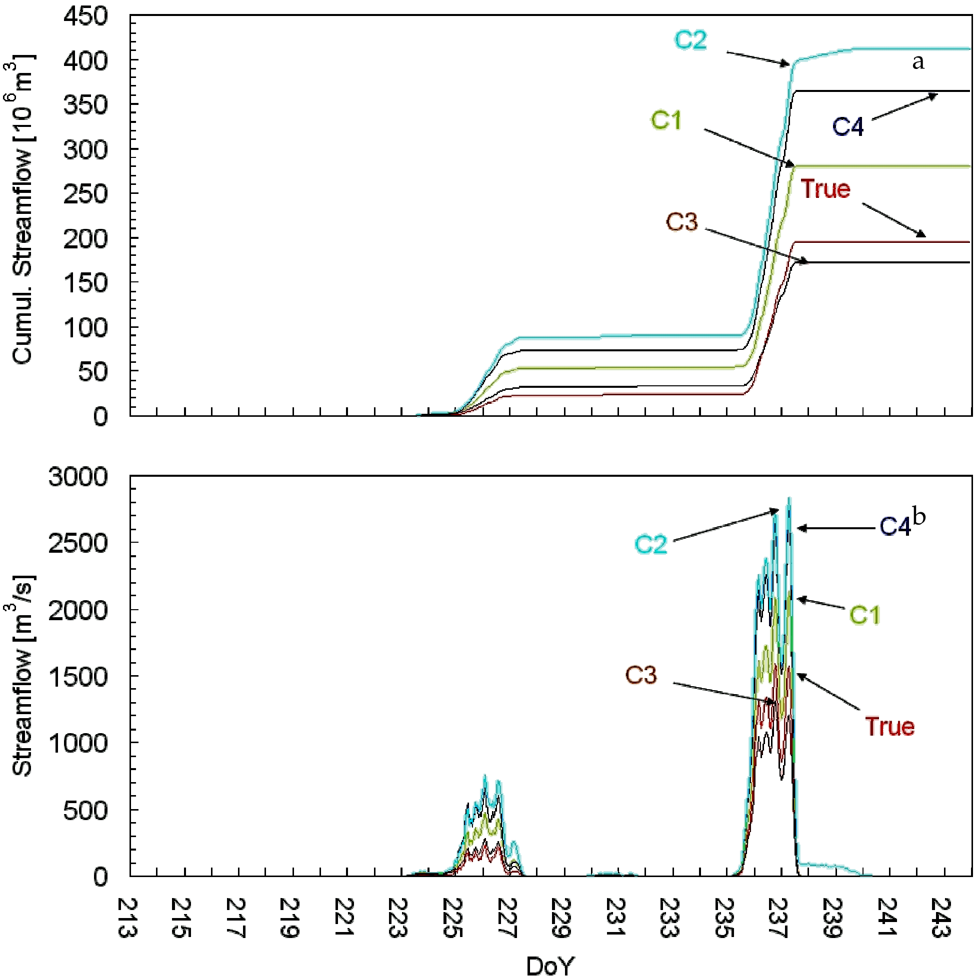

Figure A4.25. Streamflow control runs for Catchment 8 for August 2003. a) Cumulative streamflow and b) instantaneous streamflow. The numbering is explained in Table 5.1.

A4.2.3 Sensible Heat Flux and Evapotranspiration

A4.2.3.1 Catchment 1

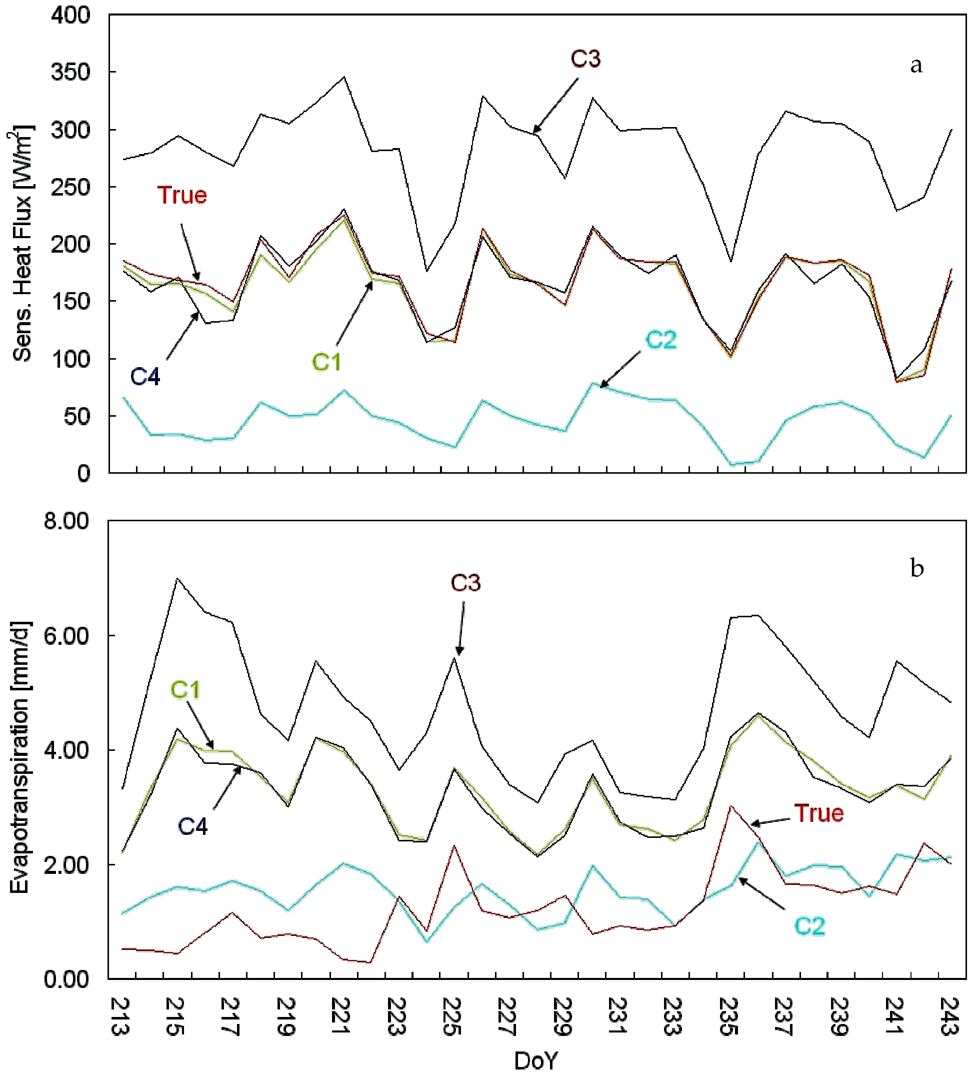

Figure A4.26. a) Sensible heat flux and b) evapotranspiration control runs for Catchment 1 for August 2003. The numbering is explained in Table 5.1.

A4.2.3.2 Catchment 2

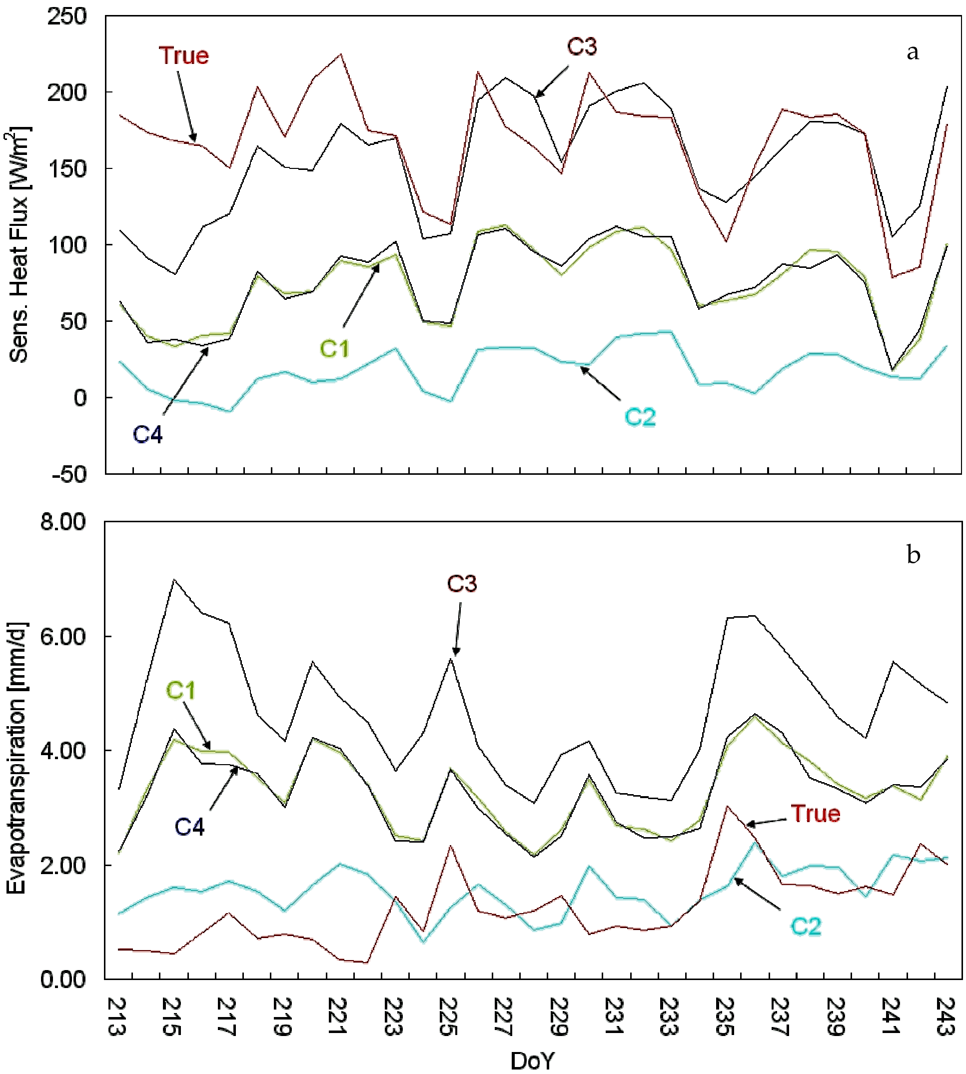

Figure A4.27. a) Sensible heat flux and b) evapotranspiration control runs for Catchment 2 for August 2003. The numbering is explained in Table 5.1.

A4.2.3.3 Catchment 3

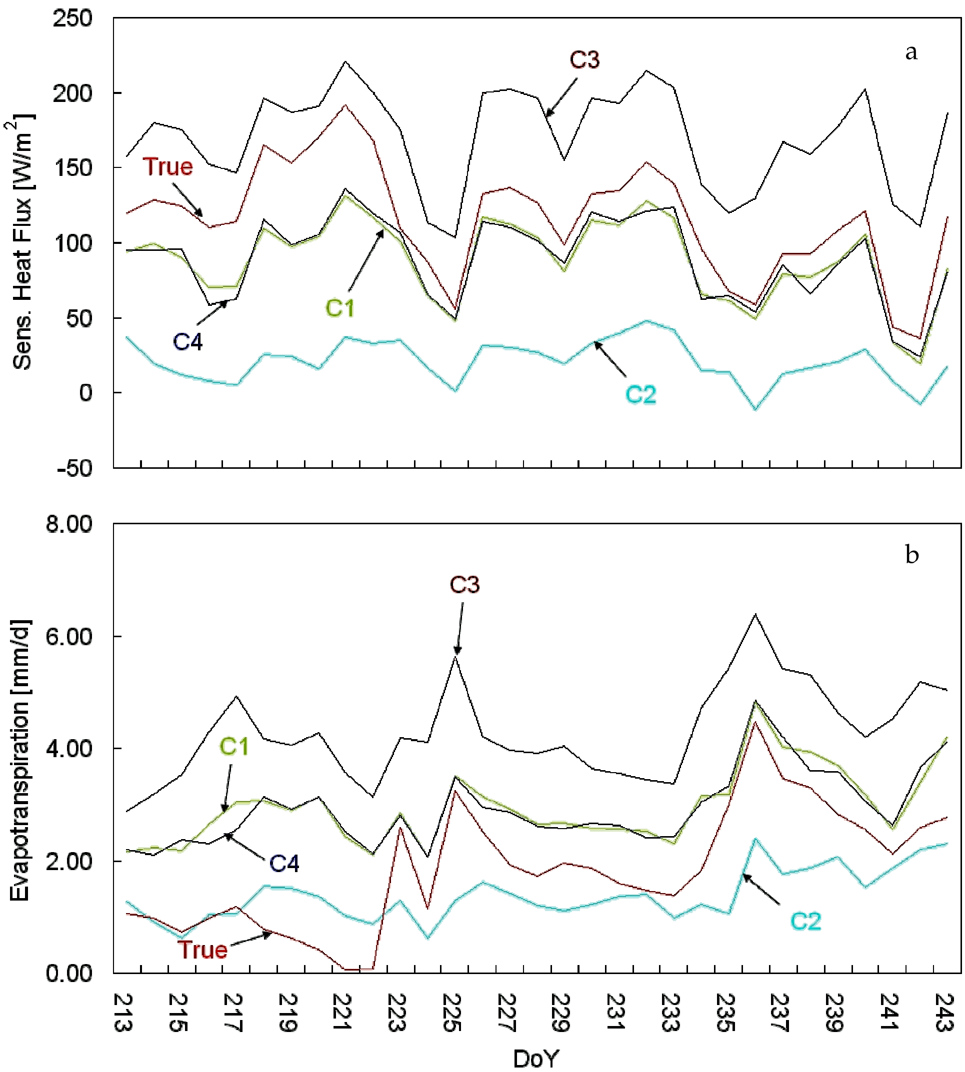

Figure A4.28. a) Sensible heat flux and b) evapotranspiration control runs for Catchment 3 for August 2003. The numbering is explained in Table 5.1.

A4.2.3.4 Catchment 4

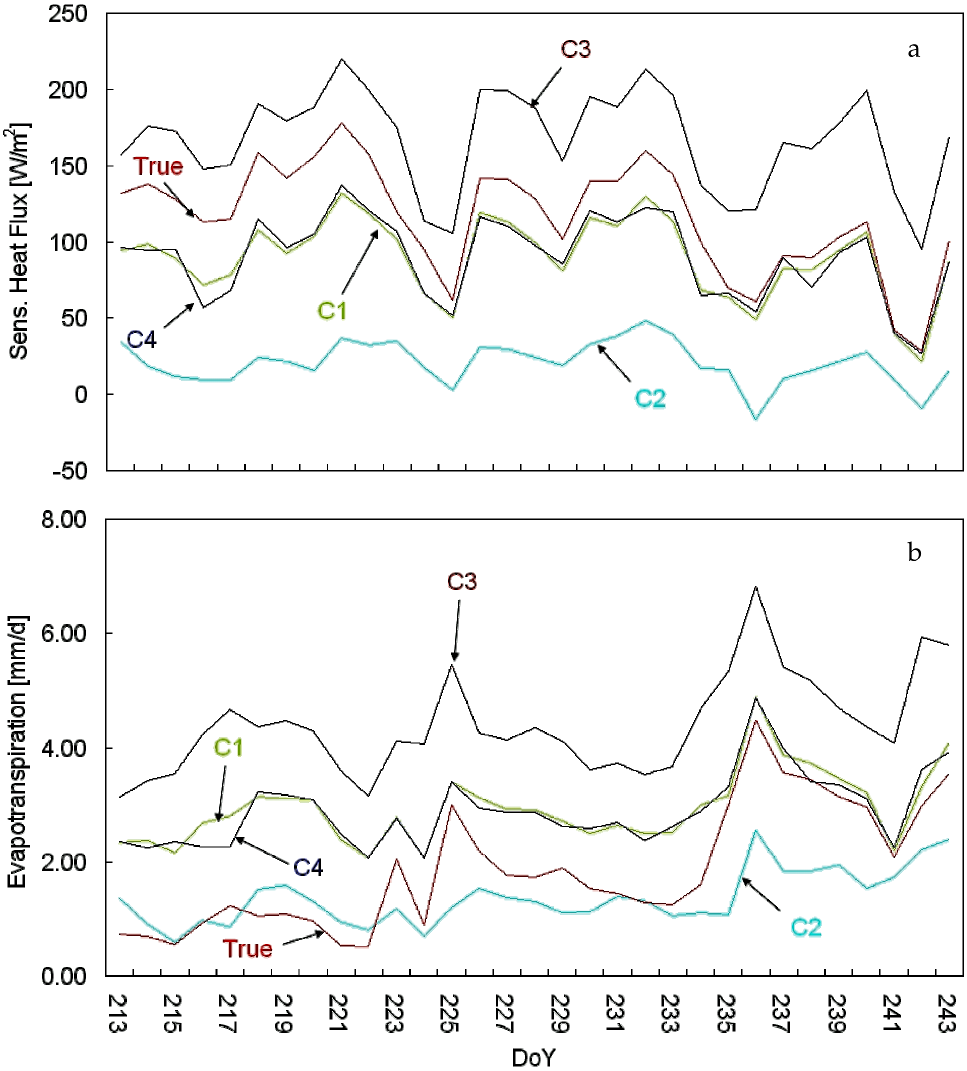

Figure A4.29. a) Sensible heat flux and b) evapotranspiration control runs for Catchment 4 for August 2003. The numbering is explained in Table 5.1.

A4.2.3.5 Catchment 5

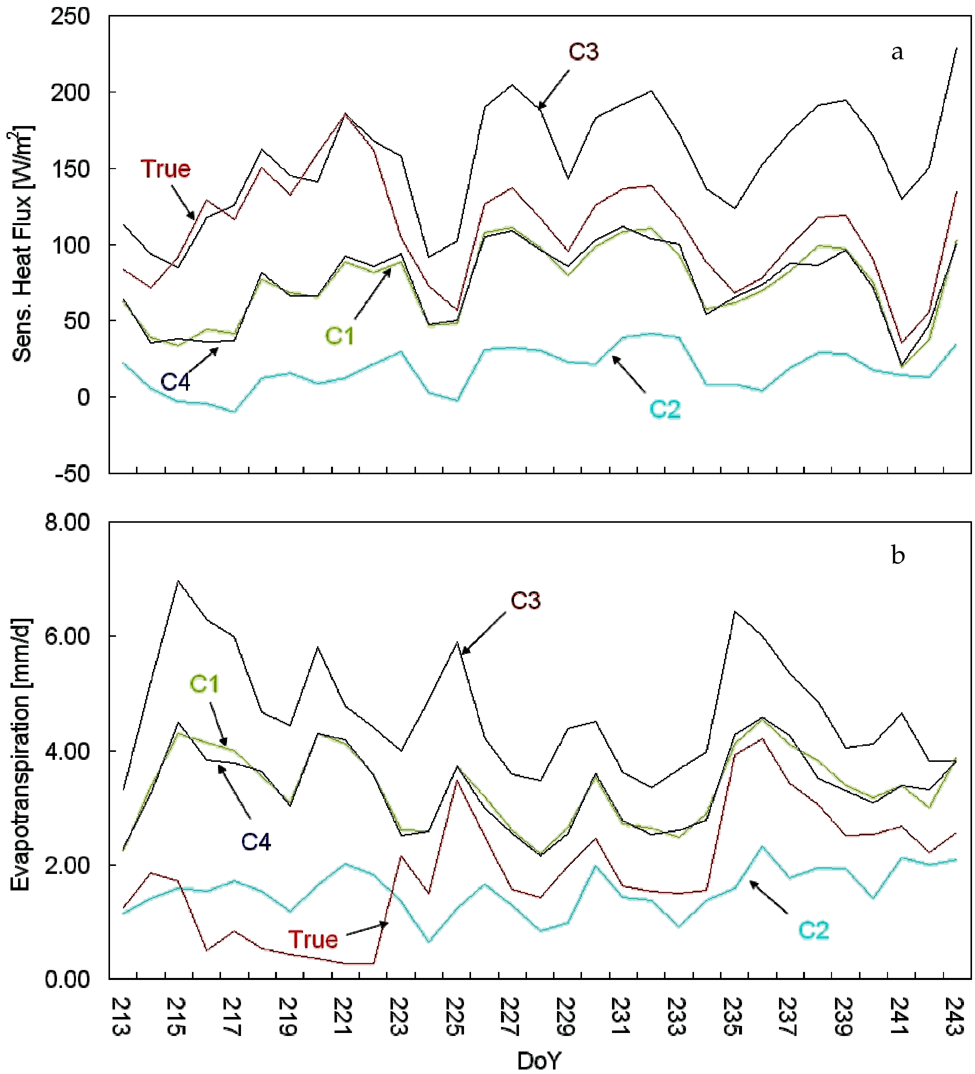

Figure A4.30. a) Sensible heat flux and b) evapotranspiration control runs for Catchment 5 for August 2003. The numbering is explained in Table 5.1.

A4.2.3.6 Catchment 6

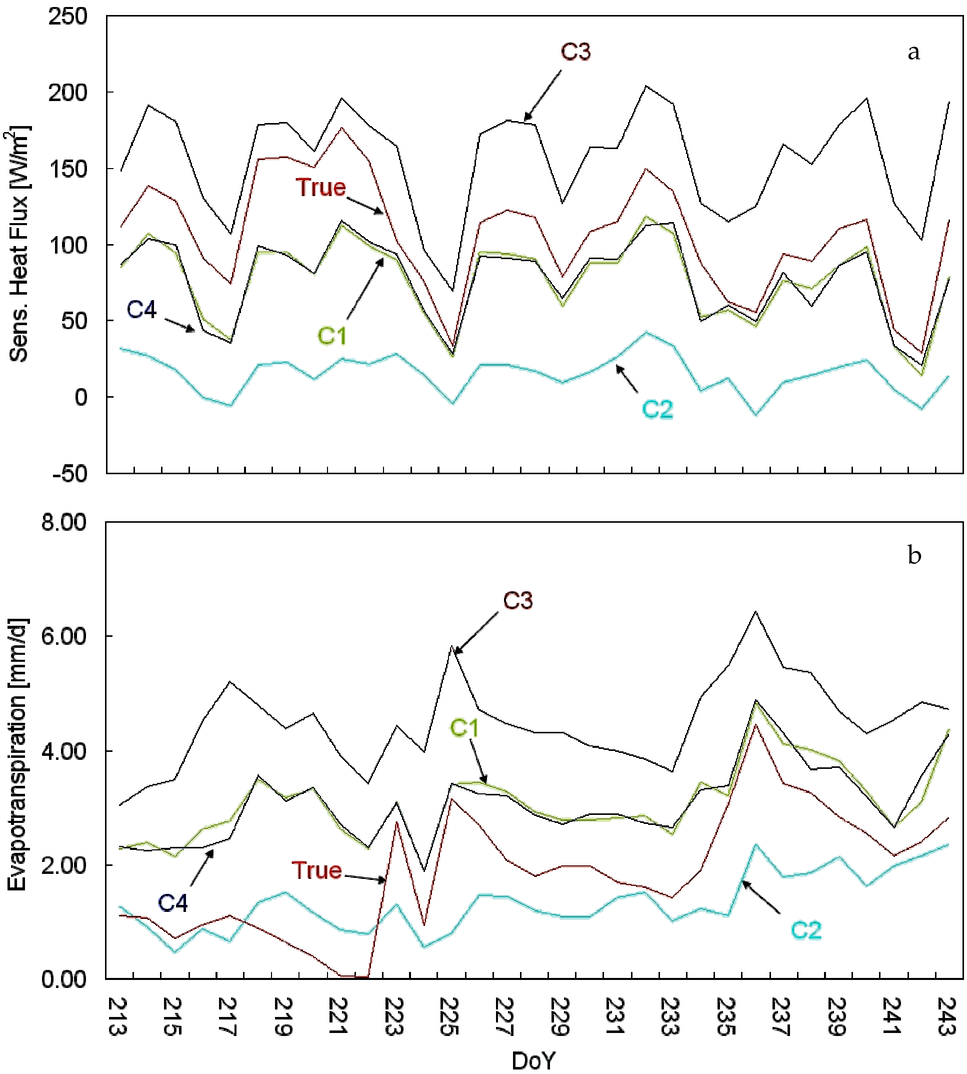

Figure A4.31. a) Sensible heat flux and b) evapotranspiration control runs for Catchment 6 for August 2003. The numbering is explained in Table 5.1.

A4.2.3.7 Catchment 7

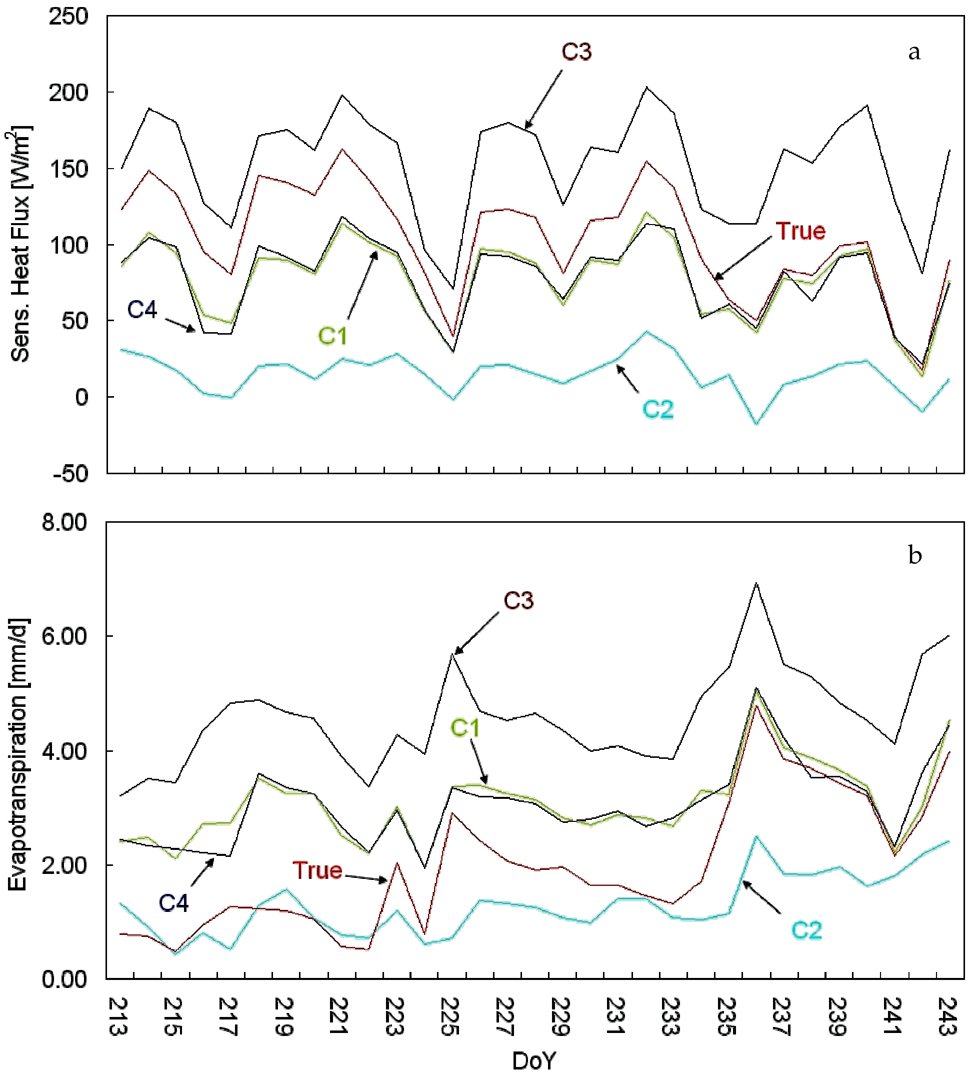

Figure A4.32. a) Sensible heat flux and b) evapotranspiration control runs for Catchment 7 for August 2003. The numbering is explained in Table 5.1.

A4.2.3.8 Catchment 8

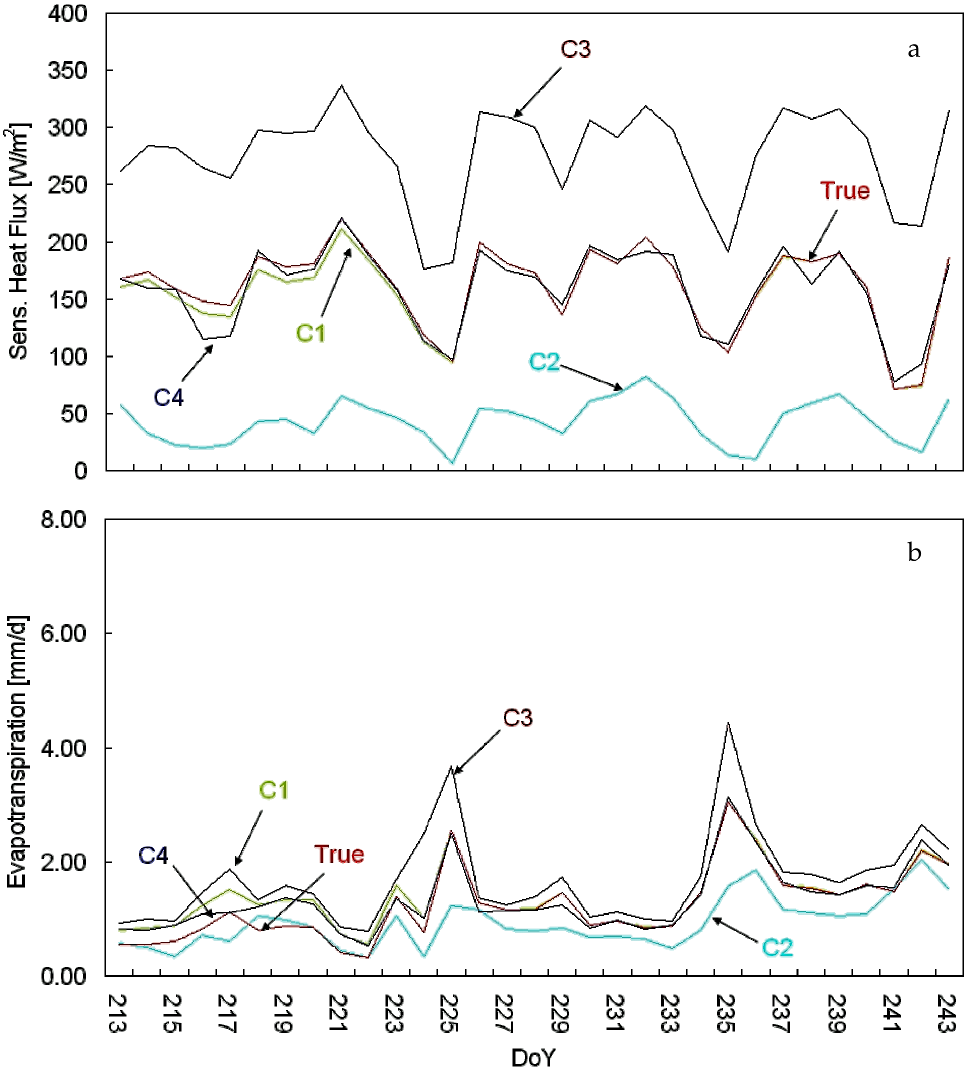

Figure A4.33. a) Sensible heat flux and b) evapotranspiration control runs for Catchment 8 for August 2003. The numbering is explained in Table 5.1.